

A THEORETICAL AND EXPERIMENTAL STUDY
OF DYNAMIC HIGHWAY LOADING

by

Nasser I. Al-Rashid
Clyde E. Lee
William P. Dawkins

Research Report Number 108-1F

Dynamics of Highway Loading
Research Project 3-8-67-108

conducted for

The Texas Highway Department

in cooperation with the
U. S. Department of Transportation
Federal Highway Administration

by the

CENTER FOR HIGHWAY RESEARCH
THE UNIVERSITY OF TEXAS AT AUSTIN

May 1972

The contents of this report reflect the views of the authors, who are responsible for the facts and the accuracy of the data presented herein. The contents do not necessarily reflect the official views or policies of the Federal Highway Administration. This report does not constitute a standard, specification, or regulation.

PREFACE

This is the first and final report on Research Study No. 3-8-67-108, entitled "Dynamics of Highway Loading." The study was begun in 1967 with the primary objective of developing a methodology for experimental measurement and characterization of the dynamic forces applied normal to the surface of highway pavements and other structures by moving traffic. The investigation is part of the Cooperative Research Program of the Center for Highway Research at The University of Texas at Austin; the Texas Highway Department; and the U. S. Department of Transportation, Federal Highway Administration, Bureau of Public Roads.

Dynamic forces applied to the roadway surface by the wheels of moving vehicles are largely responsible for certain types of pavement distress which lead ultimately to unacceptable serviceability of the pavement structure. A theoretical technique which utilizes the power of mathematical simulation and high-speed digital computation in predicting the magnitude and position of the normal components of dynamic wheel loads is described in this report. The validity of this technique is supported by the results of an experimental program which involved the measurement and analysis of dynamic wheel load forces applied to actual pavement structures by different classes of vehicles. This experimentally verified model provides a new tool for further investigation and understanding of the dynamic loading characteristics of highway pavements and is a step forward in improving present analysis and design procedures.

The authors of this report wish to express their appreciation and extend thanks to the many individuals associated with several agencies who have contributed generously of their talents and time during the conduct of this research program.

Center for Highway Research personnel include Harold H. Dalrymple, Research Engineer Associate, who perfected the instrumentation for the portable electronic data collection system; and Roger Walker, Research Engineer Associate; John Ruser; Randy Machemehl; Robert Inman; Ahmad Al-Sari; and Charlie Copeland who assisted in data reduction and analysis and other aspects of this study.

Ed Hamilton of Rainhart Company, Austin, Texas collaborated on the design improvements of the wheel load transducers, and resources of this company expedited the field experiments greatly.

The statistical design for the major experimental program was originated by Dr. Virgil L. Anderson, Professor of Statistics at Purdue University.

Kenneth Hankins of the Texas Highway Department and Carl S. Armbrister and Howard McCann of the Bureau of Public Roads served as contact individuals for their respective organizations and gave advice and continuous assistance.

Joe E. Wright and other personnel of the Planning Survey Division of the Texas Highway Department and the late Thomas K. Wood, District 14, and his maintenance personnel assisted in the field experimental program.

Lloyd J. Wolf of Lloyd J. Wolf and Sons, Inc., Dallas, Texas, as well as the Ford Motor Company provided valuable information about truck and trailer suspension characteristics. Their assistance is most appreciated.

Hubert A. Henry, Automation Division, Texas Highway Department, his staff, and personnel of the computation facilities at The University of Texas at Austin cooperated in the data processing.

Other personnel of the Center for Highway Research and the Texas Highway Department too numerous to acknowledge individually have assisted in many ways in the course of this study.

A supplementary appendices section, which includes the documentation of the computer program, experimental results, and other information related to the experimental program, is bound in a separate volume on file at the Center for Highway Research. This volume will be supplied to the sponsor on request.

Nasser I. Al-Rashid

Clyde E. Lee

William P. Dawkins

Austin, Texas

May 1972

ABSTRACT

A generalized mathematical model which characterizes the dynamic behavior of five different classes of highway vehicles is described in this report. The model consists of a series of interconnected masses, springs, and dashpots and is used to predict the magnitude, duration, and location of dynamic wheel loads applied normal to the roadway surface by the wheels of single unit and articulated vehicles operating under various conditions. The model may be forced by a simulated road profile made up of an array of bumps with different sizes and arrangements in each wheel path, or more realistically, it may be forced by a natural profile recorded in the field by a road profilometer and converted to a suitable digital format. Besides the roadway profile, required input for the model consists of static wheel loads, numerical quantities assigned to the physical characteristics of the vehicle suspension system, and axle spacing. A computer program which solves the sets of differential equations used to describe the motion of each vehicle and calculates the forces between the tire and the road surface has been written in FORTRAN language for the CDC 6600 computer and is documented with example problems.

In a statistically designed experimental program, dynamic wheel forces were measured at nine selected positions along a 64-foot section of roadway by special strain-gage type wheel load transducers. Five representative test vehicles made three passes at each of three speeds over four patterns of artificial road surface roughness and resulted in 3,672 observations of wheel load in the left wheel path and 1,836 measurements in the right wheel path. A description of the wheel load transducer and the electronic data collection system used in this program is included in this report. The results of the experimental program were used to calibrate the model and to provide a validation of the accuracy of the model. The effects of pavement roughness, speed, vehicle type, and their interactions on the magnitude of dynamic wheel loads are discussed.

Experimental devices for measuring bridge deflection and differential movement between the axle and the body of a moving test vehicle were

used along with the mathematical model to study bridge-vehicle interaction. The instrumentation, techniques, and results are described and analyzed.

The accuracy with which dynamic wheel load transducers can be used to predict static vehicle weights is assessed through the use of regression techniques. The analysis indicates that static loads can be estimated with sufficient accuracy for many traffic survey purposes, and that the large sample size made feasible with no inconvenience or hazard to traffic recommends the in-motion weighing technique as a potential substitute for loadometer weighing.

SUMMARY

Highway pavements and bridges are subjected to millions of repetitions of dynamic wheel loads during their useful lives, but current structural design procedures are based on static loading criteria for materials evaluation and for stress analysis. Techniques for characterizing the magnitude and location of dynamic vehicular traffic loads and their relation to static wheel weights are needed so that improved structural design methods can be developed.

In this research study, mathematical models of five representative classes of highway vehicles have been formulated and verified by extensive field experimentation. Good agreement was found between computed and measured wheel forces for all vehicle types, vehicle speeds (10 to 60 mph), and road surface roughness patterns investigated. These mathematical simulation models which describe realistic dynamic loading patterns can now be used directly for design of pavements and bridges and for research on improved structural design procedures.

The pavement loading experiments demonstrated that the complex interaction between a moving vehicle and a road surface profile with irregularities less than 3/4-inch high resulted in dynamic wheel loads that were up to double the static weights. Similarly, an investigation of a three-span continuous steel girder bridge indicated that even though the small total deflection of the structure (about 0.1-inch maximum in a 50-foot span) had little effect on the behavior of the test vehicle, road surface roughness on the approach pavement or on the bridge deck produced impact wheel loads more than 100 percent greater than static weight. The inertia of massive structures attenuates the effects of these dynamic wheel loads, but pavement surfaces and bridge decks experience the full impact.

A statistical analysis of the experimental data showed that a single pair of dynamic scales installed flush with the pavement surface can be used to estimate static wheel loads and gross vehicle weights with accuracy acceptable for traffic survey purposes with the advantages of safety, convenience, and economy to both the highway department and the road users.

This page replaces an intentionally blank page in the original.

-- CTR Library Digitization Team

IMPLEMENTATION STATEMENT

A series of mathematical simulation models which utilize representative vehicle characteristics and measured road surface profiles to predict dynamic wheel loading patterns have been developed. Research has shown that maximum dynamic wheel loads more than twice the static weight can be generated by surface roughness less than 3/4-inch high. Pavements and bridge decks should be designed to account for these loads, and maintenance should be programmed to minimize the surface roughness that produces excessive dynamic loads.

By using this new computational tool, structural engineers can determine more realistic design loads, maintenance engineers can assess the effects of various profile roughness patterns, materials engineers can develop more representative testing procedures, and researchers can formulate improved pavement design and structural design procedures.

Field experimentation demonstrated the feasibility of in-motion weighing for traffic survey purposes. This technique should be implemented in the interest of safety, convenience to the road user, and overall economy to the highway department and to the road users.

This page replaces an intentionally blank page in the original.

-- CTR Library Digitization Team

TABLE OF CONTENTS

PREFACE	iii
ABSTRACT	v
SUMMARY	vii
IMPLEMENTATION STATEMENT	ix
LIST OF TABLES	xv
LIST OF FIGURES	xvii
NOMENCLATURE	xxiii
CHAPTER 1. INTRODUCTION	
The Problem	1
Objectives	3
Scope and Limitations	4
CHAPTER 2. FACTORS AFFECTING DYNAMIC LOADS	
General	7
Vehicle Factors	7
Vehicle Type	7
Suspension System	9
Tires	9
Wind Effects	10
Speed	10
Roadway Factors	10
Road Profile and Surface Roughness	11
Grade	11
CHAPTER 3. THEORY OF VEHICLE DYNAMICS	
General	13
Systems with One Degree of Freedom	13
Systems with Multiple Degrees of Freedom	15
Vehicle Suspension System	18

CHAPTER 4. GENERALIZED MODEL DEVELOPMENT

Preliminary Considerations	23
Selection of Vehicle Types	24
Equations of Motion	24
Class I	24
Class II	31
Class III	37
Class IV	43
Class V	50
Solution of Equations of Motion	58
Dynamic Wheel Loads	59
Description of the Computer Program	63
Artificial Profile	64
Natural Profile	64

CHAPTER 5. MEASUREMENT OF MOVING WHEEL LOAD FORCES

General	69
Wheel Load Transducer	70
Design Description	70
Frame and Bearing Pads	70
Sealing	75
Load Cell Chassis	75
Structural Plates	75
Leveling Screws	75
Top Cover	75
Load Cells	77
Improved Wheel Load Transducer	81
Laboratory Calibration	81
Field Calibration	83
Signal Recording	86
Signal Playback and Reduction	89

CHAPTER 6. EXPERIMENTAL PROGRAM

General	91
Selection of Factors	91
Selection of Test Site	92
Selection of Test Vehicles	92
Preliminary Testing Program	95
Major Experiment	97
Instrumentation	102
Testing Procedure	105
Data Reduction	107
Manual Data Reduction	109
Computer Reduction of Data	111

CHAPTER 7. VALIDATION OF THE MODEL

General	115
Predicted versus Observed Forces - Comparative Study	115
Study of Dynamic Load Component	134
Summary	141

CHAPTER 8. DISCUSSION OF EXPERIMENTAL RESULTS

General	143
Analysis of Variance	144
Main Variable Effects	144
Speed - Scale Location Interaction (V×S)	152
Scale Location - Roughness Interaction (S×T)	152
Speed - Axles Interaction (V×A)	153
Axle - Scale Interaction (A×S)	153
Axle - Roughness Interaction (A×T)	155
Speed - Roughness Interaction (V×T)	155
Speed - Roughness - Scale Interaction (V×T×S)	155
Speed - Scale - Axle Interaction (V×S×A)	157
Roughness - Scale - Axle Interaction (T×S×A)	157
Summary Discussion	158

CHAPTER 9. MODEL REFINEMENT

Sensitivity Analysis	161
Tire Subsystem	162
Suspension Subsystem	162
Suspension Damping	167
Model Refinements	167
Tire Enveloping	171
Tandem-Axle Modifications	171
Summary	171

CHAPTER 10. BRIDGE STUDY

Experimental Program	175
Bridge Instrumentation	176
Vehicle Instrumentation	176
Experimental Measurements	179
Data Reduction and Analysis	179
Summary of Bridge Study	187

CHAPTER 11. ESTIMATING STATIC VEHICULAR WEIGHTS

Static Wheel Weights	189
Static Gross Vehicle Weight	197
Summary	200

CHAPTER 12. CONCLUSIONS AND RECOMMENDATIONS

Conclusions	203
Recommendations	208
Model Refinement	208
Field Experimentation	208
Bridge Studies	209
REFERENCES	211
APPENDIX A. STATIC WHEEL LOADS OF TEST VEHICLES	217
APPENDIX B. EXPERIMENT DESIGN	233
APPENDIX C. EXPERIMENTAL RESULTS	239

LIST OF TABLES

Table	Page
1 Class I Summary	27
2 Class II Summary	33
3 Class III Summary	39
4 Class IV Summary	45
5 Class V Summary	52
6 Channel-Scale Arrangement	104
7 Random Order of Test Runs	107
8 Duration of Maximum Level of Pulse	108
9 Printout of Computer Reduced Wheel Loads	113
10 Comparative Study Summary of the Difference in Observed and Predicted Wheel Loads	117
11 Comparative Study Summary of the Difference in Observed and Predicted Wheel Loads from Tandem Axles	119
12 Analysis of Variance	145
13 Main Variables Average Effects	146
14 Axle-Speed Interaction (A×V)	154
15 Axle-Scale Interaction (A×S)	156
16 Test Vehicle Characteristics	178
17 Regression Analysis for Wheel Weight Study	194
18 Analysis of Static Cross Weights	198
B.1 Analysis of Variance Table	234
C.1-C.36 Experimental Results	240-275
C.37-C.48 Dynamic Component (percent of static)	276-287

This page replaces an intentionally blank page in the original.

-- CTR Library Digitization Team

LIST OF FIGURES

Figure		Page
1	Schematic representation of the approach to the research program	5
2	Vehicle-road system	8
3	System with one degree of freedom	14
4	System with two degrees of freedom	17
5	Simple moving vehicle suspension	19
6	Typical half-vehicle model	21
7	Selected classes of vehicles	25
8	Class I vehicle model	26
9	Main body motion analysis	28
10	Class II vehicle model	32
11	Class III vehicle model	38
12	Class IV vehicle model	44
13	Class V vehicle model	51
14	Artificial profile example	65
15	Surface dynamics load profilometer	66
16	Summary flow of program DYMOL	67
17	Cutaway top view sections of Model 880 transducer	71
18	Exploded view of Model 880 transducer	72
19	Components of Model 880 transducer	73
20	Load cell chassis placed in frame	74
21	Center structural plate in place	74

Figure		Page
22	Assembled unit	74
23	Wheatstone bridge circuit	76
24	Top view and section showing dimensions of load cell	78
25	Top and bottom view of load cell in aluminum casting	79
26	Load cell calibration curves	80
27	Grooved structural plate	82
28	Frame latch-catch	82
29	Load cell chassis laboratory calibration setup	84
30	Load cell chassis laboratory calibration curves	85
31	Field calibration setup	87
32	Calibration load versus scale output	87
33	Recording logic block diagram	88
34	Classification of truck traffic northbound on IH-35, Austin, Texas	94
35	Preliminary installation	96
36	View of field installation	96
37	Arrangement of scales array	98
38	Driver view of field installation	99
39	Patterns of roughness	101
40	Recording system block diagram	103
41	Recording equipment	106
42	Recording equipment-field setup	106
43	Typical force pulse	108
44	Typical oscillograph analog record	110
45	Computer reduction summary flow	112
46	Predicted and observed dynamic wheel load (Class I, loaded)	121

Figure		Page
47	Predicted and observed dynamic wheel load (Class I, loaded)	122
48	Predicted and observed dynamic wheel load (Class I, loaded)	123
49	Predicted and observed dynamic wheel load (Class I, empty)	124
50	Predicted and observed dynamic wheel load (Class I, empty)	125
51	Predicted and observed dynamic wheel load (Class II)	126
52	Predicted and observed dynamic wheel load (Class III)	127
53	Predicted and observed dynamic wheel load (Class IV)	128
54	Predicted and observed dynamic wheel load (Class V)	129
55	Continuous record of predicted load and roadway profile (R-4)	130
56	Continuous record of predicted load and roadway profile (R-4)	131
57	Continuous record of predicted load and roadway profile (R-4)	132
58	Continuous record of predicted load and roadway profile (R-4)	133
59	Predicted and observed cumulative frequency distribution of dynamic load components	135
60	Predicted and observed cumulative frequency distribution of dynamic load components	136
61	Predicted and observed cumulative frequency distribution of dynamic load components	137
62	Predicted and observed cumulative frequency distribution of dynamic load components	138
63	Predicted and observed cumulative frequency distribution of dynamic load components	139
64	Predicted and observed cumulative frequency distribution of dynamic load components	140

Figure		Page
65	Effect of axles on measured average dynamic wheel loads	148
66	Effect of scale location on measured average dynamic wheel loads	149
67	Effect of speed on measured average dynamic wheel loads	150
68	Effect of roughness on measured average dynamic wheel loads	151
69(a)	Tire stiffness (4,000 lb/in) increased 50%	163
69(b)	Tire stiffness (4,000 lb/in) decreased 50%	163
70(a)	Zero tire damping	164
70(b)	Tire damping 5% of critical	164
70(c)	Tire damping 10% of critical	165
71	Class I model showing optimum parameter settings	166
72	Suspension stiffness double values shown in Fig 71	168
73(a)	Suspension damping 1% of critical	169
73(b)	Suspension damping 10% of critical	169
73(c)	Suspension damping 20% of critical	170
74(a)	Moving average of computed tire forces over 8-inch interval	172
74(b)	Computed tire forces resulting from an eight-inch (46 point) moving average of the input profile	172
75	Strain-gaged cantilever beams supported by sand-filled containers at ground level beneath bridge	177
76	Potentiometers for measuring axle-body deflections	180
77	Roughness patterns for bridge study	181
78	Theoretical and experimental axle-frame displacements for truck traveling at 30 mph	183
79	Predicted tire forces, vehicle speed 60 mph, roughness K	184
80	Predicted tire forces, vehicle speed 30 mph, roughness K	184
81	Predicted tire forces, vehicle speed 30 mph, roughness L	185
82	Predicted tire forces, vehicle speed 30 mph, roughness M	185

Figure		Page
83	Predicted tire forces, vehicle speed 30 mph, roughness N . . .	186
84	Predicted vs static wheel weights, vehicle speed 10 mph . . .	190
85	Predicted vs static wheel weights, vehicle speed 30 mph . . .	191
86	Predicted vs static wheel weights, vehicle speed 60 mph . . .	192
A.1	Static weighing operation (front axle)	218
A.2	Static weighing operation (rear axle)	218
A.3	Summary of static weights (vehicle No. I-1)	219
A.4	Summary of static weights (vehicle No. I-2)	220
A.5	Summary of static weights (vehicle No. I-3)	221
A.6	Summary of static weights (vehicle No. I-4)	222
A.7	Summary of static weights (vehicle No. II-1)	223
A.8	Summary of static weights (vehicle No. III-1)	224
A.9	Summary of static weights (vehicle No. IV-1)	225
A.10	Summary of static weights (vehicle No. V-1)	226
A.11	Summary of static weights (vehicle No. V-2)	227
A.12	Summary of static weights (vehicle No. V-3)	228
A.13	Summary of static weights (vehicle No. V-4)	229
B.1	Major experiment layout	234

This page replaces an intentionally blank page in the original.

-- CTR Library Digitization Team

NOMENCLATURE

<u>Symbol</u>	<u>Typical Units</u>	<u>Definition</u>
A	in.	Distance between cab-trailer connection and second axle
β	-	Integration parameter
Cs _{1R}	lb/in/sec	Suspension damping rate for right side of axle 1
Cs _{1L}	lb/in/sec	Suspension damping rate for left side of axle 1
Cs _{2R}	lb/in/sec	Suspension damping rate for right side of axle 2
Cs _{2L}	lb/in/sec	Suspension damping rate for left side of axle 2
Cs _{3R}	lb/in/sec	Suspension damping rate for right side of axle 3, etc.
Cs _{23R}	lb/in/sec	Suspension damping rate for right side of first tandem for Class V vehicles
Cs _{23L}	lb/in/sec	Suspension damping rate for left side of first tandem for Class III and V vehicles
Cs _{34R}	lb/in/sec	Suspension damping rate for right side of tandem axle for Class IV vehicles
Cs _{34L}	lb/in/sec	Suspension damping rate for left side of tandem axle for Class IV vehicles
Cs _{45R}	lb/in/sec	Suspension damping rate for right side of second tandem for Class V vehicles
Cs _{45L}	lb/in/sec	Suspension damping rate for left side of second tandem for Class V vehicles
Ct _{1R}	lb/in/sec	Damping rate for right tire of axle 1
Ct _{1L}	lb/in/sec	Damping rate for left tire of axle 1

<u>Symbol</u>	<u>Typical Units</u>	<u>Definition</u>
C_{2R}^t	lb/in/sec	Damping rate for right tire of axle 2, etc.
D_{1R}, D_{1L}	in.	Combined movements of the right and left corners of the main body at axle 1 due to vertical translation, rolling, and pitching
D_{2R}, D_{2L}	in.	Combined movements of the right and left corners of the main body at axle 2
D_{23R}, D_{23L}	in.	Combined movements of the right and left sides of the cab (Class V) at first tandem due to vertical translation, rolling, and pitching of the cab
D_{45R}, D_{45L}	in.	Combined movements of the right and left sides of the trailer (Class V) at second tandem due to vertical translation, rolling, and pitching of the trailer
D_{34R}, D_{34L}	in.	Combined movements of the right and left of the trailer (Class IV) at tandem axle due to vertical translation, rolling, and pitching of the trailer
D_b	in.	Movement of the cab at cab-trailer connection
D_c	in.	Movement of the trailer at cab-trailer connection
F_{DY1R}	lb	Dynamic force at right side of axle 1
F_{DY1L}	lb	Dynamic force at left side of axle 1
F_{ST1R}	lb	Static force at right side of axle 1
F_{ST1L}	lb	Static force at left side of axle 1
F_{T01R}	lb	Total force at right side of axle 1
F_{T01L}	lb	Total force at left side of axle 1
g	ft/sec ²	Acceleration of gravity
h	sec	Integration increments

<u>Symbol</u>	<u>Typical Units</u>	<u>Definition</u>
I_X	lb-sec ² -in	Rolling mass moment of inertia of main body (Class I and III)
I_Z	lb-sec ² -in	Pitching mass moment of inertia of main body (Class I and III)
I_{X1}	lb-sec ² -in	Rolling mass moment of inertia of the cab
I_{Z1}	lb-sec ² -in	Pitching mass moment of inertia of the cab
I_{X2}	lb-sec ² -in	Rolling mass moment of inertia of the trailer
I_{Z2}	lb-sec ² -in	Pitching mass moment of inertia of the trailer
I_{TZ}	lb-sec ² -in	Pitching mass moment of inertia of tandem axle (Class III)
I_{TZ1}	lb-sec ² -in	Pitching mass moment of inertia of tandem 1 (Class V)
I_{TZ2}	lb-sec ² -in	Pitching mass moment of inertia of tandem 2 (Class V)
K_s	lb/in	Suspension spring rate of cab-trailer connection
K_{s1R}	lb/in	Suspension spring rate of right side of axle 1
K_{s1L}	lb/in	Suspension spring rate of left side of axle 1
K_{s2R}	lb/in	Suspension spring rate of right side of axle 2
K_{s2L}	lb/in	Suspension spring rate of left side of axle 2, etc.
K_{s23R}	lb/in	Suspension spring rate of right side of tandem axle 1 (Class V)
K_{s23L}	lb/in	Suspension spring rate of left side of tandem axle 1 (Class V)

<u>Symbol</u>	<u>Typical Units</u>	<u>Definition</u>
$K_{s_{45R}}$	lb/in	Suspension spring rate of right side of tandem axle 2 (Class V)
$K_{s_{45L}}$	lb/in	Suspension spring rate of left side of tandem axle 2 (Class V)
$K_{s_{34R}}$	lb/in	Suspension spring rate of right side of tandem axle (Class IV)
$K_{s_{34L}}$	lb/in	Suspension spring rate of left side of tandem axle (Class IV)
$K_{t_{1R}}$	lb/in	Stiffness coefficient of right tire of axle 1
$K_{t_{1L}}$	lb/in	Stiffness coefficient of left tire of axle 1
$K_{t_{2R}}$	lb/in	Stiffness coefficient of right tire(s) of axle 2
$K_{t_{2L}}$	lb/in	Stiffness coefficient of left tire(s) of axle 2, etc.
M_0	lb-sec ² /in	Mass of main body (Class I and III)
M_{01}	lb-sec ² /in	Mass of cab
M_{02}	lb-sec ² /in	Mass of trailer
M_{1R}	lb-sec ² /in	Mass of right tire and appropriate portion of axle 1
M_{1L}	lb-sec ² /in	Mass of left tire and appropriate portion of axle 1
M_{2R}	lb-sec ² /in	Mass of right tire and appropriate portion of axle 2
M_{2L}	lb-sec ² /in	Mass of left tire and appropriate portion of axle 2, etc.
T_{RL}	in.	Trailer length
V	in/sec	Vehicle speed

<u>Symbol</u>	<u>Typical Units</u>	<u>Definition</u>
V_{1R} , V_{1L}	in.	Road profile input at right and left tires, axle 1
V_{2R} , V_{2L}	in.	Road profile input at right and left tires, axle 2
V_{3R} , V_{3L}	in.	Road profile input at right and left tires, axle 3, etc.
$W_1 , W_2 \dots$	in.	Width of axle 1, axle 2, ...
X_1	in.	Distance between center of gravity of the main body and axle 1 (Class I)
X_2	in.	Distance between center of gravity of the main body and axle 2 (Class I)
X_3	in.	Distance between center of gravity of the main body and axle 3 (Class III)
X_{12}	in.	Distance between axle 1 and axle 2
X_{13}	in.	Distance between axle 1 and axle 3
X_{23}	in.	Distance between axle 2, axle 3, etc.
X_{C1}	in.	Distance between center of gravity of cab and axle 1
X_{C2}	in.	Distance between center of gravity of cab and axle 2
X_{C23}	in.	Distance between center of gravity of cab and first tandem (Class V)
X_{TR2}	in.	Distance between center of gravity of trailer and axle 2
X_{TR23}	in.	Distance between center of gravity of trailer and first tandem
X_{TR45}	in.	Distance between center of gravity of trailer and second tandem
X_T	in.	Distance between center of gravity of main body and tandem (Class III)
X_{TRT}	in.	Distance between center of gravity of trailer and tandem (Class IV)

<u>Symbol</u>	<u>Typical Units</u>	<u>Definition</u>
Y_0	in.	Vertical displacement of main body (Class I and III)
Y_{01}	in.	Vertical displacement of cab
Y_{02}	in.	Vertical displacement of trailer
Y_{1R} , Y_{1L}	in.	Vertical displacement of right and left sides of axle 1
Y_{2R} , Y_{2L}	in.	Vertical displacement of right and left sides of axle 2
Y_{23R} , Y_{23L}	in.	Vertical displacement of right and left sides of first tandem (Class V)
Y_{45R} , Y_{45L}	in.	Vertical displacement of right and left sides of second tandem (Class V)
Y_{34R} , Y_{34L}	in.	Vertical displacement of right and left sides of tandem axle (Class IV)
ϕ_X	radians	Angle of roll of main body (Class I and III)
ϕ_{X1}	radians	Angle of roll of cab
ϕ_{X2}	radians	Angle of roll of trailer
ϕ_Z	radians	Angle of pitch of main body (Class I and III)
ϕ_{Z1}	radians	Angle of pitch of cab
ϕ_{Z2}	radians	Angle of pitch of trailer
θ_{ZR}	radians	Angle of pitch of right tandem axle (Class III and IV)
θ_{ZL}	radians	Angle of pitch of left tandem axle (Class III and IV)
θ_{Z1R}	radians	Angle of pitch of first right tandem axle (Class V)
θ_{Z1L}	radians	Angle of pitch of first left tandem axle (Class V)

<u>Symbol</u>	<u>Typical Units</u>	<u>Definition</u>
θ_{Z2R}	radians	Angle of pitch of second right tandem axle (Class V)
θ_{Z2L}	radians	Angle of pitch of second left tandem axle (Class V)

CHAPTER 1. INTRODUCTION

In the past two decades, motor vehicle traffic on the streets and highways of America has increased rapidly. Engineers are continually searching for improved methods of designing highway structures which will carry larger and heavier vehicles without experiencing premature failure.

The moving wheels of highway vehicles subject pavements and bridges to dynamic wheel loads which vary considerably from the static wheel weights that are normally used as the basis for structural design. In recognition of the need for a better understanding of the relationship between static wheel weight and dynamic wheel force, this research study was initiated in 1967.

Recent advances in instrumentation technology and in data processing now make it feasible to measure accurately the forces applied to the road surface by the wheels of moving vehicles. Likewise, numerical modeling techniques utilizing the power of modern digital computers facilitate the interpretation and generalization of experimental data.

These new tools are combined in this research study. Mathematical models of five representative classes of highway vehicles are developed and used to predict the magnitude and position of dynamic wheel forces which result from the movement of a particular type of vehicle along a defined road profile. Wheel forces and profiles measured in field experiments are then used to validate the series of models.

Information developed in this study provides highway design engineers with a better understanding of the nature of dynamic loading. By combining these more realistic structural loading conditions with an accurate analysis of the behavior of construction materials under dynamic loads, design procedures which will result in safer, more efficient, and more economical pavements and bridges can be developed.

The Problem

Transportation facilities such as highway pavements and bridges are designed to carry vehicular traffic safely and conveniently for several years

with minimum maintenance and reconstruction costs. Currently accepted procedures for designing these structures attempt to balance the strength of construction materials as determined by static testing with the static loads that will be applied by anticipated traffic.

In reality, highway structures during their design life are subjected to a few applications of static forces, but normally they are subjected to millions of repetitions of dynamic forces that vary in magnitude, duration, and frequency. This fact has long been recognized by highway engineers and by agencies responsible for setting design standards. But because of the complex nature of the dynamic forces and the lack of an adequate understanding of the response of highway structures to dynamic loads, static forces rather than dynamic forces have been used as loading criteria in design. Some efforts at accounting for dynamic loading effects have involved the application of traffic factors or impact factors (Ref 41). Such improvements to present design methods are temporary measures, and the need for methods which realistically account for many complex factors including the effects of dynamic loading by mixed traffic still exists.

Such a need was emphasized rather dramatically by the results of the AASHO Road Test, a full-scale pavement research study which was conducted near Ottawa, Illinois between 1958 and 1960 (Ref 42). After the conclusion of the AASHO Road Test, several research programs, in the form of satellite studies, were initiated for the purpose of studying the effects of dynamic loading on highway structures. One such study was conducted at the University of Illinois and involved further investigation, analysis, and interpretation of dynamic test data from the bridge studies at the Road Test. In this research (Ref 15), strains produced in different types of test bridges by stationary and by moving vehicles served as the basis for evaluating bridge characteristics such as stiffness and lateral distribution of applied loads. Observed strains were compared with strains predicted from theory. Excellent agreement was found between the experimental and the theoretical strains in cases where loading parameters and structural properties of the bridge elements were well defined, but even under the controlled traffic used at the AASHO Road Test, dynamic loads applied to the bridges by moving vehicles were not characterized precisely.

Other research efforts have been directed towards studying the response of highway structures to varying deterministic dynamic loads (Refs 40 and 49)

or to varying assumed loads which are stochastic in nature and magnitude (Refs 14 and 45). Several investigators have resorted to the use of mathematical models to represent vehicle suspension systems (Refs 2, 4, 8, 11, 16, 22, 44, and 49) in studying the effects of the different vehicle characteristics on dynamic forces and on vehicle-road interaction. In most of these investigations, little emphasis has been placed on evaluating the accuracy with which the predicted or the estimated dynamic forces represent, whether in magnitude or in characteristics, the real loads applied to the road by moving traffic.

Advances in electronic data processing now facilitate mathematical modeling. Parameters included in the model can be varied over wide ranges and the results can be evaluated immediately. Before a mathematical model can be used confidently to represent actual field conditions, however, it must be validated by comparing predicted results with observed results. Recent investigations have recognized this fact. In these investigations, dynamic wheel forces have been predicted theoretically by computer simulation and then compared with forces measured experimentally by on-board measuring devices (Ref 21) or by dynamic scales embedded in the pavement surface (Refs 17, 33, and 34). Results of these studies have led to a better definition of the factors which influence dynamic wheel loads, but no general technique for predicting the magnitude of these forces has been developed.

The need for a better understanding of the nature of dynamic loading on highway structures still remains. Techniques for predicting dynamic wheel forces from easily measured or estimated vehicle and roadway characteristics are needed before highway structural designers can incorporate realistic loading parameters into design procedures.

Objectives

The purpose of this research investigation was to accomplish the following objectives:

- (1) Develop a generalized mathematical model, or a series of models, which describes the dynamic behavior governing the magnitude and variation of dynamic wheel loads applied normal to the roadway surface by the wheels of the several classes of vehicles that represent mixed commercial highway traffic.
- (2) Prepare and document a digital computer program that solves the differential equations of motion used in the mathematical model for predicting dynamic wheel loads. Provision should be made in the

program for using either a generated artificial profile or a natural road profile, which can be recorded by a profilometer, to represent the surface over which the wheels move.

- (3) Design, construct, assemble, and test a portable electronic data collection system capable of sampling the forces applied normal to the roadway surface by the wheels of vehicles moving at speeds up to 70 miles per hour at 12 selected locations in a traffic lane. This system will produce on magnetic tape an analog record which may be used to determine the magnitude of normal wheel forces in addition to vehicle speed, number of axles, axle spacing, and vehicle length. Significant data will then be displayed for visual evaluation, or it will be converted to digital form for electronic processing, tabulation, and analysis.
- (4) Measure and record the wheel forces applied to a pavement surface by representative classes of vehicles running at different speeds and under different loading conditions. Various patterns of artificial pavement roughness in the form of step-bump obstructions will be used.
- (5) Measure and record the wheel forces applied to a relatively smooth pavement by a sample of mixed commercial traffic moving at normal and at maximum highway speeds.
- (6) Analyze the characteristics of dynamic loads applied to highway structures and attempt to define and characterize the significant factors which influence the magnitude and variation of these loads.
- (7) Compare the predicted dynamic forces with the measured dynamic forces.
- (8) Attempt to define the relationship between the static wheel loads and the dynamic wheel loads for various classes of vehicular traffic and roadway conditions.

The research program was divided into two phases: (1) the theoretical phase which involved the development of the mathematical model and preparation of the computer program (objectives 1 and 2), and (2) the experimental phase which involved the design of the data collection system and the measurement of wheel loads (objectives 3, 4, and 5). A schematic representation of the approach to this investigation is shown in Fig 1.

Scope and Limitations

The accomplishment of some of the objectives cited above has been limited by practical, economical, and time factors. Consequently, only five representative classes of vehicles have been used in this investigation. The series of field tests were conducted at a location on Interstate Highway I-35 near

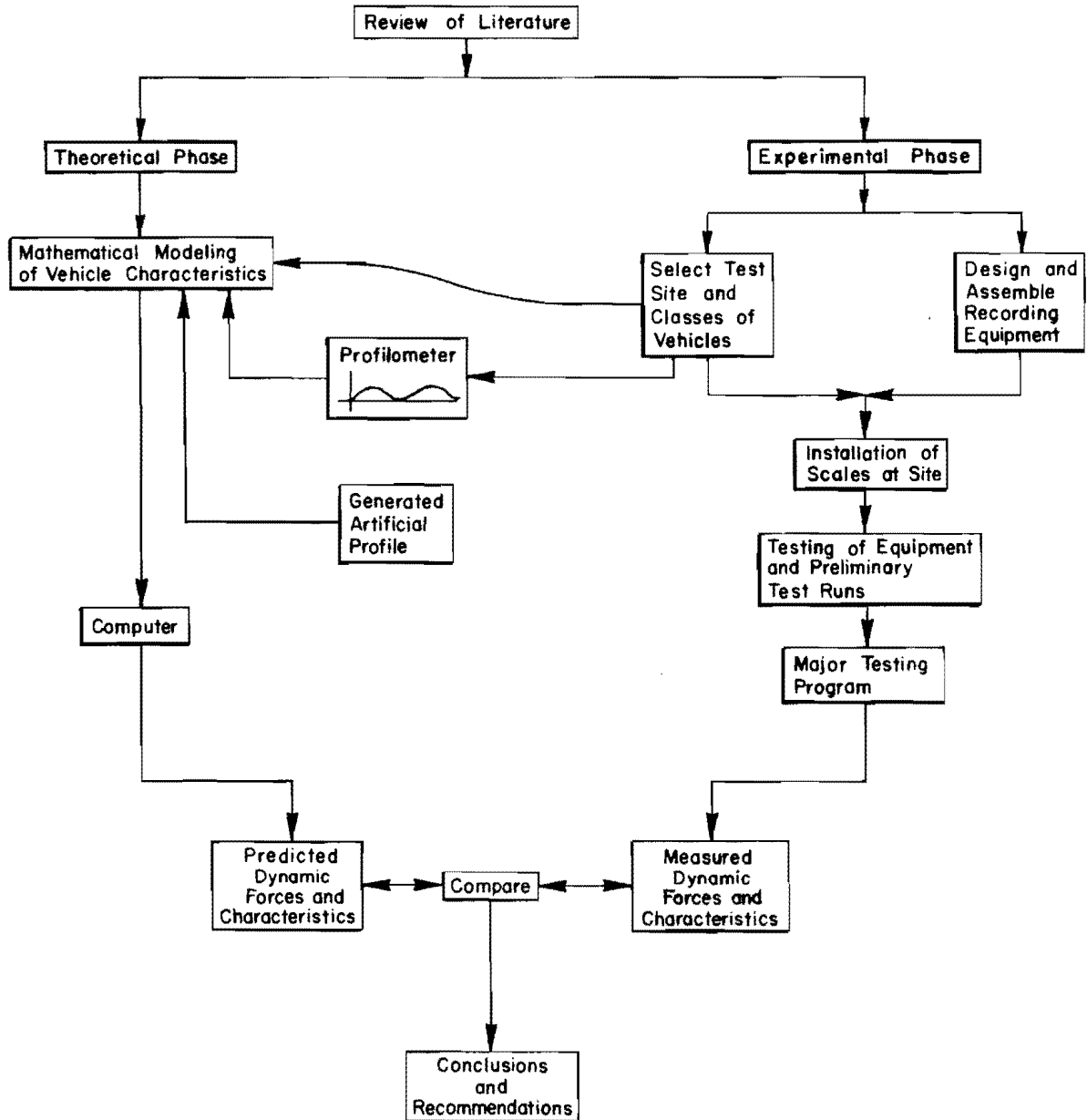


Fig 1. Schematic representation of the approach to the research program.

Austin, Texas according to a statistically designed experiment. Before selecting the five classes of test vehicles, a classification survey of approximately 1,400 commercial vehicles was conducted at the test site over a period of about 80 consecutive hours. This survey and the different classes of vehicles selected are discussed later in this report.

CHAPTER 2. FACTORS AFFECTING DYNAMIC LOADS

General

The forces produced on the roadway surface by the wheels of a moving vehicle vary continuously with time in an extremely complex fashion. An exact and complete description of this variation is a very difficult, if not impossible, task. Investigators with a wide range of interests have dealt with the problem. Mechanical engineers, on one hand, have approached the problem for the purpose of improving the riding comfort and handling characteristics of vehicles (Refs 2, 4, 5, 22, and 29). On the other hand, highway and transportation engineers have approached the problem from the standpoint of evaluating the destructive effects of dynamic wheel loads on pavements and bridges. The purpose of this chapter is to examine briefly some of the factors that make dynamic wheel loads different from static wheel loads.

In general, the problem of "road loading mechanics" involves a system in which the vehicle interacts with the roadway surface. Consequently, the factors that contribute to the generated dynamic forces may be classified into vehicular factors and roadway factors. Each of these classes is influenced by prevailing ambient conditions such as wind gusts and other climatic conditions. The vehicle-road system is shown schematically in Fig 2.

Vehicle Factors

There are several elements in the makeup of the vehicle that influence either directly or indirectly the magnitude and the frequency of dynamic wheel loads. It must be emphasized, however, that it is the overall interaction of these elements that influences the dynamic behavior of the vehicle. Thus, in discussing the influence of any particular element, its bearing or interaction with other elements or factors must also be discussed at the same time.

Vehicle Type. The classification of a vehicle, or its type, is generally determined by the number of axles, the axle arrangement and proximity, and by its size and weight.

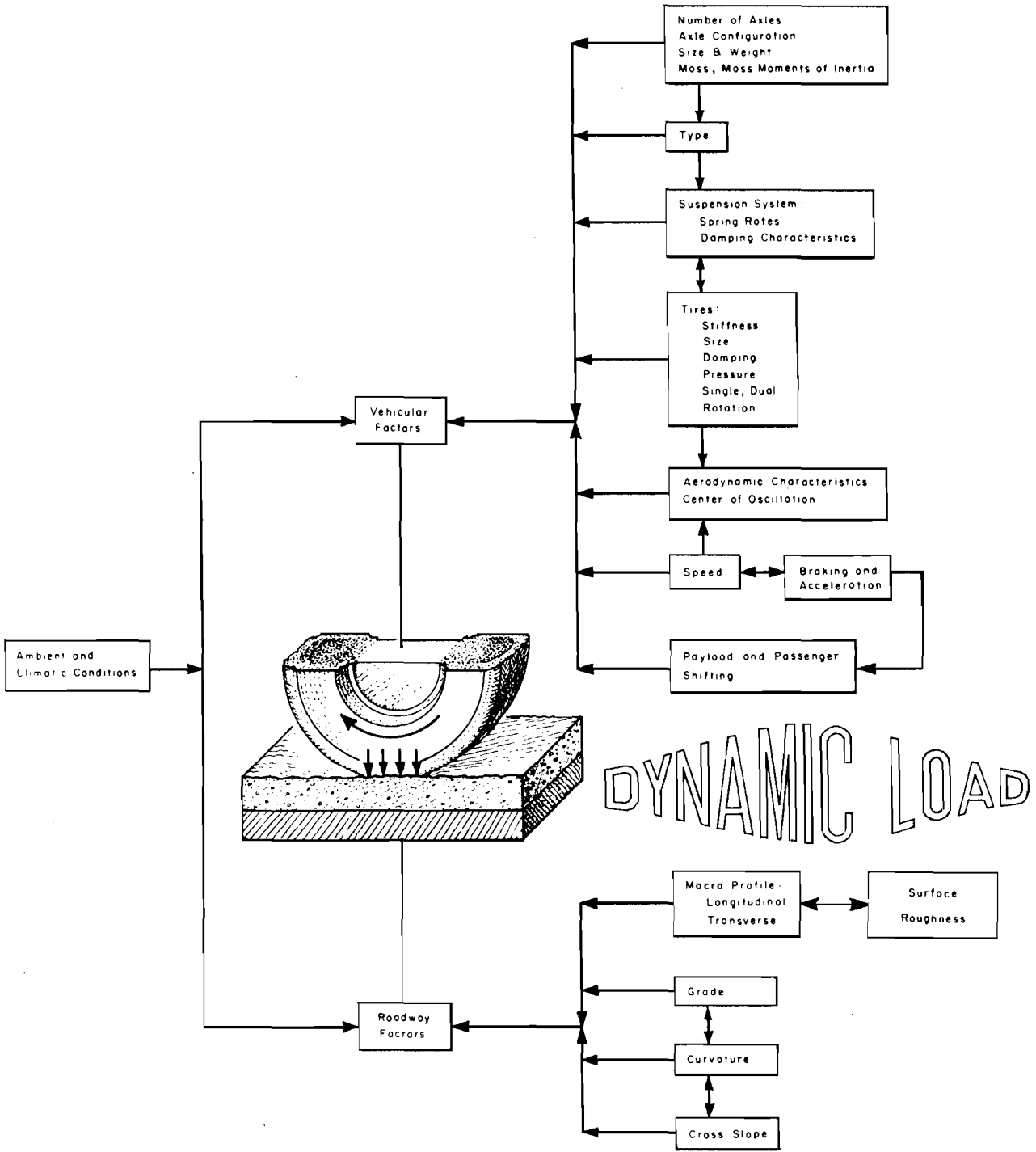


Fig 2. Vehicle-road system.

Therefore, vehicle type is considered to be one of the major factors that influences the magnitudes and distribution of dynamic wheel loads. An investigation of the dynamic loads produced by heavy highway vehicles was conducted by General Motors Corporation (Ref 21) and revealed some of these effects. Three types of vehicles were used. First, the forces produced by the rear axle of a two-axle single unit (2-D) truck were measured. Second, the forces produced by the forward axle of the tandem drive on a five-axle truck-trailer combination (3S-2) were measured. Third, the forces produced by the trailer axle of a four-axle truck-trailer combination (3S-1) were measured. The results of the investigation indicated that the amplitudes and frequencies of dynamic forces varied differently for each type. Other investigations (Ref 15) have shown that the variations in the dynamic forces were greater for two-axle vehicles than for three-axle truck-trailer vehicles. This difference was attributed to the coupling between the truck and the trailer.

Suspension System. The dynamic wheel forces exerted on the roadway surface are dependent on the characteristics of the suspension system of the vehicle. Most commercial vehicles use leaf spring suspensions joining the body mass and the unsprung mass that includes the axles, wheels, tires, and brakes. Other vehicles have different types of suspension systems such as air, coil springs, or other special purpose systems. The studies of bridges on the AASHO Road Test conducted at the University of Illinois and noted earlier in the preceding chapter (Ref 15) revealed that locking the springs of the test vehicles increased the dynamic forces by as much as a factor of three depending on the vehicle type.

Tires. The combined weight of the vehicle body, the frame, the suspension system, and the pay load is carried by the tires. The tires in turn transmit the load to the pavement surface as a constant force when the vehicle is stopped or as a varying dynamic force when the vehicle is moving. Perhaps the most important tire characteristics which influence the dynamic force are inflation pressure, stiffness, and speed of rotation. The inflation pressure and stiffness determine the deflection of the tire and consequently the magnitude of the dynamic load. Generally, variations in the tire pressure influence the frequencies of dynamic wheel loads, with lower pressures tending to decrease these frequencies (Ref 34). In addition, previous work has shown that the magnitudes of the dynamic forces increase with increased tire pressure (Ref 21). Finally, considerable variation in the magnitudes of the

wheel loads has been shown to occur with different rotation speeds of the wheel due to nonuniformity and unbalance (Ref 21).

Wind Effects. Wind gusts act on a vehicle in several ways. First, uplift effects on the body of the vehicle may result. Second, in the case of cross winds, additional roll (rotation around a longitudinal axis) of the vehicle body may take place. Third, head or tail winds may cause added pitching effects (rotation around the lateral axis). Regardless of the kind of wind that acts on a moving vehicle, it influences the dynamic behavior of the vehicle. However, consideration of wind effects is beyond the scope of this report.

Speed. Most investigators concur in concluding that the magnitudes of dynamic loads increase with increasing speeds (Refs 15, 21, and 34), possibly because high speeds increase the frequency of excitation. In addition, high vehicle speeds increase the oscillations produced by any unbalance that exists in the tires of the vehicle, due to increased wheel rotation speed as noted above. The variation of the dynamic forces with speed, however, depends largely on the type of vehicle. This has been discussed earlier in this section. Finally, it must be emphasized that while speed has an effect on the magnitude of the dynamic forces, it has little or no effect on the natural frequency of the vehicle (Ref 34).

Roadway Factors

The pavement structure with its surface profile and subsurface layers is the second major component of the system involved in road loading mechanics. Extensive investigations of the pavement structure conducted in the past fifteen years have provided highway engineers with an improved understanding of the factors involved in the performance of pavement structures under the action of repeated dynamic loads. This was one of the primary objectives of the AASHO Road Test in which approximately 800 pavement sections were subjected to more than 1,100,000 repetitions of dynamic load (Ref 42). Static or dynamic wheel loads applied at the pavement surface are carried either by beam action, in the case of rigid pavements, or by load transfer through successive layers with varying strengths in the case of flexible pavements. Excessive magnitudes or high repetition of these loads combine with such climatic

conditions as volume changes due to variations in moisture and frost heaving to cause failures in the pavement surface or in the underlying layers. These failures are eventually reflected in surface unevenness or distress. Among other roadway factors, this distress has an effect on the magnitude and frequency of the dynamic wheel loads, and therefore, will be discussed briefly.

Road Profile and Surface Roughness. Theoretically a vehicle traveling on a perfectly smooth and horizontal surface produces constant dynamic wheel forces which are equal to the static wheel forces assuming no tire unbalance. In reality, however, a road of this type is nonexistent because it is economically not feasible and practically not safe. Therefore, every roadway surface has definite profile characteristics and a varying degree of roughness depending on the type of material and the construction method used.

The general profile of a roadway surface may be described for two directions: longitudinal and transverse. Both the transverse and the longitudinal profiles of a roadway surface contribute to the excitation of the vehicle and are mainly responsible for generating dynamic wheel forces. Any form of surface distress including cracking, spalling, rutting, faulting, raveling, plastic deformation, stripping, and degradation of aggregates, or any disintegration of the structural materials resulting from effects of either dynamic loading, subsurface failures, or environmental and climatic conditions helps determine the surface profile and therefore influences the magnitudes of the dynamic wheel loads.

Grade. Although the effect of grade on the dynamic behavior of a vehicle is still a subject that needs investigation, it is expected that load transfer from one axle to the other may vary with acceleration, deceleration, braking, and other operating characteristics of a vehicle. These characteristics, especially in the case of commercial vehicles, are influenced by the grade. Roadway grades vary from 0 to 20 percent.

This page replaces an intentionally blank page in the original.

-- CTR Library Digitization Team

CHAPTER 3. THEORY OF VEHICLE DYNAMICS

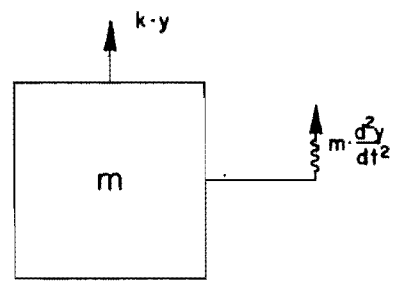
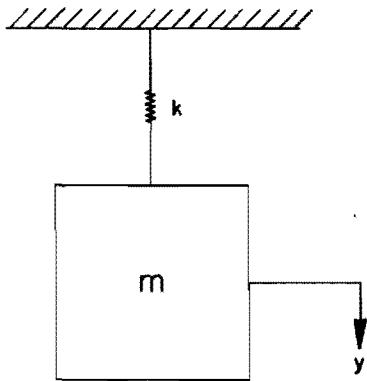
General

The purpose of this chapter is to review the theory of vibration and some of the laws of mechanics which govern vehicle dynamics. This brief review will be helpful in developing and evaluating the mathematical model presented in Chapter 4. The review considers a single degree of freedom system and then, briefly, systems with two or more degrees of freedom. Finally, a discussion of vehicle suspension systems is presented before the generalized vehicle model is developed.

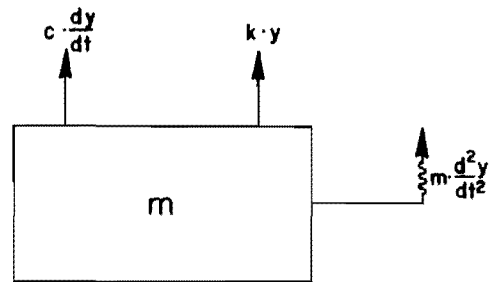
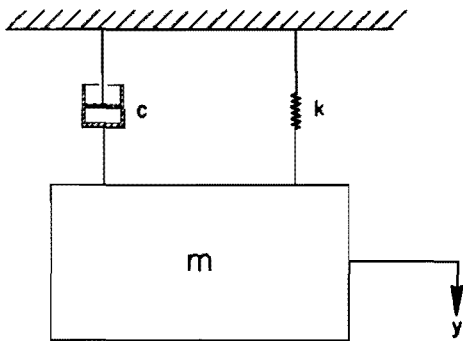
Systems with One Degree of Freedom. An example of a model of a system with one degree of freedom is shown in Fig 3(a). The system consists of a mass suspended by a massless linear spring. An exchange of energy takes place between the mass and the spring during vibration; potential energy in the spring is converted to kinetic energy of the mass. In the absence of damping or energy dissipation, the total energy of the system remains constant and the system is said to be conservative. As the system vibrates, the position of the mass is determined by the parameter y which is a function of time. The free body diagram shows the system in dynamic equilibrium with two forces acting on it: (1) the spring force, equal to the spring rate times the extension and (2) the inertia force, equal to the mass times the acceleration and acting in a direction opposite to the acceleration. The equation of motion readily follows as

$$m \frac{d^2 y}{dt^2} + k y = 0 \quad (3.1)$$

The solution of this equation shows (Refs 7, 13, 43, and 47) that the motion of the system is harmonic with a natural circular frequency that is a function of only the physical constants of the system (k and m),

ModelFree Body Diagram

(a) No damping.



(b) With damping.

Fig 3. System with one degree of freedom.

regardless of the amplitude of motion. The natural frequency of this system (ω_o) is found to be

$$\omega_o = \sqrt{\frac{k}{m}} \text{ rad/sec} \quad (3.2)$$

The frequency (f_o) and the period (T) of motion are

$$\begin{aligned} f_o &= \frac{\omega_o}{2\pi} \text{ Hz} \\ &= \frac{1}{2\pi} \sqrt{\frac{k}{m}} \end{aligned} \quad (3.3)$$

$$\begin{aligned} T &= \frac{1}{f_o} \text{ sec} \\ &= 2\pi \sqrt{\frac{m}{k}} \end{aligned} \quad (3.4)$$

A SDF system which includes the effects of viscous damping is shown in Fig 3b. The equation of motion of this system is

$$m \frac{d^2 y}{dt^2} + c \frac{dy}{dt} + k y = 0 \quad (3.5)$$

where

$$c = \text{damping rate (lb/in/sec)}$$

Systems with Multiple Degrees of Freedom. The analysis of mechanical systems with two or more degrees of freedom is discussed briefly in this section. As in the preceding section, the discussion will be confined to the development of equations of motion.

In the case of free vibration of a single degree of freedom system the motion is harmonic with one natural frequency; the vibration of a system

having several degrees of freedom is generally not harmonic (Refs 13 and 47). Instead, it is the result of a combination of several harmonic motions having different natural or characteristic frequencies. In the multiple degree of freedom case, the number of natural frequencies is equal to the number of degrees of freedom.

The hypothetical system shown in Fig 4 has two degrees of freedom: (1) the system can translate in the vertical direction and (2) it can rotate in the plane of the figure (pitch motion). Two equations of motion are required to determine the position of the system at any instant.

From a summation of vertical forces:

$$m \frac{d^2 y}{dt^2} + F_{s1} + F_{c1} + F_{s2} + F_{c2} = 0 \quad (3.6)$$

where

$$\begin{aligned} F_{s1} &= k_1 (y + X_1 \theta) , \\ F_{c1} &= c_1 \left(\frac{dy}{dt} + X_1 \frac{d\theta}{dt} \right) , \\ F_{s2} &= k_2 (y - X_2 \theta) , \\ F_{c2} &= c_2 \left(\frac{dy}{dt} - X_2 \frac{d\theta}{dt} \right) \end{aligned}$$

The magnitude of θ is assumed to be small.

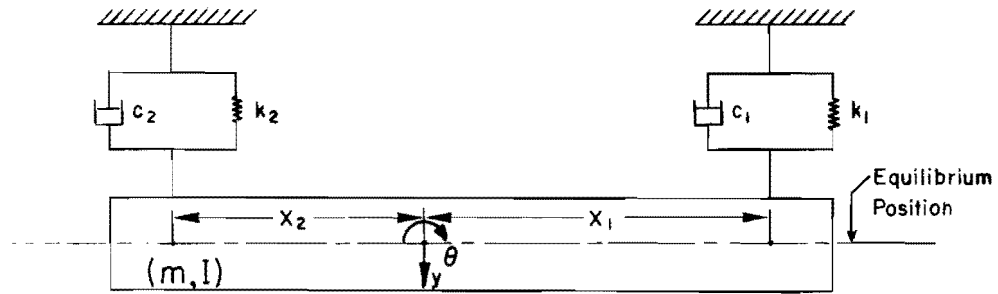
From a summation of moments about the mass center

$$I \frac{d^2 \theta}{dt^2} + (F_{c1} + F_{s1})X_1 - (F_{c2} + F_{s2})X_2 = 0 \quad (3.7)$$

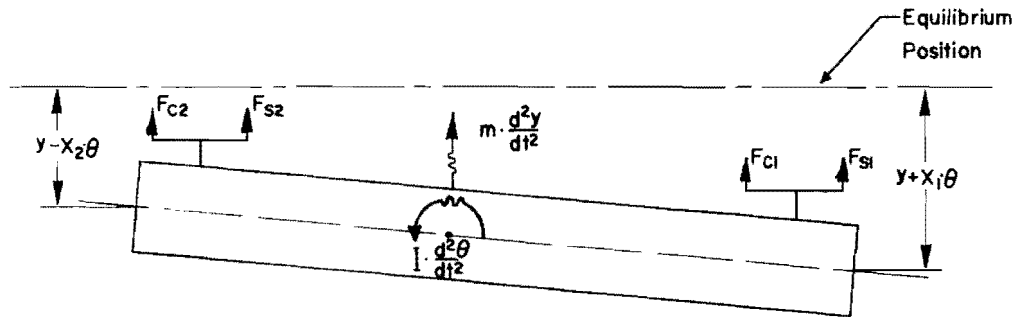
where

I = mass moment of inertia about the mass center.

When the expressions for F_{c1} , F_{s1} , F_{c2} , and F_{s2} are substituted, Eqs 3.6 and 3.7 become



(a) Model.



(b) Free body diagram.

Fig 4. System with two degrees of freedom.

$$\begin{aligned}
m \frac{d^2 y}{dt^2} + (c_1 + c_2) \frac{dy}{dt} + (k_1 + k_2)y + (k_1 X_1 - k_2 X_2)\theta \\
+ (c_1 X_1 - c_2 X_2) \frac{d\theta}{dt} = 0
\end{aligned} \tag{3.6a}$$

$$\begin{aligned}
I \frac{d^2 \theta}{dt^2} + (c_1 X_1 - c_2 X_2) \frac{dy}{dt} + (k_1 X_1 - k_2 X_2)y + (k_1 X_1^2 + k_2 X_2^2)\theta \\
+ (c_1 X_1^2 + c_2 X_2^2) \frac{d\theta}{dt} = 0
\end{aligned} \tag{3.7a}$$

When Eqs 3.6(a) and 3.7(a) are solved, the first and second natural frequencies can be determined.

Vehicle Suspension System

The basic principles involved in the analysis of systems with one or more degrees of freedom apply in the case of vehicle suspension systems. Generally, the vehicle is considered to be a damped system with several degrees of freedom. In its simplest representation, the vehicle suspension system consists of a mass resting on an elastic spring attached to a rigid wheel and has one degree of freedom (Refs 7 and 47). This model is shown in Fig 5. If the total static deflection of the spring under the action of the supported mass is d , then the spring stiffness K_s is

$$K_s = \frac{mg}{d}$$

According to Eq 3.3 the frequency of oscillation is given by

$$f_o = \frac{1}{2\pi} \sqrt{\frac{K_s}{m}}$$

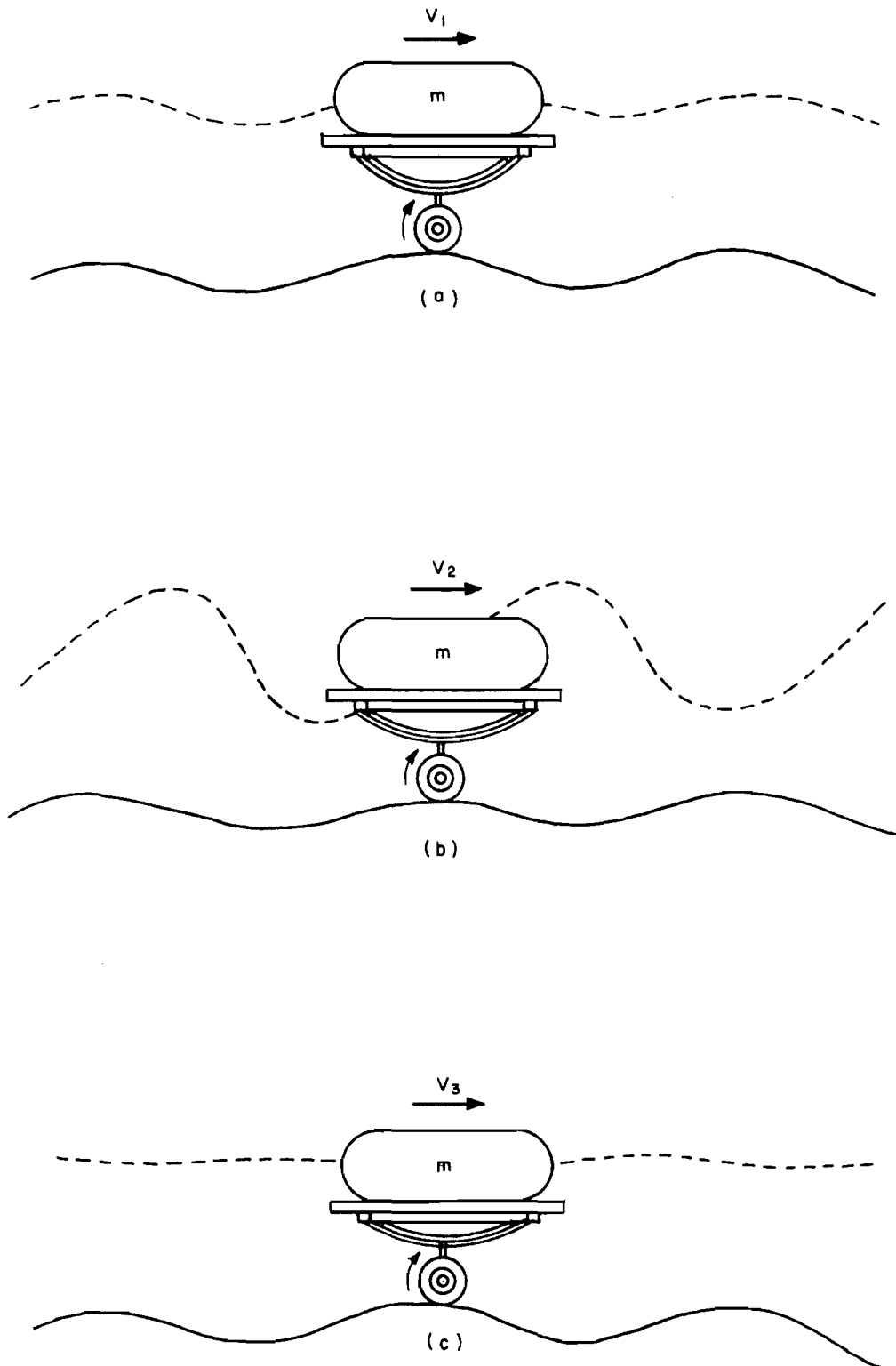


Fig 5. Simple moving vehicle suspension.

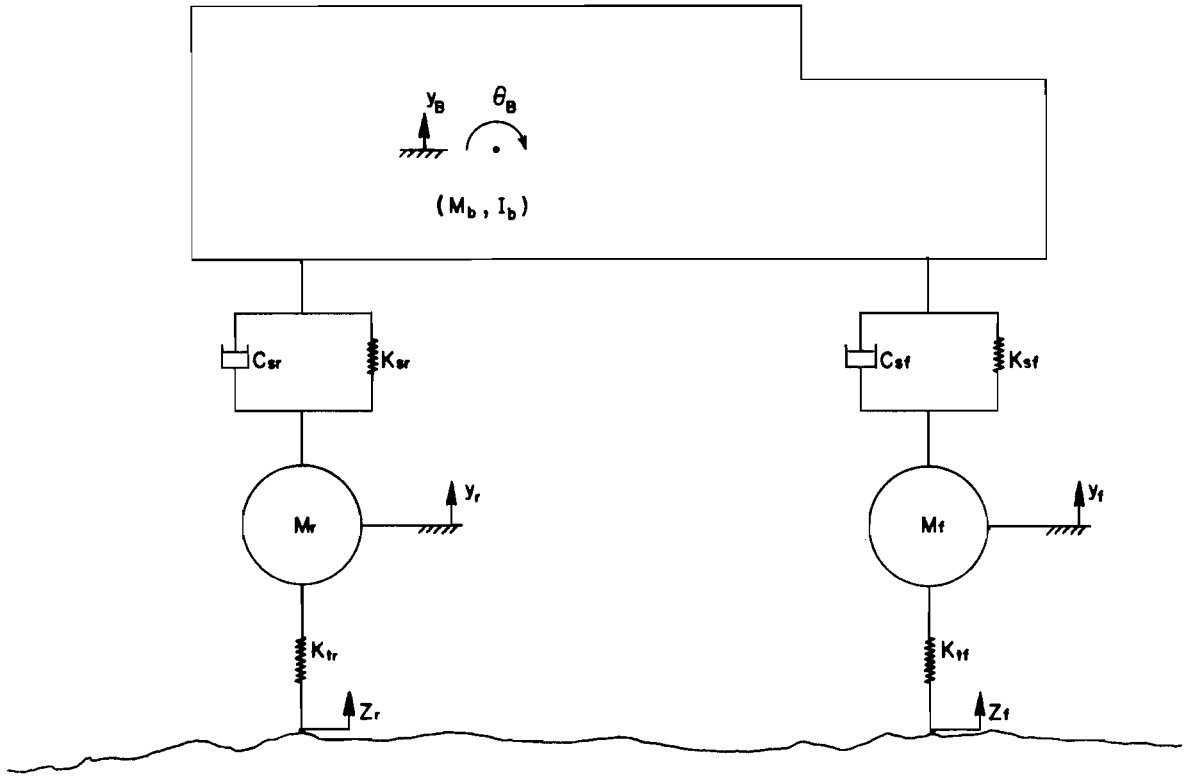
This reduces to

$$f_o = \frac{1}{2\pi} \sqrt{\frac{g}{d}} \quad (3.8)$$

A possible response of a system of this type to an undulating roadway profile at a low velocity V_1 is shown in Fig 5(a). At a higher speed V_2 the frequency of excitation increases. When this frequency coincides with the natural frequency of the system given by Eq 3.8, resonance is reached and the amplitude of vibration reaches a maximum. Damping is necessary in this situation to prevent any possible damage to the spring (Ref 7).

Theoretically (Ref 7), as speed increases beyond the critical speed corresponding to resonance, the vibration of the mass subsides with the path described by the mass becoming approximately smooth at higher speeds.

This simplified system does not realistically account for all the variables involved in the vehicle suspension system. The mass of the main body of the vehicle and its payload should be separated from the mass of the axles and wheels since each can vibrate independently. In addition, the deflection of the tires should be accounted for in the mathematical model. The literature is rich in mathematical models of vehicle suspension systems (Refs 2, 4, 5, 8, 16, 22, 29, 35, 38, 40, and 49). The majority of these models, however, assume that the two sides of the vehicle are symmetrical and consider only one of these sides. This is certainly a valid assumption, in many cases, but with such a model it is not possible to study the rolling (rotation about longitudinal axis) of the vehicle and its significance on the dynamic loads. A typical model of a vehicle, the half-vehicle model, which is most commonly used is shown in Fig 6. This model has four degrees of freedom as follows: (1) vertical translation of the front axle, (2) vertical translation of the rear axle, (3) vertical translation of the main body, and (4) rotation or pitching of the main body. Usually the tire elastic action is represented by a single spring since damping is negligible in the majority of cases (Refs 2, 4, 8, 16, 40, and 45). The procedure followed in writing the four equations of motion is similar to that described in the preceding section and therefore will not be repeated.



Mass System	Degrees of Freedom	System Constants	Variables
Front Axle	1	M_f	y_f
Rear Axle	1	M_r	y_r
Main Body	2	M_b, I_b	y_b, θ_b

Fig 6. Typical half-vehicle model.

This page replaces an intentionally blank page in the original.

-- CTR Library Digitization Team

CHAPTER 4. GENERALIZED MODEL DEVELOPMENT

The need for developing a generalized model, or a system of models, that simulates different classes of vehicles representing a wide spectrum of commercial vehicles is evident. Such a model may find several uses besides predicting the dynamic loads and studying the dynamic behavior of these classes of vehicles under variable roadway and vehicular input. For example, the model may be used to generate various types of dynamic load for investigations in the area of structural behavior of pavement slabs or bridges.

Preliminary Considerations

The elements of the vehicle suspension system which are of interest in developing a vehicle model are the main body, which is assumed to be rigid; the springs; the shock absorbers; the axle assembly which includes brakes, wheels, and steering mechanism; and finally the tires. These elements may be combined to allow a conventional two-axle vehicle (class 2-D) to be represented as three distinct masses: (1) the main body, (2) the front axle, and (3) the rear axle.

The main body of the vehicle rests on the two axles through four springs, which may be of different types, and a shock absorber is connected in parallel with each spring. The two axles in turn rest on at least four tires which may be simulated by springs and dashpots.

When this system of masses, springs, and dashpots is excited, it vibrates in an extremely complicated manner. For example the main body can undergo three independent translational movements and three independent rotations. Therefore, the two-axle-vehicle suspension system with its three main masses (body and two axles) has a total of 18 degrees of freedom. Exact description of vehicle position at an instant of time with respect to all of these movements is time-wise a prohibitive process and leads to very long and complex equations of motion. In order to facilitate the development of these equations, certain simplifying assumptions can be made. It can be noticed, for example, that several of these motions are rather insignificant as far as the analysis

is concerned and can thus be neglected in favor of the following important motions (Ref 13): (1) vertical translation of the main body, (2) main body pitching, (3) main body rolling, (4) vertical translation of the front axle, (5) vertical translation of the rear axle, (6) rolling of the front axle, and (7) rolling of the rear axle. The last four motions of the axles may be accounted for, by considering vertical translation of each of the individual tires.

Selection of Vehicle Types

A traffic classification survey conducted for the purpose of selecting the most common classes of vehicles to be included in this generalized model will be discussed later in this report under the discussion of the experimental phase of this research investigation. The five classes of vehicles chosen are shown in Fig 7 for convenience.

Equations of Motion

The different elements of the vehicle suspension system discussed above are taken into account in the mathematical representation or modeling of each vehicle. In this section, the differential equations of motion for each individual class are derived. A complete list of the notations used with associated definitions is included at the beginning of this report.

Class I. Elements of the mathematical model describing this class of vehicle (2-D), two-axle single unit, are represented in Fig 8. The total number of degrees of freedom is seven; these are summarized in Table 1.

In an attempt to simplify the derivation of expressions for the differential equations of motion, the movements of the main body are analyzed separately as described in Fig 9. The four sides of the main body are shown in this figure and the translation of the four corners due to each of these movements is determined. The combined translation due to all three independent movements are designated by: D_{1R} , for the right front corner; D_{1L} , for the left front corner; D_{2R} , for the right rear corner; and D_{2L} , for the left rear corner. The resulting expressions for these combined translations are:

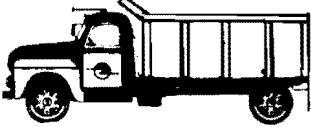
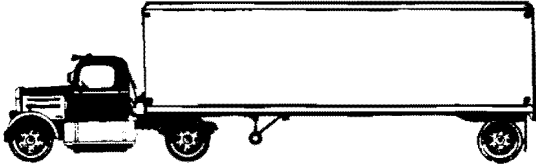
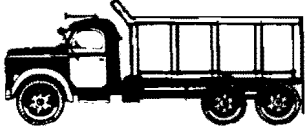

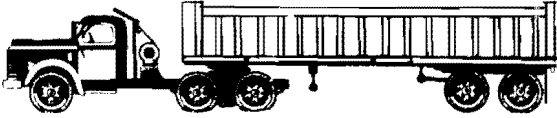
	Class	Designation
	I	2-D
	II	2S-1
	III	3-A
	IV	2S-2
	V	3S-2

Fig 7. Selected classes of vehicles.

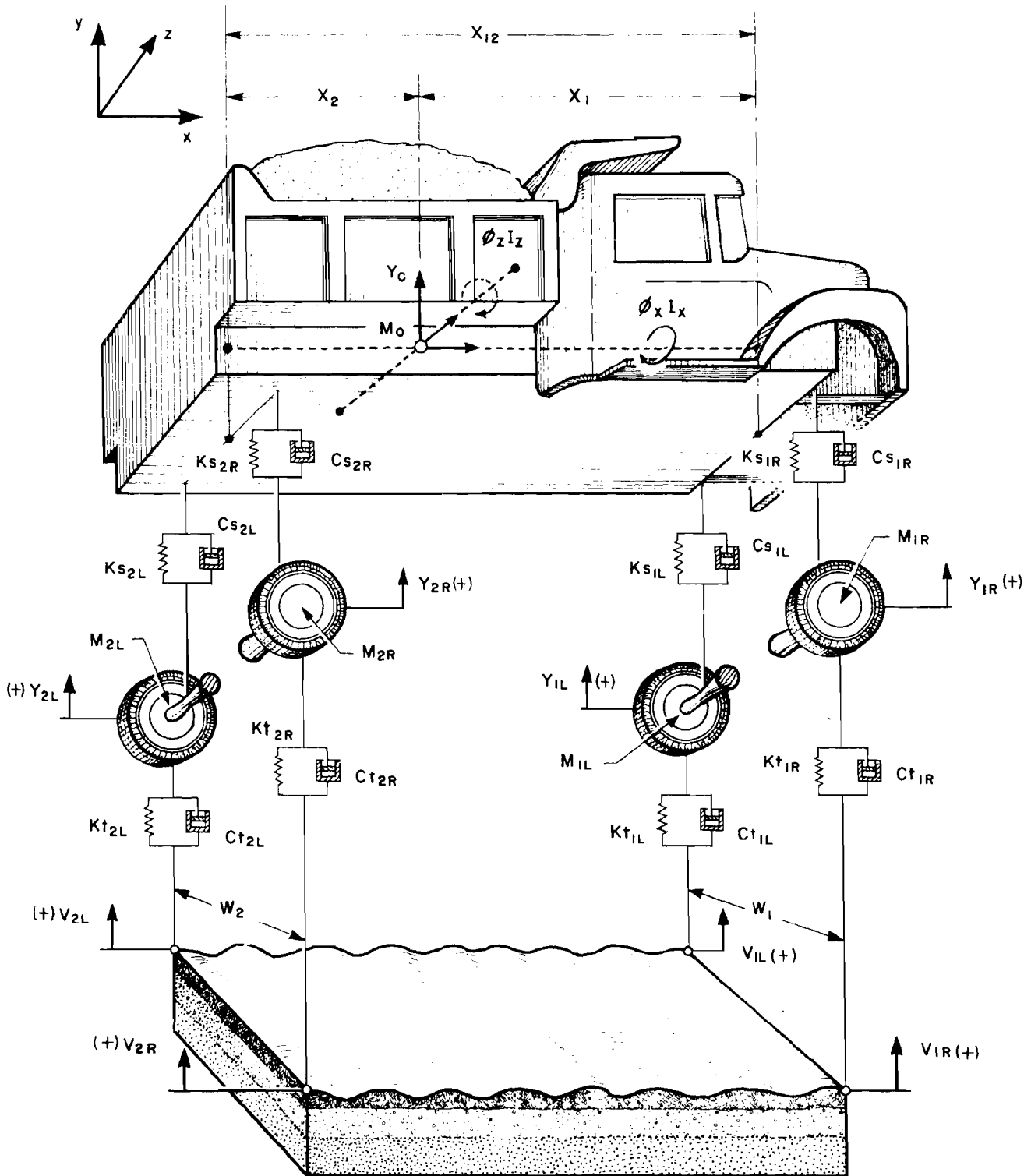


Fig 8. Class I vehicle model.

TABLE 1. CLASS I SUMMARY

Degree of Freedom	Mass System	Variables	Differential Eq of Motion
1. Vertical Translation (V.T.)	M_0	Y_0	4.5
2. Rolling		ϕ_X	4.6
3. Pitching		ϕ_Z	4.7
4. V.T.	M_{1R}	Y_{1R}	4.8
5. V.T.	M_{1L}	Y_{1L}	4.9
6. V.T.	M_{2R}	Y_{2R}	4.10
7. V.T.	M_{2L}	Y_{2L}	4.11

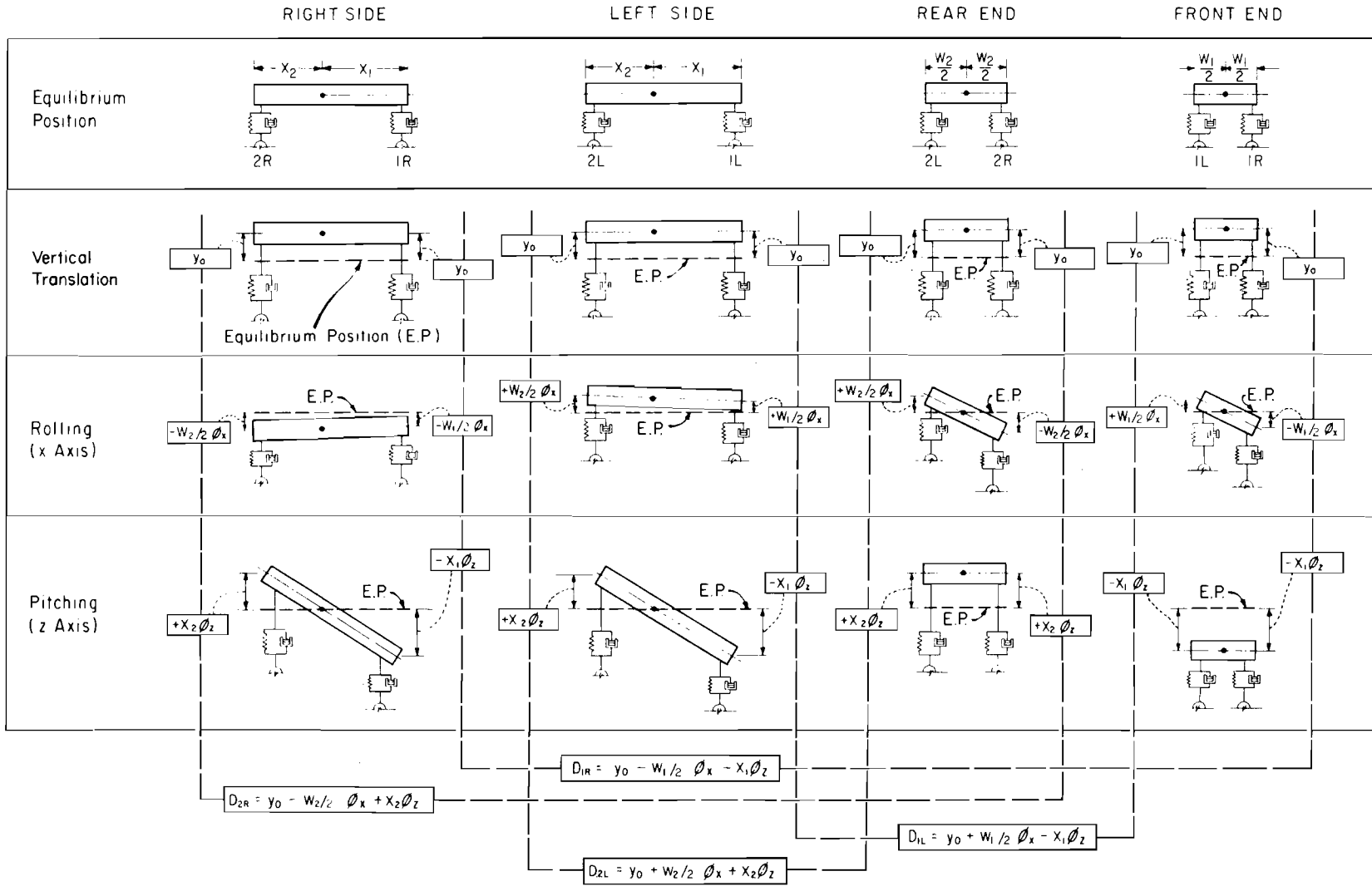


Fig 9. Main body motion analysis.

$$D_{1R} = Y_0 - \left(\frac{W_1}{2} \right) (\phi_X) - (X_1)(\phi_Z) \quad (4.1)$$

$$D_{1L} = Y_0 + \left(\frac{W_1}{2} \right) (\phi_X) - (X_1)(\phi_Z) \quad (4.2)$$

$$D_{2R} = Y_0 - \left(\frac{W_2}{2} \right) (\phi_X) + (X_2)(\phi_Z) \quad (4.3)$$

$$D_{2L} = Y_0 + \left(\frac{W_2}{2} \right) (\phi_X) + (X_2)(\phi_Z) \quad (4.4)$$

The required equations of motion are

$$\begin{aligned} & Ks_{1R}(D_{1R} - Y_{1R}) + Cs_{1R} \left(\frac{dD_{1R}}{dt} - \frac{dY_{1R}}{dt} \right) + Ks_{1L}(D_{1L} - Y_{1L}) \\ & + Cs_{1L} \left(\frac{dD_{1L}}{dt} - \frac{dY_{1L}}{dt} \right) + Ks_{2R}(D_{2R} - Y_{2R}) \\ & + Cs_{2R} \left(\frac{dD_{2R}}{dt} - \frac{dY_{2R}}{dt} \right) + Ks_{2L}(D_{2L} - Y_{2L}) \\ & + Cs_{2L} \left(\frac{dD_{2L}}{dt} - \frac{dY_{2L}}{dt} \right) + M_0 \frac{d^2 Y_0}{dt^2} = 0 \end{aligned} \quad (4.5)$$

$$\begin{aligned}
& \left(\frac{W_1}{2} \right) \left[K_{s1R} (D_{1R} - Y_{1R}) + C_{s1R} \left(\frac{dD_{1R}}{dt} - \frac{dY_{1R}}{dt} \right) - K_{s1L} (D_{1L} - Y_{1L}) \right. \\
& \quad \left. - C_{s1L} \left(\frac{dD_{1L}}{dt} - \frac{dY_{1L}}{dt} \right) \right] + \left(\frac{W_2}{2} \right) \left[K_{s2R} (D_{2R} - Y_{2R}) \right. \\
& \quad \left. + C_{s2R} \left(\frac{dD_{2R}}{dt} - \frac{dY_{2R}}{dt} \right) - K_{s2L} (D_{2L} - Y_{2L}) \right. \\
& \quad \left. - C_{s2L} \left(\frac{dD_{2L}}{dt} - \frac{dY_{2L}}{dt} \right) \right] - I_X \frac{d^2 \phi_X}{dt^2} = 0 \tag{4.6}
\end{aligned}$$

$$\begin{aligned}
& X_1 \left[K_{s1R} (D_{1R} - Y_{1R}) + C_{s1R} \left(\frac{dD_{1R}}{dt} - \frac{dY_{1R}}{dt} \right) + K_{s1L} (D_{1L} - Y_{1L}) \right. \\
& \quad \left. + C_{s1L} \left(\frac{dD_{1L}}{dt} - \frac{dY_{1L}}{dt} \right) \right] - X_2 \left[K_{s2R} (D_{2R} - Y_{2R}) \right. \\
& \quad \left. + C_{s2R} \left(\frac{dD_{2R}}{dt} - \frac{dY_{2R}}{dt} \right) + K_{s2L} (D_{2L} - Y_{2L}) \right. \\
& \quad \left. + C_{s2L} \left(\frac{dD_{2L}}{dt} - \frac{dY_{2L}}{dt} \right) \right] - I_Z \frac{d^2 \phi_Z}{dt^2} = 0 \tag{4.7}
\end{aligned}$$

$$\begin{aligned}
& K_{s1R} (D_{1R} - Y_{1R}) + C_{s1R} \left(\frac{dD_{1R}}{dt} - \frac{dY_{1R}}{dt} \right) - K_{t1R} (Y_{1R} - V_{1R}) \\
& \quad - C_{t1R} \left(\frac{dY_{1R}}{dt} - \frac{dV_{1R}}{dt} \right) - M_{1R} \frac{d^2 Y_{1R}}{dt^2} = 0 \tag{4.8}
\end{aligned}$$

$$K_{s1L} (D_{1L} - Y_{1L}) + C_{s1L} \left(\frac{dD_{1L}}{dt} - \frac{dY_{1L}}{dt} \right) - K_{t1L} (Y_{1L} - V_{1L})$$

$$Ct_{1L} \left(\frac{dY_{1L}}{dt} - \frac{dV_{1L}}{dt} \right) - M_{1L} \frac{d^2 Y_{1L}}{dt^2} = 0 \quad (4.9)$$

$$Ks_{2R}(D_{2R} - Y_{2R}) + Cs_{2R} \left(\frac{dD_{2R}}{dt} - \frac{dY_{2R}}{dt} \right) - Kt_{2R}(Y_{2R} - V_{2R}) \\ - Ct_{2R} \left(\frac{dY_{2R}}{dt} - \frac{dV_{2R}}{dt} \right) - M_{2R} \frac{d^2 Y_{2R}}{dt^2} = 0 \quad (4.10)$$

$$Ks_{2L}(D_{2L} - Y_{2L}) + Cs_{2L} \left(\frac{dD_{2L}}{dt} - \frac{dY_{2L}}{dt} \right) - Kt_{2L}(Y_{2L} - V_{2L}) \\ - Ct_{2L} \left(\frac{dY_{2L}}{dt} - \frac{dV_{2L}}{dt} \right) - M_{2L} \frac{d^2 Y_{2L}}{dt^2} = 0 \quad (4.11)$$

Class II. The model describing this vehicle type (2S-1), three-axle truck-trailer combination, is shown in Fig 10. Twelve degrees of freedom are considered to be significant (Table 2).

The differential equations of motion may again be simplified quite considerably by expressing the movements of the corners of the truck and of the trailer in the same manner used for Class I. The expressions for these movements are given in Eqs 4.12 through 4.17. In addition, the vertical movements of the truck and the trailer at their connection point, designated respectively by D_b and D_c are expressed by Eqs 4.18 and 4.19.

$$D_{1R} = Y_{01} - \left(\frac{W_1}{2} \right) (\phi_{X1}) - (X_{C1})(\phi_{Z1}) \quad (4.12)$$

$$D_{1L} = Y_{01} + \left(\frac{W_1}{2} \right) (\phi_{X1}) - (X_{C1})(\phi_{Z1}) \quad (4.13)$$

$$D_{2R} = Y_{01} - \left(\frac{W_2}{2} \right) (\phi_{X1}) + (X_{C2})(\phi_{Z1}) \quad (4.14)$$

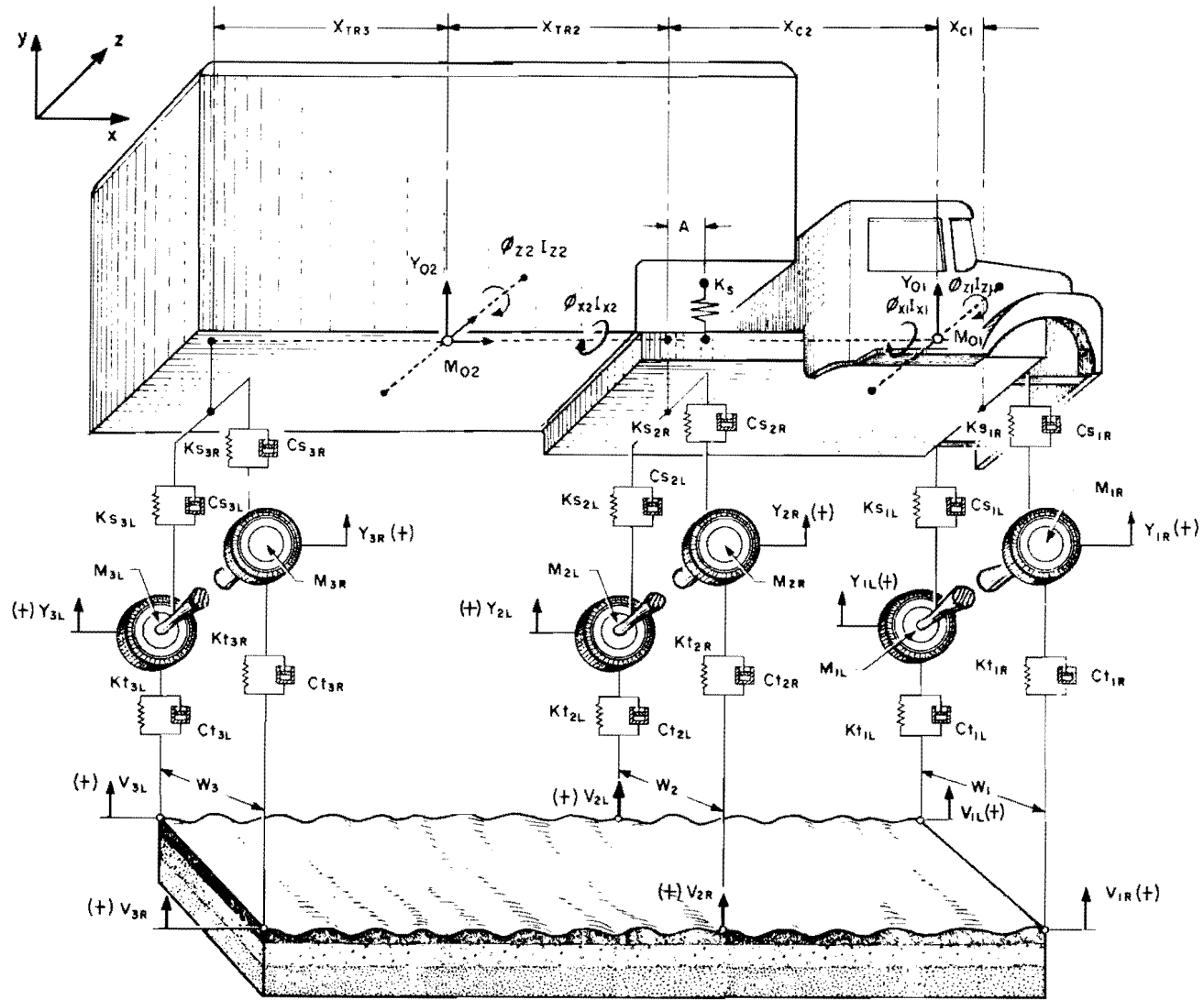


Fig 10. Class II vehicle model.

TABLE 2. CLASS II SUMMARY

Degree of Freedom	Mass System	Variables	Differential Eq of Motion
1. Vertical Translation (V.T.)	M_{01}	Y_{01}	4.20
2. Rolling		ϕ_{X1}	4.21
3. Pitching		ϕ_{Z1}	4.22
4. V.T.	M_{02}	Y_{02}	4.23
5. Rolling		ϕ_{X2}	4.24
6. Pitching		ϕ_{Z2}	4.25
7. V.T.	M_{1R}	Y_{1R}	4.26
8. V.T.	M_{1L}	Y_{1L}	4.27
9. V.T.	M_{2R}	Y_{2R}	4.28
10. V.T.	M_{2L}	Y_{2L}	4.29
11. V.T.	M_{3R}	Y_{3R}	4.30
12. V.T.	M_{3L}	Y_{3L}	4.31

$$D_{2L} = Y_{01} + \left(\frac{W_2}{2} \right) (\phi_{X1}) + (X_{C2})(\phi_{Z1}) \quad (4.15)$$

$$D_{3R} = Y_{02} - \left(\frac{W_3}{2} \right) (\phi_{X2}) + (X_{TR3})(\phi_{Z2}) \quad (4.16)$$

$$D_{3L} = Y_{02} + \left(\frac{W_3}{2} \right) (\phi_{X2}) + (X_{TR3})(\phi_{Z2}) \quad (4.17)$$

$$D_b = \frac{[A(D_{1R} + D_{1L}) + (X_{12} - A)(D_{2R} + D_{2L})]}{2X_{12}} \quad (4.18)$$

$$D_c = Y_{02} - (X_{TR2} + A)(\phi_{Z2}) \quad (4.19)$$

The twelve differential equations of motion are

$$\begin{aligned} & Ks_{1R}(D_{1R} - Y_{1R}) + Cs_{1R} \left(\frac{dD_{1R}}{dt} - \frac{dY_{1R}}{dt} \right) + Ks_{1L}(D_{1L} - Y_{1L}) \\ & + Cs_{1L} \left(\frac{dD_{1L}}{dt} - \frac{dY_{1L}}{dt} \right) + Ks_{2R}(D_{2R} - Y_{2R}) \\ & + Cs_{2R} \left(\frac{dD_{2R}}{dt} - \frac{dY_{2R}}{dt} \right) + Sk_{2L}(D_{2L} - Y_{2L}) \\ & + Cs_{2L} \left(\frac{dD_{2L}}{dt} - \frac{dY_{2L}}{dt} \right) - Ks(D_c - D_b) + M_{01} \frac{d^2 Y_{01}}{dt^2} = 0 \quad (4.20) \end{aligned}$$

$$\begin{aligned} & \left(\frac{W_1}{2} \right) \left[Ks_{1L}(D_{1L} - Y_{1L}) + Cs_{1L} \left(\frac{dD_{1L}}{dt} - \frac{dY_{1L}}{dt} \right) - Ks_{1R}(D_{1R} - Y_{1R}) \right. \\ & \left. - Cs_{1R} \left(\frac{dD_{1R}}{dt} - \frac{dY_{1R}}{dt} \right) \right] + \left(\frac{W_2}{2} \right) \left[Ks_{2L}(D_{2L} - Y_{2L}) \right. \end{aligned}$$

$$\begin{aligned}
& + C_{s2L} \left(\frac{dD_{2L}}{dt} - \frac{dY_{2L}}{dt} \right) - K_{s2R} (D_{2R} - Y_{2R}) \\
& - C_{s2R} \left(\frac{dD_{2R}}{dt} - \frac{dY_{2R}}{dt} \right) \Big] + I_{X1} \frac{d^2 \phi_{X1}}{dt^2} = 0 \tag{4.21}
\end{aligned}$$

$$\begin{aligned}
& X_{C1} \left[K_{s1R} (D_{1R} - Y_{1R}) + C_{s1R} \left(\frac{dD_{1R}}{dt} - \frac{dY_{1R}}{dt} \right) + K_{s1L} (D_{1L} - Y_{1L}) \right. \\
& \left. + C_{s1L} \left(\frac{dD_{1L}}{dt} - \frac{dY_{1L}}{dt} \right) \right] - X_{C2} \left[K_{s2R} (D_{2R} - Y_{2R}) \right. \\
& \left. + C_{s2R} \left(\frac{dD_{2R}}{dt} - \frac{dY_{2R}}{dt} \right) + K_{s2L} (D_{2L} - Y_{2L}) \right. \\
& \left. + C_{s2L} \left(\frac{dD_{2L}}{dt} - \frac{dY_{2L}}{dt} \right) \right] + (X_{C2} - A) K_s (D_c - D_b) \\
& - I_{Z1} \frac{d^2 \phi_{Z1}}{dt^2} = 0 \tag{4.22}
\end{aligned}$$

$$\begin{aligned}
& K_s (D_c - D_b) + K_{s3R} (D_{3R} - Y_{3R}) + C_{s3R} \left(\frac{dD_{3R}}{dt} - \frac{dY_{3R}}{dt} \right) \\
& + K_{s3L} (D_{3L} - Y_{3L}) + C_{s3L} \left(\frac{dD_{3L}}{dt} - \frac{dY_{3L}}{dt} \right) \\
& + M_{O2} \frac{d^2 Y_{O2}}{dt^2} = 0 \tag{4.23}
\end{aligned}$$

$$\begin{aligned}
& \left(\frac{W_3}{2} \right) \left[K_{s3R} (D_{3R} - Y_{3R}) + C_{s3R} \left(\frac{dD_{3R}}{dt} - \frac{dY_{3R}}{dt} \right) - K_{s3L} (D_{3L} - Y_{3L}) \right. \\
& \left. - C_{s3L} \left(\frac{dD_{3L}}{dt} - \frac{dY_{3L}}{dt} \right) \right] - I_{X2} \frac{d^2 \phi_{X2}}{dt^2} = 0 \tag{4.24}
\end{aligned}$$

$$\begin{aligned}
& X_{TR3} \left[Ks_{3R} (D_{3R} - Y_{3R}) + Cs_{3R} \left(\frac{dD_{3R}}{dt} - \frac{dY_{3R}}{dt} \right) + Ks_{3L} (D_{3L} - Y_{3L}) \right. \\
& \quad \left. + Cs_{3L} \left(\frac{dD_{3L}}{dt} - \frac{dY_{3L}}{dt} \right) \right] - (X_{TR2} + A)Ks(D_c - D_b) \\
& \quad + I_{Z2} \frac{d^2 \phi_{Z2}}{dt^2} = 0
\end{aligned} \tag{4.25}$$

$$\begin{aligned}
& Ks_{1R} (D_{1R} - Y_{1R}) + Cs_{1R} \left(\frac{dD_{1R}}{dt} - \frac{dY_{1R}}{dt} \right) - Kt_{1R} (Y_{1R} - V_{1R}) \\
& \quad - Ct_{1R} \left(\frac{dY_{1R}}{dt} - \frac{dV_{1R}}{dt} \right) - M_{1R} \frac{d^2 Y_{1R}}{dt^2} = 0
\end{aligned} \tag{4.26}$$

$$\begin{aligned}
& Ks_{1L} (D_{1L} - Y_{1L}) + Cs_{1L} \left(\frac{dD_{1L}}{dt} - \frac{dY_{1L}}{dt} \right) - Kt_{1L} (Y_{1L} - V_{1L}) \\
& \quad - Ct_{1L} \left(\frac{dY_{1L}}{dt} - \frac{dV_{1L}}{dt} \right) - M_{1L} \frac{d^2 Y_{1L}}{dt^2} = 0
\end{aligned} \tag{4.27}$$

$$\begin{aligned}
& Ks_{2R} (D_{2R} - Y_{2R}) + Cs_{2R} \left(\frac{dD_{2R}}{dt} - \frac{dY_{2R}}{dt} \right) - Kt_{2R} (Y_{2R} - V_{2R}) \\
& \quad - Ct_{2R} \left(\frac{dY_{2R}}{dt} - \frac{dV_{2R}}{dt} \right) - M_{2R} \frac{d^2 Y_{2R}}{dt^2} = 0
\end{aligned} \tag{4.28}$$

$$\begin{aligned}
& Ks_{2L} (D_{2L} - Y_{2L}) + Cs_{2L} \left(\frac{dD_{2L}}{dt} - \frac{dY_{2L}}{dt} \right) - Kt_{2L} (Y_{2L} - V_{2L}) \\
& \quad - Ct_{2L} \left(\frac{dY_{2L}}{dt} - \frac{dV_{2L}}{dt} \right) - M_{2L} \frac{d^2 Y_{2L}}{dt^2} = 0
\end{aligned} \tag{4.29}$$

$$\begin{aligned}
& K_{s_{3R}}(D_{3R} - Y_{3R}) + C_{s_{3R}} \left(\frac{dD_{3R}}{dt} - \frac{dY_{3R}}{dt} \right) - K_{t_{3R}}(Y_{3R} - V_{3R}) \\
& - C_{t_{3R}} \left(\frac{dY_{3R}}{dt} - \frac{dV_{3R}}{dt} \right) - M_{3R} \frac{d^2 Y_{3R}}{dt^2} = 0
\end{aligned} \tag{4.30}$$

$$\begin{aligned}
& K_{s_{3L}}(D_{3L} - Y_{3L}) + C_{s_{3L}} \left(\frac{dD_{3L}}{dt} - \frac{dY_{3L}}{dt} \right) - K_{t_{3L}}(Y_{3L} - V_{3L}) \\
& - C_{t_{3L}} \left(\frac{dY_{3L}}{dt} - \frac{dV_{3L}}{dt} \right) - M_{3L} \frac{d^2 Y_{3L}}{dt^2} = 0
\end{aligned} \tag{4.31}$$

Class III. The model for this vehicle type (3-D), single unit tandem, is shown in Fig 11. The total number of degrees of freedom is 9 (Table 3).

The movements of the four corners of the main body are given by the following equations:

$$D_{1R} = Y_0 - \left(\frac{W_1}{2} \right) \phi_X - (X_1) \phi_Z \tag{4.32}$$

$$D_{1L} = Y_0 + \left(\frac{W_1}{2} \right) \phi_X - (X_1) \phi_Z \tag{4.33}$$

$$D_{23R} = Y_0 - \left(\frac{W_2}{2} \right) \phi_X + (X_T) \phi_Z \tag{4.34}$$

$$D_{23L} = Y_0 + \left(\frac{W_2}{2} \right) \phi_X + (X_T) \phi_Z \tag{4.35}$$

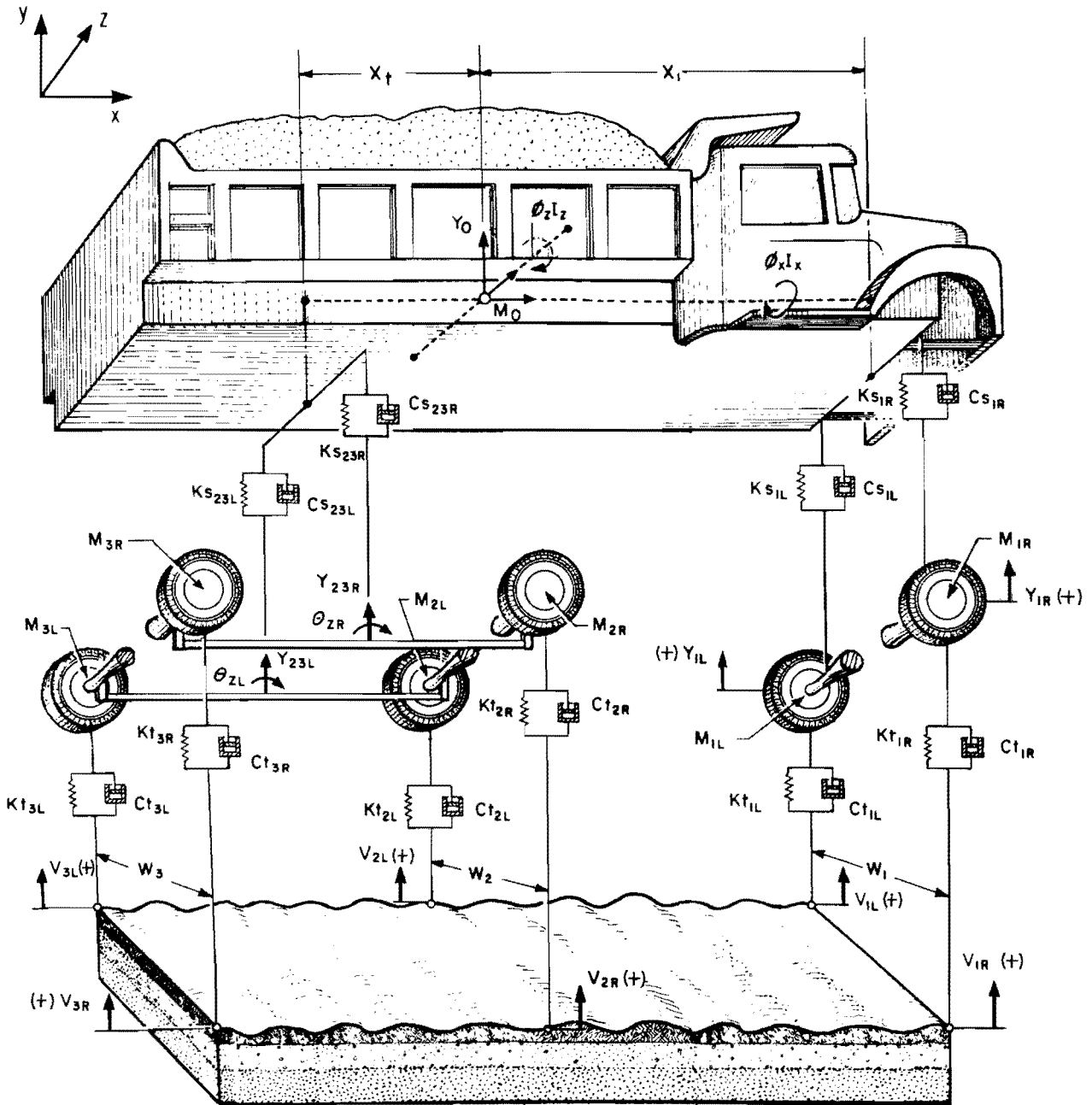


Fig 11. Class III vehicle model.

TABLE 3. CLASS III SUMMARY

Degree of Freedom	Mass System	Variables	Differential Eq of Motion
1. Vertical Translation (V.T.)	M_0	Y_0	4.36
2. Rolling		ϕ_X	4.37
3. Pitching		ϕ_Z	4.38
4. V.T.	M_{1R}	Y_{1R}	4.39
5. V.T.	M_{1L}	Y_{1L}	4.40
6. V.T.	$M_{2R} + M_{3R}$	Y_{23R}	4.41
7. V.T.	$M_{2L} + M_{3L}$	Y_{23L}	4.42
8. Pitching		θ_{ZR}	4.43
9. Pitching		θ_{ZL}	4.44

The equations of motion are:

$$\begin{aligned}
& K_{s_{1R}}(D_{1R} - Y_{1R}) + C_{s_{1R}} \left(\frac{dD_{1R}}{dt} - \frac{dY_{1R}}{dt} \right) + K_{s_{1L}}(D_{1L} - Y_{1L}) \\
& + C_{s_{1L}} \left(\frac{dD_{1L}}{dt} - \frac{dY_{1L}}{dt} \right) + K_{s_{23R}}(D_{23R} - Y_{23R}) \\
& + C_{s_{23R}} \left(\frac{dD_{23R}}{dt} - \frac{dY_{23R}}{dt} \right) + K_{s_{23L}}(D_{23L} - Y_{23L}) \\
& + C_{s_{23L}} \left(\frac{dD_{23L}}{dt} - \frac{dY_{23L}}{dt} \right) + M_0 \frac{d^2 Y_0}{dt^2} = 0 \tag{4.36}
\end{aligned}$$

$$\begin{aligned}
& \left(\frac{W_1}{2} \right) \left[K_{s_{1R}}(D_{1R} - Y_{1R}) + C_{s_{1R}} \left(\frac{dD_{1R}}{dt} - \frac{dY_{1R}}{dt} \right) - K_{s_{1L}}(D_{1L} - Y_{1L}) \right. \\
& \left. - C_{s_{1L}} \left(\frac{dD_{1L}}{dt} - \frac{dY_{1L}}{dt} \right) \right] + \left(\frac{W_2}{2} \right) \left[K_{s_{23R}}(D_{23R} - Y_{23R}) \right. \\
& \left. + C_{s_{23R}} \left(\frac{dD_{23R}}{dt} - \frac{dY_{23R}}{dt} \right) - K_{s_{23L}}(D_{23L} - Y_{23L}) \right. \\
& \left. - C_{s_{23L}} \left(\frac{dD_{23L}}{dt} - \frac{dY_{23L}}{dt} \right) \right] - I_X \frac{d^2 \phi_X}{dt^2} = 0 \tag{4.37}
\end{aligned}$$

$$\begin{aligned}
& X_1 \left[K_{s_{1L}}(D_{1L} - Y_{1L}) + C_{s_{1L}} \left(\frac{dD_{1L}}{dt} - \frac{dY_{1L}}{dt} \right) + K_{s_{1R}}(D_{1R} - Y_{1R}) \right. \\
& \left. + C_{s_{1R}} \left(\frac{dD_{1R}}{dt} - \frac{dY_{1R}}{dt} \right) \right] - X_T \left[K_{s_{23L}}(D_{23L} - Y_{23L}) \right.
\end{aligned}$$

$$\begin{aligned}
& + C_{s_{23L}} \left(\frac{dD_{23L}}{dt} - \frac{dY_{23L}}{dt} \right) + K_{s_{23R}} (D_{23R} - Y_{23R}) \\
& + C_{s_{23R}} \left(\frac{dD_{23R}}{dt} - \frac{dY_{23R}}{dt} \right) \Big] - I_Z \frac{d^2 \phi_Z}{dt^2} = 0
\end{aligned} \tag{4.38}$$

$$\begin{aligned}
& K_{s_{1R}} (D_{1R} - Y_{1R}) + C_{s_{1R}} \left(\frac{dD_{1R}}{dt} - \frac{dY_{1R}}{dt} \right) - K_{t_{1R}} (Y_{1R} - V_{1R}) \\
& - C_{t_{1R}} \left(\frac{dY_{1R}}{dt} - \frac{dV_{1R}}{dt} \right) - M_{1R} \frac{d^2 Y_{1R}}{dt^2} = 0
\end{aligned} \tag{4.39}$$

$$\begin{aligned}
& K_{s_{1L}} (D_{1L} - Y_{1L}) + C_{s_{1L}} \left(\frac{dD_{1L}}{dt} - \frac{dY_{1L}}{dt} \right) - K_{t_{1L}} (Y_{1L} - V_{1L}) \\
& - C_{t_{1L}} \left(\frac{dD_{1L}}{dt} - \frac{dV_{1L}}{dt} \right) - M_{1L} \frac{d^2 Y_{1L}}{dt^2} = 0
\end{aligned} \tag{4.40}$$

$$\begin{aligned}
& K_{s_{23R}} (D_{23R} - Y_{23R}) + C_{s_{23R}} \left(\frac{dD_{23R}}{dt} - \frac{dY_{23R}}{dt} \right) - K_{t_{2R}} \left(Y_{23R} \right. \\
& \left. - \frac{X_{23}}{2} \theta_{ZR} - V_{2R} \right) - C_{t_{2R}} \left(\frac{dY_{23R}}{dt} - \frac{X_{23}}{2} \frac{d\theta_{ZR}}{dt} - \frac{dV_{2R}}{dt} \right) \\
& - K_{t_{3R}} \left(Y_{23R} + \frac{X_{23}}{2} \theta_{ZR} - V_{3R} \right) - C_{t_{3R}} \left(\frac{dY_{23R}}{dt} + \frac{X_{23}}{2} \frac{d\theta_{2R}}{dt} \right. \\
& \left. - \frac{dV_{3R}}{dt} \right) - M_{2R} \frac{d^2 Y_{23R}}{dt^2} - M_{3R} \frac{d^2 Y_{23R}}{dt^2} = 0
\end{aligned} \tag{4.41}$$

$$\begin{aligned}
& K_{s23L} (D_{23L} - Y_{23L}) + C_{s23L} \left(\frac{dD_{23L}}{dt} - \frac{dY_{23L}}{dt} \right) - K_{t2L} \left(Y_{23L} \right. \\
& \left. - \frac{X_{23}}{2} \theta_{ZL} - V_{2L} \right) - C_{t2L} \left(\frac{dY_{23L}}{dt} - \frac{X_{23}}{2} \frac{d\theta_{ZL}}{dt} - \frac{dV_{2L}}{dt} \right) \\
& - K_{t3L} \left(Y_{23L} + \frac{X_{23}}{2} \theta_{ZL} - V_{3L} \right) - C_{t3L} \left(\frac{dY_{23L}}{dt} + \frac{X_{23}}{2} \frac{d\theta_{ZL}}{dt} \right. \\
& \left. - \frac{dV_{3L}}{dt} \right) - M_{2L} \frac{d^2 Y_{23L}}{dt^2} - M_{3L} \frac{d^2 Y_{23L}}{dt^2} = 0 \tag{4.42}
\end{aligned}$$

$$\begin{aligned}
& \left(\frac{X_{23}}{2} \right) \left[K_{t2R} \left(Y_{23R} - \frac{X_{23}}{2} \theta_{ZR} - V_{2R} \right) + C_{t2R} \left(\frac{dY_{23R}}{dt} - \frac{X_{23}}{2} \frac{d\theta_{ZR}}{dt} \right. \right. \\
& \left. \left. - \frac{dV_{2R}}{dt} \right) - K_{t3R} \left(Y_{23R} + \frac{X_{23}}{2} \theta_{ZR} - V_{3R} \right) - C_{t3R} \left(\frac{dY_{23R}}{dt} \right. \right. \\
& \left. \left. + \frac{X_{23}}{2} \frac{d\theta_{ZR}}{dt} - \frac{dV_{3R}}{dt} \right) \right] - I_{TZ} \frac{d^2 \theta_{ZR}}{dt^2} = 0 \tag{4.43}
\end{aligned}$$

$$\begin{aligned}
& \left(\frac{X_{23}}{2} \right) \left[K_{t2L} \left(Y_{23L} - \frac{X_{23}}{2} \theta_{ZL} - V_{2L} \right) + C_{t2L} \left(\frac{dY_{23L}}{dt} - \frac{X_{23}}{2} \frac{d\theta_{ZL}}{dt} \right. \right. \\
& \left. \left. - \frac{dV_{2L}}{dt} \right) - K_{t3L} \left(Y_{23L} + \frac{X_{23}}{2} \theta_{ZL} - V_{3L} \right) - C_{t3L} \left(\frac{dY_{23L}}{dt} \right. \right. \\
& \left. \left. + \frac{X_{23}}{2} \frac{d\theta_{ZL}}{dt} - \frac{dV_{3L}}{dt} \right) \right] - I_{TZ} \frac{d^2 \theta_{ZL}}{dt^2} = 0 \tag{4.44}
\end{aligned}$$

Class IV. The model for this class of vehicles (2S-2), four-axle truck-trailer combinations, is shown in Fig 12. The total number of degrees of freedom is 14 (Table 4).

The movements of the corners of the truck and trailer and for the truck-trailer connection point are expressed in Eqs 4.45 through 4.52.

$$D_{1R} = Y_{01} - \left(\frac{W_1}{2} \right) \phi_{X1} - (X_{C1})\phi_{Z1} \quad (4.45)$$

$$D_{1L} = Y_{01} + \left(\frac{W_1}{2} \right) \phi_{X1} - (X_{C1})\phi_{Z1} \quad (4.46)$$

$$D_{2R} = Y_{01} - \left(\frac{W_2}{2} \right) \phi_{X1} + (X_{C2})\phi_{Z1} \quad (4.47)$$

$$D_{2L} = Y_{01} + \left(\frac{W_2}{2} \right) \phi_{X1} + (X_{C2})\phi_{Z1} \quad (4.48)$$

$$D_b = \frac{[(D_{1R} + D_{1L})A + (D_{2R} + D_{2L})(X_{12} - A)]}{2X_{12}} \quad (4.49)$$

$$D_c = Y_{02} - (X_{TR2} + A)\phi_{Z2} \quad (4.50)$$

$$D_{34R} = Y_{02} - \left(\frac{W_3}{2} \right) \phi_{X2} + (X_{TRT})\phi_{Z2} \quad (4.51)$$

$$D_{34L} = Y_{02} + \left(\frac{W_3}{2} \right) \phi_{X2} + (X_{TRT})\phi_{Z2} \quad (4.52)$$

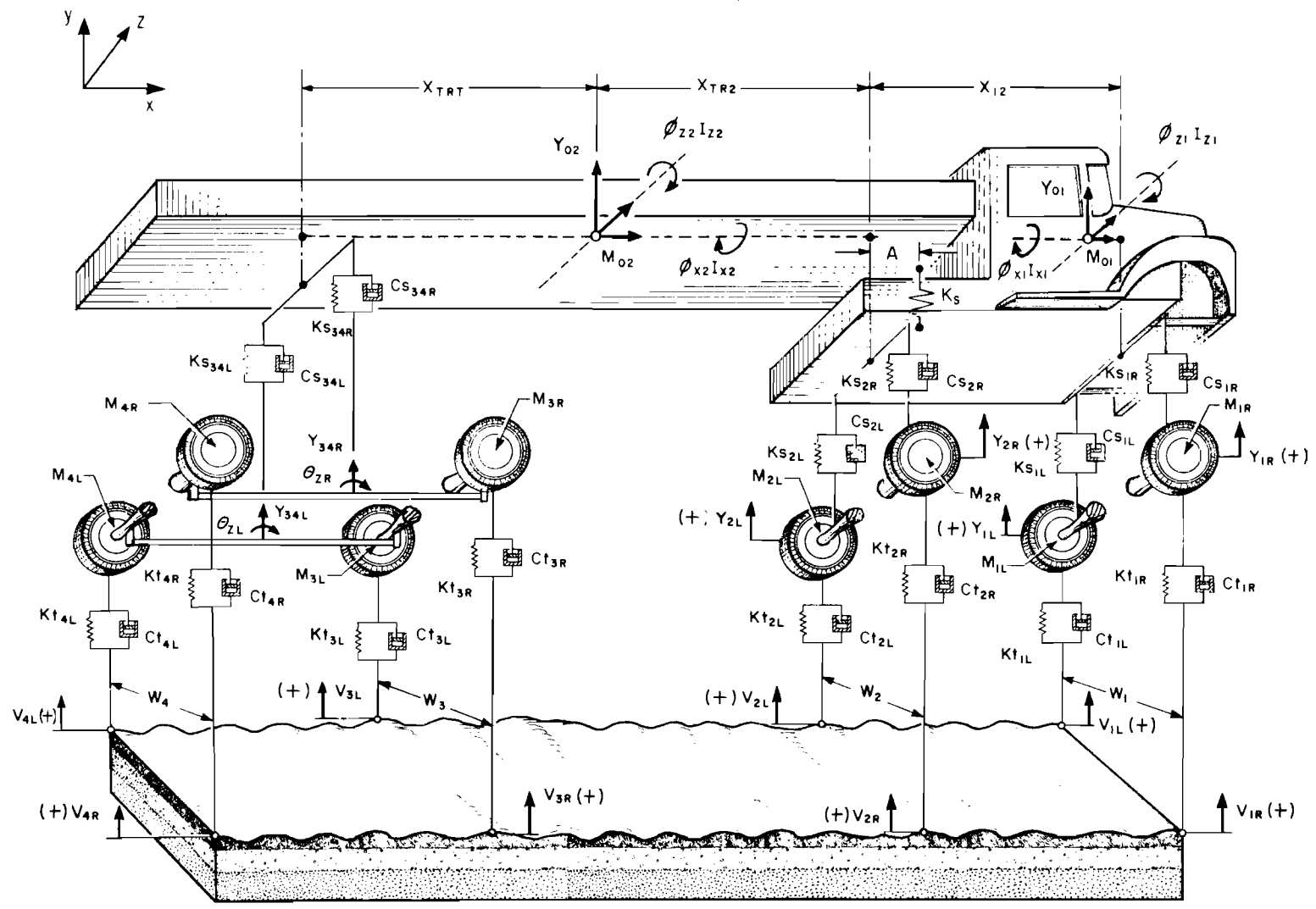


Fig 12. Class IV vehicle model.

TABLE 4. CLASS IV SUMMARY

	Degrees of Freedom	Mass System	Variables	Differential Eq of Motion
1.	Vertical Translation (V.T.)	M_{01}	Y_{01}	4.53
2.	Rolling		ϕ_{X1}	4.54
3.	Pitching		ϕ_{Z1}	4.55
4.	V.T.	M_{02}	Y_{02}	4.56
5.	Rolling		ϕ_{X2}	4.57
6.	Pitching		Y_{02}	4.58
7.	V.T.	M_{1R}	Y_{1R}	4.59
8.	V.T.	M_{1L}	Y_{1L}	4.60
9.	V.T.	M_{2R}	Y_{2R}	4.61
10.	V.T.	M_{2L}	Y_{2L}	4.62
11.	V.T.	$M_{3R} + M_{4R}$	Y_{34R}	4.63
12.	V.T.	$M_{3L} + M_{4L}$	Y_{34L}	4.64
13.	Pitching		θ_{ZR}	4.65
14.	Pitching		θ_{ZL}	4.66

The equations of motion are given in Eqs 4.53 through 4.66.

$$\begin{aligned}
& K_{s1R}(D_{1R} - Y_{1R}) + C_{s1R} \left(\frac{dD_{1R}}{dt} - \frac{dY_{1R}}{dt} \right) + K_{s1L}(D_{1L} - Y_{1L}) \\
& + C_{s1L} \left(\frac{dD_{1L}}{dt} - \frac{dY_{1L}}{dt} \right) + K_{s2R}(D_{2R} - Y_{2R}) + C_{s2R} \left(\frac{dD_{2R}}{dt} \right. \\
& \left. - \frac{dY_{2R}}{dt} \right) + K_{s2L}(D_{2L} - Y_{2L}) + C_{s2L} \left(\frac{dD_{2L}}{dt} - \frac{dY_{2L}}{dt} \right) \\
& - K_s(D_c - D_b) + M_{01} \frac{d^2 Y_{01}}{dt^2} = 0 \tag{4.53}
\end{aligned}$$

$$\begin{aligned}
& \left(\frac{W_1}{2} \right) \left[K_{s1R}(D_{1R} - Y_{1R}) + C_{s1R} \left(\frac{dD_{1R}}{dt} - \frac{dY_{1R}}{dt} \right) - K_{s1L}(D_{1L} - Y_{1L}) \right. \\
& \left. - C_{s1L} \left(\frac{dD_{1L}}{dt} - \frac{dY_{1L}}{dt} \right) \right] + \left(\frac{W_2}{2} \right) \left[K_{s2R}(D_{2R} - Y_{2R}) \right. \\
& \left. + C_{s2R} \left(\frac{dD_{2R}}{dt} - \frac{dY_{2R}}{dt} \right) - K_{s2L}(D_{2L} - Y_{2L}) - C_{s2L} \left(\frac{dD_{2L}}{dt} \right. \right. \\
& \left. \left. - \frac{dY_{2L}}{dt} \right) \right] - I_{X1} \frac{d^2 \phi_{X1}}{dt^2} = 0 \tag{4.54}
\end{aligned}$$

$$\begin{aligned}
& X_{C1} \left[K_{s1R}(D_{1R} - Y_{1R}) + C_{s1R} \left(\frac{dD_{1R}}{dt} - \frac{dY_{1R}}{dt} \right) + K_{s1L}(D_{1L} - Y_{1L}) \right. \\
& \left. + C_{s1L} \left(\frac{dD_{1L}}{dt} - \frac{dY_{1L}}{dt} \right) \right] - X_{C2} \left[K_{s2R}(D_{2R} - Y_{2R}) \right.
\end{aligned}$$

$$\begin{aligned}
& + C_{s2R} \left(\frac{dD_{2R}}{dt} - \frac{dY_{2R}}{dt} \right) + K_{s2L} (D_{2L} - Y_{2L}) + C_{s2L} \left(\frac{dD_{2L}}{dt} \right. \\
& \left. - \frac{dY_{2L}}{dt} \right) \Big] + (X_{C2} - A)K_s(D_c - D_b) - I_{Z1} \frac{d^2 \phi_{Z1}}{dt^2} = 0 \quad (4.55)
\end{aligned}$$

$$\begin{aligned}
& K_s(D_c - D_b) + K_{s34R} (D_{34R} - Y_{34R}) + C_{s34R} \left(\frac{dD_{34R}}{dt} - \frac{dY_{34R}}{dt} \right) \\
& + K_{s34L} (D_{34L} - Y_{34L}) + C_{s34L} \left(\frac{dD_{34L}}{dt} - \frac{dY_{34L}}{dt} \right) \\
& + M_{O2} \frac{d^2 Y_{O2}}{dt^2} = 0 \quad (4.56)
\end{aligned}$$

$$\begin{aligned}
& \left(\frac{W_3}{2} \right) \left[K_{s34R} (D_{34R} - Y_{34R}) + C_{s34R} \left(\frac{dD_{34R}}{dt} - \frac{dY_{34R}}{dt} \right) \right. \\
& \left. - K_{s34L} (D_{34L} - Y_{34L}) - C_{s34L} \left(\frac{dD_{34L}}{dt} - \frac{dY_{34L}}{dt} \right) \right] \\
& - I_{X2} \frac{d^2 \phi_{X2}}{dt^2} = 0 \quad (4.57)
\end{aligned}$$

$$\begin{aligned}
& K_s(X_{TR2} + A)(D_c - D_b) - X_{TRT} \left[K_{s34R} (D_{34R} - Y_{34R}) + C_{s34R} \left(\frac{dD_{34R}}{dt} \right. \right. \\
& \left. \left. - \frac{dY_{34R}}{dt} \right) + K_{s34L} (D_{34L} - Y_{34L}) + C_{s34L} \left(\frac{dD_{34L}}{dt} - \frac{dY_{34L}}{dt} \right) \right] \\
& - I_{Z2} \frac{d^2 \phi_{Z2}}{dt^2} = 0 \quad (4.58)
\end{aligned}$$

$$\begin{aligned}
& K_{s_{1R}}(D_{1R} - Y_{1R}) + C_{s_{1R}} \left(\frac{dD_{1R}}{dt} - \frac{dY_{1R}}{dt} \right) - K_{t_{1R}}(Y_{1R} - V_{1R}) \\
& - C_{t_{1R}} \left(\frac{dY_{1R}}{dt} - \frac{dV_{1R}}{dt} \right) - M_{1R} \frac{d^2 Y_{1R}}{dt^2} = 0
\end{aligned} \tag{4.59}$$

$$\begin{aligned}
& K_{s_{1L}}(D_{1L} - Y_{1L}) + C_{s_{1L}} \left(\frac{dD_{1L}}{dt} - \frac{dY_{1L}}{dt} \right) - K_{t_{1L}}(Y_{1L} - V_{1L}) \\
& - C_{t_{1L}} \left(\frac{dY_{1L}}{dt} - \frac{dV_{1L}}{dt} \right) - M_{1L} \frac{d^2 Y_{1L}}{dt^2} = 0
\end{aligned} \tag{4.60}$$

$$\begin{aligned}
& K_{s_{2R}}(D_{2R} - Y_{2R}) + C_{s_{2R}} \left(\frac{dD_{2R}}{dt} - \frac{dY_{2R}}{dt} \right) - K_{t_{2R}}(Y_{2R} - V_{2R}) \\
& - C_{t_{2R}} \left(\frac{dY_{2R}}{dt} - \frac{dV_{2R}}{dt} \right) - M_{2R} \frac{d^2 Y_{2R}}{dt^2} = 0
\end{aligned} \tag{4.61}$$

$$\begin{aligned}
& K_{s_{2L}}(D_{2L} - Y_{2L}) + C_{s_{2L}} \left(\frac{dD_{2L}}{dt} - \frac{dY_{2L}}{dt} \right) - K_{t_{2L}}(Y_{2L} - V_{2L}) \\
& - C_{t_{2L}} \left(\frac{dY_{2L}}{dt} - \frac{dV_{2L}}{dt} \right) - M_{2L} \frac{d^2 Y_{2L}}{dt^2} = 0
\end{aligned} \tag{4.62}$$

$$\begin{aligned}
& K_{s_{34R}}(D_{34R} - Y_{34R}) + C_{s_{34R}} \left(\frac{dD_{34R}}{dt} - \frac{dY_{34R}}{dt} \right) - K_{t_{3R}} \left(Y_{34R} \right. \\
& \left. - \frac{X_{34}}{2} \theta_{ZR} - V_{3R} \right) - C_{t_{3R}} \left(\frac{dY_{34R}}{dt} - \frac{X_{34}}{2} \frac{d\theta_{ZR}}{dt} - \frac{dV_{3R}}{dt} \right)
\end{aligned}$$

$$\begin{aligned}
& - Kt_{4R} \left(Y_{34R} + \frac{X_{34}}{2} \theta_{ZR} - V_{4R} \right) - Ct_{4R} \left(\frac{dY_{34R}}{dt} + \frac{X_{34}}{2} \frac{d\theta_{ZR}}{dt} \right. \\
& \left. - \frac{dV_{4R}}{dt} \right) - M_{3R} \frac{d^2 Y_{34R}}{dt^2} - M_{4R} \frac{d^2 Y_{34R}}{dt^2} = 0 \quad (4.63)
\end{aligned}$$

$$\begin{aligned}
& Ks_{34L} (D_{34L} - Y_{34L}) + Cs_{34L} \left(\frac{dD_{34L}}{dt} - \frac{dY_{34L}}{dt} \right) - Kt_{3L} \left(Y_{34L} \right. \\
& \left. - \frac{X_{34}}{2} \theta_{ZL} - V_{3L} \right) - Ct_{3L} \left(\frac{dY_{34L}}{dt} - \frac{X_{34}}{2} \frac{d\theta_{ZL}}{dt} - \frac{dV_{3L}}{dt} \right) \\
& - Kt_{4L} \left(Y_{34L} + \frac{X_{34}}{2} \theta_{ZL} - V_{4L} \right) - Ct_{4L} \left(\frac{dY_{34L}}{dt} + \frac{X_{34}}{2} \frac{d\theta_{ZL}}{dt} \right. \\
& \left. - \frac{dV_{4L}}{dt} \right) - M_{3L} \frac{d^2 Y_{34L}}{dt^2} - M_{4L} \frac{d^2 Y_{34L}}{dt^2} = 0 \quad (4.64)
\end{aligned}$$

$$\begin{aligned}
& \left(\frac{X_{34}}{2} \right) \left[Kt_{3R} \left(Y_{34R} - \frac{X_{34}}{2} \theta_{ZR} - V_{3R} \right) + Ct_{3R} \left(\frac{dY_{34R}}{dt} \right. \right. \\
& \left. \left. - \frac{X_{34}}{2} \frac{d\theta_{ZR}}{dt} - \frac{dV_{3R}}{dt} \right) - Kt_{4R} \left(Y_{34R} + \frac{X_{34}}{2} \theta_{ZR} - V_{4R} \right) \right. \\
& \left. - Ct_{4R} \left(\frac{dY_{34R}}{dt} + \frac{X_{34}}{2} \frac{d\theta_{ZR}}{dt} - \frac{dV_{4R}}{dt} \right) \right] - I_{TZ} \frac{d^2 \theta_{ZR}}{dt^2} = 0 \quad (4.65)
\end{aligned}$$

$$\begin{aligned}
& \left(\frac{X_{34}}{2} \right) \left[Kt_{3L} \left(Y_{34L} - \frac{X_{34}}{2} \theta_{ZL} - V_{3L} \right) + Ct_{3L} \left(\frac{dY_{34L}}{dt} \right. \right. \\
& \left. \left. - \frac{X_{34}}{2} \frac{d\theta_{ZL}}{dt} - \frac{dV_{3L}}{dt} \right) - Kt_{4L} \left(Y_{34L} + \frac{X_{34}}{2} \theta_{ZL} - V_{4L} \right) \right. \\
& \left. - Ct_{4L} \left(\frac{dY_{34L}}{dt} + \frac{X_{34}}{2} \frac{d\theta_{ZL}}{dt} - \frac{dV_{4L}}{dt} \right) \right] - I_{TZ} \frac{d^2 \theta_{ZL}}{dt^2} = 0 \quad (4.66)
\end{aligned}$$

Class V. Finally, the model describing this class of vehicle (3S-2), five-axle truck-trailer combination, is shown in Fig 13. The total degrees of freedom for the system is 16 (Table 5).

The movements of the corners of the truck body and trailer body and the truck-trailer connection point are expressed by Eqs 4.67 through 4.74.

$$D_{1R} = Y_{01} - \left(\frac{W_1}{2} \right) \phi_{X1} - (X_{C1})\phi_{Z1} \quad (4.67)$$

$$D_{1L} = Y_{01} + \left(\frac{W_1}{2} \right) \phi_{X1} - (X_{C1})\phi_{Z1} \quad (4.68)$$

$$D_{23R} = Y_{01} - \left(\frac{W_2}{2} \right) \phi_{X1} + (X_{C23})\phi_{Z1} \quad (4.69)$$

$$D_{23L} = Y_{01} + \left(\frac{W_2}{2} \right) \phi_{X1} + (X_{C23})\phi_{Z1} \quad (4.70)$$

$$D_b = \frac{[(D_{1R} + D_{1L})A + (D_{23R} + D_{23L})(X_{12} - A)]}{2X_{12}} \quad (4.71)$$

$$D_c = Y_{02} - (X_{TR23} + A)\phi_{Z2} \quad (4.72)$$

$$D_{45R} = Y_{02} - \left(\frac{W_4}{2} \right) \phi_{X2} + (X_{TR45})\phi_{Z2} \quad (4.73)$$

$$D_{45L} = Y_{02} + \left(\frac{W_4}{2} \right) \phi_{X2} + (X_{TR45})\phi_{Z2} \quad (4.74)$$

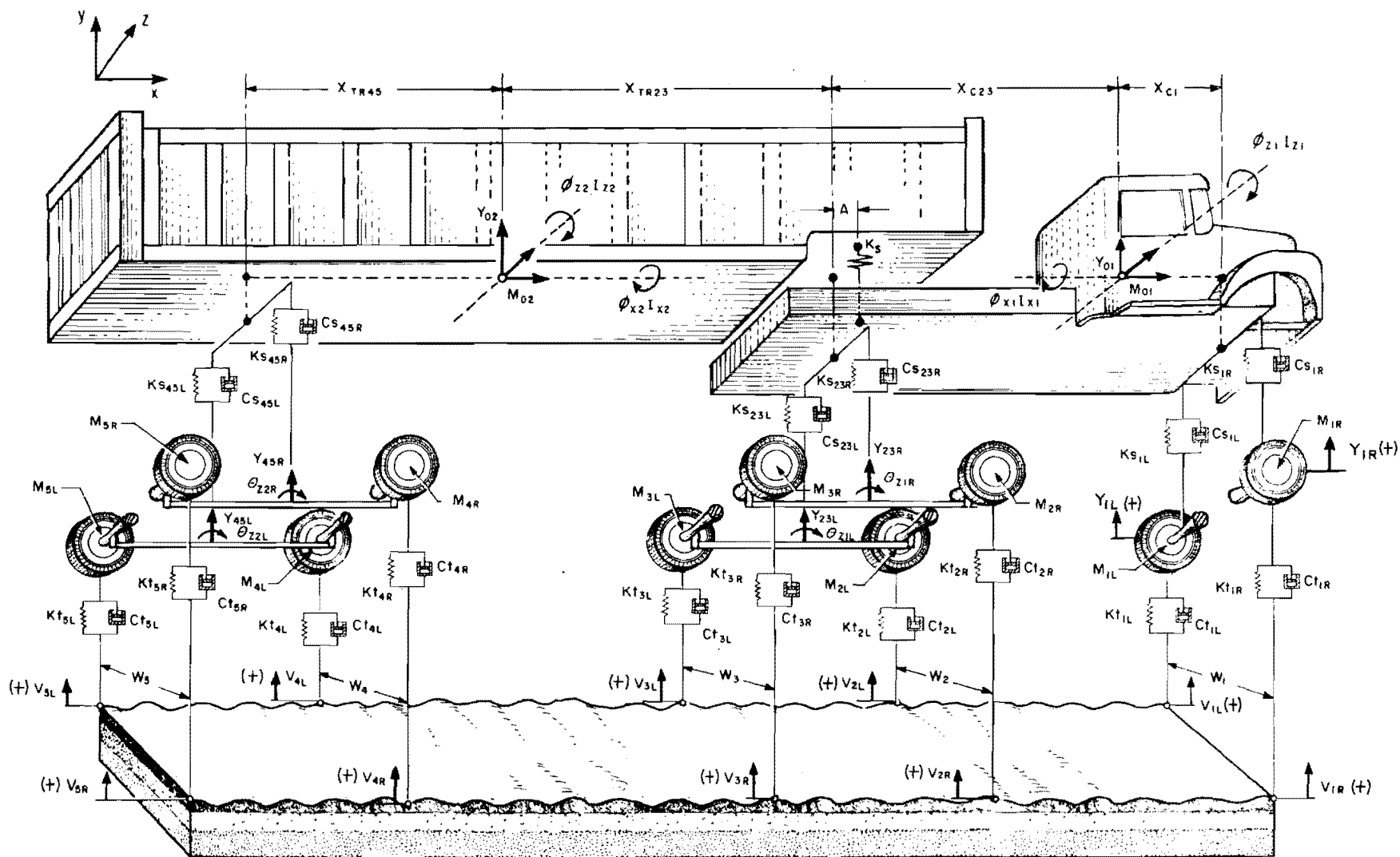


Fig 13. Class V vehicle model.

TABLE 5. CLASS V SUMMARY

	Degrees of Freedom	Mass System	Variables	Differential Eq of Motion
1.	Vertical Translation (V.T.)	M_{01}	Y_{01}	4.75
2.	Rolling		ϕ_{X1}	4.76
3.	Pitching	M_{02}	ϕ_{Z1}	4.77
4.	V.T.	M_{02}	Y_{02}	4.78
5.	Rolling		ϕ_{X2}	4.79
6.	Pitching		ϕ_{Z2}	4.80
7.	V.T.	M_{1R}	Y_{1R}	4.81
8.	V.T.	M_{1L}	Y_{1L}	4.82
9.	V.T.	$M_{2R} + M_{3R}$	Y_{23R}	4.83
10.	V.T.	$M_{2L} + M_{3L}$	Y_{23L}	4.84
11.	Pitching		θ_{Z1R}	4.85
12.	Pitching		θ_{Z1L}	4.86
13.	V.T.	$M_{4R} + M_{5R}$	Y_{45R}	4.87
14.	V.T.	$M_{4L} + M_{5L}$	Y_{45L}	4.88
15.	Pitching		θ_{Z2R}	4.89
16.	Pitching		θ_{Z2L}	4.90

The equations of motion are given in Eqs 4.75 through 4.90.

$$\begin{aligned}
& Ks(D_c - D_b) - Ks_{1R}(D_{1R} - Y_{1R}) - Cs_{1R} \left(\frac{dD_{1R}}{dt} - \frac{dY_{1R}}{dt} \right) \\
& - Ks_{1L}(D_{1L} - Y_{1L}) - Cs_{1L} \left(\frac{dD_{1L}}{dt} - \frac{dY_{1L}}{dt} \right) - Ks_{23R}(D_{23R} - Y_{23R}) \\
& - Cs_{23R} \left(\frac{dD_{23R}}{dt} - \frac{dY_{23R}}{dt} \right) - Ks_{23L}(D_{23L} - Y_{23L}) \\
& - Cs_{23L} \left(\frac{dD_{23L}}{dt} - \frac{dY_{23L}}{dt} \right) - M_{O1} \frac{d^2 Y_{O1}}{dt^2} = 0 \quad (4.75)
\end{aligned}$$

$$\begin{aligned}
& \left(\frac{W_1}{2} \right) \left[Ks_{1R}(D_{1R} - Y_{1R}) + Cs_{1R} \left(\frac{dD_{1R}}{dt} - \frac{dY_{1R}}{dt} \right) - Ks_{1L}(D_{1L} - Y_{1L}) \right. \\
& \left. - Cs_{1L} \left(\frac{dD_{1L}}{dt} - \frac{dY_{1L}}{dt} \right) \right] + \left(\frac{W_2}{2} \right) \left[Ks_{23R}(D_{23R} - Y_{23R}) \right. \\
& \left. + Cs_{23R} \left(\frac{dD_{23R}}{dt} - \frac{dY_{23R}}{dt} \right) - Ks_{23L}(D_{23L} - Y_{23L}) \right. \\
& \left. - Cs_{23L} \left(\frac{dD_{23L}}{dt} - \frac{dY_{23L}}{dt} \right) \right] - I_{X1} \frac{d^2 \phi_{X1}}{dt^2} = 0 \quad (4.76)
\end{aligned}$$

$$\begin{aligned}
& X_{C1} \left[Ks_{1R}(D_{1R} - Y_{1R}) + Cs_{1R} \left(\frac{dD_{1R}}{dt} - \frac{dY_{1R}}{dt} \right) + Ks_{1L}(D_{1L} - Y_{1L}) \right. \\
& \left. + Cs_{1L} \left(\frac{dD_{1L}}{dt} - \frac{dY_{1L}}{dt} \right) \right] - X_{C23} \left[Ks_{23R}(D_{23R} - Y_{23R}) \right.
\end{aligned}$$

$$\begin{aligned}
& + C_{s_{23R}} \left(\frac{dD_{23R}}{dt} - \frac{dY_{23R}}{dt} \right) + K_{s_{23L}} (D_{23L} - Y_{23L}) \\
& + C_{s_{23L}} \left(\frac{dD_{23L}}{dt} - \frac{dY_{23L}}{dt} \right) \Big] - I_{Z1} \frac{d^2 \phi_{Z1}}{dt^2} = 0
\end{aligned} \tag{4.77}$$

$$\begin{aligned}
& K_s (D_c - D_b) + K_{s_{45R}} (D_{45R} - Y_{45R}) + C_{s_{45R}} \left(\frac{dD_{45R}}{dt} - \frac{dY_{45R}}{dt} \right) \\
& + K_{s_{45L}} (D_{45L} - Y_{45L}) + C_{s_{45L}} \left(\frac{dD_{45L}}{dt} - \frac{dY_{45L}}{dt} \right) \\
& + M_{O2} \frac{d^2 Y_{O2}}{dt^2} = 0
\end{aligned} \tag{4.78}$$

$$\begin{aligned}
& \left(\frac{W_4}{2} \right) \Big[K_{s_{45R}} (D_{45R} - Y_{45R}) + C_{s_{45R}} \left(\frac{dD_{45R}}{dt} - \frac{dY_{45R}}{dt} \right) \\
& - K_{s_{45L}} (D_{45L} - Y_{45L}) - C_{s_{45L}} \left(\frac{dD_{45L}}{dt} - \frac{dY_{45L}}{dt} \right) \Big] \\
& - I_{X2} \frac{d^2 \phi_{X2}}{dt^2} = 0
\end{aligned} \tag{4.79}$$

$$\begin{aligned}
& K_s (X_{TR23} + A) (D_c - D_b) - X_{TR45} \Big[K_{s_{45R}} (D_{45R} - Y_{45R}) \\
& + C_{s_{45R}} \left(\frac{dD_{45R}}{dt} - \frac{dY_{45R}}{dt} \right) + K_{s_{45L}} (D_{45L} - Y_{45L}) \\
& + C_{s_{45L}} \left(\frac{dD_{45L}}{dt} - \frac{dY_{45L}}{dt} \right) \Big] - I_{Z2} \frac{d^2 \phi_{Z2}}{dt^2} = 0
\end{aligned} \tag{4.80}$$

$$\begin{aligned}
& K_{s1R}(D_{1R} - Y_{1R}) + C_{s1R} \left(\frac{dD_{1R}}{dt} - \frac{dY_{1R}}{dt} \right) - K_{t1R}(Y_{1R} - V_{1R}) \\
& - C_{t1R} \left(\frac{dY_{1R}}{dt} - \frac{dV_{1R}}{dt} \right) - M_{1R} \frac{d^2 Y_{1R}}{dt^2} = 0
\end{aligned} \tag{4.81}$$

$$\begin{aligned}
& K_{s1L}(D_{1L} - Y_{1L}) + C_{s1L} \left(\frac{dD_{1L}}{dt} - \frac{dY_{1L}}{dt} \right) - K_{t1L}(Y_{1L} - V_{1L}) \\
& - C_{t1L} \left(\frac{dY_{1L}}{dt} - \frac{dV_{1L}}{dt} \right) - M_{1L} \frac{d^2 Y_{1L}}{dt^2} = 0
\end{aligned} \tag{4.82}$$

$$\begin{aligned}
& K_{s23R}(D_{23R} - Y_{23R}) + C_{s23R} \left(\frac{dD_{23R}}{dt} - \frac{dY_{23R}}{dt} \right) - K_{t2R} \left(Y_{23R} \right. \\
& \left. - \frac{X_{23}}{2} \theta_{Z1R} - V_{2R} \right) - C_{t2R} \left(\frac{dD_{23R}}{dt} - \frac{X_{23}}{2} \frac{d\theta_{Z1R}}{dt} - \frac{dV_{2R}}{dt} \right) \\
& - K_{t3R} \left(Y_{23R} + \frac{X_{23}}{2} \theta_{Z1R} - V_{3R} \right) - C_{t3R} \left(\frac{dY_{23R}}{dt} + \frac{X_{23}}{2} \frac{d\theta_{Z1R}}{dt} \right. \\
& \left. - \frac{dV_{3R}}{dt} \right) - M_{2R} \frac{d^2 Y_{23R}}{dt^2} - M_{3R} \frac{d^2 Y_{23R}}{dt^2} = 0
\end{aligned} \tag{4.83}$$

$$\begin{aligned}
& K_{s23L}(D_{23L} - Y_{23L}) + C_{s23L} \left(\frac{dD_{23L}}{dt} - \frac{dY_{23L}}{dt} \right) - K_{t2L} \left(Y_{23L} \right. \\
& \left. - \frac{X_{23}}{2} \theta_{Z1L} - V_{2L} \right) - C_{t2L} \left(\frac{dY_{23L}}{dt} - \frac{X_{23}}{2} \frac{d\theta_{Z1L}}{dt} - \frac{dV_{2L}}{dt} \right) \\
& - K_{t3L} \left(Y_{23L} + \frac{X_{23}}{2} \theta_{Z1L} - V_{3L} \right) - C_{t3L} \left(\frac{dY_{23L}}{dt} - \frac{X_{23}}{2} \frac{d\theta_{Z1L}}{dt} \right.
\end{aligned}$$

$$- \frac{dV_{3L}}{dt} \Big) - M_{2L} \frac{d^2 Y_{23L}}{dt^2} - M_{3L} \frac{d^2 Y_{23L}}{dt^2} = 0 \quad (4.84)$$

$$\begin{aligned} & \left(\frac{X_{23}}{2} \right) \left[Kt_{2R} \left(Y_{23R} - \frac{X_{23}}{2} \theta_{Z1R} - V_{2R} \right) + Ct_{2R} \left(\frac{dY_{23R}}{dt} \right. \right. \\ & \quad \left. \left. - \frac{X_{23}}{2} \frac{d\theta_{Z1R}}{dt} - \frac{dV_{2R}}{dt} \right) - Kt_{3R} \left(Y_{23R} + \frac{X_{23}}{2} \theta_{Z1R} - V_{3R} \right) \right. \\ & \quad \left. - Ct_{3R} \left(\frac{dY_{23R}}{dt} + \frac{X_{23}}{2} \frac{d\theta_{Z1R}}{dt} - \frac{dV_{3R}}{dt} \right) \right] I_{TZ1} \frac{d^2 \theta_{Z1R}}{dt^2} = 0 \quad (4.85) \end{aligned}$$

$$\begin{aligned} & \left(\frac{X_{23}}{2} \right) \left[Kt_{2L} \left(Y_{23L} - \frac{X_{23}}{2} \theta_{Z1L} - V_{2L} \right) + Ct_{2L} \left(\frac{dY_{23L}}{dt} \right. \right. \\ & \quad \left. \left. - \frac{X_{23}}{2} \frac{d\theta_{Z1L}}{dt} - \frac{dV_{2L}}{dt} \right) - Kt_{3L} \left(Y_{23L} + \frac{X_{23}}{2} \theta_{Z1L} - V_{3L} \right) \right. \\ & \quad \left. - Ct_{3L} \left(\frac{dY_{23L}}{dt} + \frac{X_{23}}{2} \frac{d\theta_{Z1L}}{dt} - \frac{dV_{3L}}{dt} \right) \right] - I_{TZ1} \frac{d^2 \theta_{Z1L}}{dt^2} = 0 \quad (4.86) \end{aligned}$$

$$\begin{aligned} & Ks_{45R} (D_{45R} - Y_{45R}) + Cs_{45R} \left(\frac{dD_{45R}}{dt} - \frac{dY_{45R}}{dt} \right) - Kt_{4R} \left(Y_{45R} \right. \\ & \quad \left. - \frac{X_{45}}{2} \theta_{Z2R} - V_{4R} \right) - Ct_{4R} \left(\frac{dY_{45R}}{dt} - \frac{X_{45}}{2} \frac{d\theta_{Z2R}}{dt} - \frac{dV_{4R}}{dt} \right) \\ & \quad - Kt_{5R} \left(Y_{45R} + \frac{X_{45}}{2} \theta_{Z2R} - V_{5R} \right) - Ct_{5R} \left(\frac{dY_{45R}}{dt} \right. \\ & \quad \left. + \frac{X_{45}}{2} \frac{d\theta_{Z2R}}{dt} - \frac{dV_{5R}}{dt} \right) - M_{4R} \frac{d^2 Y_{45R}}{dt^2} - M_{5R} \frac{d^2 Y_{45R}}{dt^2} = 0 \quad (4.87) \end{aligned}$$

$$\begin{aligned}
& K_{s45L} (D_{45L} - Y_{45L}) + C_{s45L} \left(\frac{dD_{45L}}{dt} - \frac{dY_{45L}}{dt} \right) - K_{t4L} \left(Y_{45L} \right. \\
& \left. - \frac{X_{45}}{2} \theta_{Z2L} - v_{4L} \right) - C_{t4L} \left(\frac{dY_{45L}}{dt} - \frac{X_{45}}{2} \frac{d\theta_{Z2L}}{dt} - \frac{dv_{4L}}{dt} \right) \\
& - K_{t5L} \left(Y_{45L} + \frac{X_{45}}{2} \theta_{Z2L} - v_{5L} \right) - C_{t5L} \left(\frac{dY_{45L}}{dt} \right. \\
& \left. + \frac{X_{45}}{2} \frac{d\theta_{Z2L}}{dt} - \frac{dv_{5L}}{dt} \right) - M_{4L} \frac{d^2 Y_{45L}}{dt^2} - M_{5L} \frac{d^2 Y_{45L}}{dt^2} = 0 \quad (4.88)
\end{aligned}$$

$$\begin{aligned}
& \left(\frac{X_{45}}{2} \right) \left[K_{t4R} \left(Y_{45R} - \frac{X_{45}}{2} \theta_{Z2R} - v_{4R} \right) + C_{t4R} \left(\frac{dY_{45R}}{dt} \right. \right. \\
& \left. \left. - \frac{X_{45}}{2} \frac{d\theta_{Z2R}}{dt} - \frac{dv_{4R}}{dt} \right) - K_{t5R} \left(Y_{45R} + \frac{X_{45}}{2} \theta_{Z2R} - v_{5R} \right) \right. \\
& \left. - C_{t5R} \left(\frac{dY_{45R}}{dt} + \frac{X_{45}}{2} \frac{d\theta_{Z2R}}{dt} - \frac{dv_{5R}}{dt} \right) \right] \\
& - I_{TZ2} \frac{d^2 \theta_{Z2R}}{dt^2} = 0 \quad (4.89)
\end{aligned}$$

$$\begin{aligned}
& \left(\frac{X_{45}}{2} \right) \left[K_{t4L} \left(Y_{45L} - \frac{X_{45}}{2} \theta_{Z2L} - v_{4L} \right) + C_{t4L} \left(\frac{dY_{45L}}{dt} \right. \right. \\
& \left. \left. - \frac{X_{45}}{2} \frac{d\theta_{Z2L}}{dt} - \frac{dv_{4L}}{dt} \right) - K_{t5L} \left(Y_{45L} + \frac{X_{45}}{2} \theta_{Z2L} - v_{5L} \right) \right. \\
& \left. - C_{t5L} \left(\frac{dY_{45L}}{dt} + \frac{X_{45}}{2} \frac{d\theta_{Z2L}}{dt} - \frac{dv_{5L}}{dt} \right) \right] \\
& - I_{TZ2} \frac{d^2 \theta_{Z2L}}{dt^2} = 0 \quad (4.90)
\end{aligned}$$

Solution of Equations of Motion

In many practical problems such as the one under discussion, a closed-form solution is a lengthy and time-consuming process, and often is not possible. When such cases arise, numerical techniques are used to obtain approximate and reasonable solutions to these problems.

M. N. Newmark, in his paper entitled "A Method of Computation for Structural Dynamics" (Ref 30), described a procedure which may be used in solving the relationships between forces and displacements for structures with varying degrees of elastic and inelastic behavior.

This method has been selected for solving the equations of motion derived in the preceding section.

The procedure is based on the assumption that the displacements, the velocities, and the accelerations of the system are known at any particular time t_i . The values of these variables at time t_{i+1} where

$$t_{i+1} - t_i = h$$

are determined from the following relationship:

$$\left(\frac{dy}{dt} \right)_{i+1} = \left(\frac{dy}{dt} \right)_i + h(1 - \nu) \left(\frac{d^2y}{dt^2} \right)_i + h\nu \left(\frac{d^2y}{dt^2} \right)_{i+1} \quad (4.91)$$

and

$$\begin{aligned} (y)_{i+1} = & (y)_i + h \left(\frac{dy}{dt} \right)_i + h^2 \left(\frac{1}{2} - \beta \right) \left(\frac{d^2y}{dt^2} \right)_i \\ & + h^2 \beta \left(\frac{d^2y}{dt^2} \right)_{i+1} \end{aligned} \quad (4.92)$$

Newmark (Ref 30) has shown that a false damping will be introduced merely from the numerical procedure if ν is not taken as 1/2. Thus, with ν equal to 1/2, Eq 4.91 reduces to:

$$\left(\frac{dy}{dt} \right)_{i+1} = \left(\frac{dy}{dt} \right)_i + \frac{h}{2} \left(\frac{d^2y}{dt^2} \right)_i + \frac{h}{2} \left(\frac{d^2y}{dt^2} \right)_{i+1} \quad (4.93)$$

A β -value equal to 1/6 which corresponds to a linear variation of acceleration in the time interval was chosen for this study. The time increment h may be taken as approximately 1/5 to 1/6 of the shortest period of oscillation to assure convergence and stability of the solution. Obviously, more refined solutions may be obtained with shorter increments. For the purpose of solving the sets of equations of the generalized model described herein, the value of h depends on the speed of the vehicle. An increment of time equal to the time required for the wheel to travel a distance of 1 inch. or 0.001 second, whichever is less has been used. This criterion keeps the h -value within the ranges required for convergence and stability.

The procedure used is outlined as follows:

- (1) Assume a value for the acceleration of each mass.
- (2) Calculate the velocity and displacement for each mass by using Eqs 4.93 and 4.92, respectively.
- (3) Calculate the acceleration from the differential equation of motion.
- (4) Compare the calculated acceleration and the assumed acceleration.
- (5) Stop if the computed acceleration is equal to the assumed acceleration within a reasonable tolerance limit (10^{-6} has been used); the solution has been reached. If these are not equal, repeat step (1) above, using the calculated acceleration as a new assumed acceleration.

In case of excessive excitation any individual tire may lose contact with the road; therefore, provisions were made to eliminate tensile forces acting on the tires.

Dynamic Wheel Loads. Once the vertical translation of the tires is determined, the dynamic force components may be evaluated. Equations 4.94 through 4.115 give the expressions for the dynamic wheel forces. In order to avoid unnecessary repetition, the subscript on the parenthesis indicates the class of vehicle. Thus $(F_{DY1R})_{I...V}$ is the dynamic force at the right side of axle 1 for Class I through Class V; while $(F_{DY4R})_V$ is the dynamic force at the right side of axle 4 for Class V only, etc.

$$\left(F_{DY1R} \right)_{I...V} = Kt_{1R} (V_{1R} - Y_{1R}) + Ct_{1R} \left(\frac{dV_{1R}}{dt} - \frac{dY_{1R}}{dt} \right) \quad (4.94)$$

$$\left(F_{DY1L} \right)_{I \dots V} = Kt_{1L}(V_{1L} - Y_{1L}) + Ct_{1L} \left(\frac{dV_{1L}}{dt} - \frac{dY_{1L}}{dt} \right) \quad (4.95)$$

$$\left(F_{DY2R} \right)_{I, II, IV} = Kt_{2R}(V_{2R} - Y_{2R}) + Ct_{2R} \left(\frac{dV_{2R}}{dt} - \frac{dY_{2R}}{dt} \right) \quad (4.96)$$

$$\left(F_{DY2L} \right)_{I, II, IV} = Kt_{2L}(V_{2L} - Y_{2L}) + Ct_{2L} \left(\frac{dV_{2L}}{dt} - \frac{dY_{2L}}{dt} \right) \quad (4.97)$$

$$\left(F_{DY3R} \right)_{II} = Kt_{3R}(V_{3R} - Y_{3R}) + Ct_{3R} \left(\frac{dV_{3R}}{dt} - \frac{dY_{3R}}{dt} \right) \quad (4.98)$$

$$\left(F_{DY3L} \right)_{II} = Kt_{3L}(V_{3L} - Y_{3L}) + Ct_{3L} \left(\frac{dV_{3L}}{dt} - \frac{dY_{3L}}{dt} \right) \quad (4.99)$$

$$\begin{aligned} \left(F_{DY2R} \right)_{III} &= Kt_{2R} \left(V_{2R} - Y_{23R} + \frac{X_{23}}{2} \theta_{ZR} \right) \\ &+ Ct_{2R} \left(\frac{dV_{2R}}{dt} - \frac{dY_{23R}}{dt} + \frac{X_{23}}{2} \frac{d\theta_{ZR}}{dt} \right) \end{aligned} \quad (4.100)$$

$$\begin{aligned} \left(F_{DY2L} \right)_{III} &= Kt_{2L} \left(V_{2L} - Y_{23L} + \frac{X_{23}}{2} \theta_{ZL} \right) \\ &+ Ct_{2L} \left(\frac{dV_{2L}}{dt} - \frac{dY_{23L}}{dt} + \frac{X_{23}}{2} \frac{d\theta_{ZL}}{dt} \right) \end{aligned} \quad (4.101)$$

$$\begin{aligned} \left(F_{DY3R} \right)_{III} &= Kt_{3R} \left(V_{3R} - Y_{23R} - \frac{X_{23}}{2} \theta_{ZR} \right) \\ &+ Ct_{3R} \left(\frac{dV_{3R}}{dt} - \frac{dY_{23R}}{dt} - \frac{X_{23}}{2} \frac{d\theta_{ZR}}{dt} \right) \end{aligned} \quad (4.102)$$

$$\begin{aligned} \left(F_{DY3L} \right)_{III} &= Kt_{3L} \left(v_{3L} - Y_{23L} - \frac{X_{23}}{2} \theta_{ZL} \right) \\ &+ Ct_{3L} \left(\frac{dv_{3L}}{dt} - \frac{dY_{23L}}{dt} - \frac{X_{23}}{2} \frac{d\theta_{ZL}}{dt} \right) \end{aligned} \quad (4.103)$$

$$\begin{aligned} \left(F_{DY3R} \right)_{IV} &= Kt_{3R} \left(v_{3R} - Y_{34R} + \frac{X_{34}}{2} \theta_{ZR} \right) \\ &+ Ct_{3R} \left(\frac{dv_{3R}}{dt} - \frac{dY_{34R}}{dt} + \frac{X_{34}}{2} \frac{d\theta_{ZR}}{dt} \right) \end{aligned} \quad (4.104)$$

$$\begin{aligned} \left(F_{DY3L} \right)_{IV} &= Kt_{3L} \left(v_{3L} - Y_{34L} + \frac{X_{34}}{2} \theta_{ZR} \right) \\ &+ Ct_{3L} \left(\frac{dv_{3L}}{dt} - \frac{dY_{34L}}{dt} + \frac{X_{34}}{2} \frac{d\theta_{ZR}}{dt} \right) \end{aligned} \quad (4.105)$$

$$\begin{aligned} \left(F_{DY4R} \right)_{IV} &= Kt_{4R} \left(v_{4R} - Y_{34R} - \frac{X_{34}}{2} \theta_{ZR} \right) \\ &+ Ct_{4R} \left(\frac{dv_{4R}}{dt} - \frac{dY_{34R}}{dt} - \frac{X_{34}}{2} \frac{d\theta_{ZR}}{dt} \right) \end{aligned} \quad (4.106)$$

$$\begin{aligned} \left(F_{DY4L} \right)_{IV} &= Kt_{4L} \left(v_{4L} - Y_{34L} - \frac{X_{34}}{2} \theta_{ZL} \right) \\ &+ Ct_{4L} \left(\frac{dv_{4L}}{dt} - \frac{dY_{34L}}{dt} - \frac{X_{34}}{2} \frac{d\theta_{ZL}}{dt} \right) \end{aligned} \quad (4.107)$$

$$\left(F_{DY2R} \right)_V = Kt_{2R} \left(v_{2R} - Y_{23R} + \frac{X_{23}}{2} \theta_{Z1R} \right)$$

$$+ Ct_{2R} \left(\frac{dV_{2R}}{dt} - \frac{dY_{23R}}{dt} + \frac{X_{23}}{2} \frac{d\theta_{Z1R}}{dt} \right) \quad (4.108)$$

$$\begin{aligned} \left(F_{DY2L} \right)_V &= Kt_{2L} \left(V_{2L} - Y_{23L} + \frac{X_{23}}{2} \theta_{Z1L} \right) \\ &+ Ct_{2L} \left(\frac{dV_{2L}}{dt} - \frac{dY_{23L}}{dt} + \frac{X_{23}}{2} \frac{d\theta_{Z1L}}{dt} \right) \end{aligned} \quad (4.109)$$

$$\begin{aligned} \left(F_{DY3R} \right)_V &= Kt_{3R} \left(V_{3R} - Y_{23L} - \frac{X_{23}}{2} \theta_{Z1R} \right) \\ &+ Ct_{3R} \left(\frac{dV_{3R}}{dt} - \frac{dY_{23R}}{dt} - \frac{X_{23}}{2} \frac{d\theta_{Z1R}}{dt} \right) \end{aligned} \quad (4.110)$$

$$\begin{aligned} \left(F_{DY3L} \right)_V &= Kt_{3L} \left(V_{3L} - Y_{23L} - \frac{X_{23}}{2} \theta_{Z1L} \right) \\ &+ Ct_{3L} \left(\frac{dV_{3L}}{dt} - \frac{dY_{23L}}{dt} - \frac{X_{23}}{2} \frac{d\theta_{Z1L}}{dt} \right) \end{aligned} \quad (4.111)$$

$$\begin{aligned} \left(F_{DY4R} \right)_V &= Kt_{4R} \left(V_{4R} - Y_{45R} + \frac{X_{45}}{2} \theta_{Z2R} \right) \\ &+ Ct_{4R} \left(\frac{dV_{4R}}{dt} - \frac{dY_{45R}}{dt} + \frac{X_{45}}{2} \frac{d\theta_{Z2R}}{dt} \right) \end{aligned} \quad (4.112)$$

$$\begin{aligned} \left(F_{DY4L} \right)_V &= Kt_{4L} \left(V_{4L} - Y_{45L} + \frac{X_{45}}{2} \theta_{Z2L} \right) \\ &+ Ct_{4L} \left(\frac{dV_{4L}}{dt} - \frac{dY_{45L}}{dt} + \frac{X_{45}}{2} \frac{d\theta_{Z2L}}{dt} \right) \end{aligned} \quad (4.113)$$

$$\begin{aligned} \left(F_{DY5R} \right)_V &= Kt_{5L} \left(v_{5R} - Y_{45R} - \frac{X_{45}}{2} \theta_{Z2R} \right) \\ &+ Ct_{4R} \left(\frac{dv_{5R}}{dt} - \frac{dY_{45R}}{dt} - \frac{X_{45}}{2} \frac{d\theta_{Z2R}}{dt} \right) \end{aligned} \quad (4.114)$$

$$\begin{aligned} \left(F_{DY5L} \right)_V &= Kt_{5L} \left(v_{5L} - Y_{45L} - \frac{X_{45}}{2} \theta_{Z2L} \right) \\ &+ Ct_{4L} \left(\frac{dv_{5L}}{dt} - \frac{dY_{45L}}{dt} - \frac{X_{45}}{2} \frac{d\theta_{Z2L}}{dt} \right) \end{aligned} \quad (4.115)$$

After the dynamic force components are calculated for each wheel, the total dynamic wheel load may be determined by simply adding the static and the dynamic force components. For axle 1, these loads are given by

$$F_{TO1R} = F_{DY1R} + F_{ST1R} \quad (4.116)$$

$$F_{TO1L} = F_{DY1L} + F_{ST1L} \quad (4.117)$$

The total loads for the remaining axles are determined in similar fashion.

Description of the Computer Program

After the development of the model was completed, a computer program "DYMOL" was written in FORTRAN language for CDC 6600 available at the time through the computer facilities of The University of Texas at Austin. The program consists of eight subroutines which are monitored by a main driver routine. The solution of each set of differential equations describing the motion of each class of vehicles and the calculation of forces for that class are handled by separate subroutines. These subroutines are named CLASS I, CLASS II, CLASS III, CLASS IV, and CLASS V. In addition PROGRAM DYMOL provides two alternative forcing functions for the model: (1) the model may be forced by an artificial profile, or (2) the model may be forced by a natural profile. Each of these two alternatives is discussed briefly below.

Artificial Profile. The subroutine that generates this artificial profile is ARTPROF. The profile may be generated as a series of bumps placed on a smooth surface. The number, placement, and spacing may be varied for each of the left and right wheel paths independently. The bumps are then converted to full or half sine waves as desired. Once the characteristics of an artificial profile are specified, elevations with respect to a horizontal smooth condition are calculated at each step increment h , by subroutine ARTPROF for a maximum of 3,000 increments corresponding to profile distances of 250, 132, and 44 feet for speeds of 50, 30, and 10 miles per hour, respectively. These elevations are then used as road excitation inputs for the model. An example of such an artificial road profile for a Class V vehicle is shown in Fig 14.

Natural Profile. A more realistic prediction of the dynamic wheel loads would be one based on natural profile excitations.

The high-speed Surface Dynamics Road Profilometer (Fig 15) (improved GMR Profilometer) was available for measuring and evaluating profile characteristics. This device was used periodically in measuring the profile of the test section for subsequent use with the mathematical model. The subroutine that handles natural profile input is NATPROF subroutine.

The DYMOL program is summarized in Fig 16. A complete flow diagram, FORTRAN listing, input guide, and an example run with coded input and sample output are on file at the Center for Highway Research.

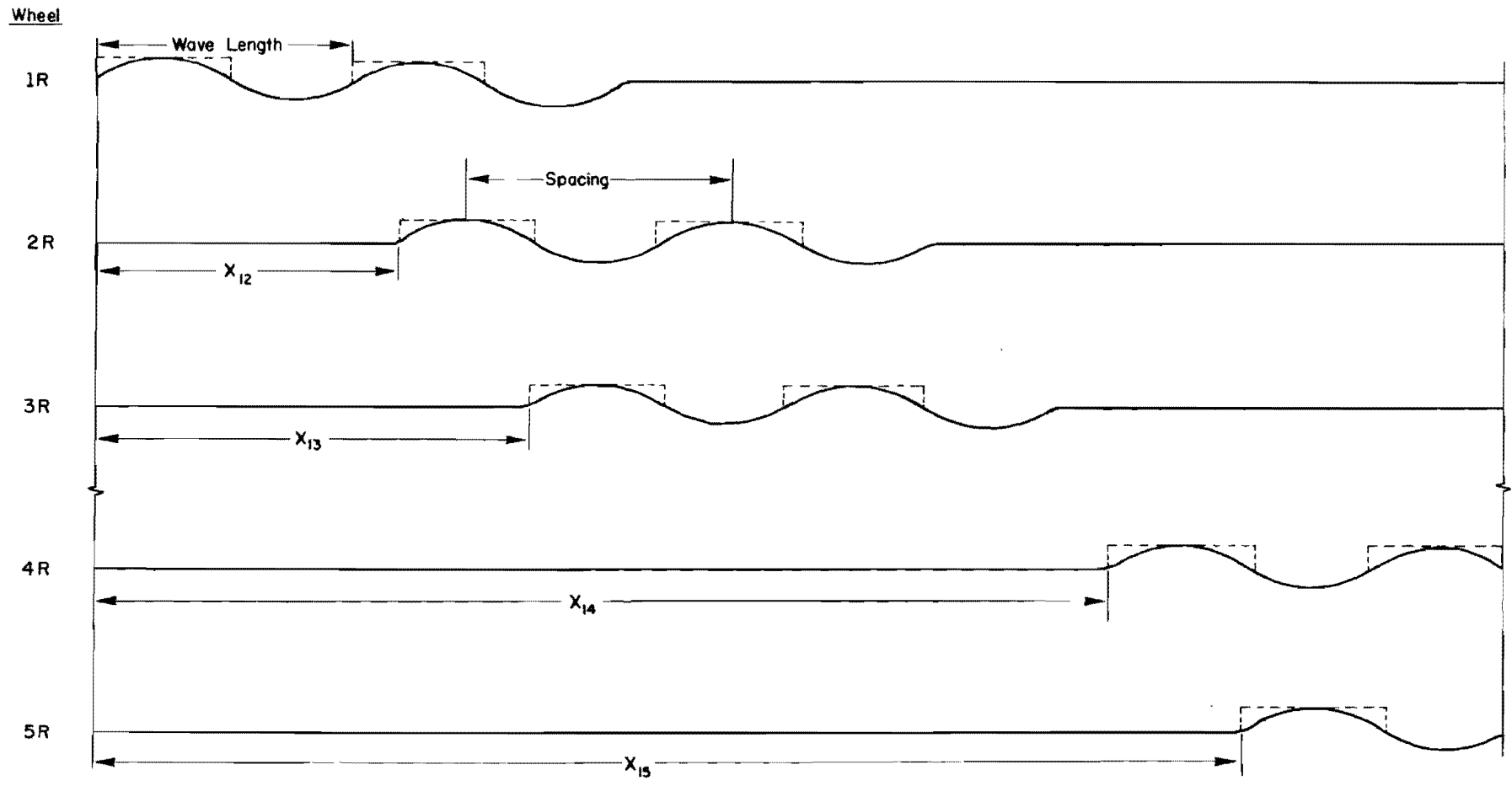


Fig 14. Artificial profile example.

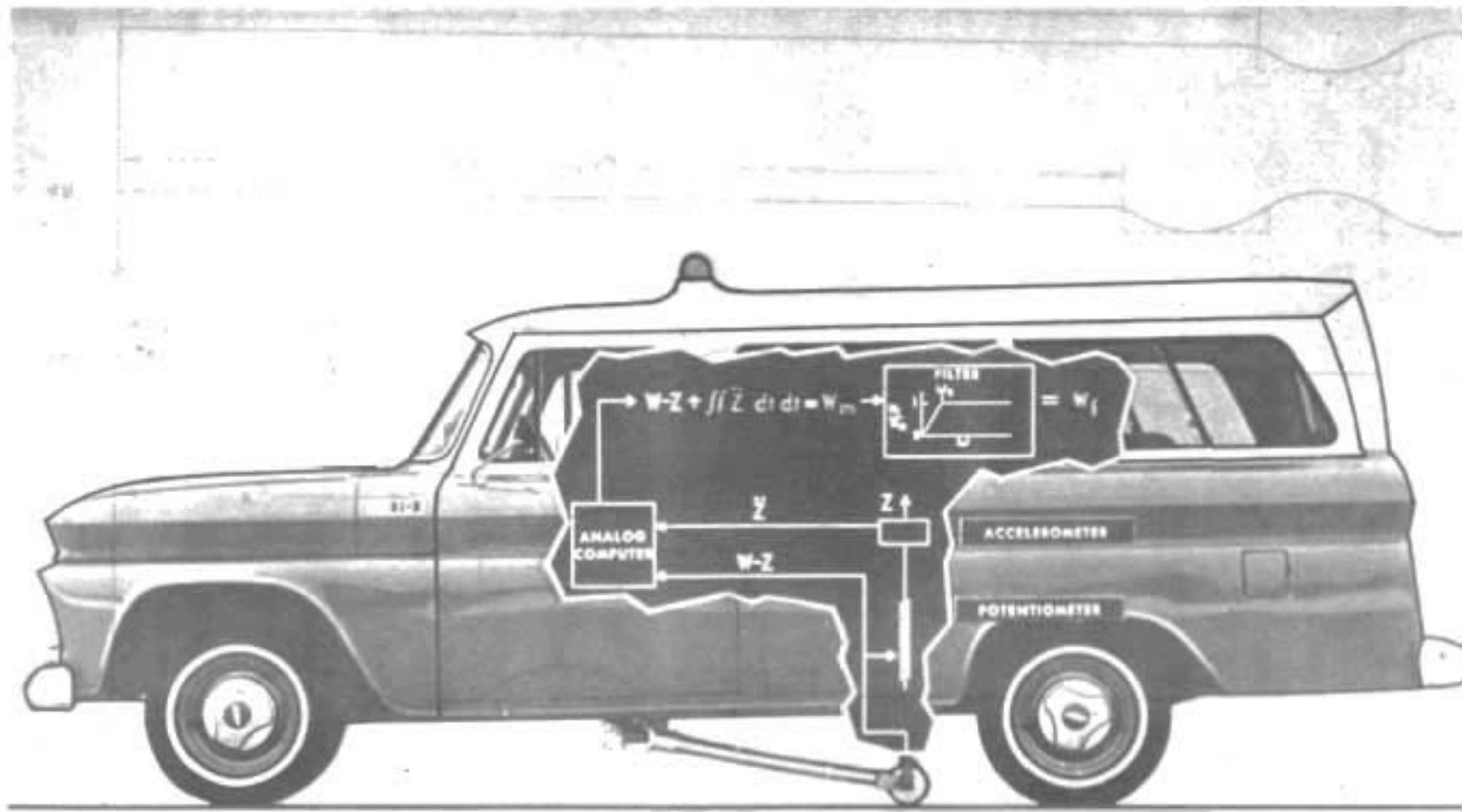


Fig 15. Surface dynamics road profilometer (Ref 25).

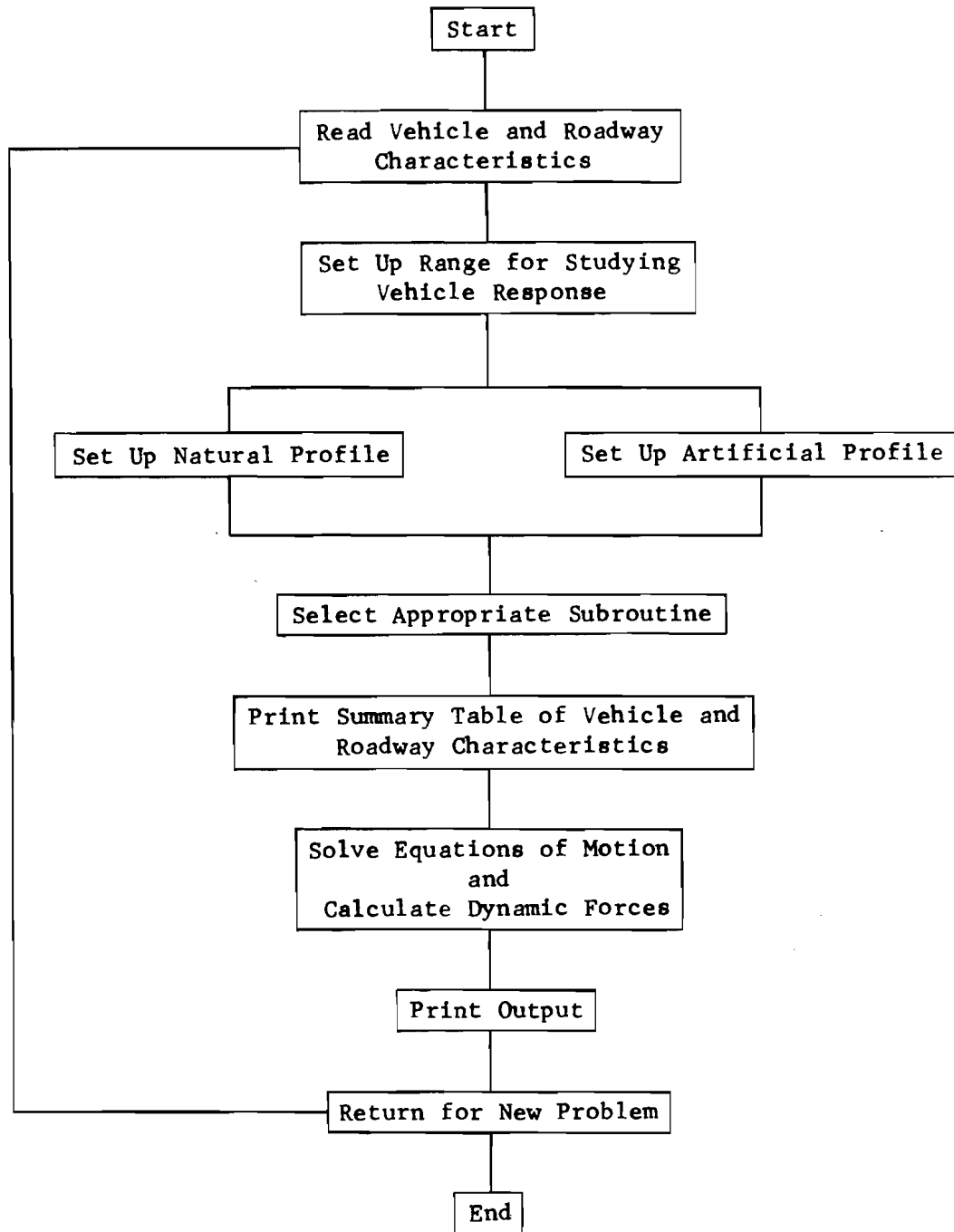


Fig 16. Summary flow of program DYMOL.

This page replaces an intentionally blank page in the original.

-- CTR Library Digitization Team

CHAPTER 5. MEASUREMENT OF MOVING WHEEL LOAD FORCES

General

The first step in the experimental phase of this investigation was to choose a technique for measuring the forces applied to the pavement by a moving wheel. Several investigators have used on-board measuring techniques (Refs 20 and 21). Although these techniques have the advantage of providing continuous records of measured wheel forces, they are not practical when several multi-wheeled test vehicles are involved or when the dynamic wheel loads of mixed traffic need to be measured. The other alternative is to place in the pavement several wheel load sensing devices, or scales, which are capable of measuring moving wheel loads. The development of such devices has been the major concern in a number of research efforts both in the United States and abroad. Attempts at developing an in-motion weighing system were reported by Norman and Hopkins (Ref 31) in the early 1950's. Their work resulted in the development of a scale platform made of a reinforced concrete slab measuring 3 feet by 10 feet in plan dimension and 12-inches deep. The slab was supported by four conventional load cells housed in a pit under the road. This scale design was slightly modified and used experimentally in Europe (Ref 3) and in the United States (Ref 39). Successful operation of these scales, however, has been hampered by a number of inherent inadequacies in the general design such as the inertia of the heavy slab and its adverse effects on the response of the scale system to rapidly varying dynamic wheel forces.

To be suitable for the research described herein, a scale system must have certain characteristics. These include such properties as portability, good compliance, insensitivity to tractive forces, uniform sensitivity to normal forces over the entire platform, ruggedness, reliability, fast response, ease of installation and maintenance, and reasonable cost. The only known portable scale satisfying the criteria suggested above and capable of sensing the dynamic forces which are applied normal to the roadway surface of a wheel of a vehicle moving at speeds up to 70 miles per hour has been developed by the Center for Highway Research at

The University of Texas at Austin. A comprehensive description of the development of this scale system is included in Research Report No. 54-F of the Center for Highway Research entitled "A Portable Electronic Scale for Weighing Vehicles in Motion" by Clyde E. Lee and Nasser I. Al-Rashid (Ref 26).

This chapter is devoted to a brief description of the basic design of this scale which was used and successively improved during the course of the experimental phase of this research program. In addition a description of the revised design details is included.

Wheel Load Transducer

The normal component of the wheel load forces acting on the pavement is detected by means of the wheel load transducer, which is the load sensing element of the dynamic scale system. These forces are converted into corresponding electrical signals ready for conditioning and recording. The major factors considered in the basic design of the transducer are size, portability, ruggedness, sensitivity, response, and capability of producing electrical signals that faithfully represent the magnitude of the applied forces.

Design Description

The wheel load transducer design has passed through several stages of improvements. The most recent design constructed in 1968 by Rainhart Company of Austin, Texas, whose product designer, Ed Hamilton, collaborated in the design improvements is shown in Figs 17 through 22. This design which is designated as Model 880 by Rainhart Company is 22 inches by 54 inches in plan dimension and about 2-1/2-inches thick. The most significant features of the transducer are the following (Ref 26).

Frame and Bearing Pads. The skeleton of the transducer is a rectangular steel frame shown in Fig 18. Eight cast aluminum bearing pads are held in position relative to the frame by a temporary jig while the frame and bearing pads are positioned in a thin layer of fresh concrete grout. The long sides of the frame extend about 3 inches into the pavement beyond the ends of the transducer in order to provide for additional anchorage and stability of the frame. After the grout is set, the jig is removed thus leaving the frame and the bearing pads supported independently in the hardened grout.

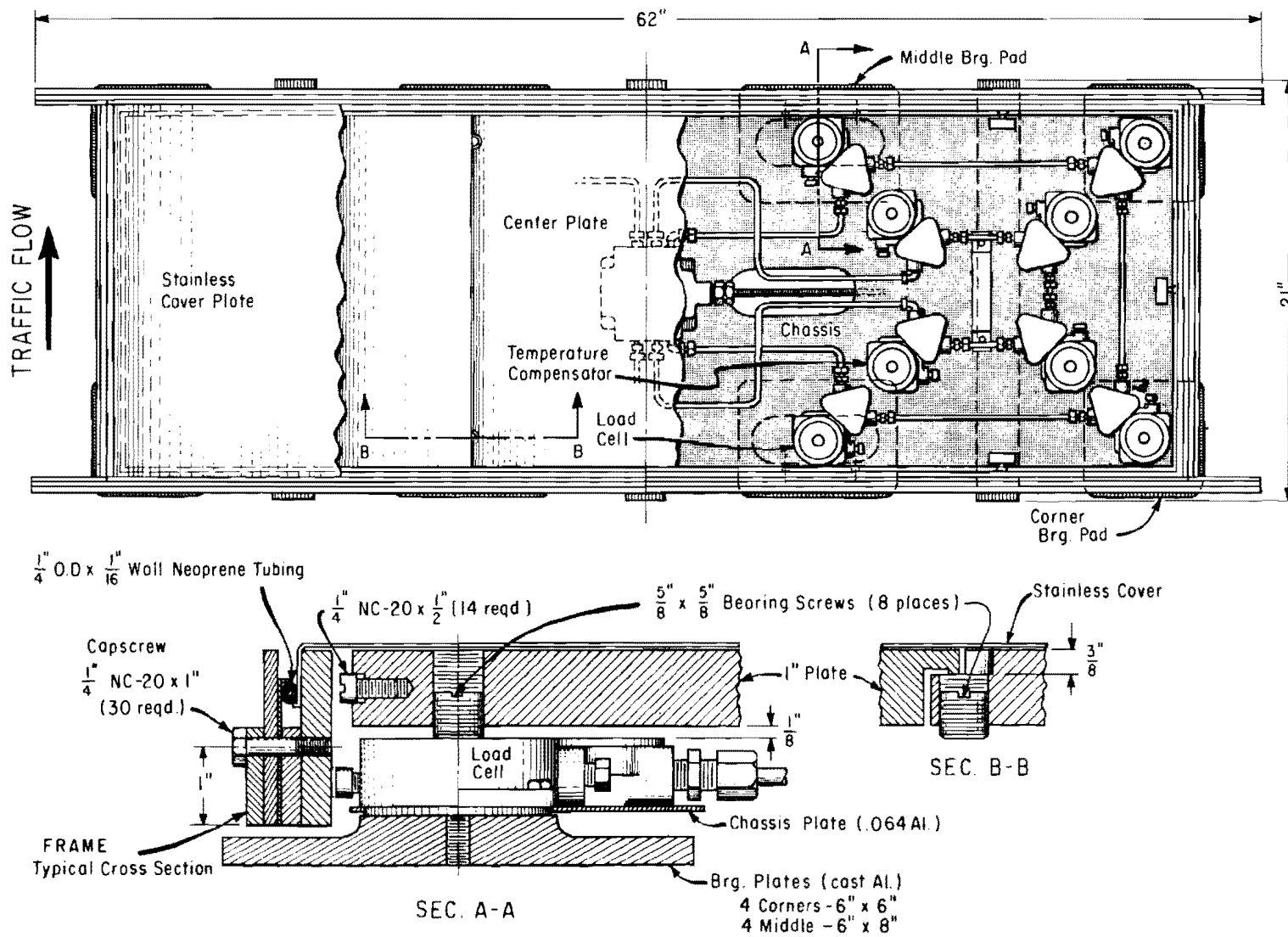


Fig 17. Cutaway top view sections of Model 880 transducer.

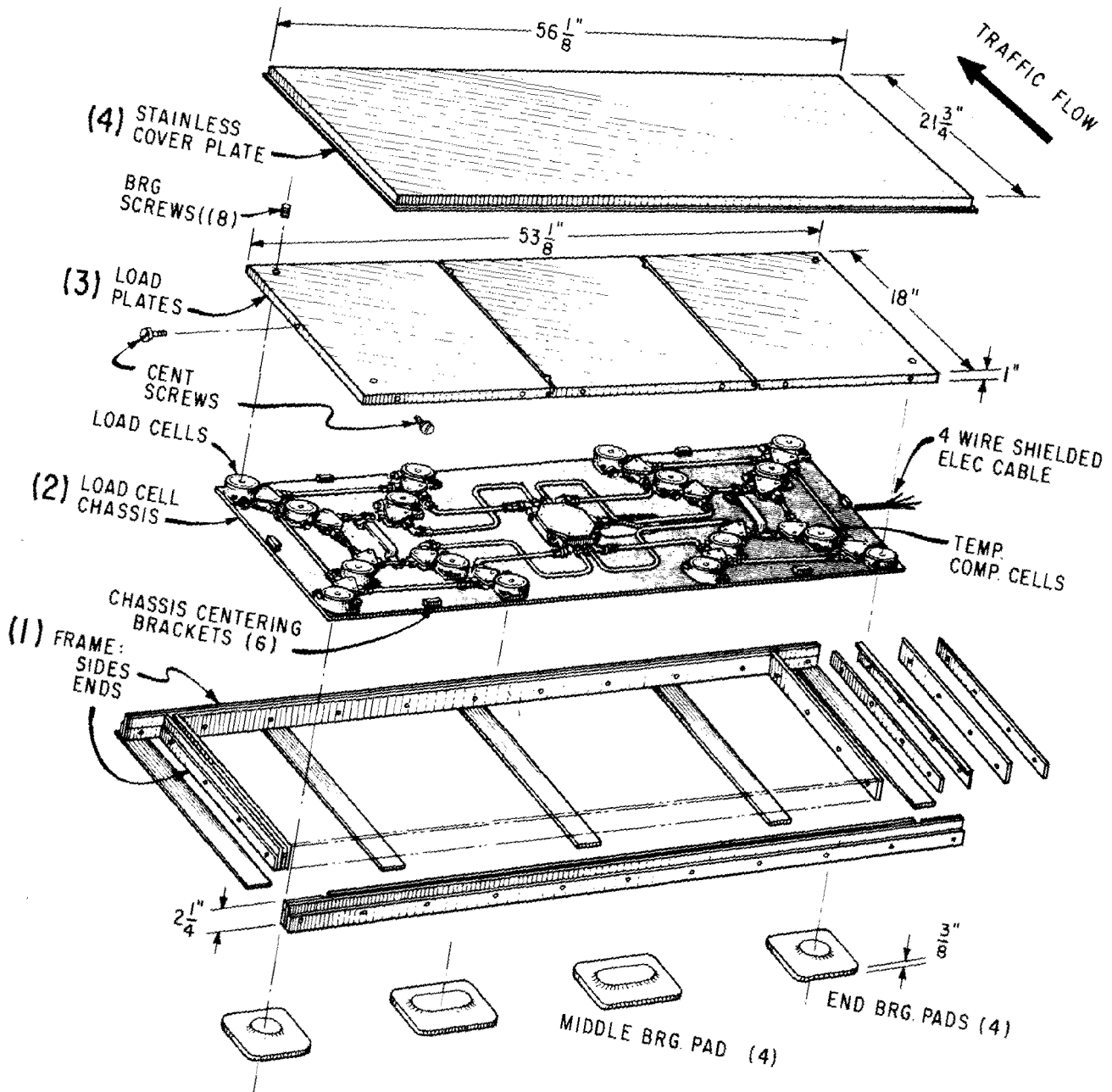


Fig 18. Exploded view of Model 880 transducer.

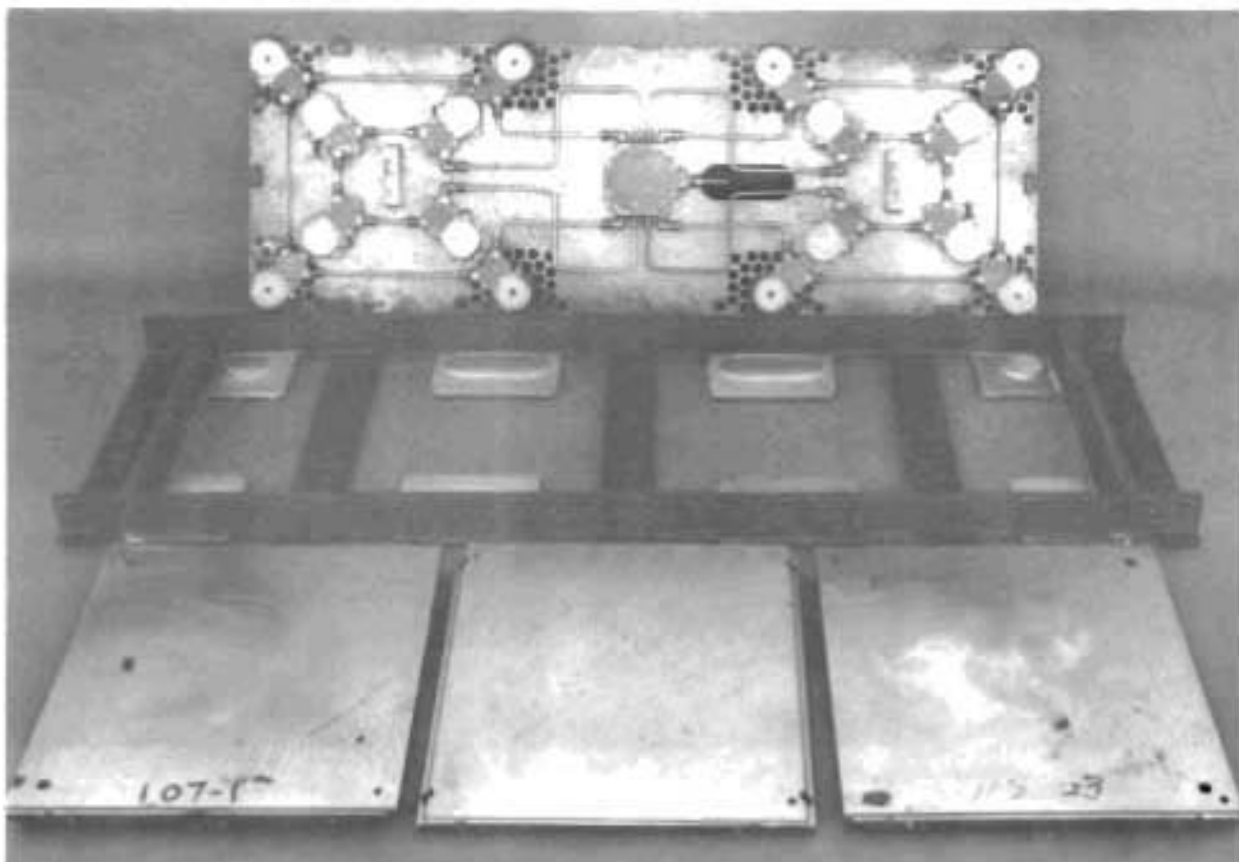


Fig 19. Components of Model 880 transducer.

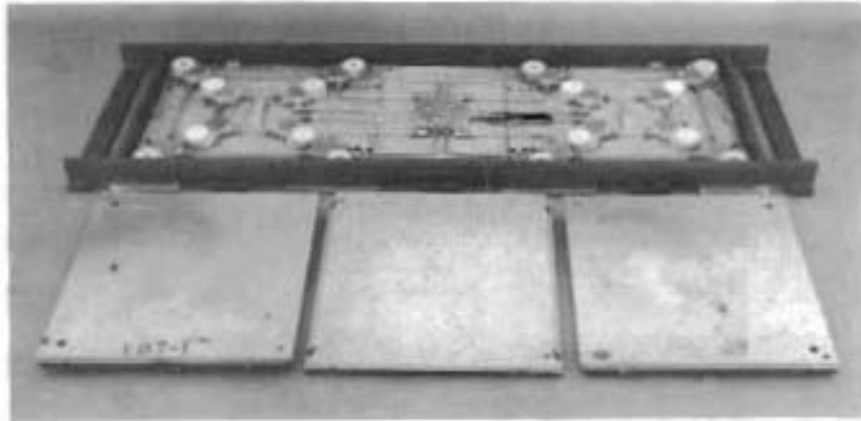


Fig 20. Load cell chassis placed in frame.

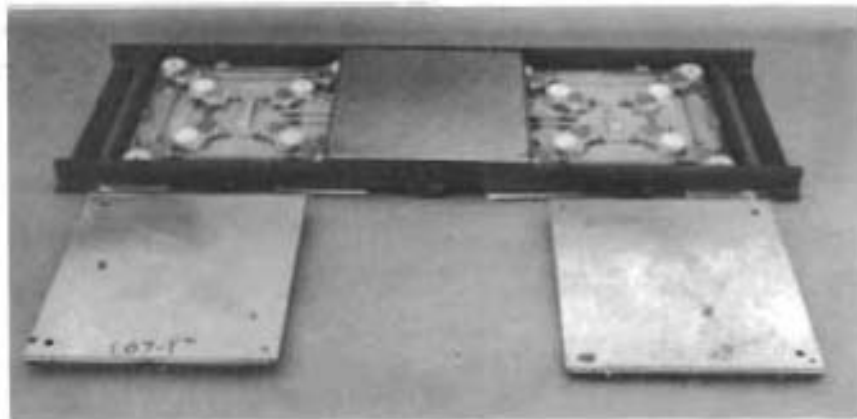


Fig 21. Center structural plate in place.

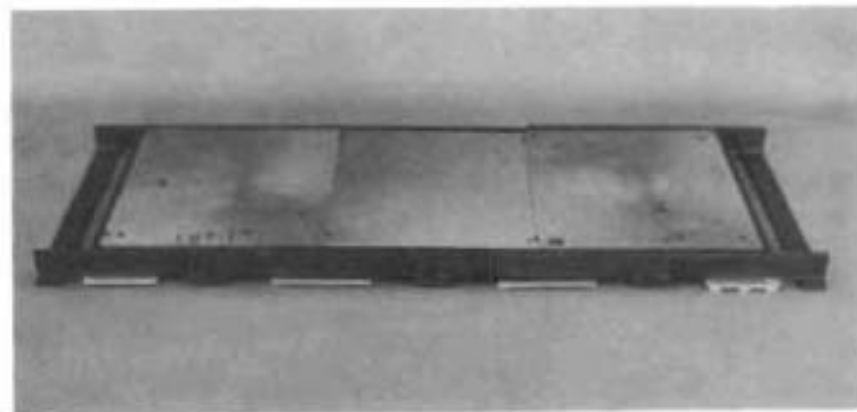


Fig 22. Assembled unit.

Sealing. Moisture has adverse effects on load cells and electrical leads. Early designs of the transducer provided for a single completely sealed unit; but maintenance and servicing of that unit was difficult and time consuming. Instead, a drain pipe extending from the unit to the road side is provided in this recent design, and each load cell is tightly sealed in a special aluminum casting. The electrical leads are housed in 1/4-inch copper tubing connected to the castings by means of threaded connectors.

Load Cell Chassis. This is a thin aluminum sheet with eight uniquely-designed bonded resistance foil strain gage load cells fixed to it in proper horizontal reference to the bearing pads. The load cells all have approximately the same initial electrical resistance and are connected in series such that a full Wheatstone bridge is formed with four active load cells in each of two opposite arms and four temperature-compensating gages in each of the remaining two arms (see Fig 23).

The magnitude of an applied load is indicated by the change in resistance of a strain gage element cemented to the body of the load cell. But since temperature changes also induce changes in resistance, it is necessary to offset the effects of temperature change by incorporating identical gages not subjected to load into the bridge circuit. This is the function of the temperature-compensating gages. The design, calibration, and matching of the load cells is described in the next section.

Structural Plates. Three structural steel plates 18 inches by 18 inches in plan dimension and 1-inch thick are used to transfer the load from the tire to the load cells. The center plate is supported at each corner by the four central load cells. This arrangement prevents uplift of the remaining plates if only one plate is loaded. Each plate weighs 90 pounds.

Leveling Screws. At each corner of the center plate and at the outer corners of the side plates, a hardened steel leveling screw bears on the spherical boss of the load cell. The purpose of these screws is to permit vertical adjustment of the structural plates with respect to the pavement surface and to provide uniform contact with the load cells.

Top Cover. This is a thin stainless steel sheet cover which was placed over the structural plates in order to eliminate or reduce tractive forces and to prevent water and deleterious debris from entering the assembled unit.

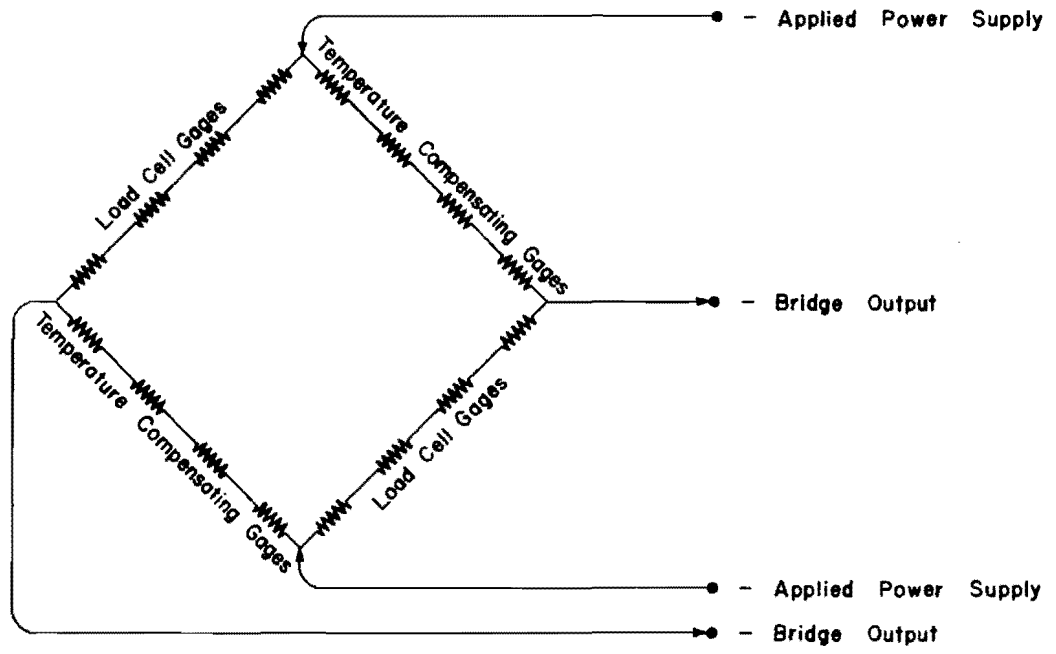


Fig 23. Wheatstone bridge circuit.

Load Cells

In the preceding section, it was mentioned that the load cells are of unique and special design. Basically, the most important characteristics of the design is the size, quick response, and the capability of the load cell to support and withstand loads up to 12,000 pounds.

The applied loads have extremely short durations, in the order of a few milliseconds, thus requiring that the load cell have a quick response. The cell consists of a circular diaphragm 1.000 inch in diameter and 0.150-inch thick and with a 120-ohm spiral etched-foil strain gage cemented to the plane surface of the diaphragm. A stiff ring 0.400-inch thick and 1.980 inches in outside diameter is made composite with the diaphragm. The load transfer to the cell is through a spherical boss 0.500 inch in diameter. These and other details of the cell are shown in Fig 24. Also shown in Fig 25 is the top and bottom views of the load cell and the special aluminum casting. The strain gage is coated with an epoxy sealant and a layer of room-temperature-vulcanized rubber for protection against moisture.

The load cells are manufactured in quantities and calibrated individually in the laboratory under static load. The calibration was accomplished by connecting the cell as an active arm in a standard Wheatstone bridge circuit powered with a constant 6-volt D.C. in order to provide the same current condition used in the wheel load transducer. The cell was then loaded to 8,000 pounds through a standard double bridge Ormond load cell with 0.25 percent accuracy and 10,000-pound capacity. A Servo-controlled hydraulic loading system was used to apply the load. After each 2-kip increment the load was held for a few moments before the next increment was added.

After the load of 8,000 pounds was reached the cell was unloaded so that hysteresis effects could be detected. The output of both the load cell and the Ormond load cell were plotted on an X-Y plotter (see Fig 26). At each 2-kip increment the output of the load cell was also printed by means of a data logging system with 0.10 percent accuracy. The sensitivity of each load cell, in pounds per millivolt, was calculated. A computer program was written for calculating these sensitivities and selecting groups of eight cells, with approximately the same sensitivities, to be used in a single transducer. The program first calculates the sensitivities, arranges the load cells in order of their sensitivities, selects groups of eight cells, and finally divides each

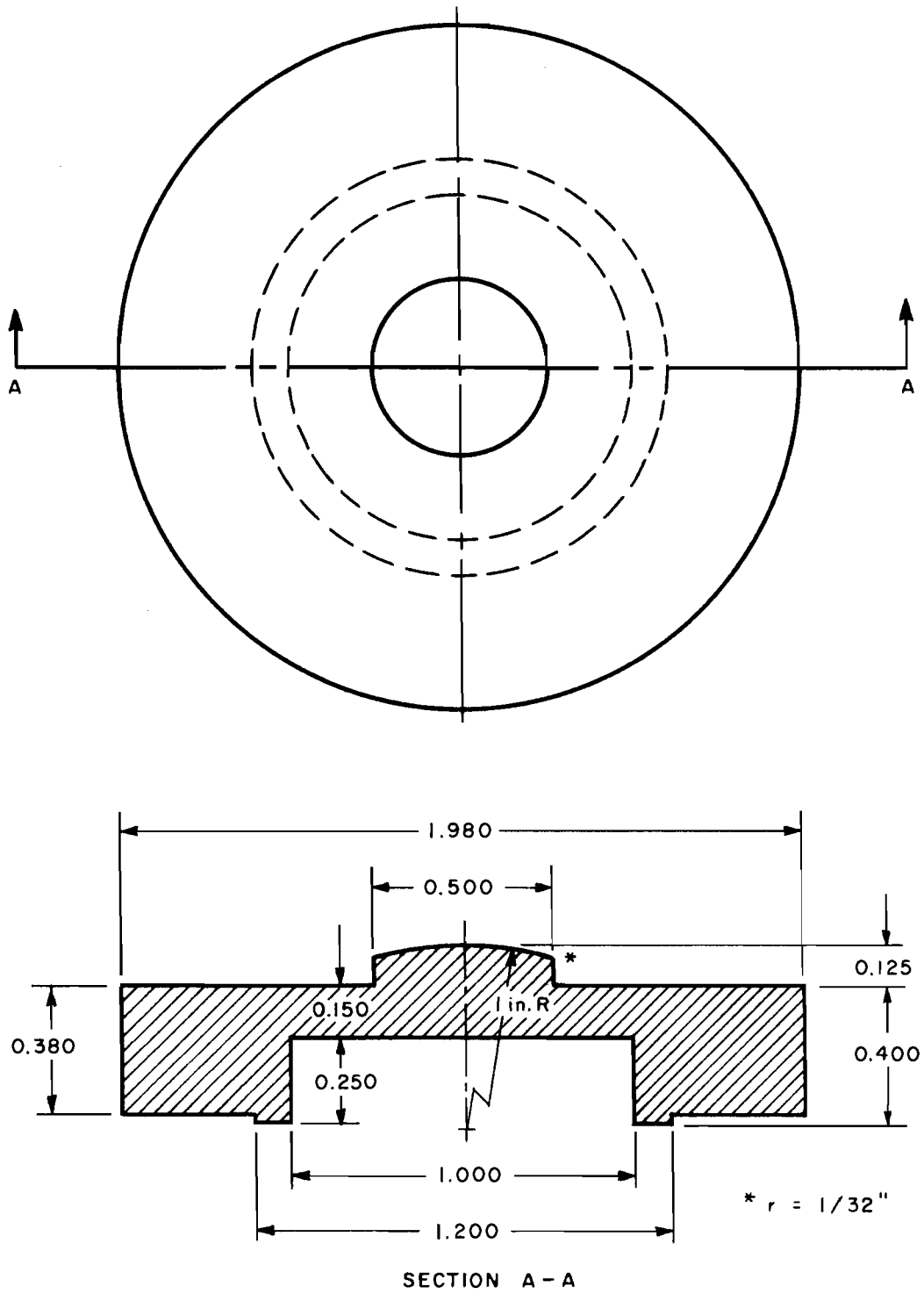


Fig 24. Top view and section showing dimensions of load cell (Ref 26).

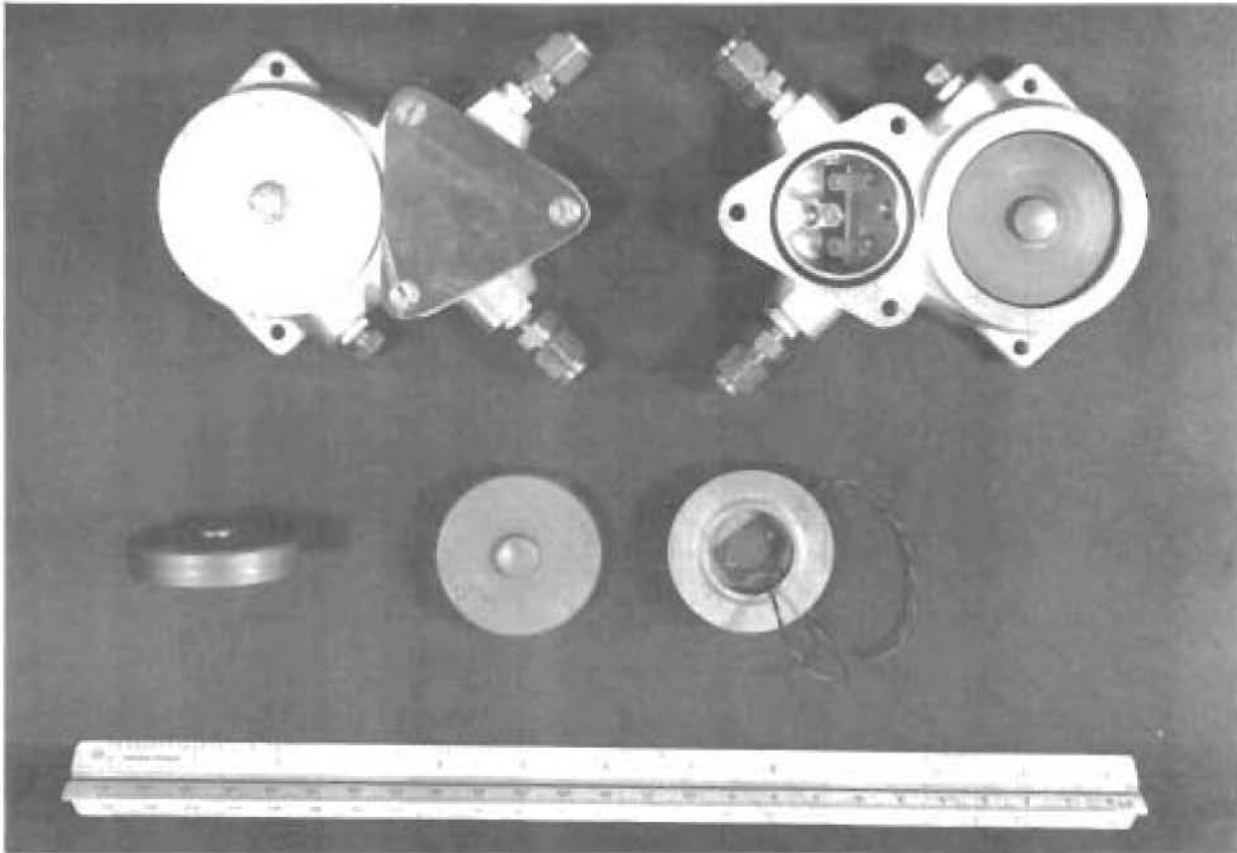


Fig 25. Top and bottom view of load cell in aluminum casting.

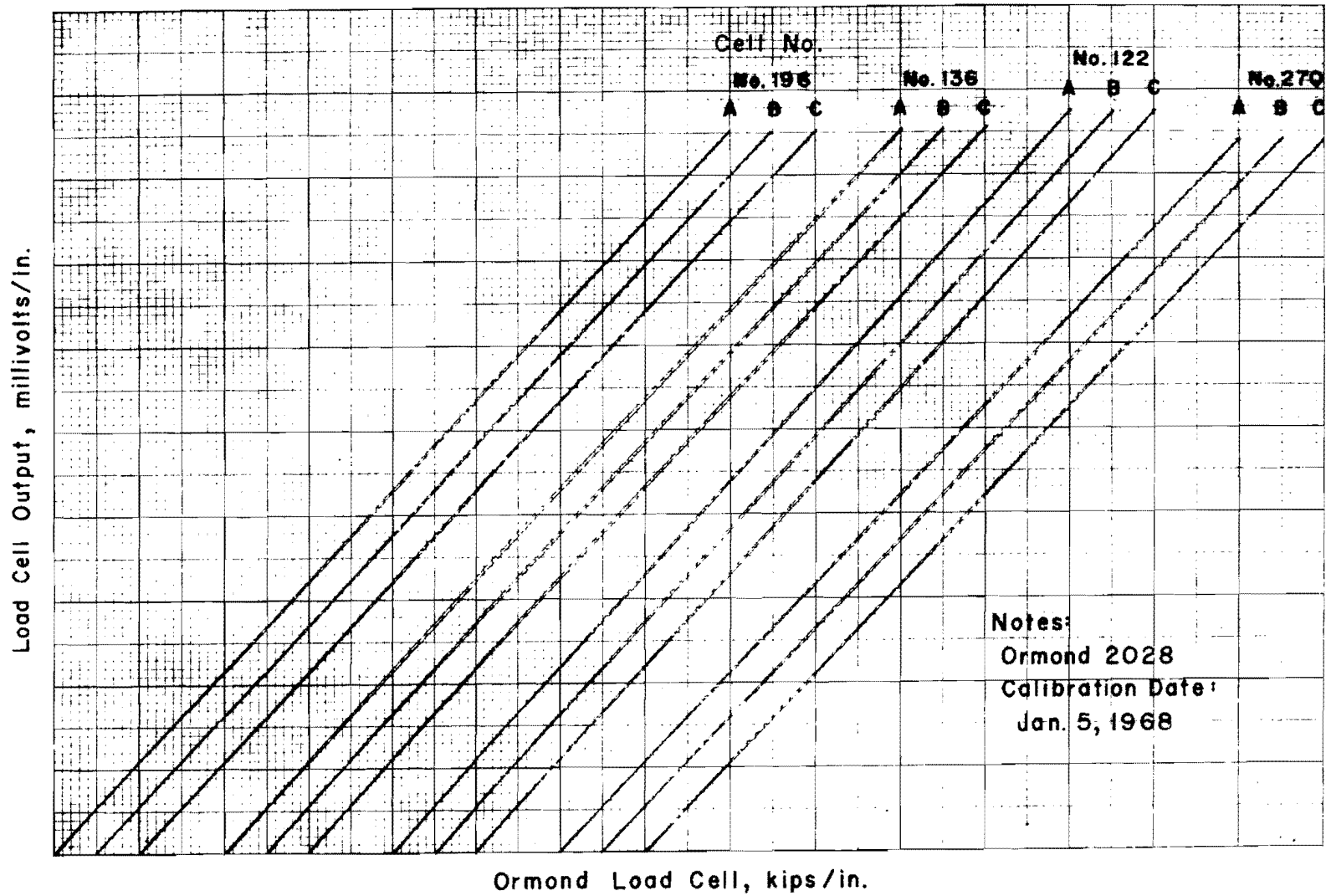


Fig 26. Load cell calibration curves.

group of eight into two subgroups of four cells such that the total resistance of the two groups is balanced.

Improved Wheel Load Transducer

The transducer described above was installed in a roadway surface and subjected to traffic loading and weather conditions. The copper tubing connections on the load cell chassis and the stainless steel sheet metal cover failed by fatigue cracking after about four months under heavy Interstate traffic. The failure of these two components of the transducer made it necessary to introduce further modifications in an attempt to eliminate these weaknesses in the design.

Revised design details were worked out in cooperation with the manufacturer (Rainhart Company), and two transducers incorporating these proposed changes were again put under traffic. The ordinary copper tubing fittings were replaced by special rubber-mounted tubing fittings and stainless steel tubing was used for all connections on the load cell chassis. In addition, a new stainless steel sheet metal cover without bolt holes was fitted on one of the transducers. Another transducer was installed without a sheet metal cover. The structural plates in this transducer were grooved on the sides to allow a neoprene tubing seal to be inserted around the periphery. Sliding aluminum latches were provided on each outer plate to prevent accidental escape from the frame.

After about one month under Interstate traffic both units continued to perform satisfactorily. Field tests utilizing accelerating and braking test vehicles showed no adverse effects of eliminating the sheet metal cover. Thus, the latter simplified design, without a cover, was selected for use in the experimental program.

Figure 27 shows one of the structural plates with the groove around the periphery and the latch that fits into a groove in the frame shown in Fig 28.

Laboratory Calibration

A procedure similar to that followed in calibrating the individual load cells was used in calibrating the transducer load cell chassis; whereby the output of the assembled load cells was compared to that from a standard Ormond

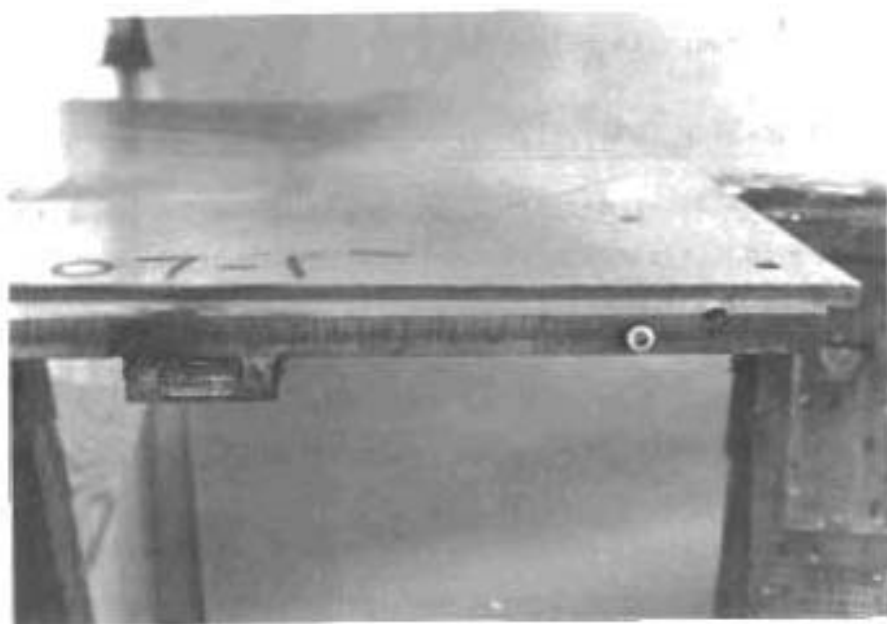


Fig 27. Grooved structural plate.

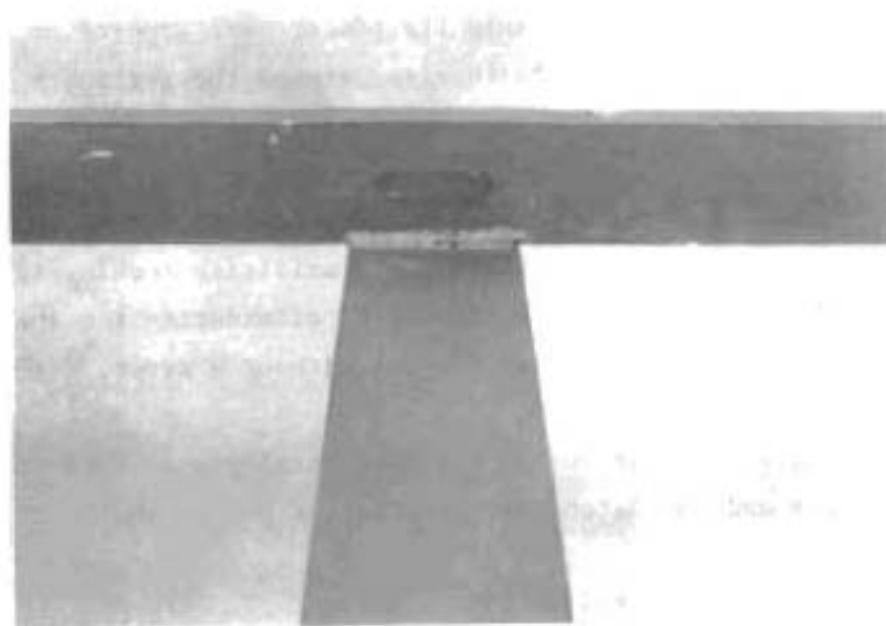


Fig 28. Frame latch-catch.

load cell. The right side, center, and the left side of the assembled wheel load transducer was loaded by applying load through wooden blocks to the structural plates. A Servo-controlled hydraulic system was used for applying the load (Fig 29) and the output of both the transducer and the Ormond cell were plotted on an X-Y plotter. Each of these three positions of the transducer was loaded three times to a maximum load of 10,000 pounds and then unloaded. The millivolt output of the transducer was measured precisely by a digital voltmeter and the voltage at the maximum applied load was recorded on the graph (Fig 30). The average of these values was divided by 10,000 pounds or 10 kips in order to obtain the calibration value or sensitivity of the transducer in millivolts per kip. This value was used later in scaling the shunt calibration step from millivolts to kips.

In addition, the laboratory calibration served as a double check on the linearity characteristics of the group action of load cells before field installation.

Field Calibration

The calibration factor which is ultimately used in reducing the electrical signals from the transducer to force units must be carefully evaluated since it may magnify or reduce the measured dynamic forces and consequently may affect the interpretation of the results. For this reason a field calibration of the scales under actual environmental and loading conditions was necessary in order to supplement the laboratory calibration of the load cell chassis.

After the installation of the scales, several methods were tried. One such method was simply allowing a vehicle with a measured static weight to roll slowly over the scales several times at approximately the same speed. The wheel loads were recorded as the vehicle passed each scale and the loads were reduced by using the calibration factor obtained in the laboratory. This factor was then adjusted based on a comparison between the measured and actual wheel load determined by a loadometer. Another procedure attempted in calibrating the scales involved stopping each tire at three different positions across the scale platform and recording the electrical signals from the transducers. Two vehicles were used in the operation. This procedure, although time consuming, had the advantage that the wheel was not moving and thus no excitations that may disturb the load were present. In both of these procedures,

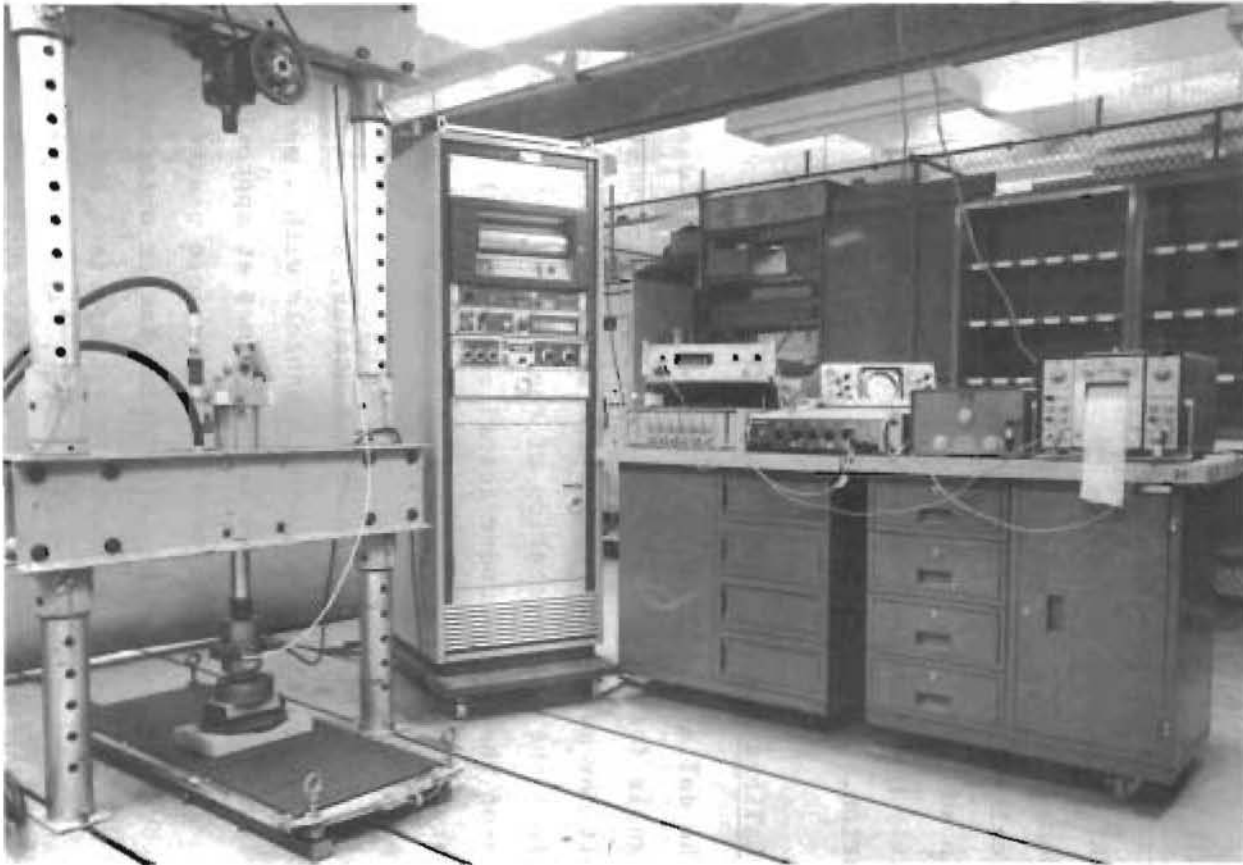


Fig 29. Load cell chassis laboratory calibration setup.

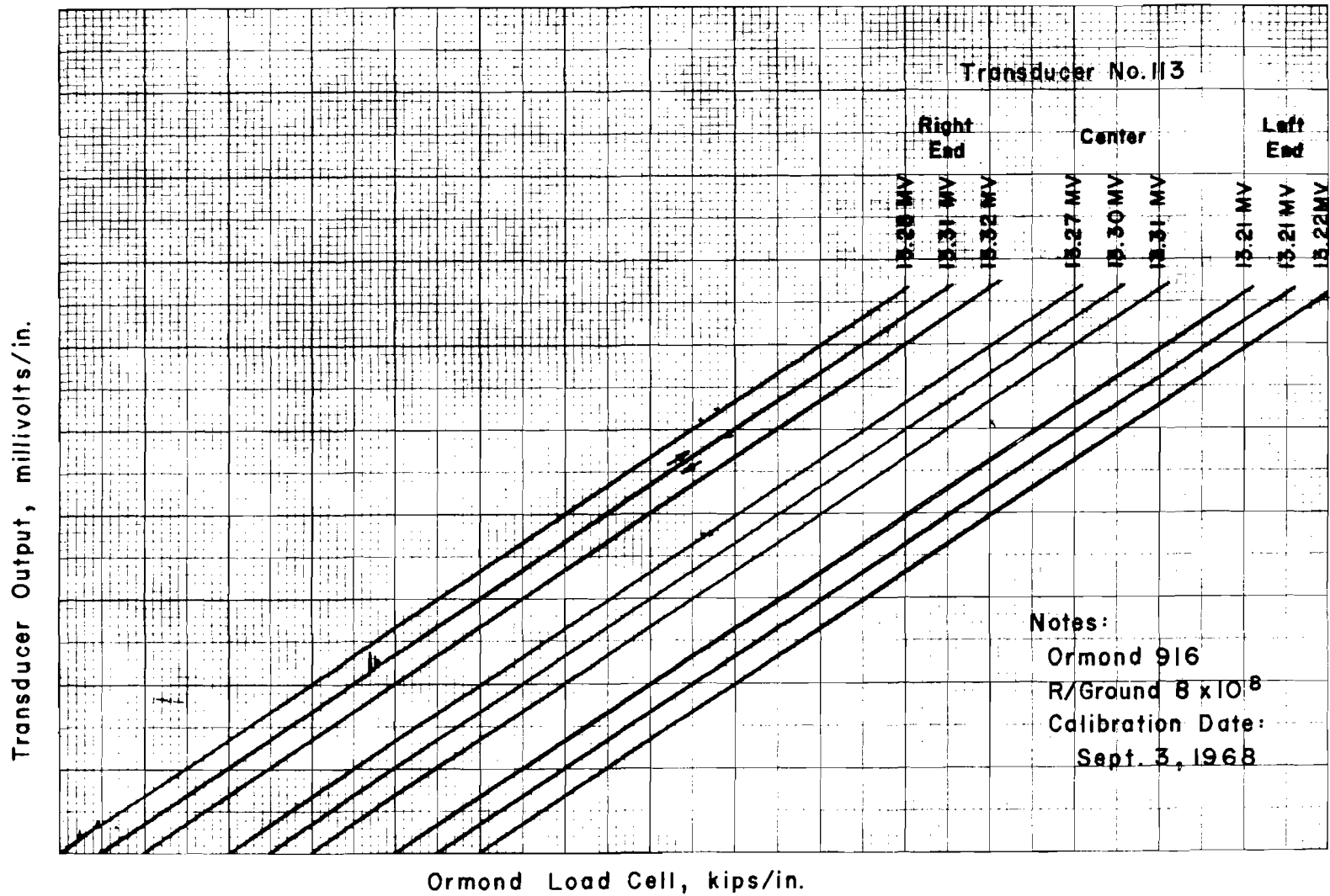


Fig 30. Load cell chassis laboratory calibration curves.

however, there were uncertainties concerning the exact magnitude of the applied wheel loads, thus it was decided that the calibration factors obtained in this manner should be checked further with a more precise calibration.

A local firm which periodically calibrates and certifies public scales in the State of Texas was contracted to perform an additional dead weight calibration in which loads with precise magnitudes are applied. In this procedure three increments of load 3,000, 6,000, and 9,000 pounds were applied at two positions across the scale platform (left and right sides). The load was then decreased by the same increments. After the addition and removal of each increment, the amplified electrical signals from the transducer were read by a digital voltmeter. In addition the calibration step size was recorded. The loading setup is shown in Fig 31.

The applied load in kips was plotted against the scale output in millivolts and a least square line was fitted through the plotted points for both the left and the right side loading positions. The value of the calibration step in pounds were then determined and used as a calibration factor. A typical curve is shown in Fig 32.

Signal Recording

The wheel load forces applied to the transducer cause an unbalance in the Wheatstone bridge circuit, described in a preceding section of this chapter, due to a change in the electrical resistance of the strain gage cemented on the load cell. This change in resistance is reflected in electrical signals varying continuously with time during the application of the load and are thus suited for direct recording in analog form. The signals are first conditioned by ordinary balancing methods to zero output with no load applied and are amplified by a factor of 333 or 1,000, depending upon the desired transducer range. After amplification, the signals are fed to the input of one channel of a Honeywell 8100, 8-channel FM magnetic tape recorder. In addition, the signals are recorded in the field on a light-beam oscillograph for subsequent manual reduction. The recording process is described in the block diagram shown in Fig 33.

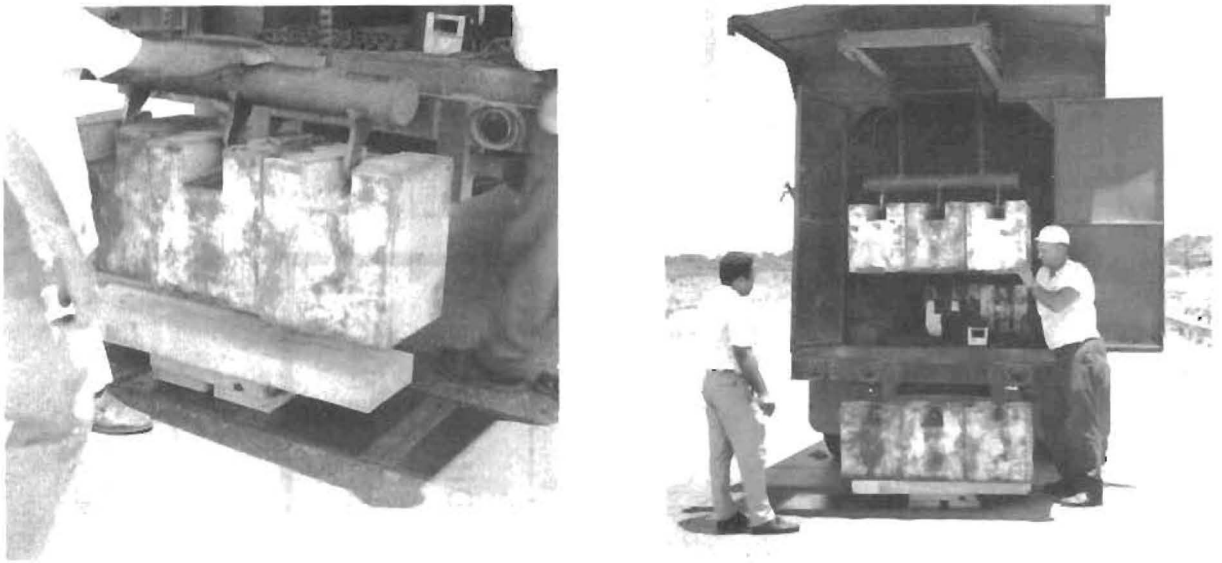


Fig 31. Field calibration setup.

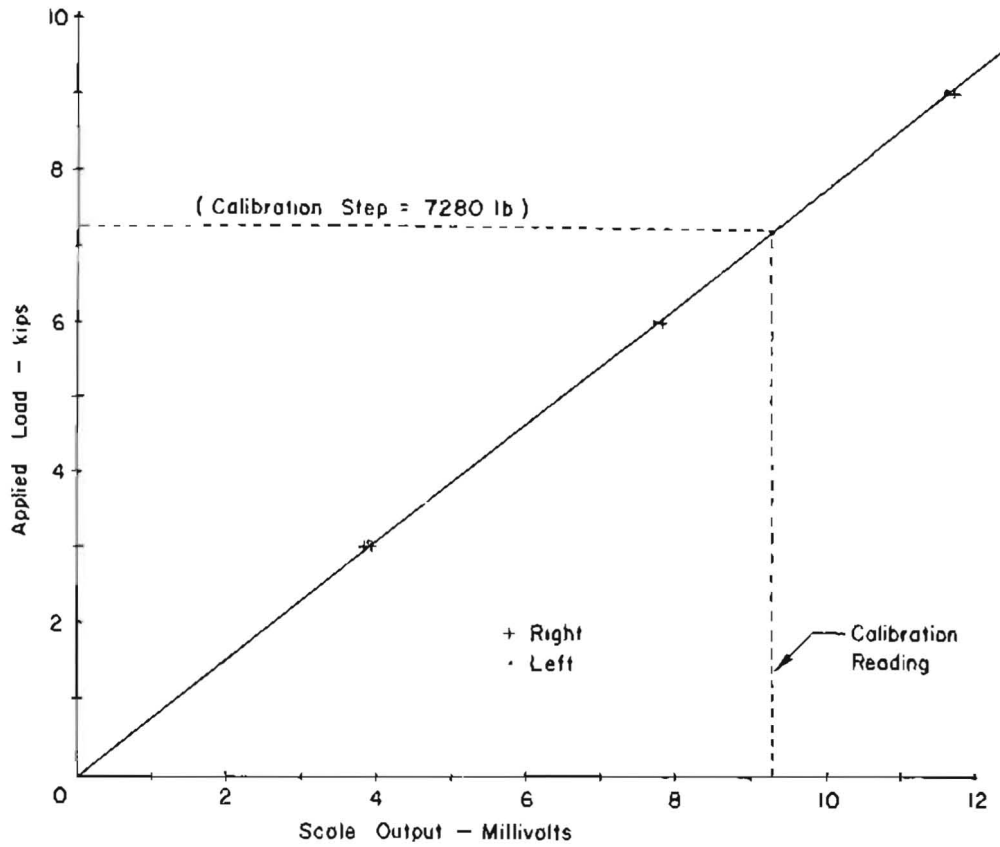


Fig 32. Calibration load versus scale output.

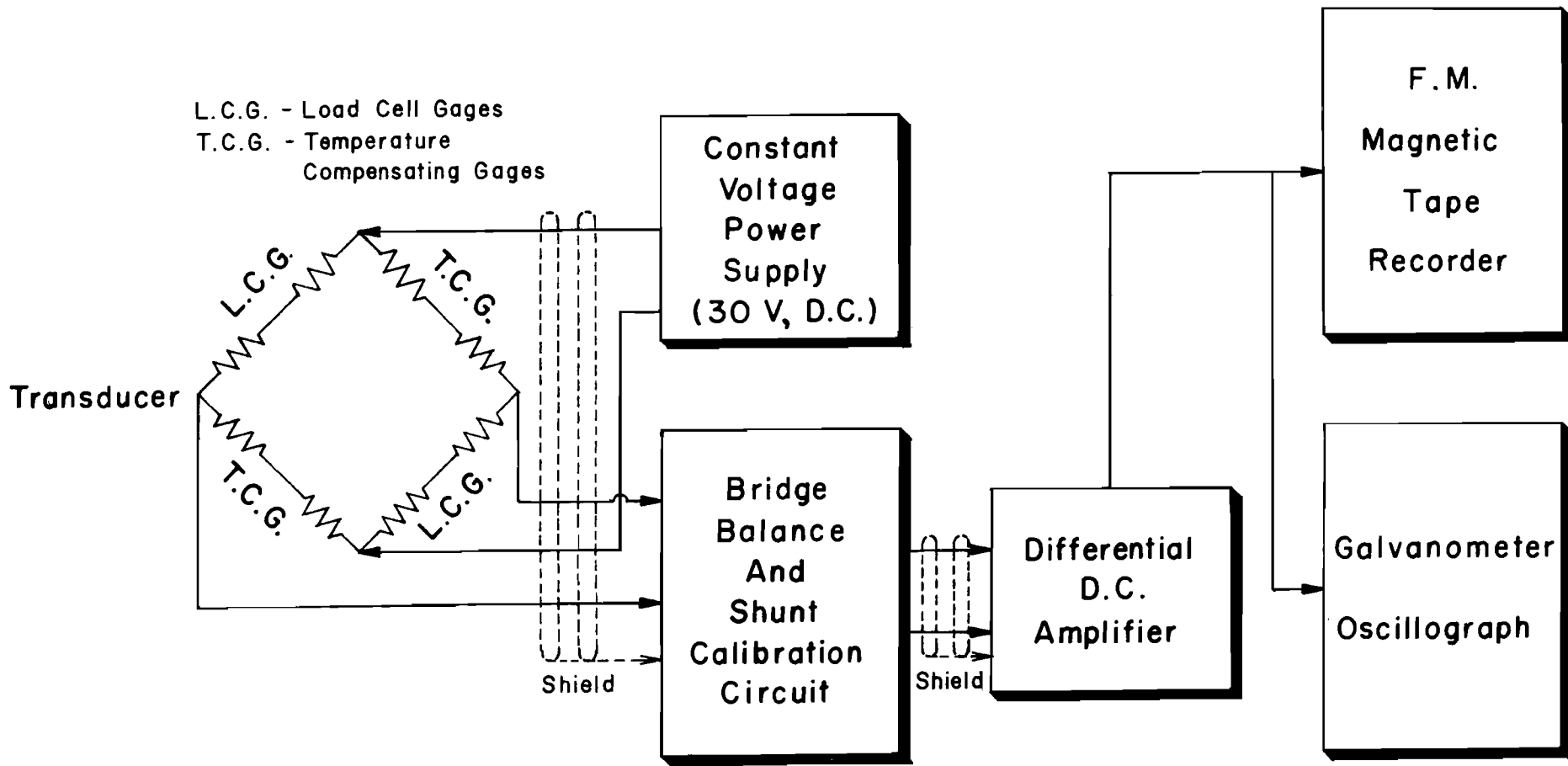


Fig 33. Recording logic block diagram.

Signal Playback and Reduction

The field analog record may be observed during or after recording by utilizing a built-in oscilloscope in the tape recorder which has the advantage of checking the recorded signals and the presence of any noise that may distort these signals. If accurate scaling of the signals is desired, the analog record can be played either in the field or in the laboratory on the screen of a storage oscilloscope such as Tektronix Type 564. This in addition to the light-beam oscillograph, mentioned in the preceding section, shows the versatility of the analog form of recording adopted for this purpose.

For precise and efficient reduction of large quantities of data an electronic computer must be used. Analog records must be converted to digital form before processing. For a more detailed description of the data processing technique used for reducing and analyzing wheel force information, the reader is referred to Ref 26.

This page replaces an intentionally blank page in the original.

-- CTR Library Digitization Team

CHAPTER 6. EXPERIMENTAL PROGRAM

General

The main purpose of this program was to define the significant factors that influence the dynamic behavior of selected classes of vehicles and determine the extent to which these factors affect the magnitude and the nature of dynamic wheel loads. Basically, the program involved the measurement of forces applied normal to the roadway surface by the wheels of vehicles moving at speeds up to 60 or 70 miles per hour at several sampling locations in a traffic lane. At each of these locations, the forces were detected by a wheel load transducer which has been described in the preceding chapter. The experimental data were then compared to the predicted forces resulting from the mathematical model simulation of the behavior of the vehicles used in the series of experimental tests. The necessary adjustments to the mathematical model were made in accordance with the results of this comparison.

The selection of factors, the site, the test vehicles, and the design of this experimental testing program are described in the early part of this chapter. The remainder of the chapter is devoted to a description of the portable electronic data collection system used in the measurement and recording of dynamic forces and to the procedure followed in the reduction and tabulation of the experimental data.

Selection of Factors

It was not possible, nor practically feasible within the limitations of this study program, to include all the factors that influence the dynamic behavior of a moving vehicle. For example, some factors such as environmental and aerodynamic effects, or wheel unbalance and rotation are quite variable and their proper investigation requires elaborate and costly experimental setups. In addition, the influence of such factors, as discussed in Chapter 2, depends on their interaction with other related variables.

Of the several factors discussed in Chapter 2, the vehicle type, vehicle speed, surface roughness, and profile characteristics were considered to have significant effects on the behavior of a moving vehicle. Thus, these factors were chosen as the main parameters to be included in the experimental program. Five different vehicle types, three levels of speed, and four patterns of surface roughness were investigated. These will be discussed under the section on experiment layout.

Selection of Test Site

One of the early efforts in this experimental program was the selection of an appropriate site for the installation of a series of wheel load transducers. It was important that the selected site meet the following requirements: (1) it must be on an Interstate Highway, (2) it must have at least three lanes in order to minimize interruptions to traffic during testing especially since the instrumented traffic lane must be blocked during testing, (3) it must be on a relatively smooth and level section, (4) it must not be located on a hill or curve section, (5) it must be conveniently located between two interchanges so that large test vehicles can turn around without excessive delay, (6) it must not be located in the vicinity of possible sources of interferences or noise that might affect the performance of the electronic recording equipment, and (7) it must have a convenient source of electric power.

Several possible locations in and around Austin, Texas were considered in the light of the above requirements. A section on the northbound lanes of Interstate Highway 35 immediately south of Williamson Creek and approximately one mile south of Ben White Boulevard near Austin was selected. Approval for occupying this site was granted by District 14 authorities of the Texas Highway Department. The profiles of the pavement surface at this site were recorded by the high-speed Surface Dynamics Road Profilometer. The profiles were evaluated and a relatively flat 100-foot strip was selected for installation of the wheel load transducers.

Selection of Test Vehicles

After the test site had been selected, the portable in-motion weighing and classification system developed for the Texas Highway Department and the Bureau of Public Roads by the Center for Highway Research (Project 3-10-63-54)

was installed approximately 40 feet in advance of the selected 100-foot test strip. This system is described in detail in Ref 26. It consists basically of a pair of wheel load transducers set side-by-side in the two-wheel paths, an inductance loop detector, pneumatic rubber tubes, and recording equipment. The system can be installed in a traffic lane in a few hours and may be operated either manually or automatically to record on magnetic tape information related to the wheel loads, speed, length, number of axles, and axle arrangements and proximities for vehicles moving at speeds up to the maximum legal limit in addition to the time of day that the vehicle passed over the system. The record may then be digitized and reduced by a high-speed computer for tabulation of the collected information.

A survey of Interstate commercial traffic was conducted over a period of seven days on a continuous basis by personnel of the Planning Survey Division of the Texas Highway Department. Traffic signs directing trucks to use the right traffic lane were placed ahead of the installation in order to insure that the majority of commercial traffic would pass over the system. From this survey a period of approximately 80 consecutive hours, during which more than 1,400 vehicles were weighed and classified as they passed over the system at speeds up to 60 to 70 miles per hour, was selected for studying the distribution of the different classes of vehicles. The results of this classification survey analyses are summarized in Fig 34. The five classes of vehicles selected for use in the experimental program represent approximately 92 percent of the vehicles observed.

Contacts were established with local contract haulers to arrange for rental of vehicles representative of the selected five classes of vehicles. In addition to the five vehicles used in the major experiment, three Class I vehicles and three Class V vehicles were also used, thus bringing the total number of test vehicles used in the experimental program to eleven. Each vehicle was given an identification number that indicates its class and a serial number within the class. For example, vehicle V-4 is the fourth vehicle of Class V group of test vehicles. Except for vehicles I-1 and I-2 which were used early in the testing program, the static weight of the wheels of each test vehicle was determined by a loadometer at least eight times. The static weight information are included in Appendix A.

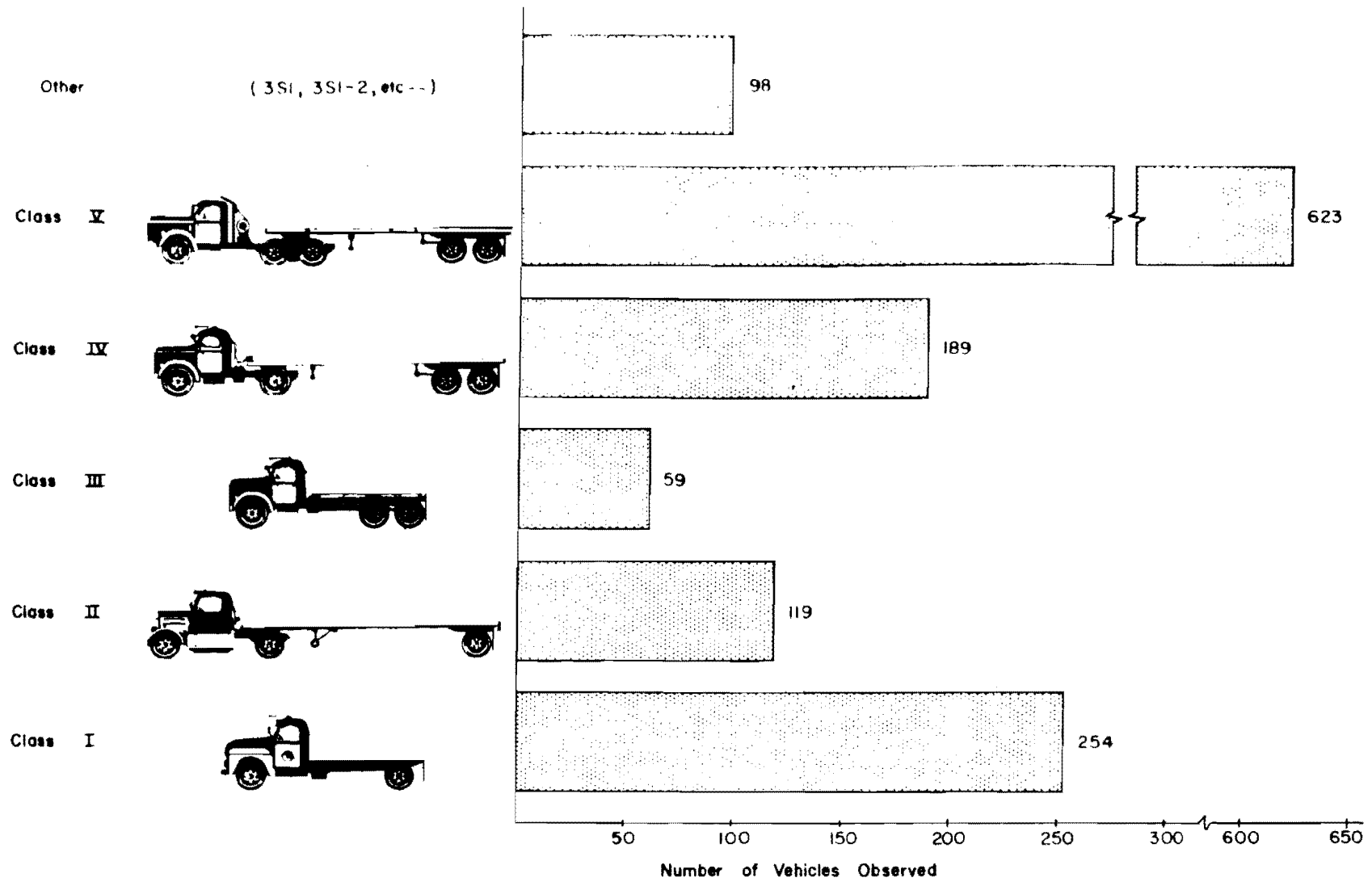


Fig 34. Classification of truck traffic northbound on IH-35, Austin, Texas.

Preliminary Testing Program

Before the major experimental program was started, six wheel load transducers were installed in the left wheel path of the 100-foot strip according to an expanding spacing shown in Fig 35. A photograph of the field installation is shown in Fig 36. Based on estimates of the period of oscillation of a vehicle suspension system, this arrangement is believed to be sufficiently long for describing at least one cycle of oscillation. A single unit two-axle vehicle with known suspension characteristics was provided by the Texas Highway Department for use in testing. The main purpose of this preliminary testing program was: (1) to check the recording equipment, (2) to develop a suitable recording technique, and (3) to check the adequacy of the spacing arrangement of sampling locations.

The first series of tests consisted of several passes of the test truck operating at different speeds and under various loading conditions. Braking and accelerating tests were made in order to check the response of the wheel load transducers and to point out any significant variations with respect to load placement across the scale platform. Performance of the system was entirely satisfactory.

The transducers were then subjected to continuous pounding of Interstate traffic for several months after which time fatigue failures in some components of the transducers occurred as mentioned in Chapter 5. Reconditioned wheel load transducers were then installed in the same positions, and an additional series of tests were conducted with two two-axle vehicles (partially loaded and fully loaded). The test vehicles made approximately 40 passes at different speed levels up to 60 miles per hour. Three patterns of artificial roughness were introduced in advance of the first wheel load transducer by means of sheets of plywood (2 by 8 feet by 3/4 inch). The same sequence of test runs was repeated with two additional patterns of roughness in individual wheel paths.

The analysis of data from these tests revealed the following:

- (1) Additional force sampling points were needed in the upstream portion of the instrumented section.
- (2) Sampling beyond the fifth scale was unnecessary due to quick damping of vehicle oscillation after it passed over the bump(s).
- (3) At certain speed roughness combinations, the tire lost contact with the roadway surface at more than one sampling point.

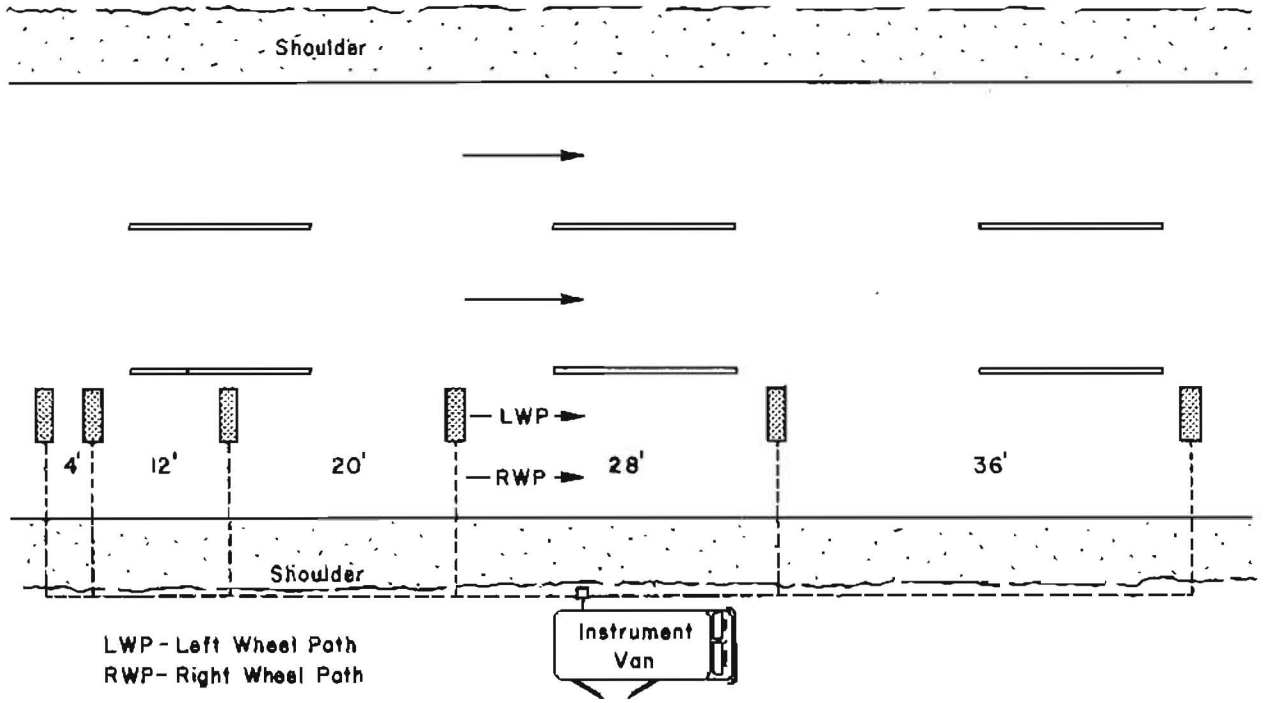


Fig 35. Preliminary installation.



Fig 36. View of field installation.

This preliminary testing program proved valuable in more than one respect in the subsequent planning of the major experimental program which is the subject of the next section.

Major Experiment

Based on the results of the preliminary testing program, a new arrangement of the transducer array was devised for the major experiment. In this arrangement the instrumented section was shortened to 64 feet (originally 100 feet). Six reconditioned wheel load transducers were installed in the left wheel path. Three additional transducers were installed in the right wheel path for the purpose of studying the roll characteristics of the test vehicles and the effect of roll on the magnitude of dynamic forces applied to the pavement surface. The new positioning arrangement is shown in Fig 37. A field view of installation is shown in Fig 38. Basically, there are seven different positions in the longitudinal direction of the test section. At some positions (1 and 4) both the left and the right wheel paths are sampled, while at other positions (2, 5, 6, and 7) only the left wheel path is sampled. The individual transducers, or scales, are designated for convenience of reference according to both their position and sampling location. Thus, scale "1-left" or simply "1L" is the first scale in the array located in the left wheel path, while scale "3R" is the scale in the third position and located in the right wheel path. Notice that there are no 2R, 3L, 5R, 6R, or 7R scales.

Essentially, except for the addition of the scales in the right wheel path and that of scale 4L, the remaining scales retained the same positions as during the preliminary testing program. The new arrangement had the advantage of providing simultaneous force measurement of the successive wheels of tandem axles at scales 1L and 2L, 3R and 4R, and again at 4L and 5L. The distance from 1L to 2L, 3R to 4R, and from 4L to 5L was made 4 feet to encompass the spectrum of spacings common to tandem axles.

Pavement roughness, speed, scale position, and axles were the main variables investigated in this experiment. Three patterns of artificial roughness were introduced by placing different sources of excitation in the wheel path of the vehicle. An 8 by 2-foot sheet of 3/4-inch plywood was placed at two different locations in advance of the first wheel load transducer in order to

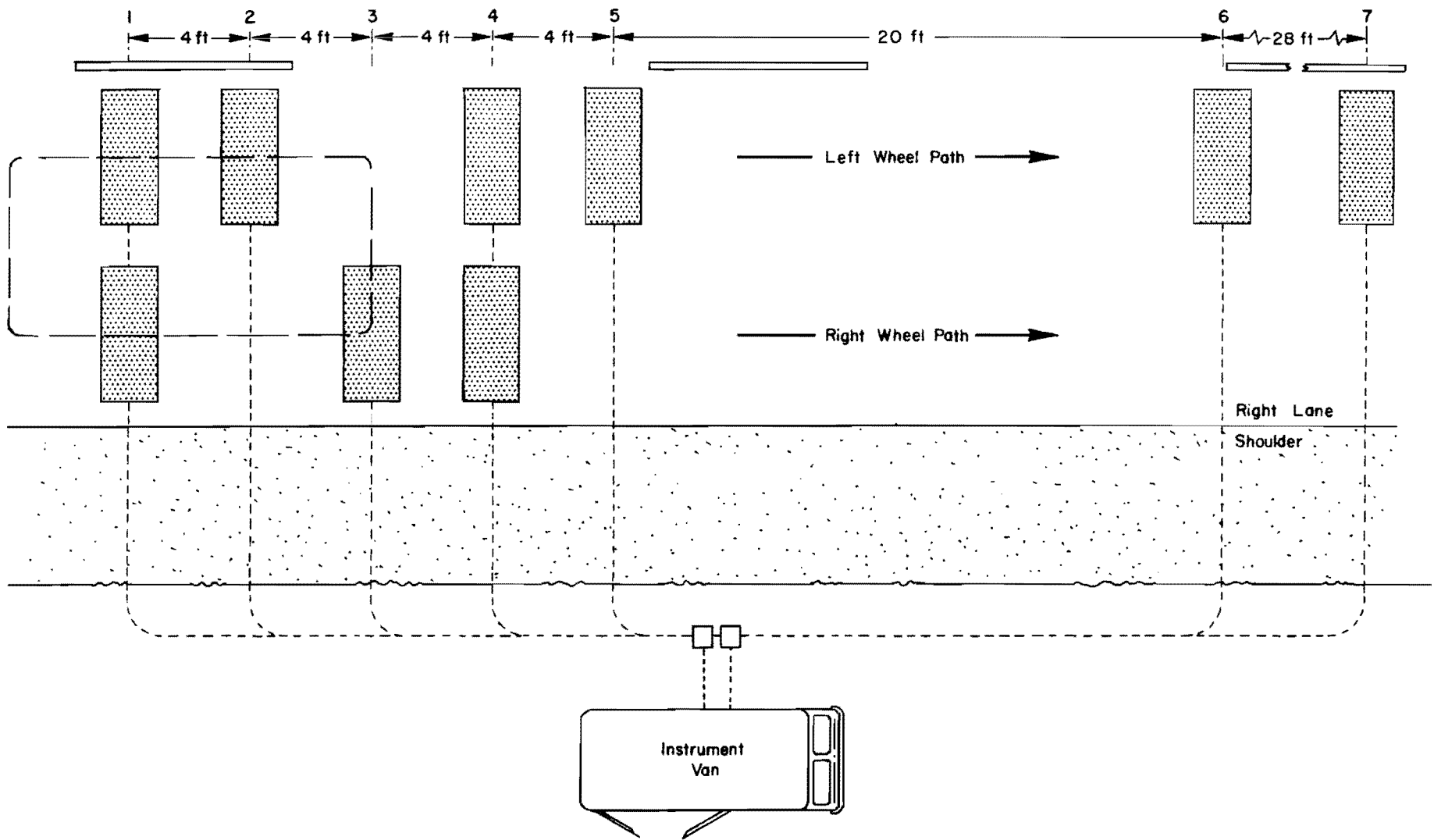


Fig 37. Arrangement of scales array.



Fig 38. Driver view of field installation.

provide two such levels of roughness. The third level was provided by placing thinner sheets of plywood (18 by 48 inches by 3/8-inch) over the platform of scales 1L and 1R. In addition, the smooth condition with no artificial roughness was also included in the experiment thus bringing the total number of levels of roughness to four. These are shown in Fig 39.

Three levels of speed 10, 30, and 60 miles per hour were used. For every speed-roughness combination, each test vehicle made three runs over the instrumented site. Thus, the total number of runs for each class of vehicles was 36, which in effect brings the total number of runs for the five classes to 180. Vehicle loading and tire pressure were kept constant.

The experiment was laid out according to a statistical experiment design in order that inference concerning the significance of the different effects and the interactions between the variables could properly and correctly be made. Several choices of statistical designs are available (Refs 1, 9, and 32). The choice of any particular design, however, depends on the nature of the experiment and the restrictions imposed on randomization by economical, practical, and other factors related to performing the experiment. For example, a completely randomized factorial design would call for running the 180 test runs in a random order. Practically, it is not feasible to change the test vehicle, the road roughness pattern, and speed between each run. In addition, a completely randomized design requires randomization of force sampling locations in the instrumented section. This requirement is virtually impossible to achieve.

A suitable procedure for running the experiment would be to use one or more test vehicles and run the required number of passes at the different speed levels for a particular roughness pattern. After this is completed, the road roughness is changed and the series of passes is repeated. At each pass the dynamic wheel loads are measured in the order of the sampling locations. Such a procedure leaves only the series of passes or experimental units in each roughness pattern to be randomized.

An experiment designed according to this procedure is referred to as a split-split-split plot. A description of this design is included in Appendix B.

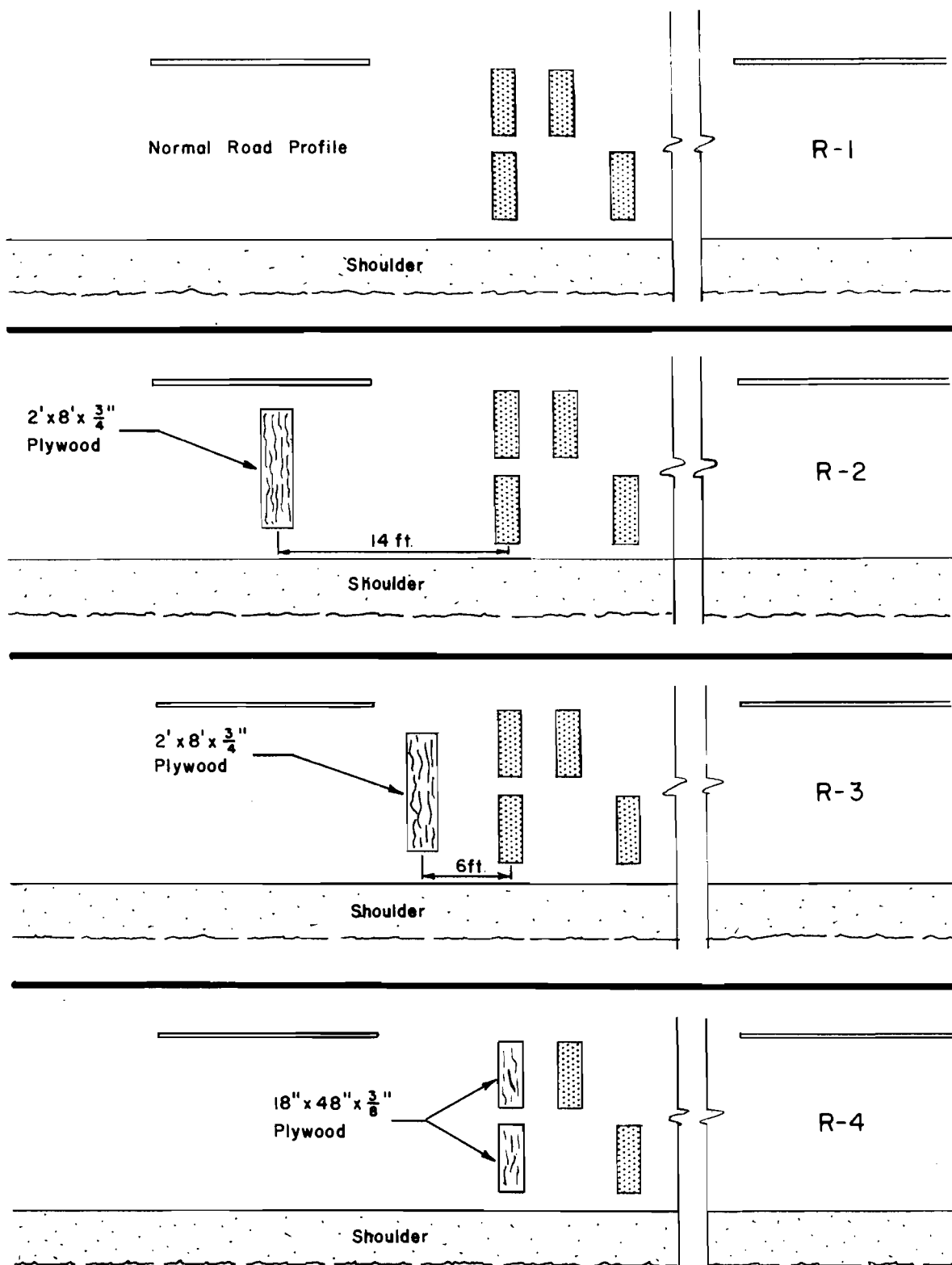


Fig 39. Patterns of roughness.

Instrumentation

In the preceding sections the preliminary and the major experimental programs were discussed. The accomplishment of these experiments as outlined required elaborate instrumentation for signal conditioning, recording, and processing. This section is devoted to a description of the portable electronic data collection system used in recording the dynamic forces at each sampling location.

This system is capable of producing on magnetic tape, or on a galvanometer oscillograph, records of the normal wheel forces, vehicle speed, number of axles, and axle spacing for each vehicle. The basic principles involved in designing this recording system are the same as those discussed briefly in Chapter 5 under signal recording.

The block diagram for this system is shown in Fig 40. For each transducer there is an individual unit which includes the constant-voltage power supply, the bridge balance-circuit, and the shunt calibration circuit. These are standard model 2480 signal conditioning units from Dymec Division of Hewlett-Packard Company. The power supply provides an adjustable voltage ranging from 0.1 to 30.0 D.C. volts and an output current of 0 to 200 milliampere. The line and load regulation of the units is within 0.002 percent.

The signal conditioning and calibration circuit provides a standard bridge balance range and remote controlled shunt calibration relays. These relays are triggered by a presence loop detector located downstream from transducer "7L," and they operate through a time delay circuit. A calibration pulse of 50 millisecond duration is provided at the end of the record simultaneously on each channel of transducer output.

The conditioned output signals from each transducer are amplified by a model 8875A Differential Amplifier from Sanborn Division of Hewlett-Packard Company. These amplifiers provide up to ± 10.0 volt output at a current ranging up to 100 milliamperere. The voltage gain of the amplifiers may be adjusted by vernier-controlled steps between 1.0 and 3000.0. In addition, the amplifiers include adjustable output filters with cutoff frequencies at 2, 200, 2,000, and 20,000 H_z . In most cases, the amplified signals from the transducers were filtered at 200 H_z in order to eliminate extraneous noise signals which may have been caused by vehicle ignition and other sources of interference.

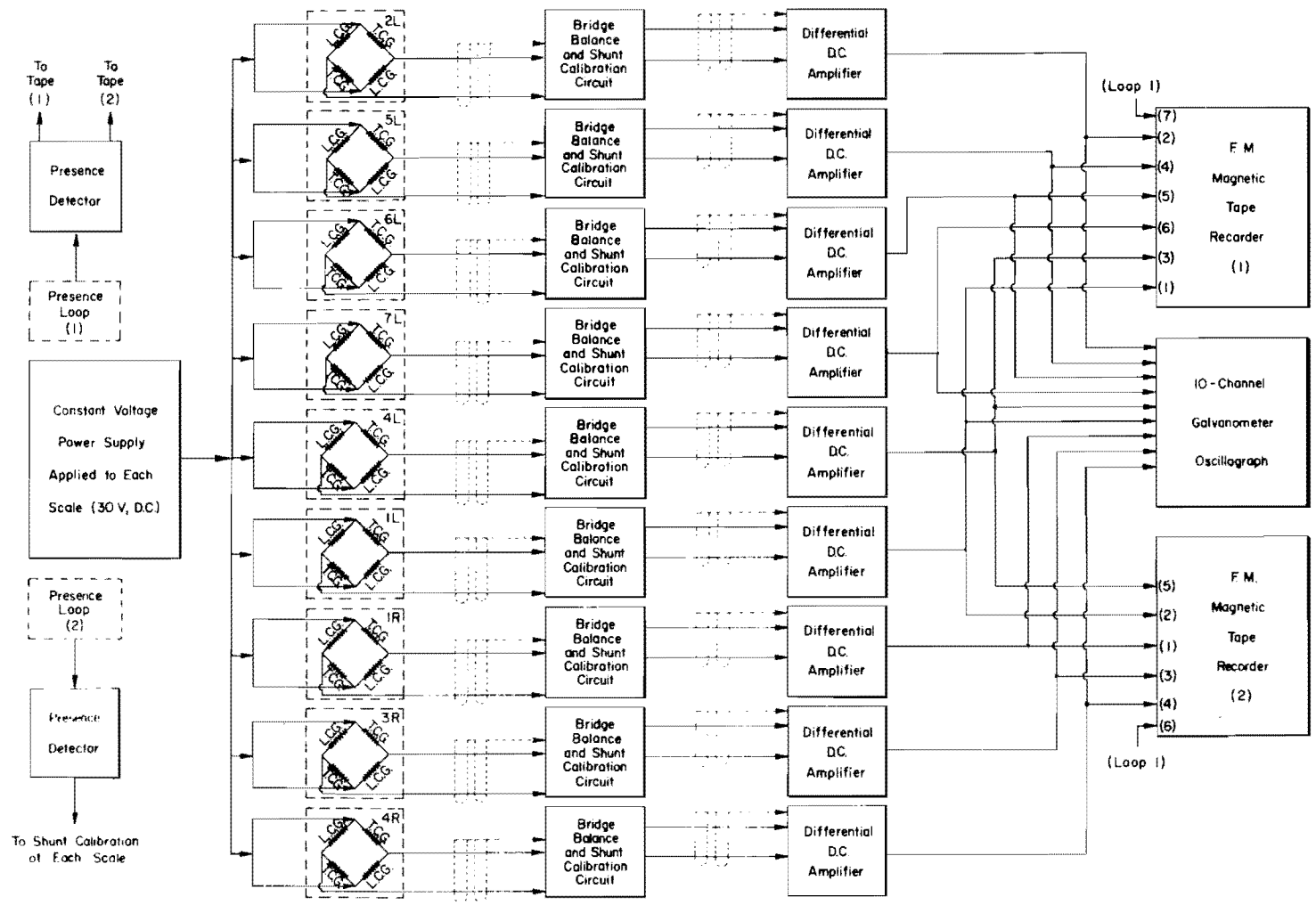


Fig 40. Recording system block diagram.

The dynamic forces and other vehicle data were recorded in analog form simultaneously on both a frequency modulated magnetic tape system and on a direct writing galvanometer oscillograph. Two 8-channel Honeywell model 8100 magnetic tape recorders were used and operated at a tape speed of 1-7/8 inches per second which provides a recording bandwidth of 0 to 625 H_z . The following table shows the channel assignments to the different scales. This information is also shown in Fig 40.

TABLE 6. CHANNEL-SCALE ARRANGEMENT

Channel	Scale	
	Tape 1	Tape 2
1	1L*	1R
2	2L	1L
3	4L*	3R
4	5L	4R
5	6L	4L
6	7L	(loop)
7	(loop)	

* Recorded on both tapes.

A model 5-114 Consolidated Electrodynamics Corporation oscillograph provided a visual recording of data as it was being recorded on the magnetic tapes. The recording galvanometers used in the oscillograph provided a flat frequency response of 0 to 500 H_z .

An inductance loop detector located over the first pair of transducers provided a vehicle presence signal which coincided with the wheel load pulses from scales 1L, 1R, and 2L and thus could be used to establish the number of axles belonging to a particular vehicle. This information was especially important in the mixed traffic study.

The output of each scale calibration and all the necessary voltage adjustments were read with a model 3440A Hewlett-Packard digital voltmeter. This meter provides 0.05 percent accuracy with ± 10 microvolt resolution in the D.C. voltage ranges.

This recording equipment (Fig 41) was housed in a van shown in Fig 42. Arrangements were made to provide a source of 115 V.A.C. power at the test site in order to avoid using portable generators which could possibly cause interference with the electronic systems and result in undesirable noise.

The equipment described above provided the flexibility and the accuracy necessary for collecting meaningful wheel load data under the varying conditions dictated by the plans for the experiments.

Testing Procedure

During the planning stage of the experimental program a general scheme for scheduling the test vehicle passes was selected and the experiment was designed accordingly. Based on this scheme a general procedure was followed throughout the major experimental program. A brief description of this procedure is included in the following paragraphs.

The three-speed levels: 10, 30, and 60 miles per hour, were designated as levels: 1, 2, and 3, respectively. These levels were arranged with the replicate numbers (three repetitions for each speed level) as such:

<u>Pass No.</u>	<u>Speed</u>	<u>Replicate</u>
1	1	1
2	1	2
3	1	3
4	2	1
5	2	2
.	.	.
.	.	.
.	.	.
9	3	3

The order of running these passes was selected at random and this order is shown in Table 7.

Each test vehicle then made nine passes according to this order of speed levels over each roughness pattern. After the test vehicle completed this series of passes, the roughness pattern was changed. The experiment was conducted over a period of several days with one or more test vehicles operated

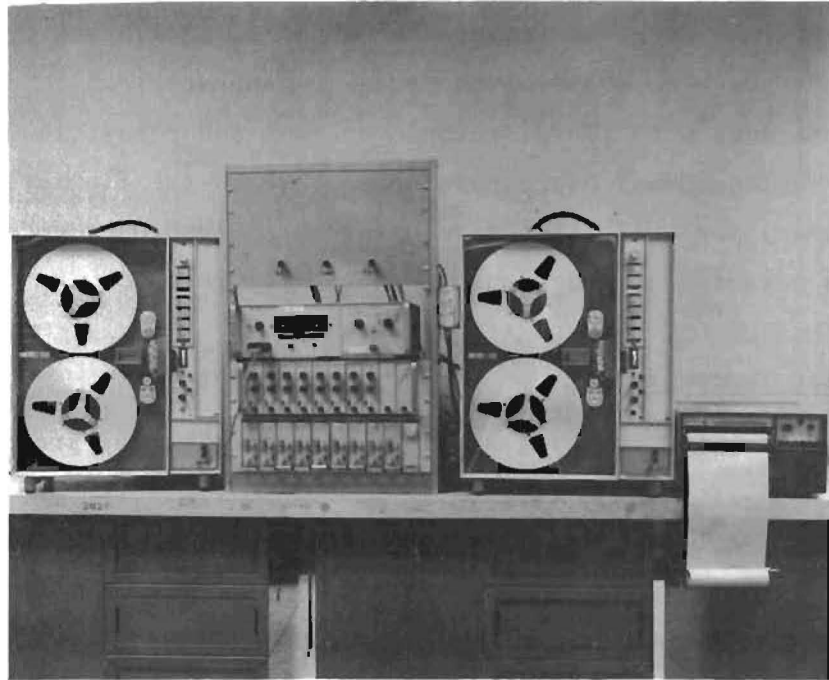


Fig 41. Recording equipment.

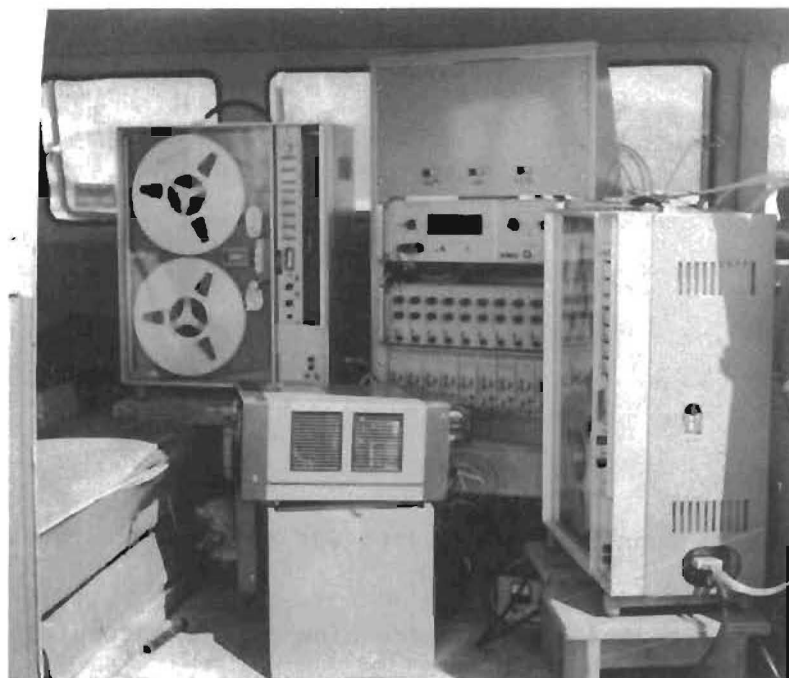


Fig 42. Recording equipment - field setup.

TABLE 7. RANDOM ORDER OF TEST RUNS

Run No.	1	2	3	4	5	6	7	8	9
Speed	60	30	30	10	10	10	60	30	60

each day. When more than one test vehicle was used, the drivers were instructed to follow the same order of passes whereby all vehicles made the run before starting on the next one. Every pass having relevance to the major experimental program was given a serial number for identification purposes.

The above procedure was found to be simple and efficient from the standpoint of field organization during data collection.

Data Reduction

The analog record for each pass made by a test vehicle starts when the test vehicle is detected by the upstream presence loop detector (around scale 1L, 1R, and 2L) and lasts until the end of the calibration pulse after the vehicle passes over the downstream loop detector located just beyond the last scale (7L). The length of the record is inversely proportional to the speed of the vehicle. For example, a record of a 10-mile per hour pass is six times as long as a record of a 60-mile per hour pass. The significant portions of the record, however, are the force waveforms or pulses that give a measure of the forces applied to the scale surface. The portions of an analog record during which a force pulse occurs correspond to the time during which the tire is being supported, partially and completely, by the scale platform. Thus, there are as many pulses as there are scales. The shape and the duration of the pulse depends on several factors including: (1) speed of the vehicle, (2) tire contact length, and (3) the effective width of the scale platform, which in this case is 18 inches. These factors are discussed in Ref 26. The general shape of a typical force pulse is shown in Fig 43. Basically, the pulse is made up of (1) a rise portion corresponding to the wheel establishing gradual contact with the scale, (2) a relatively flat maximum attained level corresponding to the wheel fully supported by the scale, and (3) a fall portion which corresponds to the wheel gradually losing contact with the scale. The portion of the pulse which is of interest in the calculation of the wheel

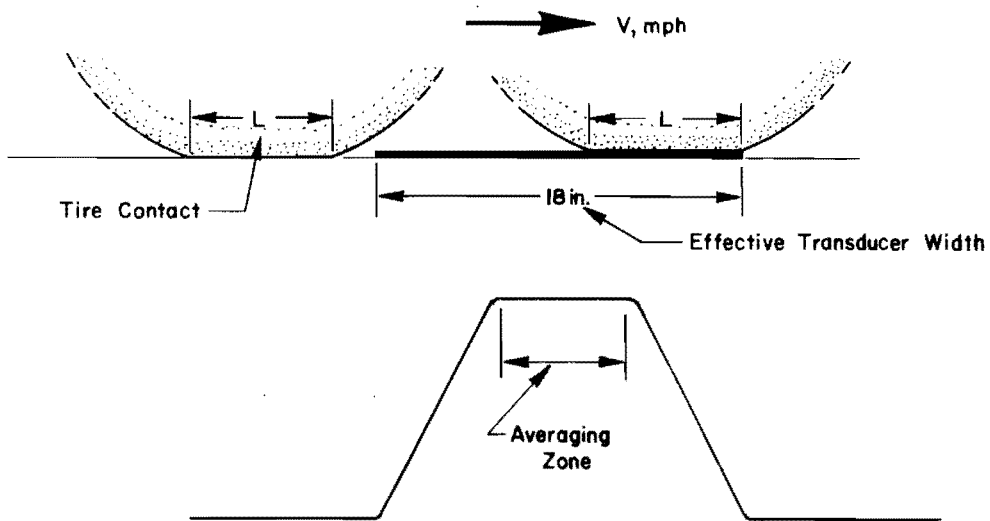


Fig 43. Typical force pulse.

TABLE 8. DURATION OF MAXIMUM LEVEL OF PULSE

Tire Contact L	Durations in Seconds for Vehicle Speeds (mph)							
	10	20	30	40	50	60	70	80
9.0	.0511	.0255	.0170	.0127	.0102	.0085	.0073	.0063
10.0	.0454	.0227	.0151	.0113	.0090	.0075	.0064	.0056
11.0	.0397	.0198	.0132	.0099	.0079	.0066	.0056	.0049
12.0	.0340	.0170	.0113	.0085	.0068	.0056	.0048	.0042
13.0	.0284	.0142	.0094	.0071	.0056	.0047	.0040	.0035
14.0	.0227	.0113	.0075	.0056	.0045	.0037	.0032	.0028

Note: Effective width of transducer = 18 inches.

load forces is the central portion which includes the maximum attained level. The duration of this portion depends again on the speed of the vehicle and the contact length of the tire. Pulse duration for several combinations of speed and tire contact length are given in Table 8.

Data reduction, which includes determining the average of the central portion of each force pulse to represent the wheel load forces, may be accomplished either manually from the strip charts which is produced by the oscillograph or electronically by the high speed computer. The latter requires digitization of the analog record before actual reduction and tabulation. Each of these methods are now discussed briefly.

Manual Data Reduction. The analog records displayed on 7-inch-wide strip charts by the galvanometer oscillograph provided one method of data reduction. An example of such records is shown in Fig 44. Each horizontal trace shown in the figure represents the signals from an individual scale whose number is given at the beginning of the trace. The photographic traces have been marked with ink to allow for adequate reproduction. The record is shown in two parts with a time reference giving the start and the end of each part. At the end of the record nine calibration pulses appear simultaneously as mentioned in the preceding section. The gain of the oscillograph amplifiers was adjusted to allow for the maximum expected dynamic force.

The following procedure was used in the reduction of each of these records:

- (1) At the bottom of each force and calibration pulse a no-load level was established by extending the trace immediately preceding the force pulse.
- (2) An average of the central portion of the pulse was determined in order to establish the height of the pulse. In the case of a smooth flat-top pulse the average was simply the maximum attained central level. But, on the other hand, the majority of force pulses, especially those produced by fast moving wheels, had high frequency wave fluctuations with relatively small amplitude superimposed on them. This has been noticed by other investigators (Refs 26, 33, and 34) and is largely attributed to the vibration of the unsprung masses of the vehicle and the scale system. It is for such force pulses that extreme caution must be exercised in establishing the average level of the central portion in order to avoid erroneous and inconsistent results.
- (3) The height of each pulse was then scaled against the corresponding calibration pulse whose value in pounds is known, thus establishing the wheel load forces which are represented by these heights.

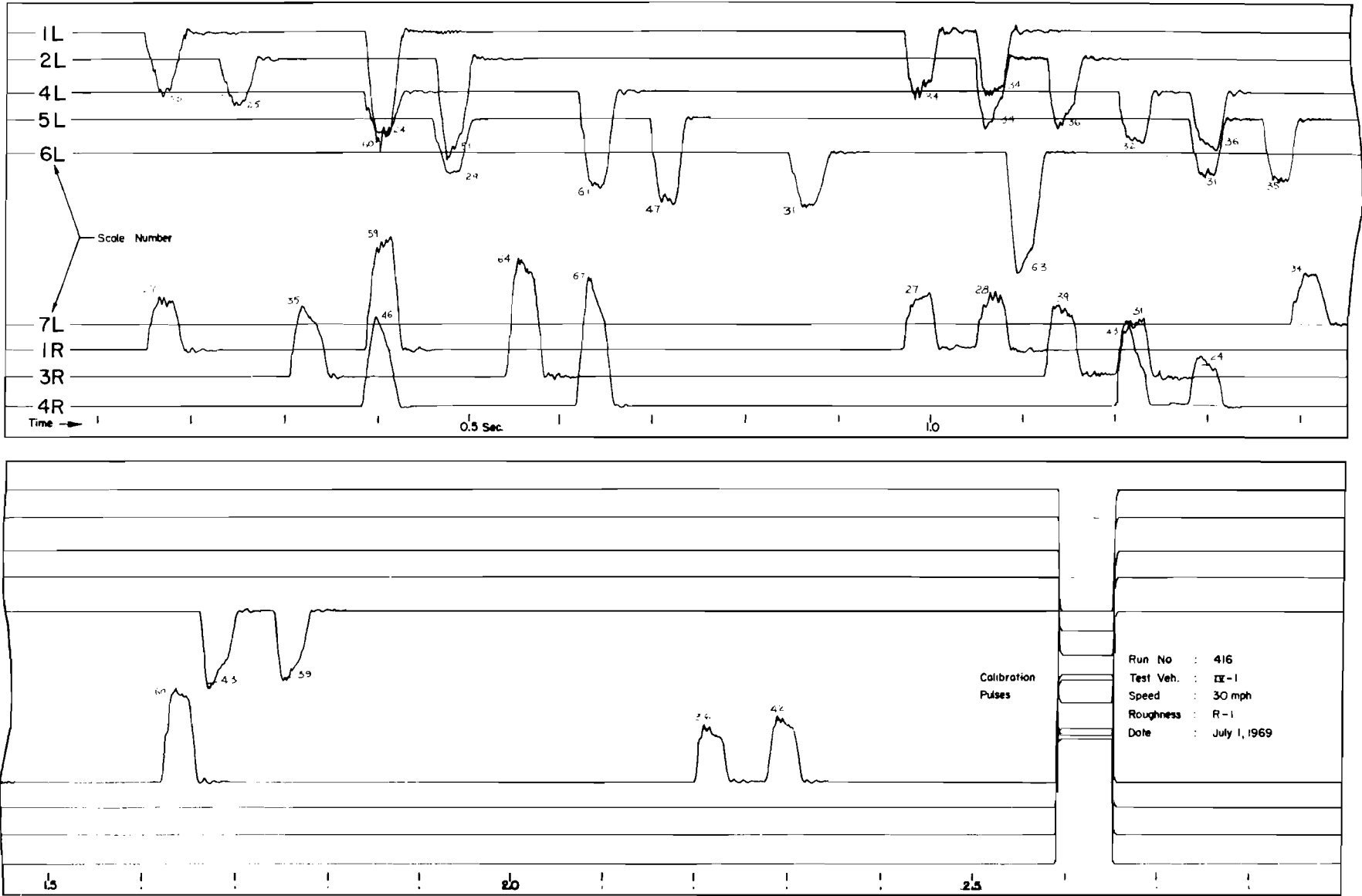


Fig 44. Typical oscillograph analog record.

The numbers given near the top of each force pulse represent the corresponding wheel load forces in 100-pound units.

Manual reduction, although time consuming, had an advantage in that human judgment could be used to eliminate extraneous noise pulses or noise signals that may have occurred within the averaging zone of a force pulse.

Computer Reduction of Data. This method of data reduction differs from the preceding method in that it is performed in stages rather than in one step directly from the analog record. The analog record must first be converted to digital form. An SDS 930 computer with special analog-to-digital capabilities has been used for this purpose. Each channel of digitized information was searched for force pulses by a digital computer program. A technique in which the magnitude of the varying electrical signals was compared with a threshold limit was used in identifying the rise and the fall of a force pulse. Furthermore, a procedure was used to isolate noise pulses of relatively short duration from valid force pulses by discarding all pulses less than 6 milliseconds in duration. Digital information describing all detected pulses was written on magnetic tape along with additional information regarding the relative time between successive pulses. At the end of each vehicle record, a calibration step pulse which simulates a constant force on each transducer was introduced as a check on instrumentation drift. The calibration steps were then used in a second computer program to scale the force pulses. Finally, since two 8-track tape recorders were used simultaneously in recording analog signals from the nine scales, a third program was used to coordinate and tabulate the forces indicated by each of the nine scales. The different steps involved in this data reduction method are summarized in Fig 45. A typical printout of the reduced data is shown in Table 9. Seven wheel load samples from the central portion of each load pulse and the average of each of these samples are tabulated in this printout.

All the experimental data were reduced by visual inspection of analog records and have been used in the analysis. A comparative study of the results of both methods of reduction showed no significant differences between the two.

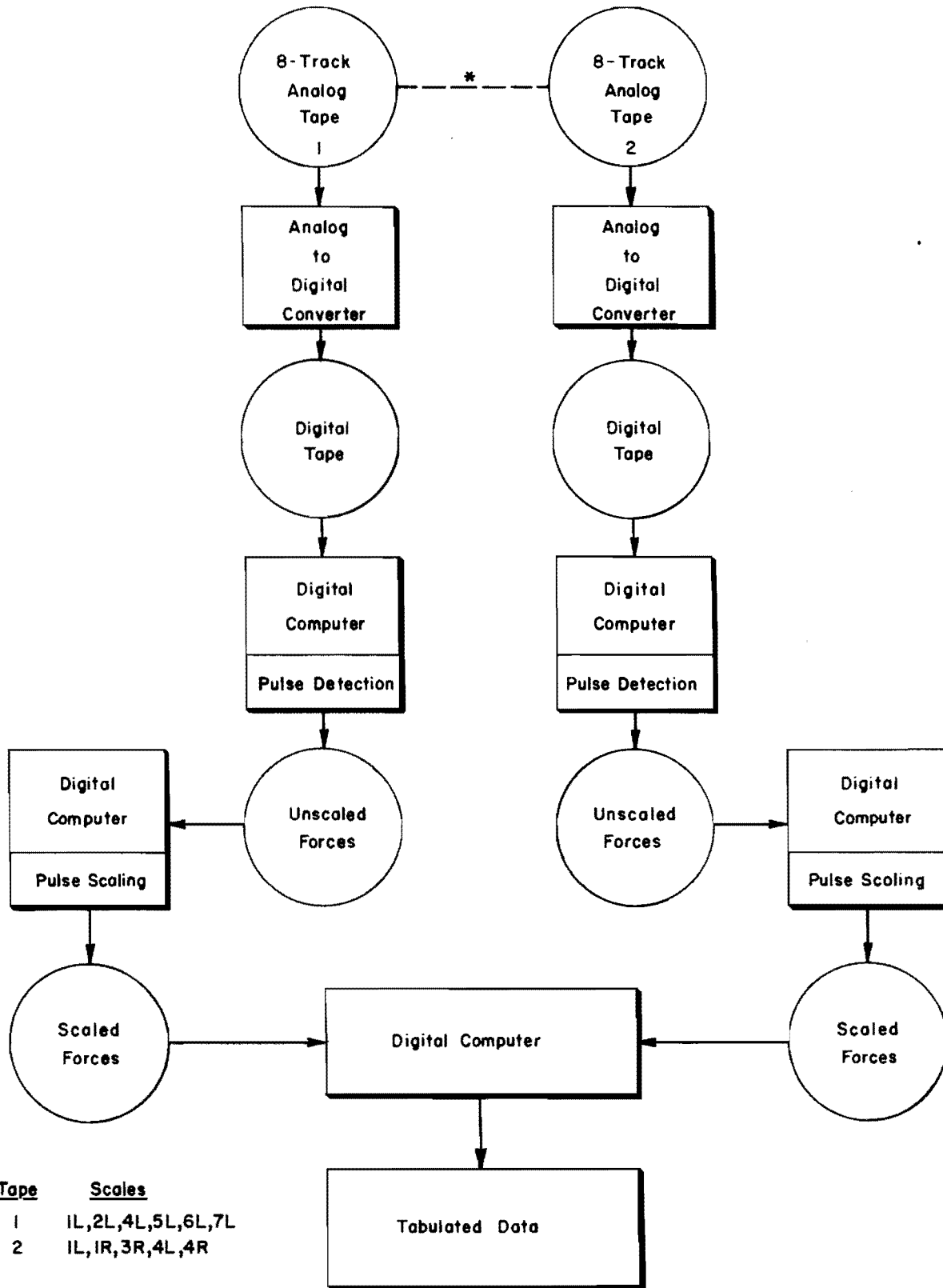


Fig 45. Computer reduction summary flow.

TABLE 9. PRINTOUT OF COMPUTER REDUCED WHEEL LOADS

SPEED 29.281 1L	NUMBER OF AXLES 5		RUN NUMBER 419		4L	4L	4H	5L	6L	7L
	1L	1R	2L	3R						
AXLE NUMBER 1										
45.476	43.608	43.667	42.770	62.214	57.007	56.693	23.189	44.356	51.788	50.235
47.209	47.046	45.475	40.193	60.191	60.315	59.259	20.703	41.683	50.094	46.198
46.439	44.754	44.842	40.986	56.916	59.112	57.518	18.862	37.878	45.671	45.509
42.395	40.876	45.204	39.995	52.966	57.709	57.151	18.033	36.027	43.789	46.986
43.743	43.608	45.746	38.311	51.810	58.310	56.693	17.757	34.999	43.977	46.789
42.780	41.317	45.746	35.437	47.378	56.406	54.494	17.388	34.176	43.695	43.047
40.951	41.229	46.830	34.446	44.103	55.604	54.494	17.849	32.531	42.377	43.047
* 44.959	40.785	45.339	39.109	53.207	56.840	55.827	21.113	38.483	45.795	45.974
AXLE NUMBER 2										
52.220	61.457	57.753	67.653	98.417	69.818	68.097	58.072	75.972	73.301	57.079
49.717	46.561	60.374	62.500	98.128	71.823	68.097	54.247	71.448	72.454	55.996
55.686	52.819	59.470	60.419	92.830	69.818	66.997	52.179	71.139	68.408	55.208
43.170	50.528	59.832	58.833	87.531	70.019	68.005	48.312	67.026	66.149	54.617
44.133	43.564	60.464	55.960	85.894	70.219	68.188	47.575	65.175	66.431	52.155
48.658	44.269	60.826	50.707	81.269	68.615	66.905	46.194	62.912	63.985	51.761
42.689	47.002	60.103	49.221	75.393	67.513	65.439	43.800	59.828	61.444	50.974
* 50.278	49.245	59.300	58.110	86.923	68.922	66.555	51.253	66.095	67.942	53.690
AXLE NUMBER 3										
48.634	45.530	46.618	51.119	77.931	58.822	58.755	39.040	54.336	51.633	51.545
36.792	36.628	34.417	52.605	73.307	60.526	60.129	32.226	48.064	47.586	49.083
44.013	44.208	45.534	47.056	72.826	61.127	60.037	28.175	41.482	45.986	46.720
41.221	38.743	47.883	38.633	68.779	60.626	60.679	25.689	36.444	44.951	46.818
36.792	36.628	47.341	36.750	65.311	61.227	60.587	25.505	33.770	43.728	45.046
37.659	39.045	41.918	34.371	60.784	61.628	60.587	23.019	30.068	41.375	43.470
40.932	40.153	46.618	29.114	58.760	60.225	59.854	20.993	26.983	40.152	40.319
* 41.736	41.154	45.969	40.731	67.159	60.281	59.525	27.776	37.016	44.946	45.880
AXLE NUMBER 4										
48.215	46.786	55.286	46.367	71.443	65.914	63.785	51.744	46.830	51.346	42.894
56.784	55.424	56.551	41.809	64.507	65.613	62.502	51.127	48.064	46.076	45.159
50.815	50.047	53.659	39.926	63.929	62.806	58.471	54.444	50.326	41.370	41.811
49.274	47.667	54.020	38.439	61.424	58.396	55.355	55.917	53.719	39.582	39.743
49.274	49.166	53.568	40.223	60.075	56.892	52.881	57.114	55.673	39.488	40.925
49.082	46.521	52.213	36.358	58.719	52.080	50.040	60.613	59.375	39.770	41.023
50.430	49.254	51.580	33.940	59.401	50.076	48.849	64.572	65.751	39.112	40.629
* 51.580	49.626	53.574	39.370	63.731	57.918	55.441	58.910	56.181	44.564	42.599
AXLE NUMBER 5										
67.808	66.111	65.747	63.744	89.916	86.488	79.926	53.850	47.015	73.541	77.428
80.420	76.600	68.549	61.563	85.195	78.669	74.153	51.456	42.901	70.530	73.686
77.050	77.041	66.289	52.050	75.851	75.863	70.030	53.482	40.944	64.789	70.437
72.429	68.843	62.855	48.483	62.460	68.645	60.042	53.666	40.639	60.648	60.885
75.606	72.369	63.397	47.888	59.859	60.826	59.767	52.837	39.097	57.637	58.719
74.451	74.308	58.969	39.564	54.078	60.325	58.026	52.745	37.143	56.037	57.340
68.963	67.433	55.805	35.303	46.661	52.005	50.604	54.310	38.274	52.931	50.545
* 74.858	73.105	62.900	48.213	65.307	67.826	66.526	53.249	41.220	61.866	62.876

* Average of the Seven Samples

This page replaces an intentionally blank page in the original.

-- CTR Library Digitization Team

CHAPTER 7. VALIDATION OF THE MODEL

General

The primary objective of this study program as stated in Chapter 1 was to develop a generalized mathematical model, or a series of models, which describe the dynamic behavior governing the magnitude and variation of dynamic wheel loads applied normal to the roadway surface by the wheels of the several classes of vehicles that represent mixed commercial highway traffic. The model was developed for both single unit vehicles and articulated multi-axle commercial vehicles. Before this model can be used confidently to simulate real-world conditions, it must be checked and validated by comparing the predicted dynamic wheel loads with observed loads under the same, or nearly the same, vehicular and roadway conditions.

This chapter describes a comparison between the predicted and the observed wheel loads in order to determine the accuracy of the model under varying operating conditions. The observed wheel loads which are used in this comparison are part of the data collected in the field during the major experimental program. These data have been properly documented and are presented in tabular form in Appendix C of this report.

Predicted versus Observed Forces - Comparative Study

The magnitude and the variation of the predicted dynamic wheel loads are greatly influenced not only by the assumptions involved in the physical and mathematical formulation of the model, but also by the vehicle and road characteristics which are used as an input for the model. An attempt has, therefore, been made to obtain information from manufacturers and other related groups regarding numerical quantities that must be assigned to the physical characteristics of the vehicles being modeled. Load deflection curves, or constants; damping characteristics; the distribution of mass, or weight of the vehicle, particularly the mass of the wheels, tires, and axles including

the differential and housing for the drive axles; and information pertaining to the flexibility of the vehicle body are among the vehicle characteristics required. Only a limited amount of information has been obtained from these sources, but field measurements on several representative vehicles permitted reasonable estimates to be made for all vehicle parameters needed in the model. A digital record of the natural profile of the test section for each pattern of roughness was recorded on a magnetic tape by the GMR profilometer in order to provide the road profile forcing function for the model. A total of 12* runs were simulated by the model for each of the five classes of vehicles. Point dynamic loads produced by the wheels of each class of vehicles were determined at 1-inch intervals over a stretch of pavement surface approximately 200-feet long including the instrumented test section. The range of predicted dynamic wheel loads was computed for the time increments when the wheel would be supported by a transducer at each sampling location. The total number of wheel load samples was 1,224** or 418 at each of 10, 30, and 60 miles per hour speeds. The observed dynamic wheel loads at every sampling location were compared with the corresponding range of predicted wheel loads. The difference between the closest observed value to the predicted range was determined. A summary of this comparative study is presented in Table 10. The model performance, as shown in this summary, appeared to be quite remarkable at low and medium speeds. This is indicated by the fact that 92 and 82 percent of the field observations were within 10 percent of the predicted range at 10 and 30 miles per hour, respectively, for all five classes of vehicles combined. For individual vehicles the percentage ranged between 85 percent for Classes II and III to 100 percent for Classes I and IV, at 10 miles per hour; and between 73 percent for Class V to 100 percent for Class I, at 30 miles per hour. At 60 miles per hour speed, however, only 53 percent of the observed values were within 10 percent of the predicted range. Again, this percentage varied for each vehicle ranging from 45 percent for Class V vehicle to approximately 65 percent for Class I vehicle. Consequently, the predicted dynamic wheel loads at this speed were inspected over the

* 4 roughness conditions \times 3 speeds = 12.

** 12 runs \times 17 axles \times 6 sampling locations (scale locations) = 1,224.

TABLE 10. COMPARATIVE STUDY SUMMARY OF THE DIFFERENCE
IN OBSERVED AND PREDICTED WHEEL LOADS

Vehicle Class	Speed, mph	Percent Within Predicted Range					
		0	5	10	15	20	≥25
I	10	82	10	8	-	-	-
	30	90	6	4	-	-	-
	60	52	2	10	4	4	28
II	10	72	10	3	8	3	4
	30	68	8	7	3	4	10
	60	50	8	1	4	15	22
III	10	78	3	4	8	1	6
	30	68	5	7	3	0	17
	60	31	10	7	11	7	34
IV	10	100	-	-	-	-	-
	30	70	5	5	2	2	16
	60	46	2	6	4	8	36
V	10	90	0	3	4	3	-
	30	62	5	6	8	4	15
	60	37	3	5	3	2	50
I - V	10	86	3	3	4	1	3
	30	70	6	6	4	2	12
	60	42	5	6	5	7	35
I - V	10, 30, 60	66	5	4	4	3	18

entire sampling section, and in many cases it was found that model oscillation was not completely in phase with the observed oscillation. Furthermore, vehicle oscillation which frequently was produced by existing unbalance in the wheels of the vehicle as well as road profile irregularities, tended to increase with the vehicle speed thus accounting, at least in part, for poorer agreement between the observed and the predicted range of dynamic wheel load at high speeds.

A separate comparative study was also made of the observed and the predicted wheel loads for the tandem axles. This involved Classes III, IV, and V and included a total of 576* samples. The results of this study are summarized in Table 11. Generally, the overall performance of the model for the tandem axle wheel loads appeared to be similar to that found in the preceding study.

In addition to these descriptive statistical studies which involved all combinations of roughness, speed, axles, and sample location, it is desirable to present a few of these comparisons in graphical form. Thus, additional instructions were incorporated in the computer program "DYMOL" to make use of plotting routines available in the CDC 6600 system at The University of Texas at Austin in order to plot the predicted left wheel path dynamic loads over the position of each scale. The plotted wheel loads were produced on microfilm from which prints were later made. A smooth curve indicating the predicted pattern of load variation over the 18-inch effective width of the scale platform was fitted through the point wheel loads. The total number of runs made by the model resulted in 204** sets of curves.

Furthermore, it was desirable to check the performance of the model under more than one loading condition since it would be expected that the dynamic behavior of moving vehicles may vary according to whether the vehicle is loaded or empty. Additional passes were thus simulated with an empty Class I vehicle for this purpose.

After these curves were completed, the average dynamic wheel forces recorded in the field at each sampling location under a specific roughness-speed condition were plotted on the corresponding curve in order to provide for an

* 4 roughnesses \times 3 speeds \times 6 scales \times (2 axles (III) + 2 axles (IV) + 4 axles (V)) = 576.

** 12 runs \times 17 axles = 204.

TABLE 11. COMPARATIVE STUDY SUMMARY OF THE DIFFERENCE IN OBSERVED
AND PREDICTED WHEEL LOADS FROM TANDEM AXLES

Vehicle Class	Speed, mph	Percent Within Predicted Range					
		0	5	10	15	20	≥25
III	10	80	4	2	6	2	6
	30	56	6	8	5	0	25
	60	25	6	8	8	9	44
IV	10	100	-	-	-	-	-
	30	61	0	4	4	4	27
	60	50	2	4	4	2	38
V	10	99	0	0	1	-	-
	30	69	3	1	8	5	14
	60	39	1	3	1	1	55
III, IV, V	10	94	1	1	2	1	1
	30	63	3	4	6	4	20
	60	38	2	5	4	3	48
III, IV, V	10, 30, 60	66	2	3	4	2	23

immediate visual comparison between the observed and the predicted wheel loads.

The observed wheel loads were recorded in analog form and reduced manually by visual inspection of analog field records (see Fig 44, page 110). The technique used in this reduction which consisted of determining the calibrated average height of the central portion of the pulses representing each wheel load, has been discussed in details in the preceding chapter.

Due to the large number of sets of these comparative curves, only those representative of both good and poor agreement between the predicted and observed wheel loads were included in this chapter. The selected curves are shown in Figs 46 through 54. In addition, the figures show the variation in the degree of replication of three repeated passes at the same roughness-speed condition. Except for a few cases where the range in the observed loads reached as much as 2,000 pounds, the degree of replication was quite satisfactory.

These segmentary curves do not show how the dynamic wheel loads varied continuously over the entire pavement test section. In order to demonstrate such variation the predicted wheel loads produced by the drive axles of Classes I (both loaded and empty), II, and IV for roughness 4 and speed 30 miles per hour are shown in Figs 55 through 58. The road profile for the stretch over which the loads are determined is also included at the bottom of each figure. High frequency oscillations were eliminated and a smooth curve has been fitted to show the overall variation of the load.

As shown in these figures, the 3/8-inch board placed over scale 1L platform resulted in impact factors* of 130 percent (Class I, empty), 90 percent (Class IV), 55 percent (Class III), and 44 percent (Class I, loaded). The duration of these impact forces was short due to the rapid variation in the magnitude of the load. For example, the wheel load for the drive axle of Class I empty vehicle dropped from a maximum of approximately 6,000 pounds (130 percent impact factor) to zero (tire losing contact with the road surface) in approximately 25 milliseconds (20 Hz). The corresponding load variation for the loaded Class I vehicle was from a maximum of 10,200 pounds (44 percent impact factor) to approximately 4600 pounds (see Fig 56) in about 25 milliseconds. Although the tire in this case did not lose contact with the

* Impact factor is the excess in dynamic force over static force expressed as percentage of static.

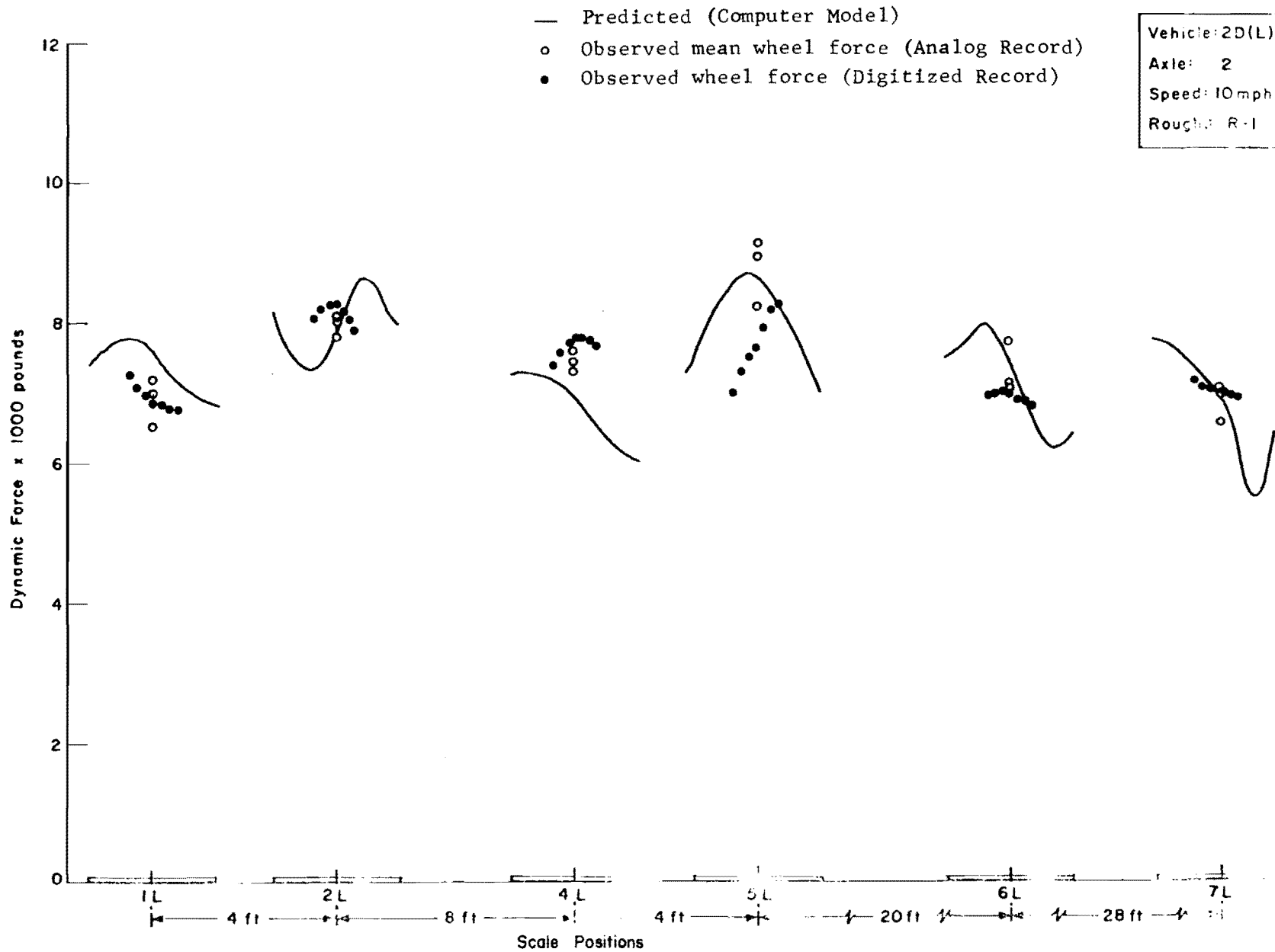


Fig 46. Predicted and observed dynamic wheel load (Class I, loaded).

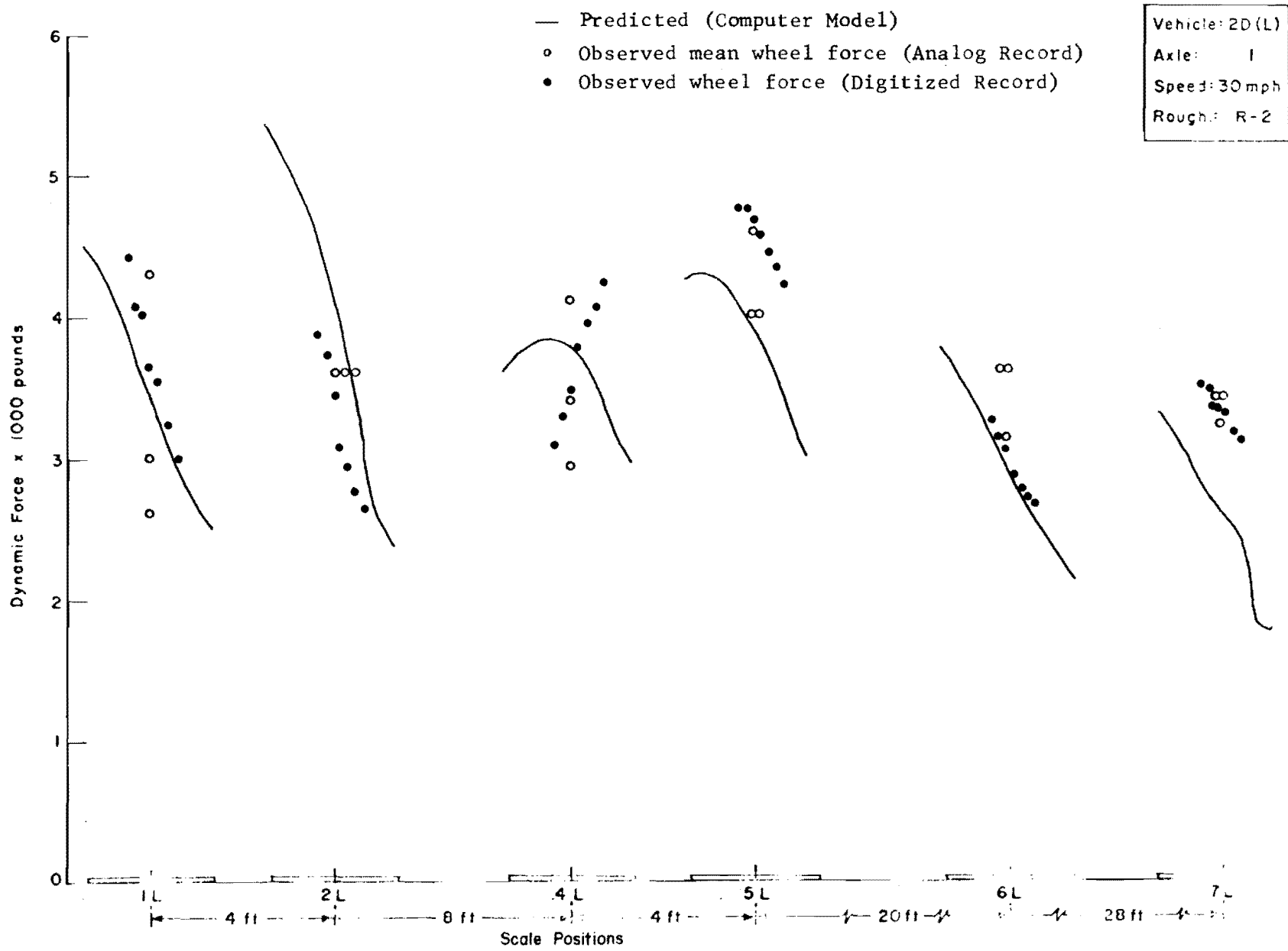


Fig 47. Predicted and observed dynamic wheel load (Class I, loaded).

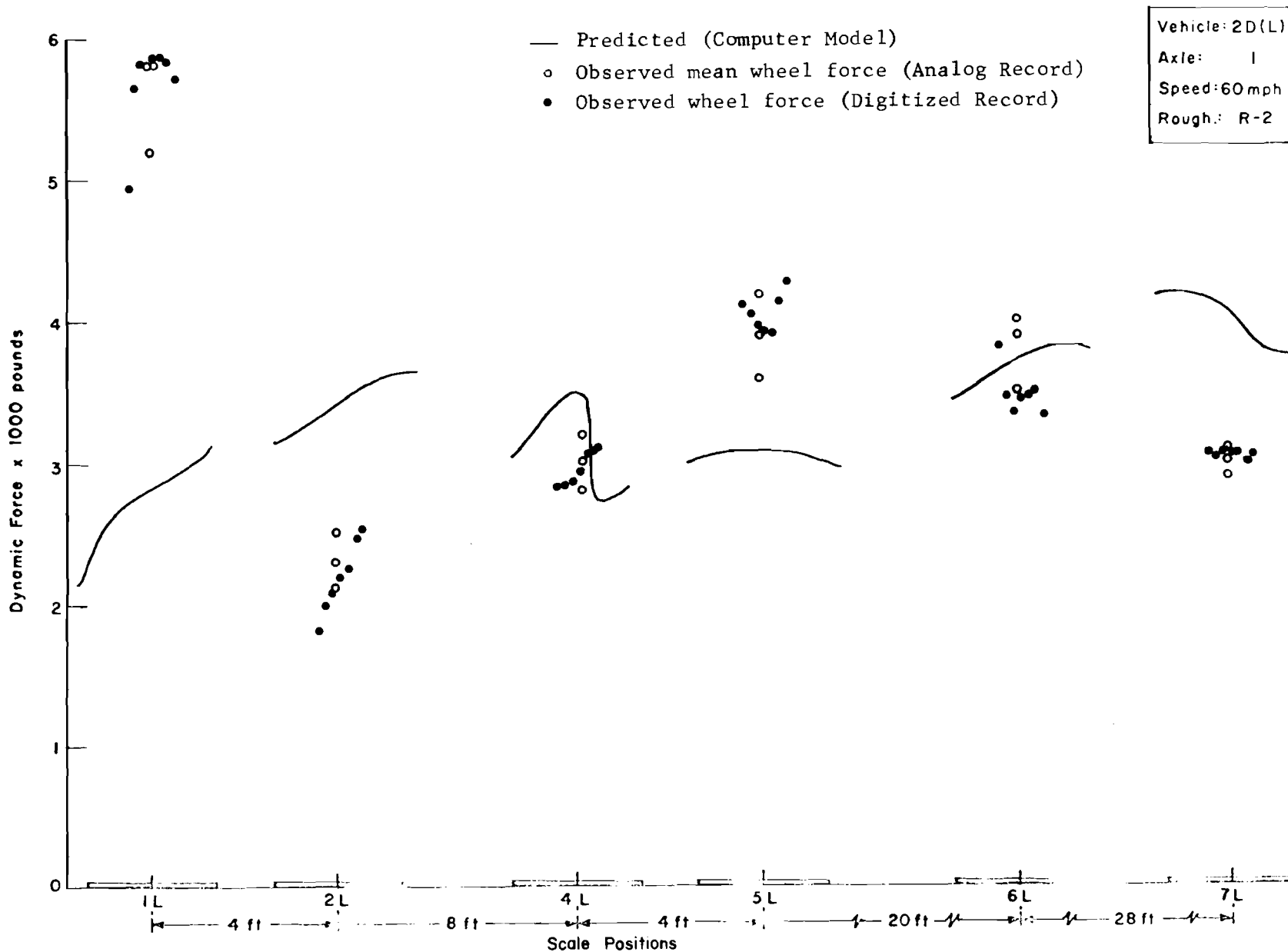


Fig 48. Predicted and observed dynamic wheel load (Class I, loaded).

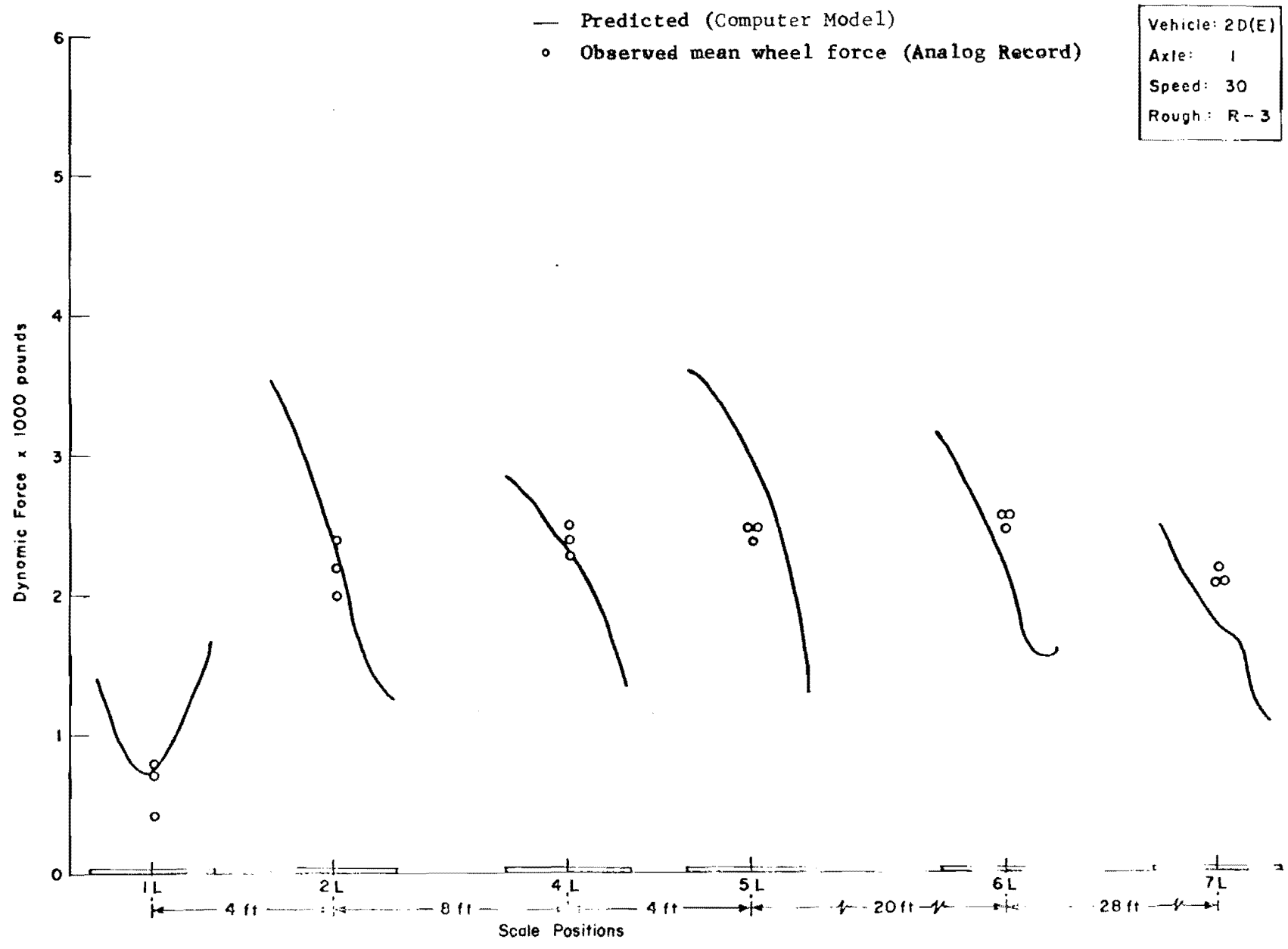


Fig 49. Predicted and observed dynamic wheel load (Class I, empty).

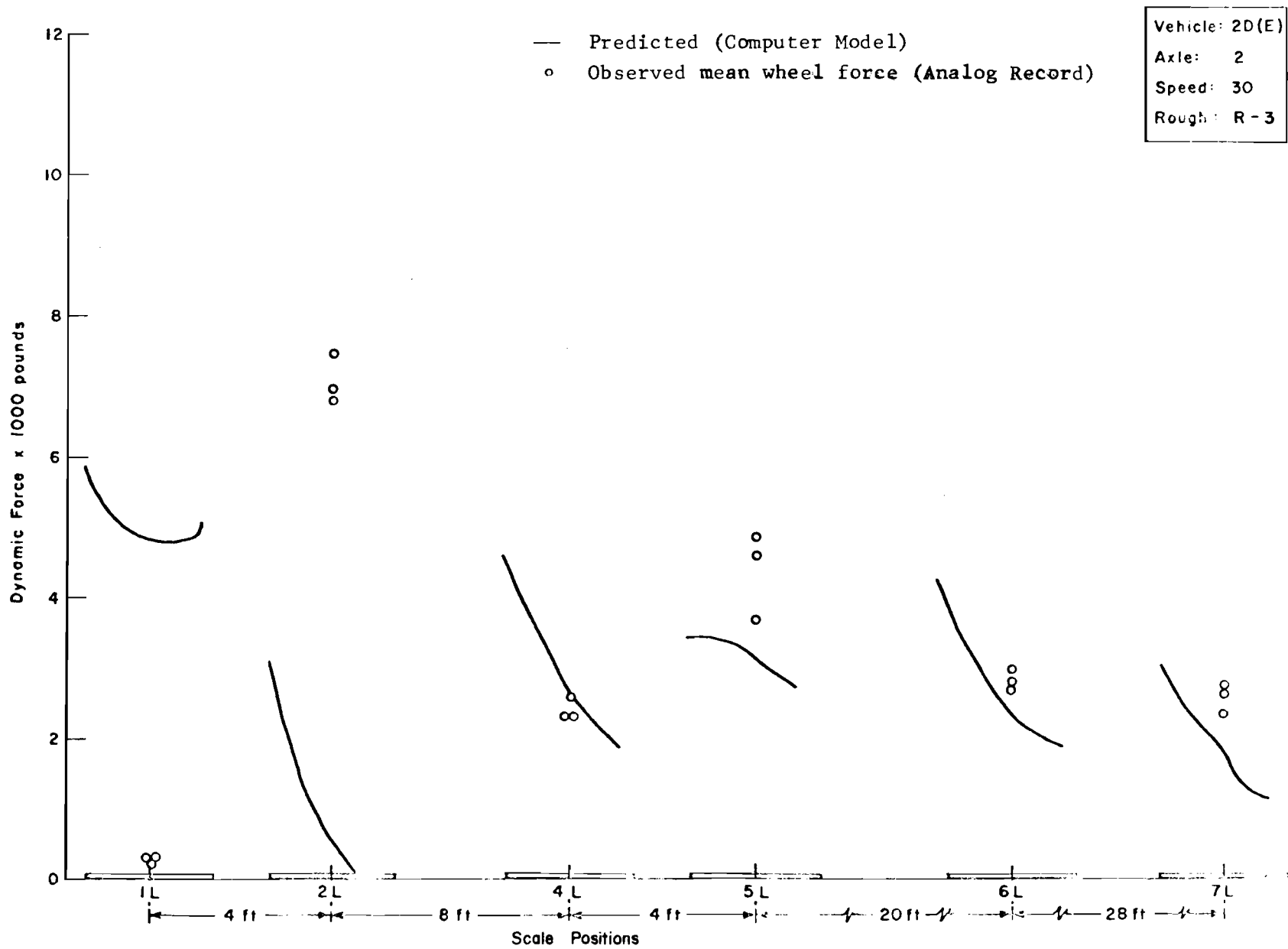


Fig 50. Predicted and observed dynamic wheel load (Class I, empty).

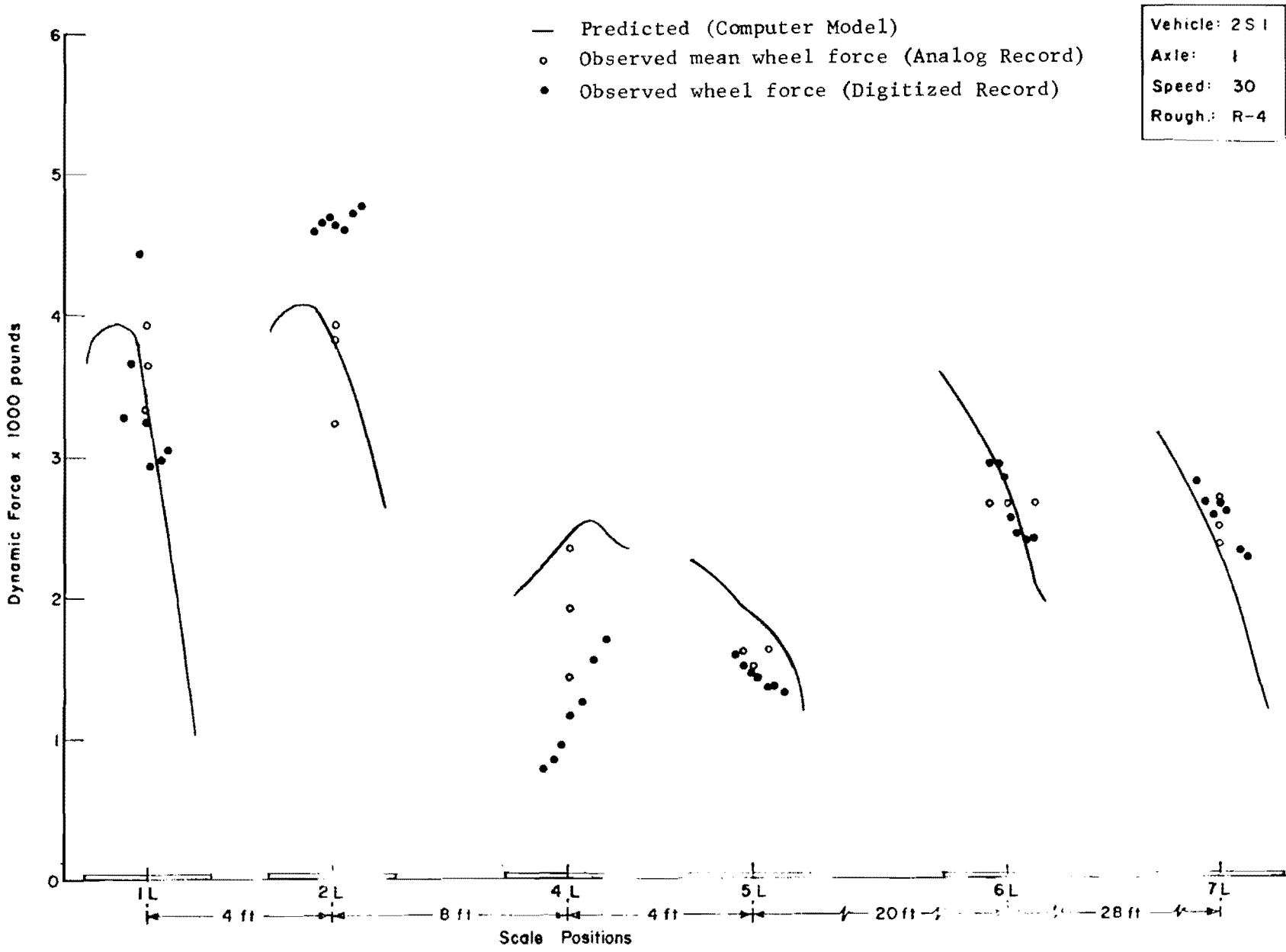


Fig 51. Predicted and observed dynamic wheel load (Class II).

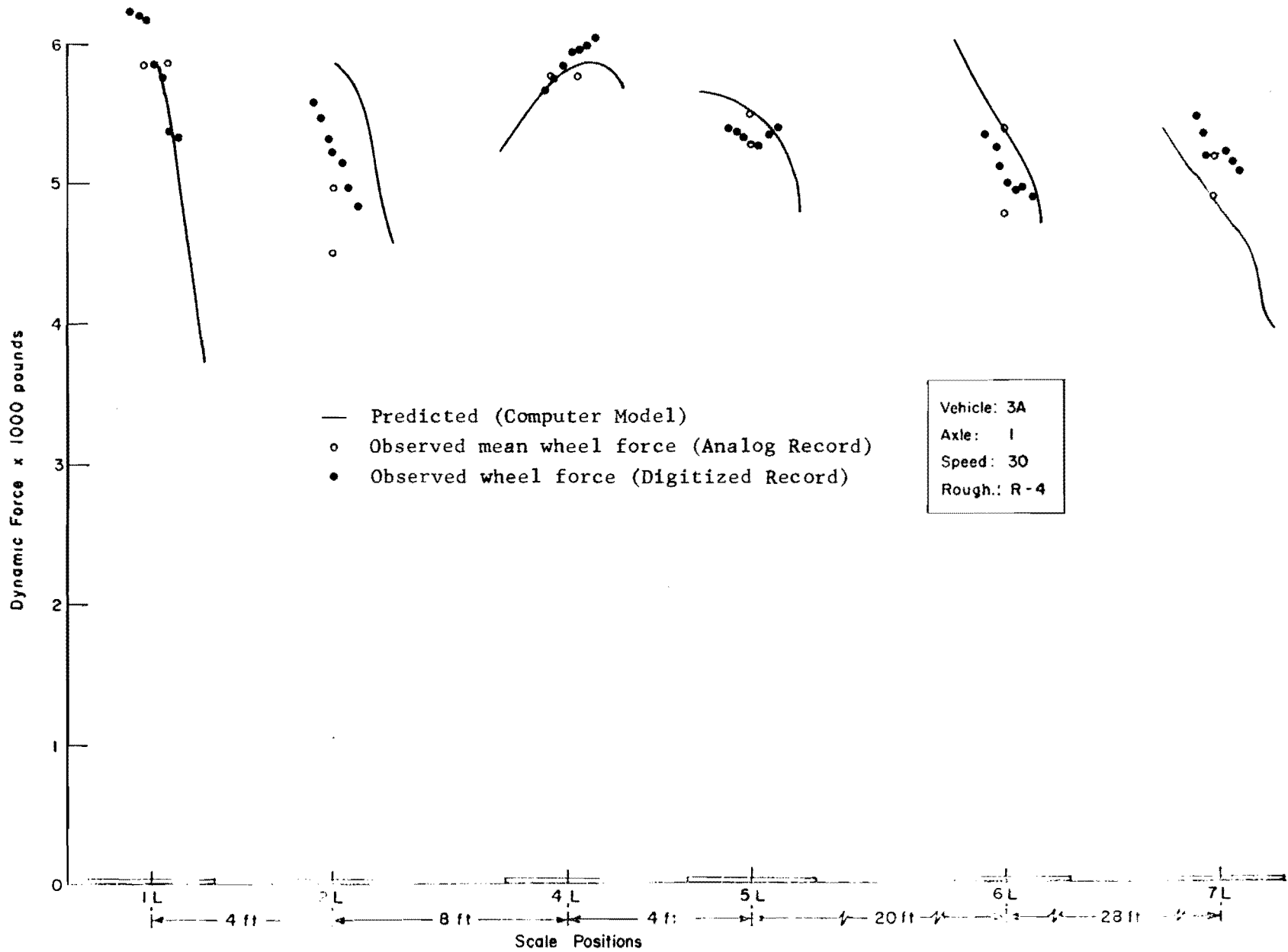


Fig 52. Predicted and observed dynamic wheel load (Class III).

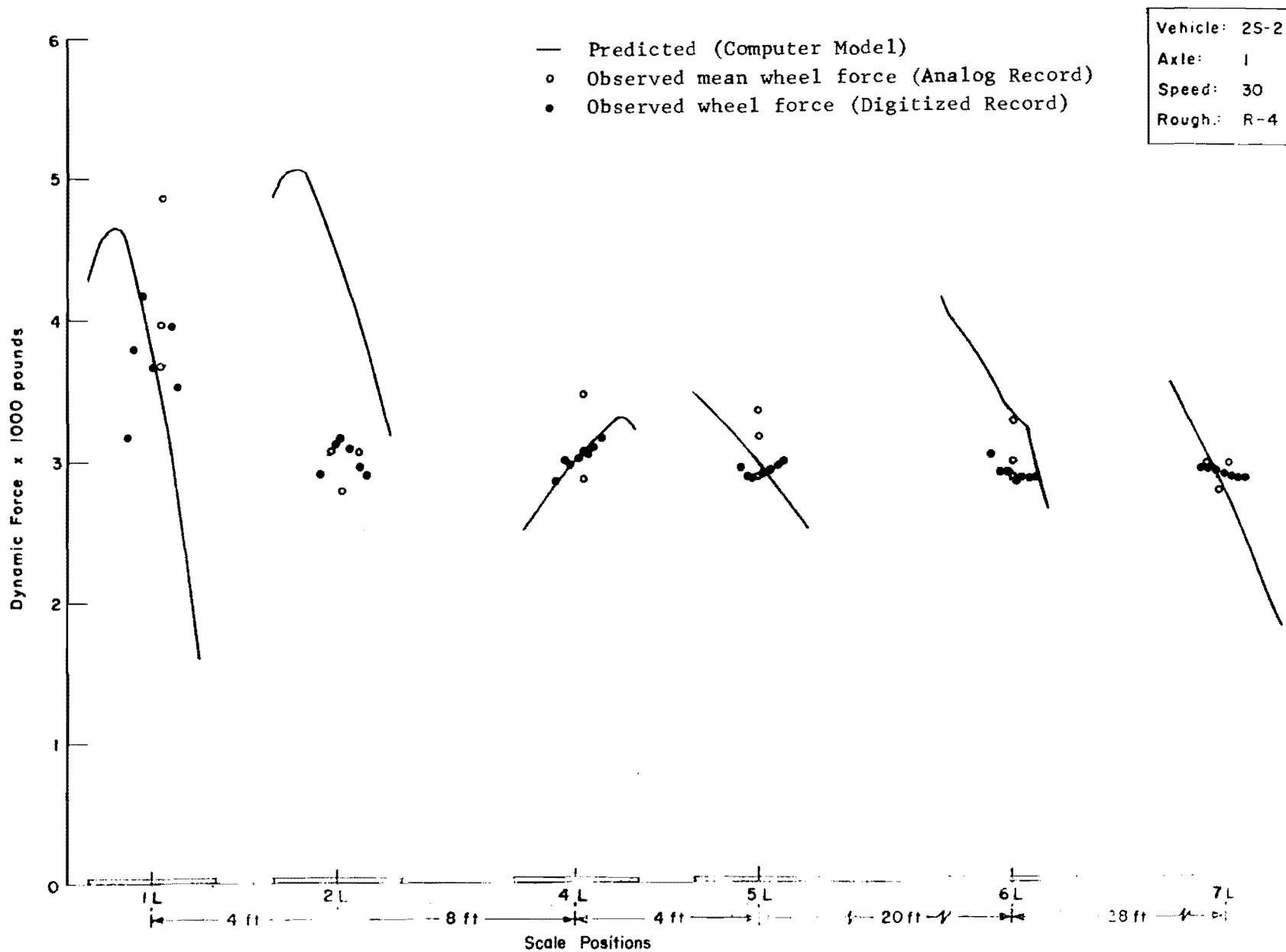


Fig 53. Predicted and observed dynamic wheel load (Class IV).

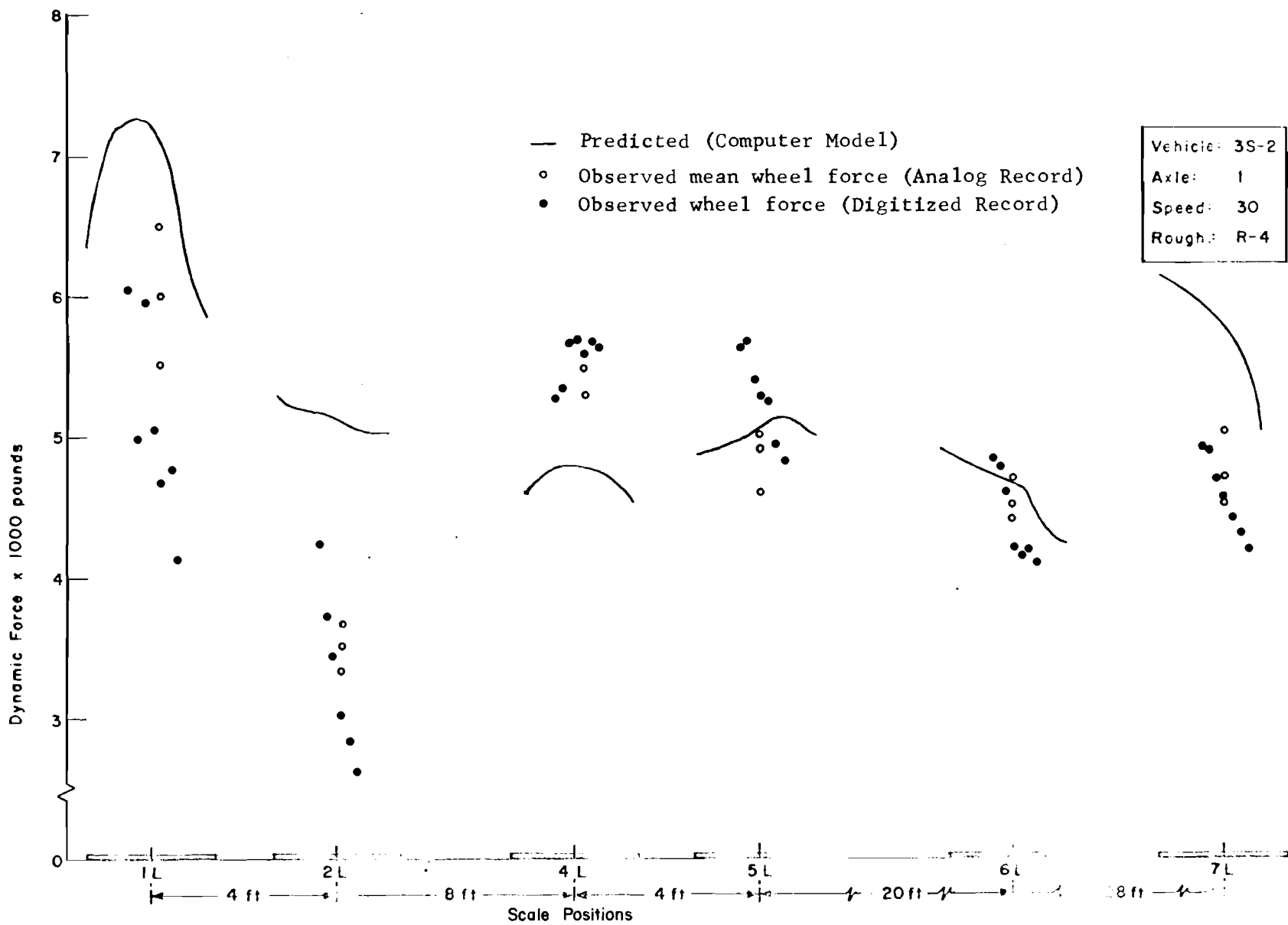


Fig 54. Predicted and observed dynamic wheel load (Class V).

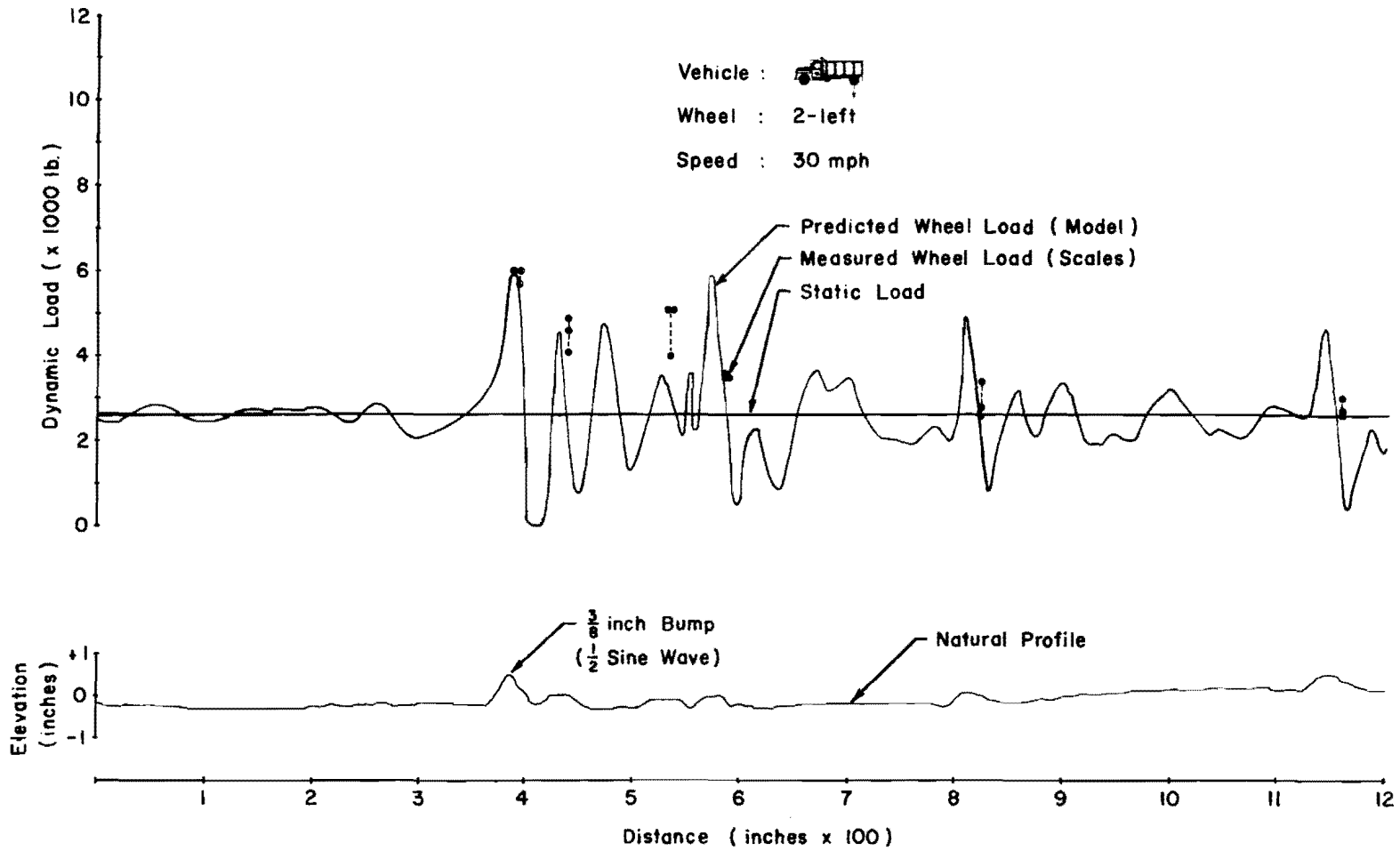


Fig 55. Continuous record of predicted load and roadway profile (R-4).

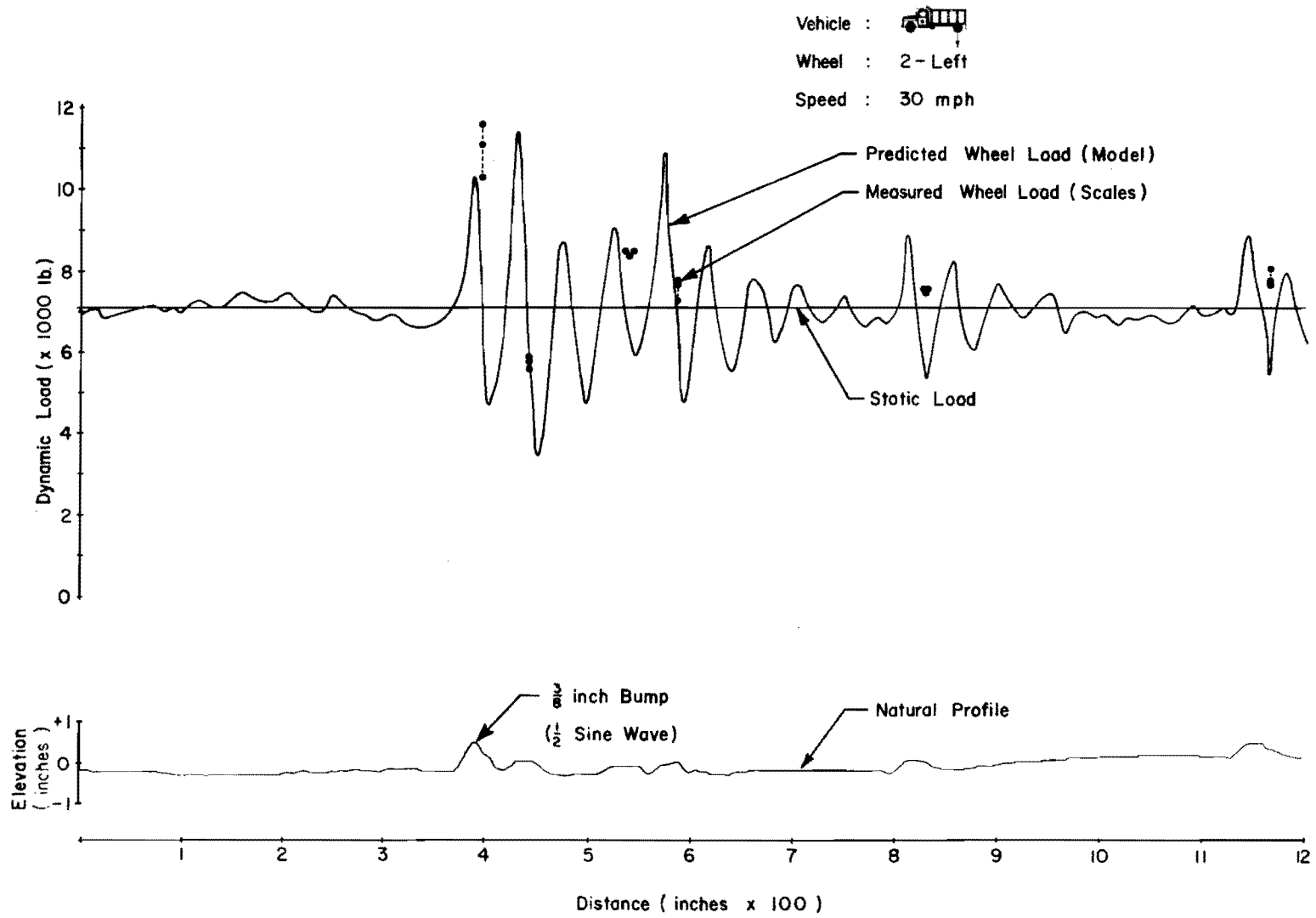


Fig 56. Continuous record of predicted load and roadway profile (R-4).

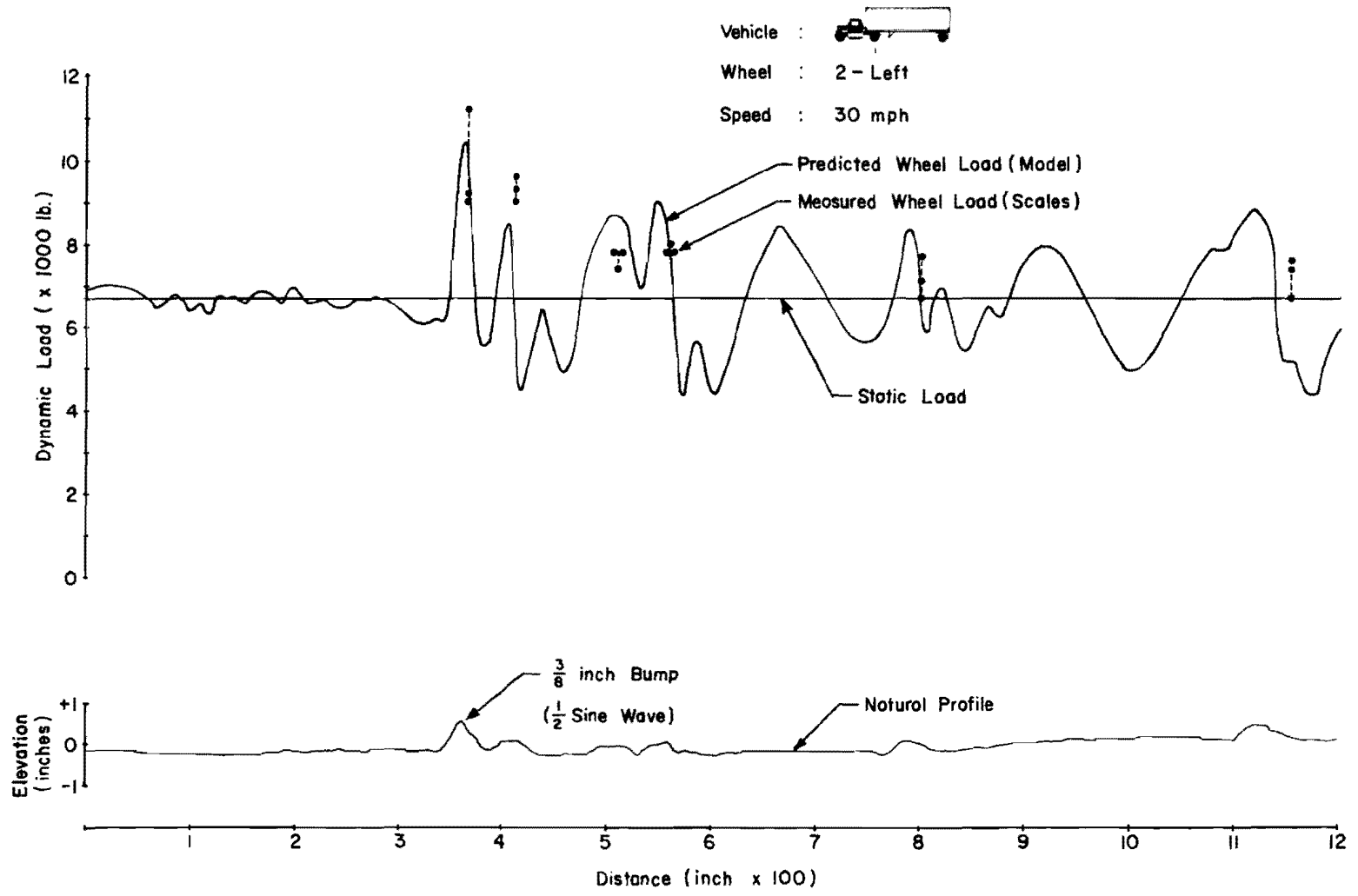


Fig 57. Continuous record of predicted load and roadway profile (R-4).

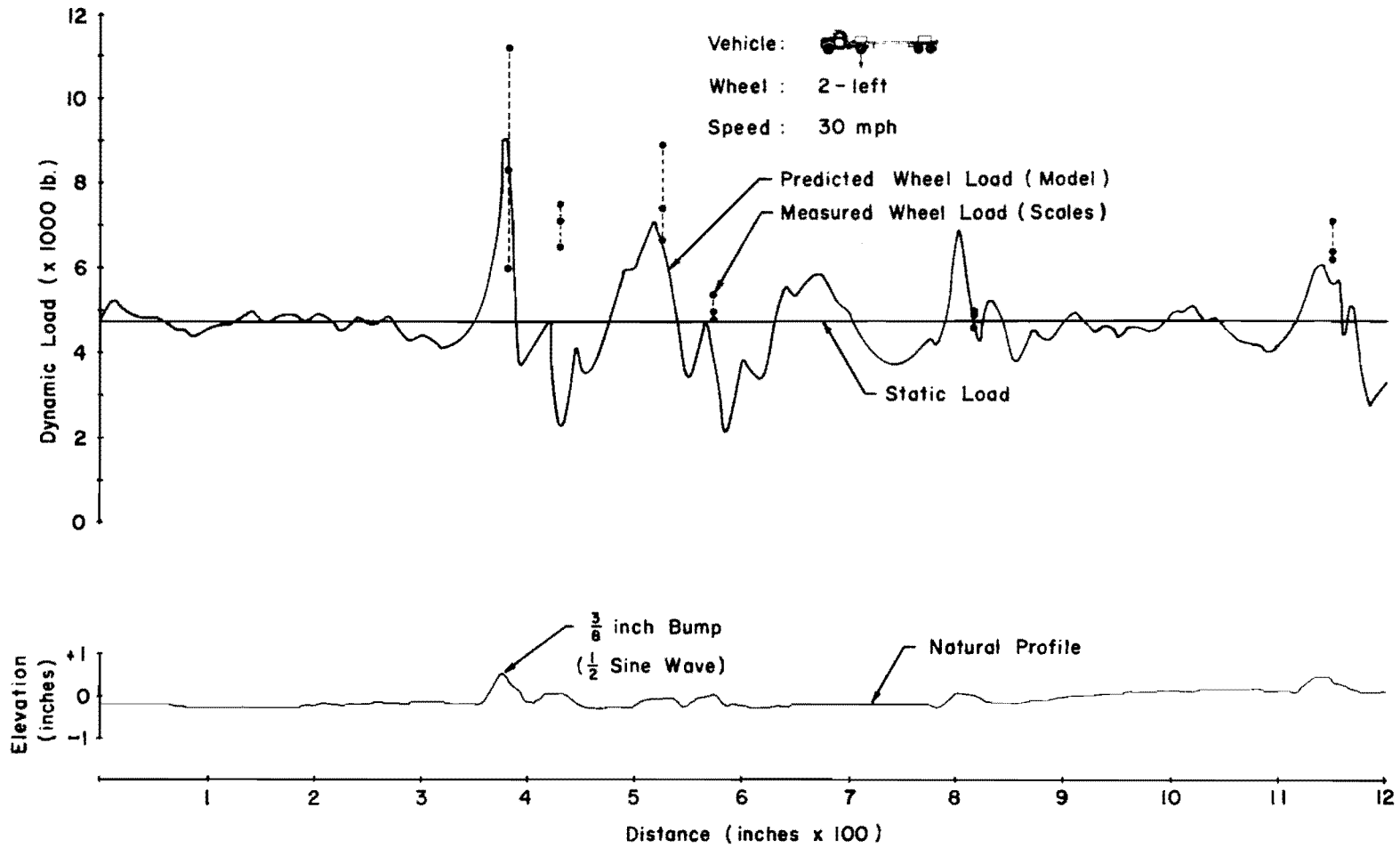


Fig 58. Continuous record of predicted load and roadway profile (R-4).

pavement surface, the rate of change of the load remained approximately the same as in the empty condition. For Class II and IV vehicles a slightly smaller rate of force change was noticed with drops amounting to about 4900 and 3600 pounds, respectively, in 25 milliseconds (see Figs 57 and 58).

Study of Dynamic Load Component*

In the preceding section the validation of the mathematical model involved a direct comparison between the predicted dynamic wheel loads and the observed loads. Although this comparative study which was presented in a descriptive statistical form, and in part in graphical form, is sufficient for the purpose of establishing the accuracy of the model, the model has been subjected to a further check involving a study of the frequency distribution of dynamic load component resulting from predicted and observed dynamic wheel loads. The dynamic component corresponding to each roughness-speed-axle combination of wheel load samples was calculated for both cases (predicted and observed). Due to the deterministic nature of the model formulation, however, only one value can be predicted at each sampling location as compared to three field observations. Thus in order to equalize the number** of samples for both cases, the average of the three observations has been used in determining the observed dynamic components. The computer program which was used in determining these components was also used in sorting and listing each component according to its absolute value. From this listing, frequency tables were formed and cumulative frequency curves were then drawn for the combined classes of vehicles as well as for individual classes. These curves are shown in Figs 59 through 64.

It must be pointed out, however, that these frequency diagrams are purely intended for comparative purposes and that no conclusion regarding the magnitude of wheel loads should be made since only the absolute values of the dynamic components have been used. In addition, the term dynamic component has been selected for this absolute difference between static and dynamic in order that it may not be confused with impact factor which normally implies positive components where the dynamic load is greater than static load.

* Dynamic load component is the difference in dynamic and static forces expressed as a percentage of static force.

** 1,224 samples (= 4 roughnesses × 3 speeds × 17 axles × 6 scales).

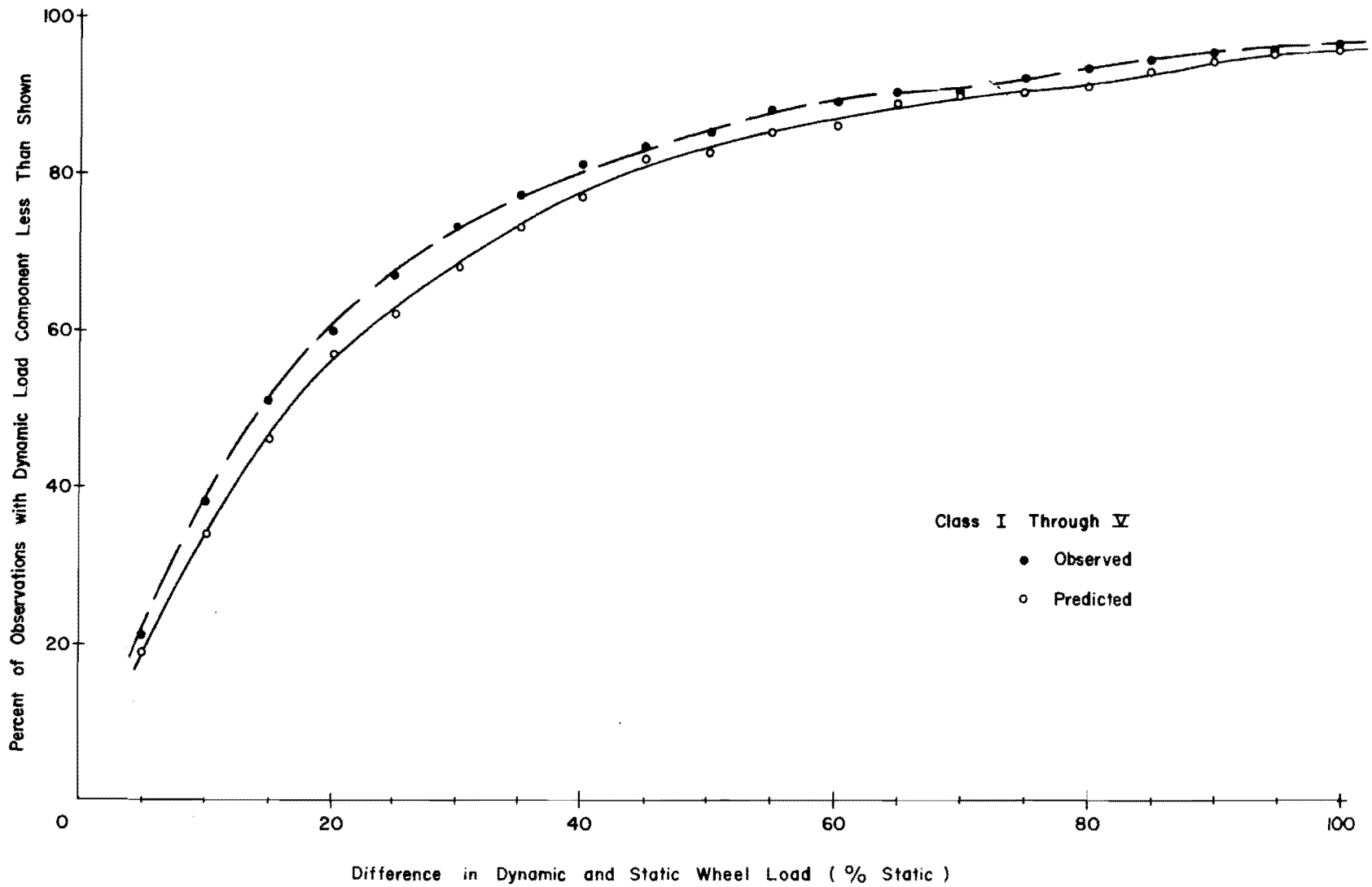


Fig 59. Predicted and observed cumulative frequency distribution of dynamic load components.

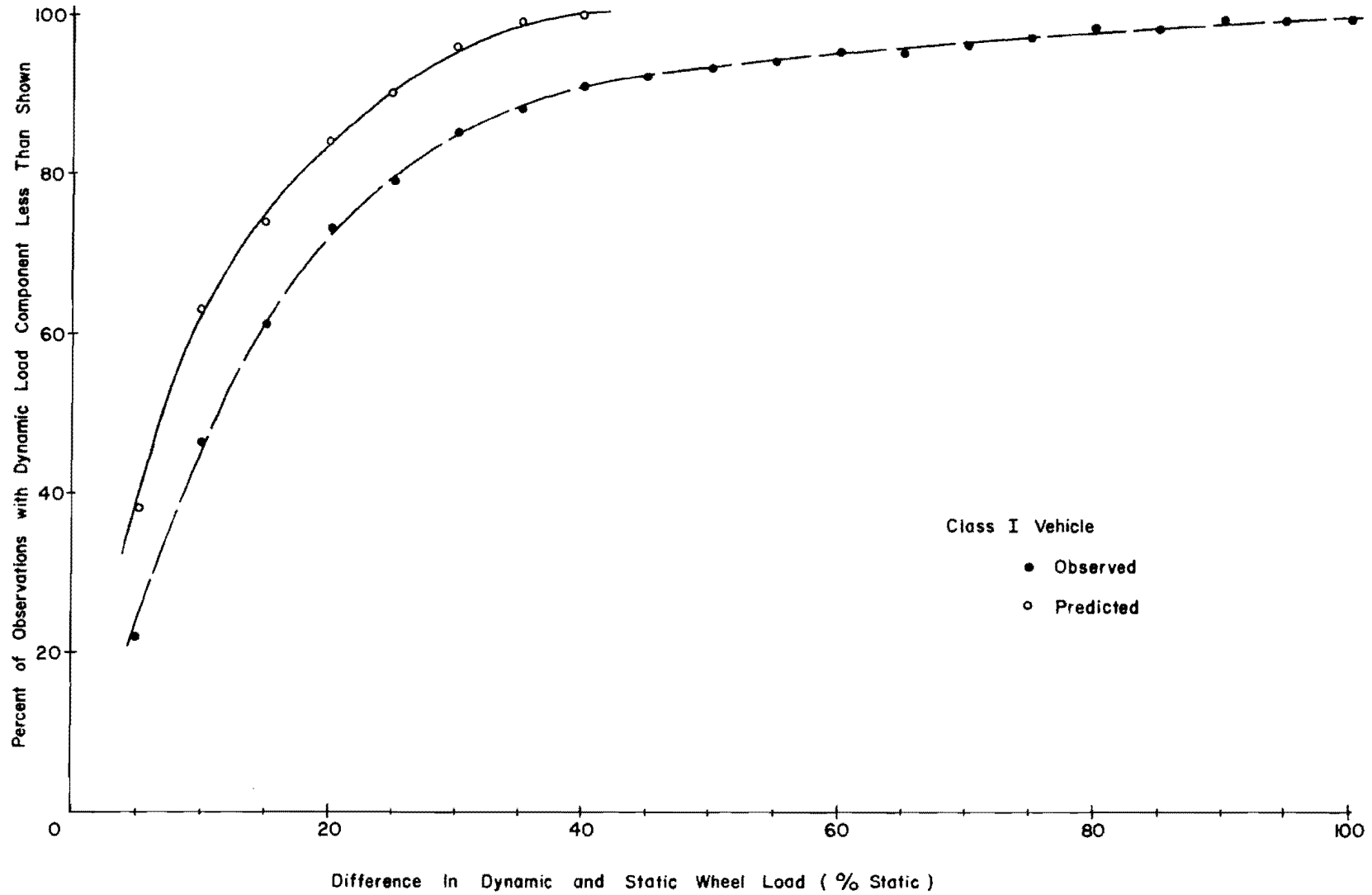


Fig 60. Predicted and observed cumulative frequency distribution of dynamic load components.

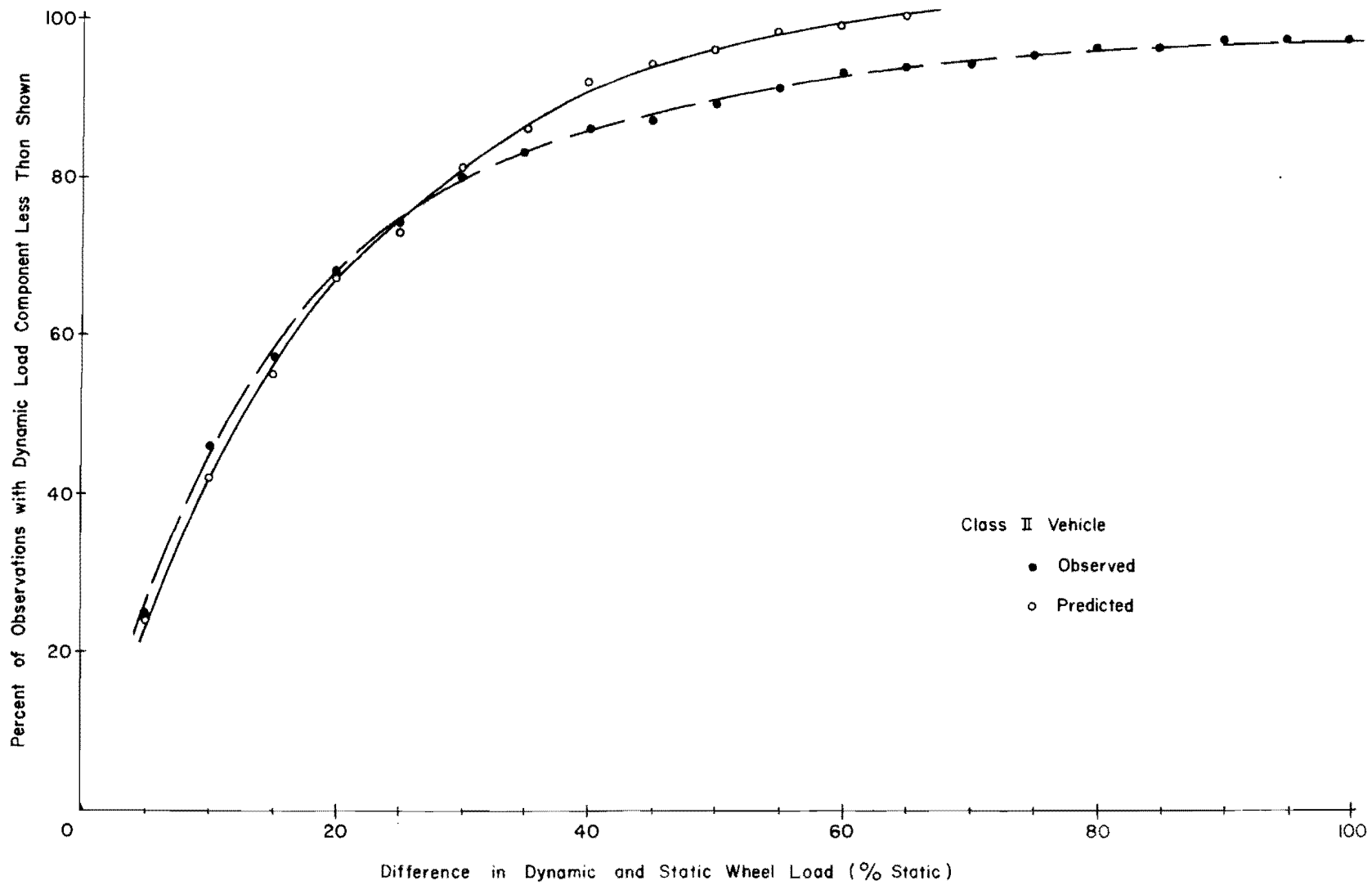


Fig 61. Predicted and observed cumulative frequency distribution of dynamic load components.

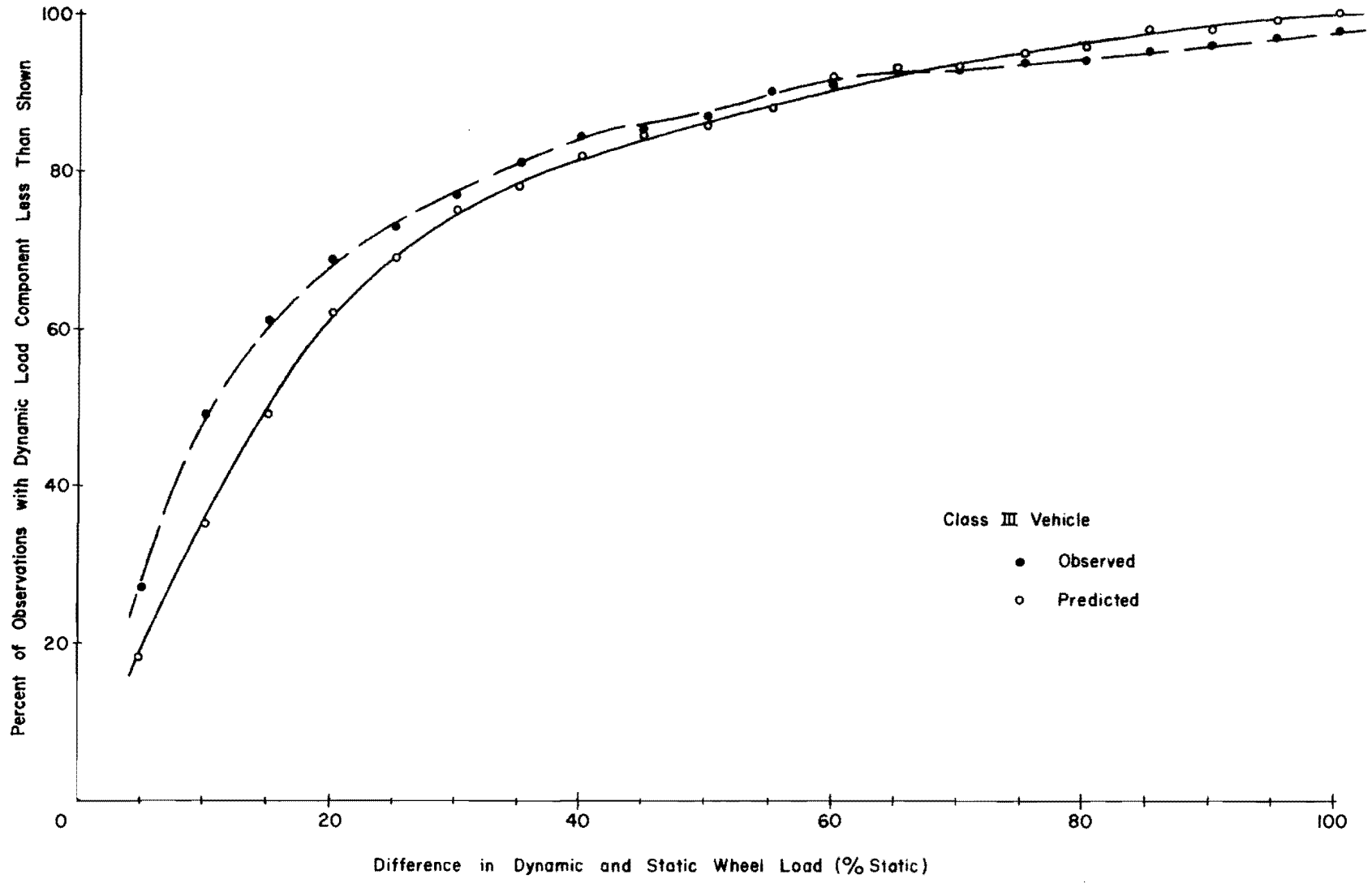


Fig 62. Predicted and observed cumulative frequency distribution of dynamic load components.

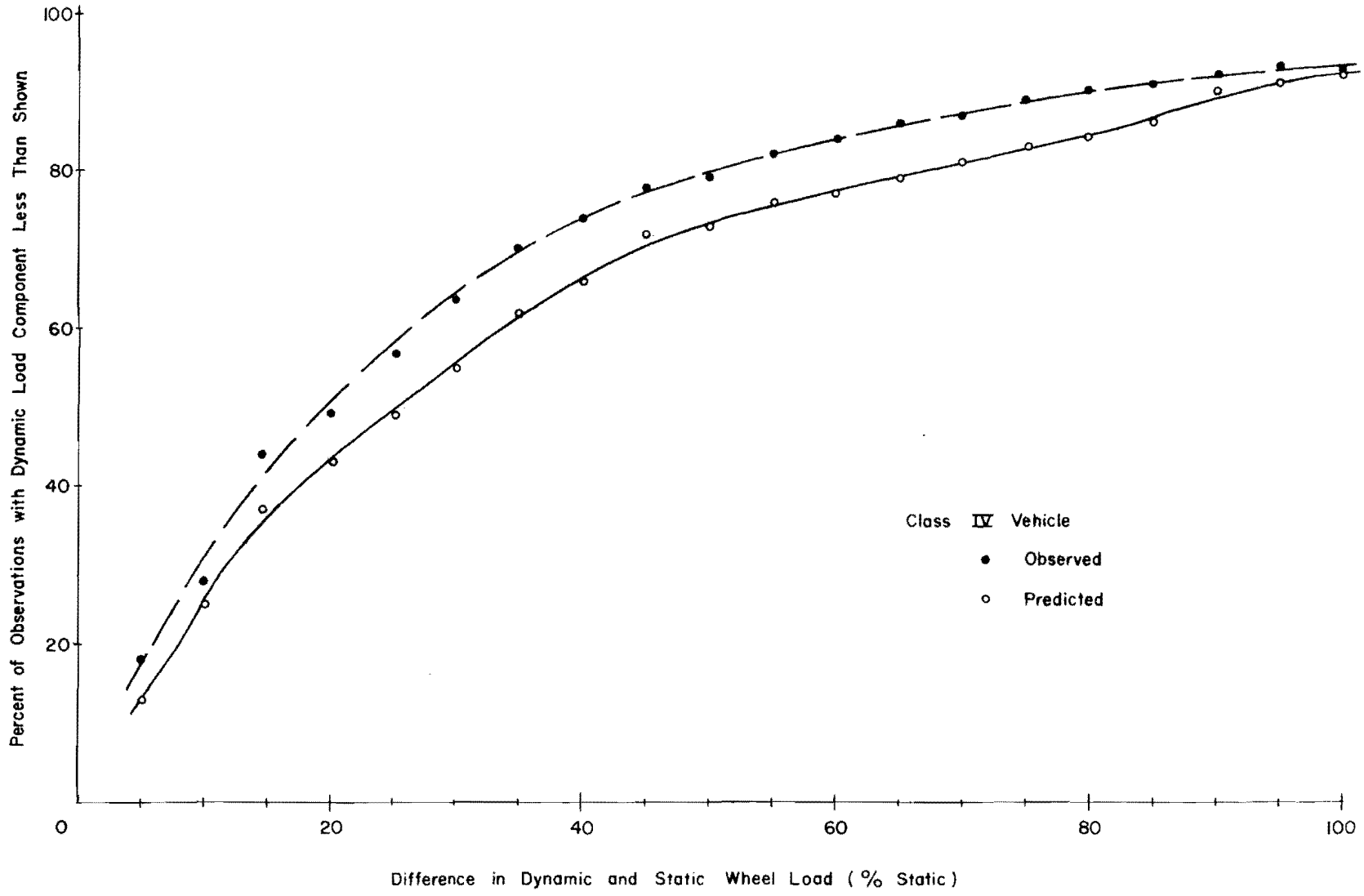


Fig 63. Predicted and observed cumulative frequency distribution of dynamic load components.

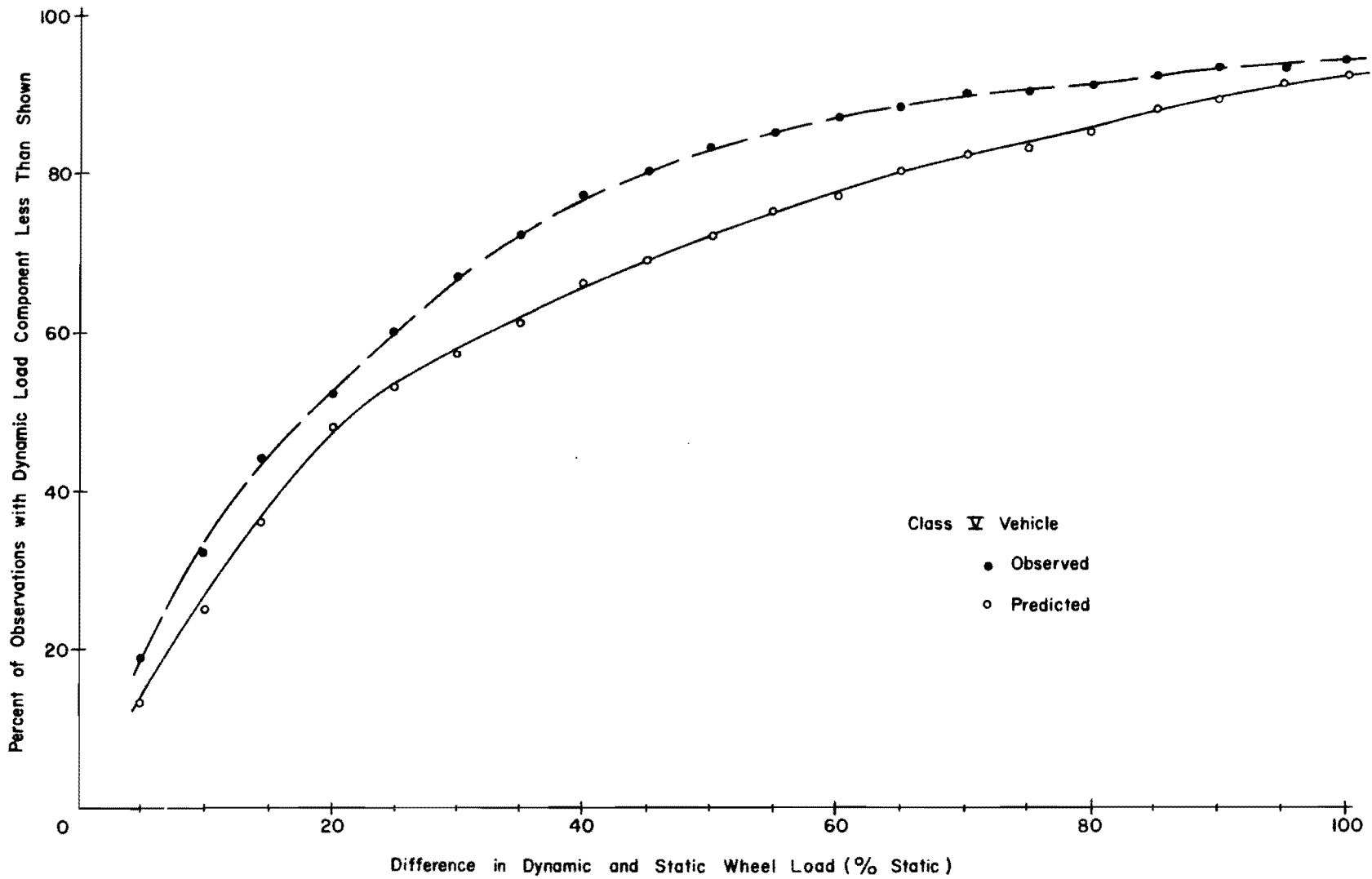


Fig 64. Predicted and observed cumulative frequency distribution of dynamic load components.

The predicted dynamic components for the combined samples of all classes of vehicles generally appear to be greater in magnitude than the observed components. This is shown in Fig 59 where the predicted curve falls below the observed curve with a maximum variation in frequency of about 5 percent. Except for the Class I vehicle, a similar comparison for individual classes of vehicles indicates that the two curves follow nearly the same pattern. The predicted cumulative frequency curve for Class I samples, however, fall above the corresponding observed curve which is an indication that the predicted components were generally lower in magnitude than the observed. Another interesting feature of these frequency curves for this class (see Fig 60) is that all of the predicted dynamic components are less than 40 percent in magnitude while only about 90 percent of the observed components fall below 40 percent in magnitude. A similar feature is shown for Class II (see Fig 61) where all of the predicted components, compared to 94 percent of the observed components, are below 65 percent in magnitude. As mentioned earlier, it cannot be determined from the figures how many of these loads were above or below the corresponding static load.

Summary

Based on the above comparative studies between the predicted and the observed dynamic wheel loads, it can be concluded that the model performance under a wide range of different conditions was in general quite good. The average difference between the observed and the predicted range of wheel loads is less than 10 percent with relatively few extreme variations. This average may be indicative of the accuracy of the model. It must be noted, however, that certain assumptions involved in the formulation of the model can be modified in order to improve the accuracy of the model, particularly with regard to modeling the tandem axles where the mass of the fore-and-aft connection frame has been ignored in comparison to the masses of the wheels. Consequently, extreme pitching of the tandem has resulted especially at high speeds. One possible means of reducing the extent of tandem pitching would be by including this mass which in turn would increase the mass moment of inertia thus reducing the pitching frequency.

Finally, the accuracy of the model predictions depends on the accuracy of the numerical quantities used for the physical characteristics of the vehicles.

The extent to which these affect the predicted forces can be determined by performing a sensitivity analysis on the model.

CHAPTER 8. DISCUSSION OF EXPERIMENTAL RESULTS

General

The experimentally measured dynamic loads applied normal to the roadway surface by the wheels of selected classes of vehicles are documented in Appendix C as noted in the preceding chapter. The general layout of the experimental program has been described earlier in this report.

The objective of this chapter is to analyze the variation in the magnitude of the dynamic wheel forces over the different levels of each factor or combination of factors included in the experiment. Basically, the hypothesis is first made that the factors selected have no significant effect on the magnitude of the wheel loads and that the observed differences at the various levels are attributable to random variation and are not due to relationships which exist between the factors and the dependent variable (dynamic load). An analysis of variance was conducted on the data in accordance with the experiment design presented in Appendix B in order that inference concerning the significance of these differences could properly be made. For example, if at a certain significance level the dynamic wheel loads recorded at one speed level are found to be significantly different from loads at the remaining speed levels then this indicates that these differences are not purely due to chance or random variation but that there is a dependence of dynamic forces on speed.

The factors and factor interactions which were found significant are discussed, and the corresponding variation in the average dynamic wheel loads over the different main effect levels are presented graphically in bar diagram form. Each bar diagram represents a dynamic wheel load obtained by averaging observations from all combinations included in that particular level. Although these average effects are helpful in interpretation of the differences between the different levels, in many instances they tend to mask extreme variations which may exist in individual measurements especially in situations involving averaging over a large number of combinations such as in the case of main effects.

Analysis of Variance

Before the analysis of variance was performed, an alpha (α) level of 0.01 was selected in order to establish a threshold which could be used to accept or reject the above stated hypothesis concerning the significance of the variation in the magnitude of dynamic wheel loads. At this level, one is 99 percent confident that differences which are found significant are in fact significant.

The choice of the α level is a matter of practical or economical consideration. Basically, the research worker selects a level in such a manner that the results are most valuable to him (Ref 1). In situations where minor differences which have no practical or economical importance are known to be significant at a certain level, a much lower level is used thus permitting the detection of only highly significant differences. The reverse is also true.

The major experiment was designed and analyzed as a split-split-split plot in order to guard against bias resulting from restrictions on randomization at several stages of the experiment. However, after the analysis of variance was performed according to the statistical model described in Appendix B, it was found that the split plot errors were not significant and that a pooled error could be used instead. The analysis of variance based on this pooled error is presented in Table 12 in which the factors and interactions are listed in the order of their relative importance. All of the factors listed were found significant at a level much lower than the selected 1 percent.

The fact that two-way and three-way interactions were found to be significant is an indicated of the dependence of one factor on the other factor(s) in the manner in which they influence the magnitude and variation of the recorded dynamic wheel loads. This dependency may be either simple or complex; but regardless of its nature, it indicates that at least some interactions must be considered if the analysis is to be complete.

Main Variable Effects. The differences between the levels of the main variables which include axles, speed, scale or sampling location, and pattern of roughness have been found significant at the 1 percent level. The average dynamic loads and the dynamic components have been determined at each level and are summarized in Table 13. Graphical representation of the variation in these

TABLE 12. ANALYSIS OF VARIANCE

Source of Variation	Degrees of Freedom	Sum of Squares	Mean Square	F	Significance Level, percent
A	16	961,539.7	60,096.2	855.6	1
S	5	70,957.4	14,191.5	202.0	1
V	2	26,033.3	13,016.7	185.3	1
VXS	10	107,563.8	10,756.4	153.1	1
TXS	15	33,098.3	2,206.5	31.4	1
T	3	5,029.6	1,676.5	23.9	1
VXTXS	30	40,399.7	1,346.7	19.2	1
AxV	32	31,150.4	973.4	13.9	1
VXSxA	160	126,315.8	789.5	11.2	1
AXS	80	58,482.5	731.0	10.4	1
AXT	48	16,588.7	345.6	7.2	1
VXSxAXT	480	191,851.8	399.7	5.7	1
AxSxT	240	89,932.1	374.7	5.3	1
VXTxA	96	32,986.1	343.6	4.9	1
VXT	6	1,660.3	276.7	3.9	1
Error	2,448	171,936.7	70.2		

Factors Legend

A - Axle
S - Scale
V - Speed
T - Roughness

TABLE 13. MAIN VARIABLES AVERAGE EFFECTS

a. Axles (A)			b. Speed (V)		c. Scale (S)		d. Roughness (T)	
Axle	Static	Dynamic	Speed	Dynamic	Scale	Dynamic	Roughness	Dynamic
1	30	35*(17)**	10	51(6)	1L	62(29)	R-1	53(10)
2	71	79(11)	30	55(15)	2L	49(2)	R-2	55(15)
			60	57(19)	4L	51(6)	R-3	54(13)
3	22	26(18)			5L	58(21)	R-4	56(17)
4	67	73(9)			6L	52(8)		
5	51	58(14)			7L	53(10)		
6	50	52(4)						
7	66	75(14)						
8	66	70(6)						
9	29	31(7)						
10	48	57(19)						
11	27	37(37)						
12	29	37(28)						
13	43	46(7)						
14	53	64(21)						
15	41	52(27)						
16	57	64(12)						
17	58	66(14)						

a. Axles: 4 (T) x 6 (S) x 3 (V) x 3 (Repetitions)
= 216 observations.

b. Speeds: 4 (T) x 6 (S) x 17 (A) x 3 (Repetitions)
= 1,224 observations.

c. Scales: 4 (T) x 3 (V) x 17 (A) x 3 (Repetitions)
= 612 observations.

d. Roughness: 4 (T) x 3 (V) x 17 (A) x 3 (Repetitions)
= 918 observations.

* All forces are in 100 pounds.

** Numbers in parenthesis represent dynamic load components (percent).

average dynamic loads are shown in Figs 65 through 68 where both static and dynamic wheel loads are indicated. The shaded portion of each bar diagram represents the excess of dynamic load over the corresponding static load. When these shaded portions are expressed as a percent of the corresponding static load, impact factors are obtained.

The highly significant nature of the variation in average dynamic wheel loads between the different axle levels (main effect A) as indicated by the analysis of variance and demonstrated in Fig 65 was, of course, anticipated since the static loads of individual wheels differ in magnitude. However, it is the relative differences in the average dynamic components produced by the left wheel(s) of each axle that is important. The following observations can be made regarding these differences:

- (1) The magnitude of these components ranged between +4 percent to +37 percent for the combined left wheels of all 17 axles.
- (2) For most of the vehicle classes, the wheel with the least static load within each class produced the largest dynamic component for that particular class.
- (3) The average dynamic components for the fore-and-aft tandem wheels were within 9 percent which indicate the similarity in their dynamic behavior.
- (4) For individual classes of vehicles, Class IV showed the largest variation in the dynamic component with a range of +7 percent for axle 1 to +37 percent for axle 3. Class V had the second largest variation with a range of +7 percent to +27 percent for axles 1 and 3, respectively.

Next in the order of significance among the main effects was the scale or sampling location along the roadway surface. This has particular importance to the highway engineer since extreme variations which produce maximum dynamic component or impact factors result in destructive effects on the pavement surface. As shown in Fig 66, the average dynamic wheel load effect for all axles ranged between 6200 and 4900 pounds within the sampling section. The corresponding dynamic components, based on an average static load of 4800 pounds, ranged between +2 and +29 percent, respectively. Since these values were averages for all axles combined, they should be considered as parameters measuring average effects rather than actual wheel loads. The two extreme values just mentioned were measured within a 4-foot interval thus indicating the rapidly varying nature of the dynamic wheel loads. Also, the pattern of load variation described by the first three samples was repeated to a lesser extent

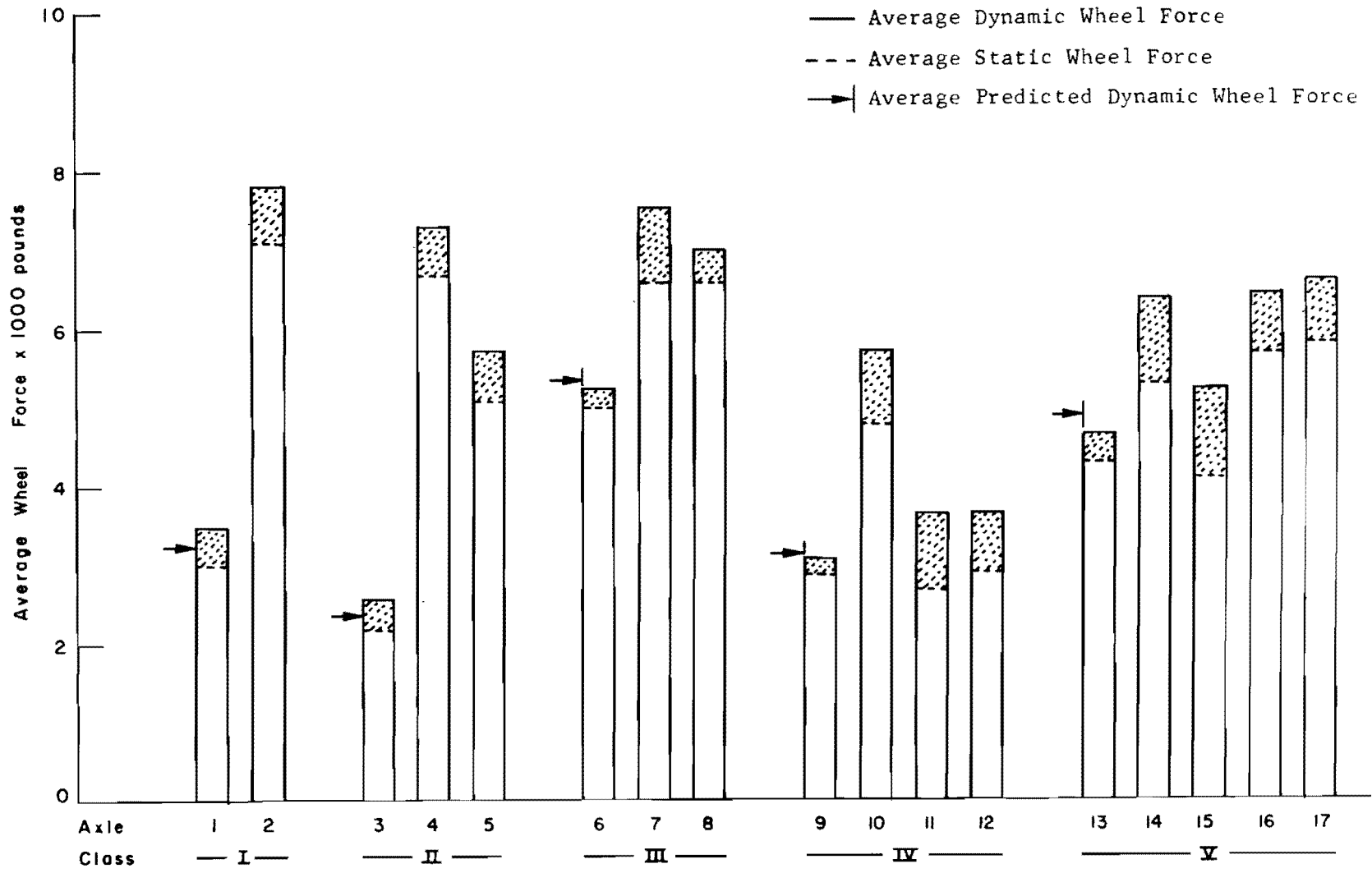


Fig 65. Effect of axles on measured average dynamic wheel loads.

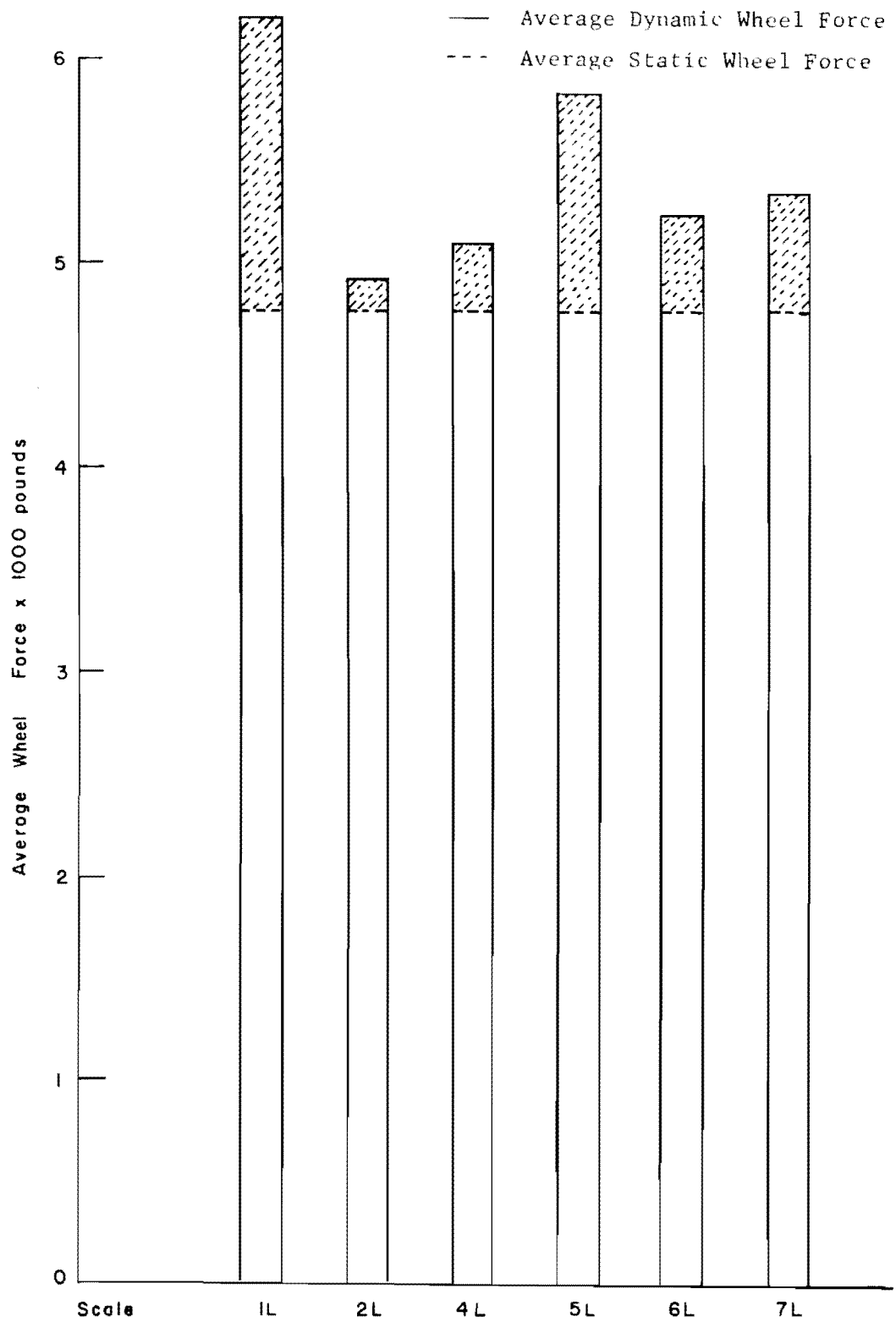


Fig 66. Effect of scale location on measured average dynamic wheel loads.

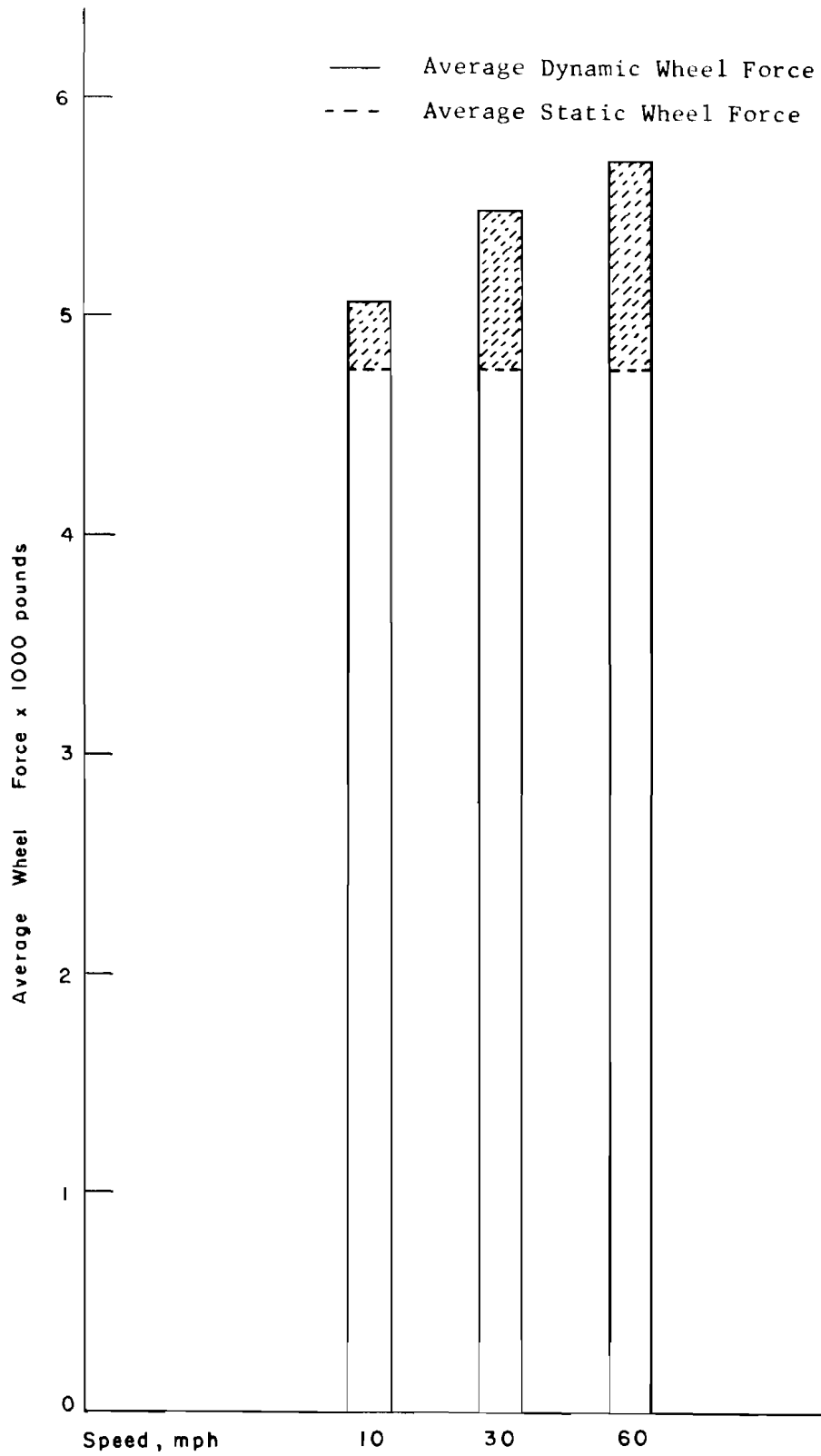


Fig 67. Effect of speed on measured average dynamic wheel loads.

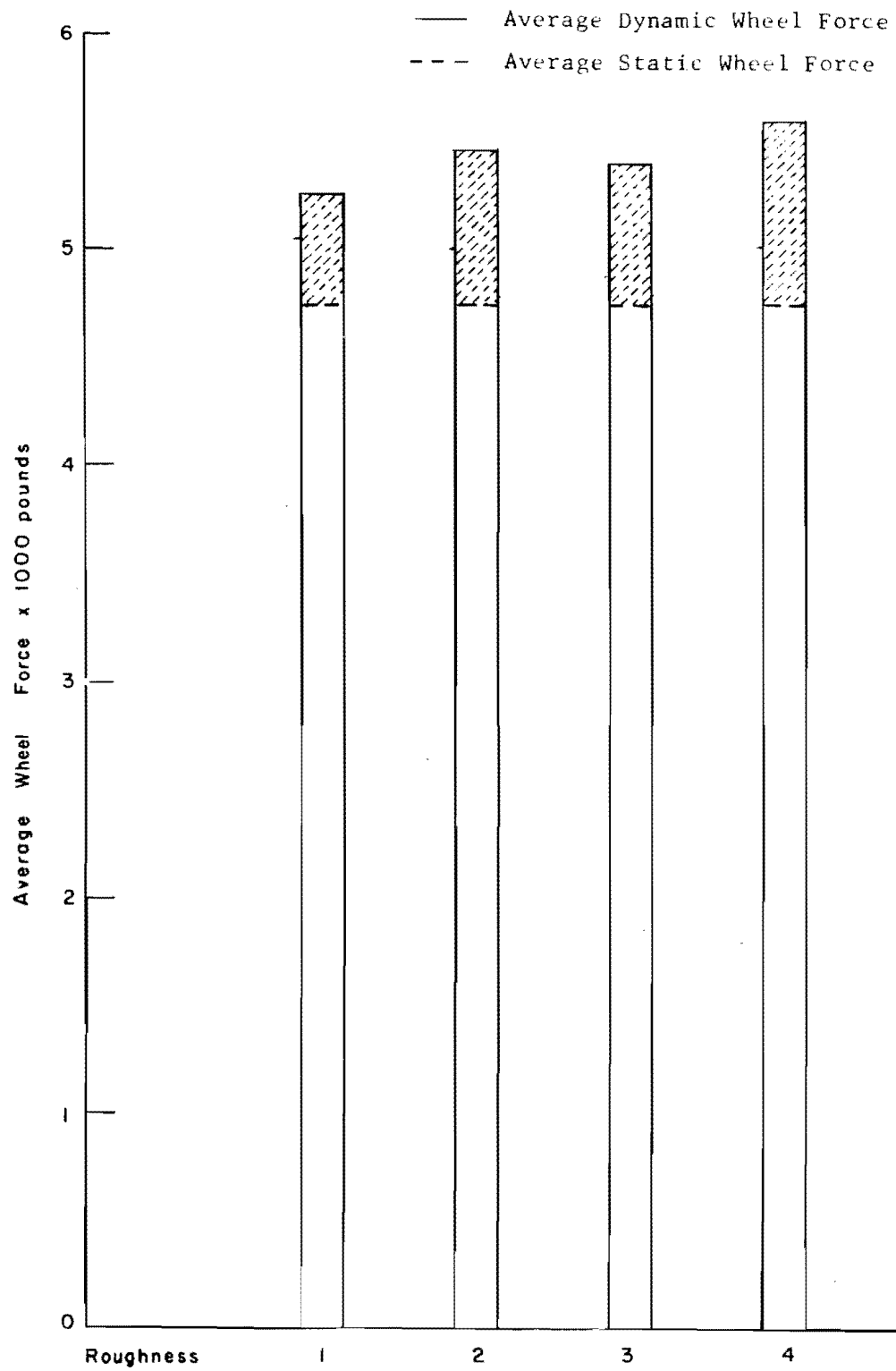


Fig 68. Effect of roughness on measured average dynamic wheel loads.

by the last three samples with a large dynamic component at the fourth sampling location decreasing at the fifth and the sixth locations. This was probably due to an unevenness in the roadway profile immediately in advance of scale 5L (fourth sampling location). This unevenness was caused partly by slight settlements in the pavement and partly by patches around the scale frame thus causing reexcitation of the vehicle suspension system. The reader is referred to Figs 55 through 58 (pages 129 through 132) for further examination of this natural profile.

The average dynamic loads at each speed level are shown in Fig 67 and an increasing trend of these loads with increasing speed is evident. When measured by the dynamic component, this increase amounted to approximately 9 and 4 percent corresponding to an increase in speed from 10 to 30 miles per hour and from 30 to 60 miles per hour, respectively.

Finally, the variations caused by the four levels of artificial patterns of roughness are shown in Fig 68. Of the four main effects this variation was found to be the least significant with an increase in the average dynamic component of approximately 6 percent between R-1 and R-4. This was no doubt due to the fact that the major differences between these artificial patterns of roughness were localized around the areas where the bumps were placed and thus only the samples nearest these areas were expected to exhibit large differences. The large differences could be detected as high order interactions involving sampling locations and roughness condition and are examined later.

Speed - Scale Location Interaction (V×S). The magnitude and variation of the average dynamic wheel loads at 10 and 30 miles per hour were considerably less than at 60 miles per hour. This is evidenced by the fact that the dynamic component ranged between minimum values of 0 and +10 percent to maximum values of +12 and +23 percent at 10 and 30 miles per hour, respectively, while the corresponding range for 60 miles per hour was between -10 percent and +56 percent. Most of the variation took place in the early part of the test section with practically no variation in the last two samples for all speeds.

Scale Location - Roughness Interaction (S×T). The maximum average dynamic loads for this interaction occurred at the first sampling location. At this location, the average dynamic component increased from 10 percent for the natural profile (R-1) to 48 percent for a 3/8-inch step bump on Scale 1. This means that a 3/8-inch bump produced an average increase in dynamic component

(or in this case impact factor) of 38 percent of static at the first scale location. This increase was equivalent to double the average effect measured at distances of 6 and 14 feet downstream from a 3/4-inch bump. The average dynamic component resulting from both R-3 and R-2 was 29 percent which represented an increase of 19 percent over R-1. At the last two scale locations almost no variation in dynamic load factor was noticeable between the four roughness patterns. This is an indication that the bumps produced no significant dynamic load effects at locations more than 36 feet downstream from the step bump.

Speed - Axles Interaction (VxA). The following observations can be made concerning this interaction after performing an analysis of variance and examining data shown in Table 14 concerning the variation of average dynamic wheel loads with respect to speed for the axles corresponding to individual vehicle classes.

- (1) In general, dynamic wheel load components increased with an increase in speed. This is evidenced by the fact that of the 34* possible speed changes from either 10 to 30 miles per hour or from 30 to 60 miles per hour:
 - (a) Twenty-four showed an increase in average dynamic wheel load components; these increases ranged between 3 percent and 37 percent when going from the lower speed to the next higher speed level.
 - (b) Six showed a decrease ranging between 4 percent and 13 percent.
 - (c) Four remained unchanged.
- (2) The maximum single axle variation with speed, measured in dynamic load component is between 0 percent at 10 miles per hour to +70 percent at 60 miles per hour (Class IV, axle 3).
- (3) The pattern of variation in dynamic load component was approximately the same for the front axle of each vehicle except for Class II which was considerably higher than the remaining axles.
- (4) For each class of vehicles, the axle with the least static load showed the maximum percent variation in the magnitude of dynamic load component with speed.
- (5) The overall variation at each speed level for all axles was from a minimum of 0, -3, and +7 percent to maximums of +17, +37, and +70 percent at 10, 30, and 60 miles per hour, respectively.

Axle - Scale Interaction (A×S). This interaction involves the variation of the average dynamic forces along the roadway surface produced by the left

* 17 axles each varying from 10 to 30 and from 30 to 60 miles per hour.

TABLE 14. AXLE-SPEED INTERACTION (A×V)

Axle	Static Load	Speed, mph		
		10	30	60
1	30	33*(10)**	36(20)	37(23)
2	71	77(9)	77(9)	83(17)
3	22	22(0)	29(32)	27(23)
4	67	67(0)	75(12)	78(16)
5	51	56(10)	56(10)	60(18)
6	50	50(0)	53(6)	55(10)
7	66	69(5)	81(23)	76(15)
8	66	71(8)	64(-3)	74(12)
9	29	30(3)	31(7)	31(7)
10	48	50(4)	60(25)	62(29)
11	27	27(0)	37(37)	46(70)
12	29	30(3)	36(24)	44(52)
13	43	43(0)	46(7)	49(14)
14	53	57(8)	69(30)	66(25)
15	41	48(17)	50(22)	58(41)
16	57	66(16)	64(12)	64(12)
17	58	64(10)	71(22)	63(9)

* Average of 72 observations, in 100 pounds.

** Numbers in parenthesis represent the dynamic component (percent).

wheels of each of the 17 axles. Thus, it serves to point out any variation, by a single axle or a group of axles, from the observed pattern of variation for all the axles combined which has been discussed earlier. The following observations can be made concerning the data presented in Table 15:

- (1) The maximum variation in the average dynamic load for the left wheels on a single axle was from 9400 pounds to 6100 pounds (axle 2, Class III), while the minimum variation was from 4800 pounds to 4500 pounds (axle 1, Class V). These two extreme variations corresponded to reductions in dynamic load components of 50 and 7 percent, respectively.
- (2) With the exception of the tandem axles of Class III and the front axle of Class V, the maximum dynamic wheel load component for each axle was recorded at the first sampling location. But in all cases a sharp reduction of the load occurred at the second and third sampling locations.
- (3) The same pattern of load variation at the first three locations was repeated at the last three locations for Classes I, III, and V with a departure from this pattern by Classes II and IV.
- (4) There were no extreme differences in load variation for the fore-and-aft tandem axles.

Axle-Roughness Interaction (A×T). The average dynamic wheel loads at roughnesses R-2, R-3, and R-4 were in general greater than the corresponding loads at roughness R-1. Differences in the dynamic load components for each axle ranged between 2 percent and 23 percent with no apparent relationship between these ranges of variation and the corresponding static wheel loads. Furthermore, the dynamic components varied for all axles from minimums of +3, +6, +4, and +6 percent to maximums of +30, +30, +48, and +33 percent for R-1, R-2, R-3, and R-4, respectively.

Speed-Roughness Interaction (V×T). According to the analysis of variance this interaction was the least significant of all interactions considered. The maximum increase in this component was 17 percent which corresponds to an increase from 6 percent at 10 miles per hour to 23 percent at 60 miles per hour.

Speed-Roughness-Scale Interaction (V×T×S). As shown in Table 12 (page 144) this is the most significant of the three-factor interactions and, therefore, the first three-way interaction that will be discussed in this chapter. The most noticeable feature of this interaction was the considerable change in the magnitude of the average dynamic wheel load at 60 miles per hour with

TABLE 15. AXLE-SCALE INTERACTION (A×S)

Axle	Static Load	Scale					
		1L	2L	4L	5L	6L	7L
1	30	41*(37)**	31(3)	33(10)	39(30)	34(13)	32(7)
2	71	86(21)	76(7)	78(10)	82(15)	75(6)	74(4)
3	22	32(45)	24(9)	23(5)	25(14)	26(18)	25(14)
4	67	77(15)	73(9)	70(4)	72(7)	74(10)	74(10)
5	51	65(27)	52(2)	53(4)	57(12)	56(10)	63(23)
6	50	59(18)	47(-6)	54(8)	55(10)	51(2)	49(-2)
7	66	90(36)	70(6)	70(6)	94(42)	61(-8)	68(3)
8	66	85(29)	55(-17)	63(-5)	86(30)	64(-1)	65(-1)
9	29	33(14)	27(-7)	33(14)	29(0)	31(7)	32(10)
10	48	68(42)	50(4)	54(12)	56(17)	57(19)	59(23)
11	27	42(56)	35(30)	32(18)	34(26)	38(41)	39(44)
12	29	43(48)	33(14)	32(10)	37(28)	37(28)	37(28)
13	43	46(7)	45(5)	45(5)	48(12)	45(5)	47(9)
14	53	72(36)	56(6)	60(13)	72(36)	64(21)	61(15)
15	41	57(39)	44(7)	45(10)	64(56)	51(24)	52(27)
16	57	75(32)	57(0)	60(5)	73(28)	59(3)	63(10)
17	58	80(38)	58(0)	63(9)	67(15)	65(12)	65(12)

* Average of 36 observations, in 100 pounds.

** Numbers in parenthesis represent the dynamic component (percent).

the change in roughness pattern. At scale 1L this amounted to an increase in the dynamic wheel load component of 54 percent (from 25 percent at R-1 to 79 percent at R-4). The corresponding increase at 10 miles per hour at the same location was 17 percent or approximately one-third of this amount. At 60 miles per hour and at the second sampling location (scale 2L), the decrease in the dynamic component for R-1 was 8 percent while the corresponding decrease for R-2, R-3, and R-4 was 80, 98, and 83 percent. Such variation in the load reflects the manner in which vehicles traveling at high speeds will respond to sudden disturbances on the roadway surface and the wide ranges in the dynamic wheel loads produced as a result of such disturbances. Again as pointed out in earlier discussions, the differences in impact loads resulting from the four patterns of roughness were considerably less noticeable for all three speeds at the last two sampling locations (scale 6L and 7L).

Speed-Scale-Axle Interaction (V×S×A). An increase in speed resulted in an increase in the magnitude and the range of variation of the average dynamic wheel load for most of the axles. For example, the dynamic component ranged between -2 percent to +15 percent at 10 miles per hour, -8 percent to +37 percent at 30 miles per hour, and 6 percent to 105 percent at 60 miles per hour at the first sampling location. At the second sampling location, these components varied by as much as 32, 62, and 134 percent for 10, 30, and 60 miles per hour, respectively.

Furthermore, the scale layout in the field (see Fig 37, page 98) allowed the left wheels of a tandem axle to be supported simultaneously once by scales 1L and 2L and again by 4L and 5L, thus permitting an examination of the pitching behavior of the tandem axle at each speed level. The extent of pitching may be measured by the difference in the dynamic load component produced simultaneously by the fore-and-aft tandems at each of these locations. These differences ranged between 2 and 30 percent, 2 and 35 percent, and 5 and 126 percent for 10, 30, and 60 miles per hour, respectively. This clearly indicates that the amount of pitching increased with speed.

Roughness-Scale-Axle Interaction (T×S×A). This interaction was the least significant of the interactions considered. The range of sample variations of the average dynamic wheel loads for each of the 17 axles changed with the pattern of artificial roughness. For R-1, the maximum variation in the dynamic

load component ranged between 11 to 37 percent, while the corresponding ranges for R-2, R-3, and R-4 were 8 to 73 percent, 11 to 63 percent, and 31 to 145 percent, respectively. Each of these percentages represent the change between the maximum and the minimum components observed for a particular wheel. Again as noted in earlier discussions most of this variation, particularly for R-4, took place in the upstream part of the sampling section.

Summary Discussion

In the preceding statistical analysis, all the main variable effects and the two-factor and three-factor interactions were found significant at the selected confidence level of 99 percent. These factors and the associated interactions were then arranged in a hierarchical order of decreasing significance and discussed individually. In this discussion it was pointed out that the dynamic behavior of individual axles measured in terms of the magnitude of dynamic load components produced by the left wheels varied by as much as 33 percent with a mean of approximately 16 percent for all left wheels of the 17 axles. Dynamic wheel loads were also found to vary in magnitude along the roadway surface, and the general pattern of this variation was presented. Furthermore, the effect of vehicle speed on the average magnitude of dynamic wheel loads was discussed. Both the magnitude and the rate of variation of these average loads were found to increase with an increase in speed. The effects of each of the four patterns of artificial roughness were found to be localized in areas near the bumps.

Extreme variations in the magnitude of individual dynamic wheel loads have not been included in the above discussion of average dynamic wheel load effects. While in actuality these extreme variations are considered in establishing the statistical significance of the main factors and interactions, they were somewhat masked by the process of obtaining average effects as noted earlier in this chapter. An example of an extreme condition was observed in the field where the tire actually lost contact with the roadway surface and thus registered no load at one or several sampling locations. Generally, this occurred at high speeds and within the first 16 feet of the instrumented roadway. Such behavior is of particular importance to pavement or bridge design engineers since in many cases impact factors of more than 100 percent were produced as the tire(s) again came in contact with the roadway surface.

In one instance, this off-ground-on-ground behavior was noticed to take place over a stretch of roadway extending about 30 feet from the source of disturbance* with nearly the same pattern for all three passes of the test truck (see tandem axle pairs 4 and 5 of Class V, Tables C.12, C.15, and C.18, pages 242, 245, and 248, respectively). Extreme pitching of this tandem axle may be noticed by examining the wheel loads at scales 1L and 2L and at 4L and 5L. While the left tires on the forward axle were completely off the roadway surface, the left tires on the back axle were applying a dynamic force exceeding twice the corresponding static force. There are other instances in which the dynamic wheel load resulting from a 3/8-inch board exceeded twice the static load not only at high speeds but also at medium speeds. Examples of such cases may be found by referring to Tables C.47 and C.48 (pages 277 and 278).

Finally, it must be recognized that the comments and observations presented in the course of the discussion in this chapter are applicable only within the inference space which is defined by the different levels of the main variables or main effects. For example, conclusions cannot be drawn or inference be made with the same level of confidence regarding the magnitude and variation of dynamic loads beyond the test section, at speeds higher than 60 miles per hour, for vehicles which are different from those used in the experiment, or for other patterns of roughness. Thus the comments upon which these conclusions are subsequently made are primarily based on what has been observed in the field within the framework of the experiment and this in turn depends on tolerances in the experimental measurement and visual reduction of field data.

* 8 feet by 2 feet by 3/4-inch plywood placed 14 feet in advance of scale 1L, "R-2."

This page replaces an intentionally blank page in the original.

-- CTR Library Digitization Team

CHAPTER 9. MODEL REFINEMENT

A detailed description of the development of several vehicle models and the procedures used for validating the models are given in previous chapters. Since only one set of input parameters was used to characterize the tire and suspension components of each vehicle in these studies, subsequent sensitivity analyses described in this chapter were devoted to determining the best values of spring stiffness and damping to use as input to the vehicle models. The need for some minor refinements in the model configurations became apparent after the effects of extreme as well as small variations in model input parameters were evaluated. These are described in the last sections of this chapter.

Sensitivity Analysis

The procedure used to evaluate the input parameters that are required for calibrating the vehicle models was performed in three phases. In the first phase, the class of vehicle, speed, and profile roughness were all held constant while parameters describing the suspension and tire systems were varied until the best feasible agreement was obtained between model output and experimental data. In the next phase, the speed was allowed to vary, and a slightly altered set of suspension and tire system parameters were obtained. In the third phase, the profile roughness, as well as speed, was varied, and the final set of most generally agreeable input parameters was chosen. This same three-phase process was carried out for the model of each of the five classes of vehicles. In the following discussion, all examples are taken from the analysis of the Class I vehicle model.

This heuristic, or step learning, type of analysis was performed using the interactive graphics capability of the CDC 252 cathode ray tube display system which is part of the CDC 6600 computer system at The University of Texas at Austin. It was recognized that a more nearly "closed-form" solution to model calibration could probably be obtained, but several factors discouraged the development of such a solution. First, the method employed here permitted the

observation of the final "best" solution as well as all intermediate solutions which led to it. The numerous intermediate solutions allowed the overall effects of each input parameter to be evaluated qualitatively and quantitatively. Second, since facilities for immediate visual display of all numeric results were readily accessible, an overall saving in time could be realized by using human judgment to evaluate the displayed results as soon as computations were completed.

Tire Subsystem. The tire subsystem used in the vehicle models consists of a paralleled spring and dashpot (see Fig 8). Values for the spring stiffnesses and for the dashpot damping coefficients must be selected as input to the vehicle model.

Representative values of tire stiffness were obtained from several sources as mentioned in Chapter 7, and for a tire inflation pressure of 65 to 70 psi, these values were approximately 4000 pounds per inch of deflection. When this value was used in the model, there was good agreement between computed and observed wheel forces for low vehicular speeds (30 mph or less). Figure 69 shows the results of varying the 4000 pounds per inch by \pm 50 percent. It is obvious that the model is quite sensitive to changes in tire stiffness, since doubling the tire stiffness approximately doubled the magnitude of the peak dynamic loads for this particular road profile roughness pattern.

After varying the tire stiffness in this manner and studying the resulting agreement between theoretical and experimental data, it was noted that a tire stiffness of 4000 pounds per inch of deflection produced the best results for speeds up to 30 mph. Studies of higher speeds (approximately 60 mph) showed that it was necessary to increase tire stiffness slightly with speed, up to about 4500 pounds per inch at a speed of about 60 mph in order to have good agreement between computed and observed forces.

Even though it is known that truck tires have no great capacity for damping, a small amount of damping in the model subsystem produced the best results. Various amounts of damping were tried, from zero to 10 percent of critical, as shown in Fig 70. The best agreement was finally obtained when a damping factor of approximately 2 percent of critical for both front and rear tires was used (see Fig 71).

Suspension Subsystem. As may be seen in the schematic diagrams of the models for the five classes of vehicles that are included in Chapter 4, the

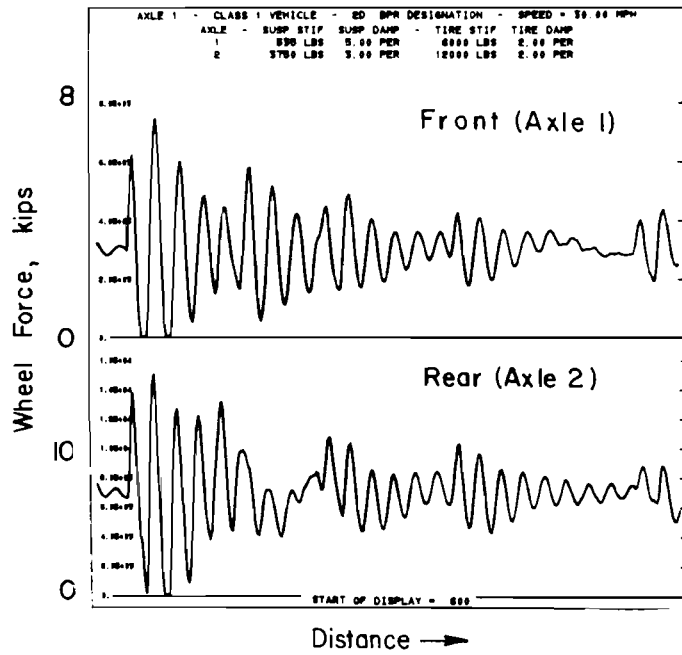


Fig 69(a). Tire stiffness (4,000 lb/in) increased 50%.

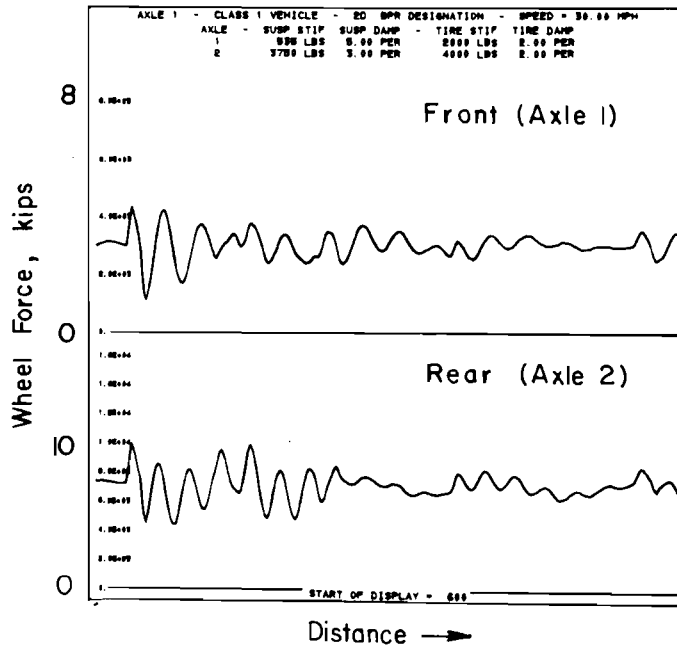


Fig 69(b). Tire stiffness (4,000 lb/in) decreased 50%.

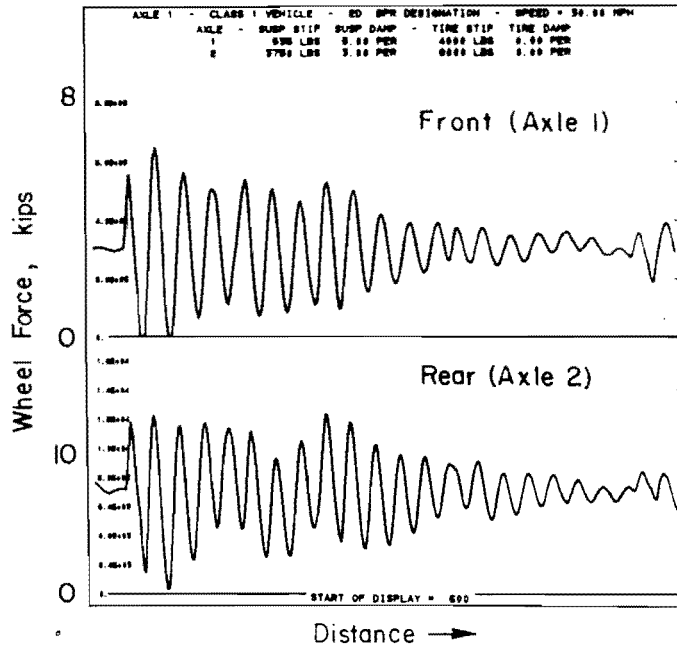


Fig 70(a). Zero tire damping.

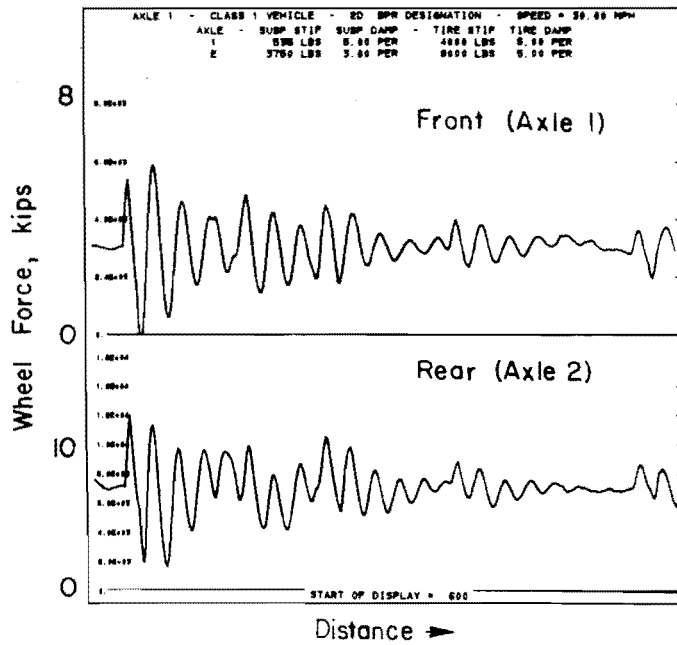


Fig 70(b). Tire damping 5% of critical.

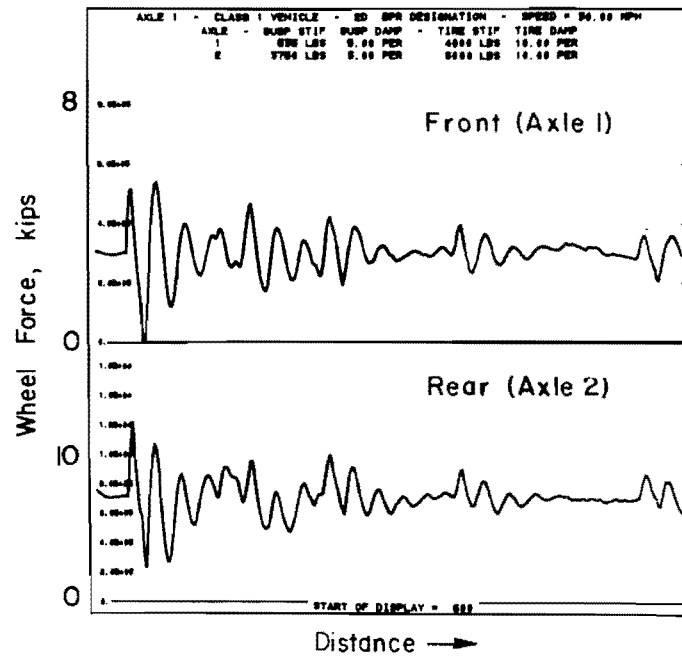


Fig 70(c). Tire damping 10% of critical.

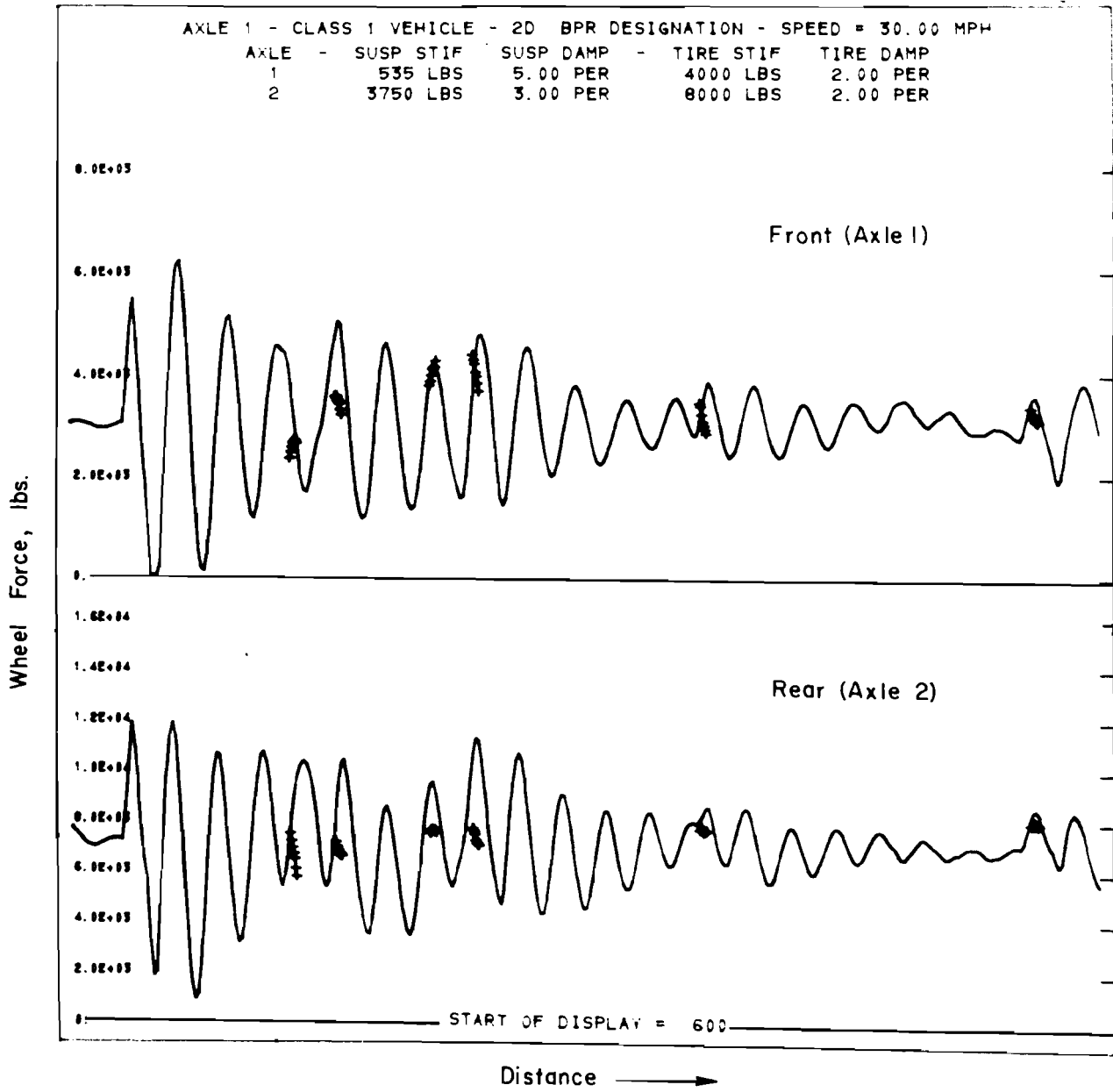


Fig 71. Class I model showing optimum parameter settings.

vehicle suspension system is also simulated by springs and dashpots connected in parallel. The stiffness of the springs under static loading can be simply and accurately determined experimentally by applying incremental loads and measuring the resulting deflection. For the Class I vehicle, representative numbers were found to be 535 and 3750 pounds per inch of deflection for the front and rear suspension subsystems, respectively. Doubling these experimentally determined values resulted in dramatic changes in the computed wheel forces, as shown in Fig 72. These changes, as well as the variations in tire stiffness discussed earlier, primarily affected variations in amplitude of the computed wheel forces but had little effect on the frequency of oscillation.

Suspension Damping. Since most large trucks do not have shock absorbers as such, the damping that occurs in the suspension system is largely that which is due to friction and the resulting energy dissipation. Although the models described herein utilize viscous instead of friction damping, it was found that viscous damping allowed good approximation of wheel forces, especially in the zone of peak dynamic force where the suspension system usually experiences high-frequency oscillation.

In this study, the critical damping factor for the tire-suspension-axle system was computed and the damping coefficient was expressed as a percent of this critical value. Many combinations were tried, and the resulting theoretical force diagrams were compared with the experimental information. Figure 73 shows the results of varying the suspension damping between a maximum of 20 percent of critical and a minimum of 1 percent of critical. As may be seen, these changes again primarily affected the overall amplitude of the computed wheel force curves, but they also produced some small changes in frequency. After viewing these results and simulating different speeds of each vehicle class over various roughness patterns, a compromise situation was reached for the Class I vehicle. Coefficients of 5 percent and 2 percent of critical are recommended for the front and rear wheel suspension elements, respectively.

Model Refinements

The sensitivity analysis pointed out the need for some refinements in the model configuration. These refinements are outlined in the following paragraphs.

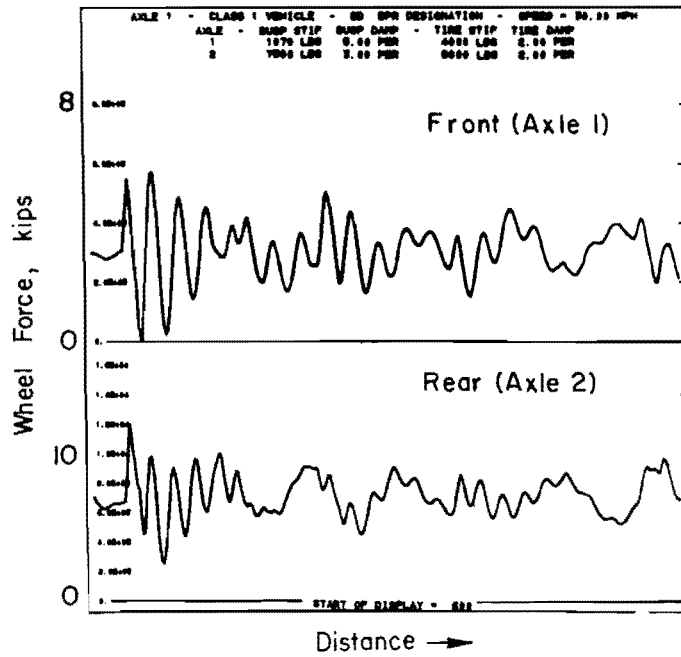


Fig 72. Suspension stiffness double values shown in Fig 71.

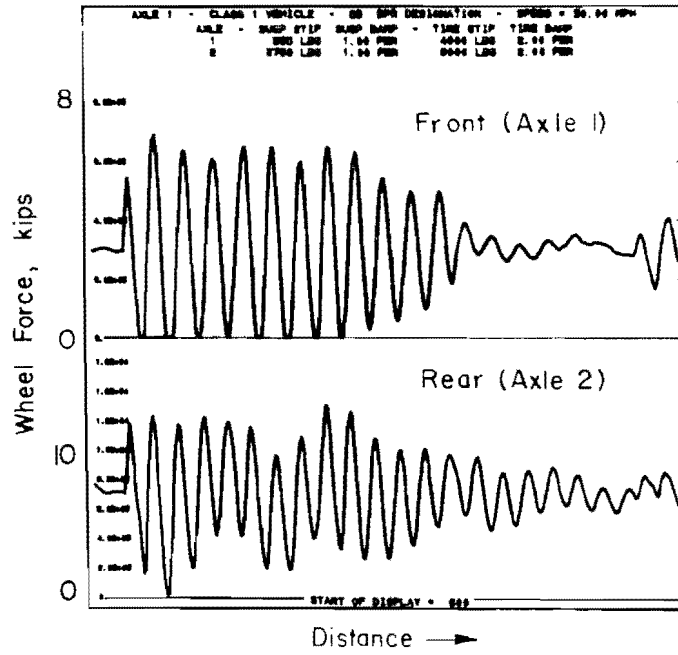


Fig 73(a). Suspension damping 1% of critical.

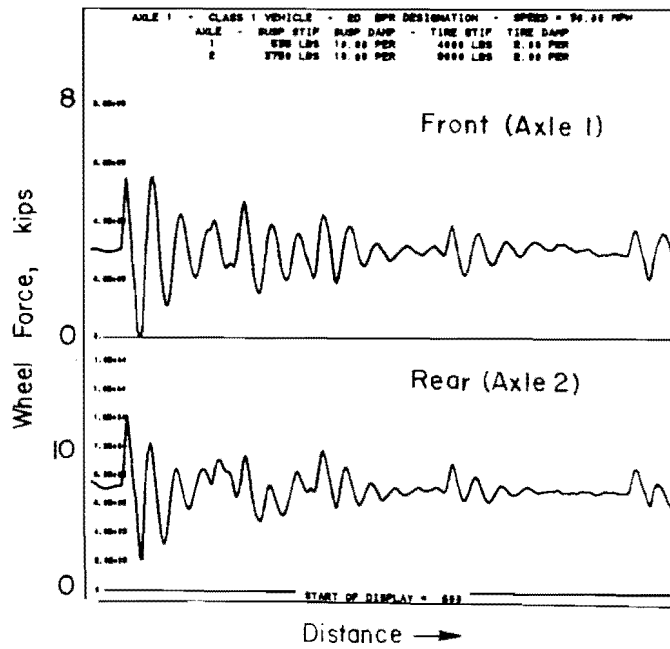


Fig 73(b). Suspension damping 10% of critical.

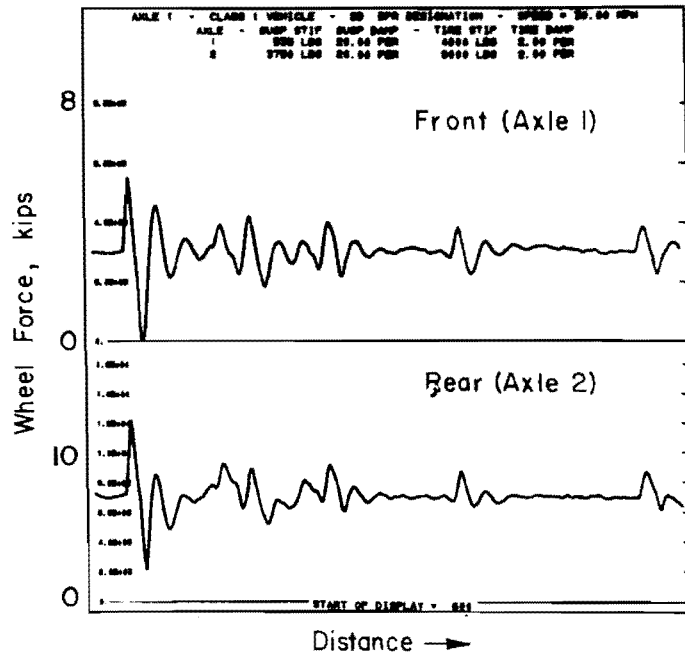


Fig 73(c). Suspension damping 20% of critical.

Tire Enveloping. Pneumatic tires of highway vehicles have an enveloping action. That is, rather than maintaining point contact with the road surface, the tire has a finite contact length ranging from about 4 to 10 inches, depending on the size and stiffness of the tire. This enveloping action reduces the effect of small changes in the road surface profile, allowing the effects of small bumps or depressions to be completely absorbed by the tire, without displacing the axle.

The mathematical model was originally configured to receive profile elevations on a point-by-point basis, thus not allowing for the tire enveloping action. This caused the model to predict abnormally high wheel forces for small or abrupt surface irregularities.

To overcome this problem, two possible solutions were considered. The first involved averaging computed wheel forces. That is, the arithmetic mean of the wheel forces over a distance roughly equal to the length of the actual tire envelope were computed on a point-by-point basis. The other solution was to average the surface profile over some distance again equal to the length of the tire envelope prior to inputting the profile into the model.

Since both of these solutions produce similar results (see Fig 74), the profile-averaging technique was chosen for two reasons. First, it seemed to be the more logical of the two since it represents mathematically the actual tire enveloping action. Second, it allows the computed axle and body movements to be more nearly equal to the true values and thus facilitates the study of differential movements between the axles and the vehicle body.

Tandem-Axle Modifications. As noted in Chapter 4, the original version of the model ignored the mass of the fore-aft connecting member on tandem axles (see Fig 51). Use of this "massless" bar resulted in extreme pitching of the tandem axles, especially at high speeds. To overcome this problem, the model was revised to take into consideration the mass of the connecting members. The extra mass increased the mass moment of inertia which in turn helped reduce the severe tandem axle pitching phenomenon predicted by the model.

Summary

The sensitivity analysis and calibration procedure yielded the following information:

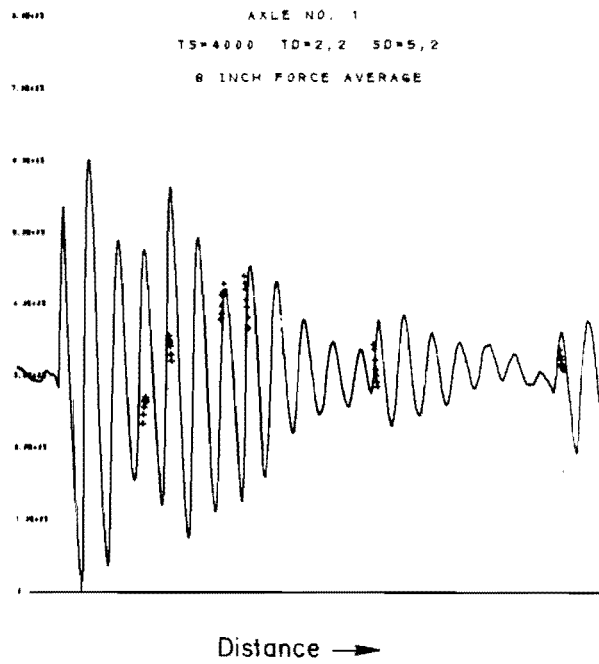


Fig 74(a). Moving average of computed tire forces over 8-inch distance.

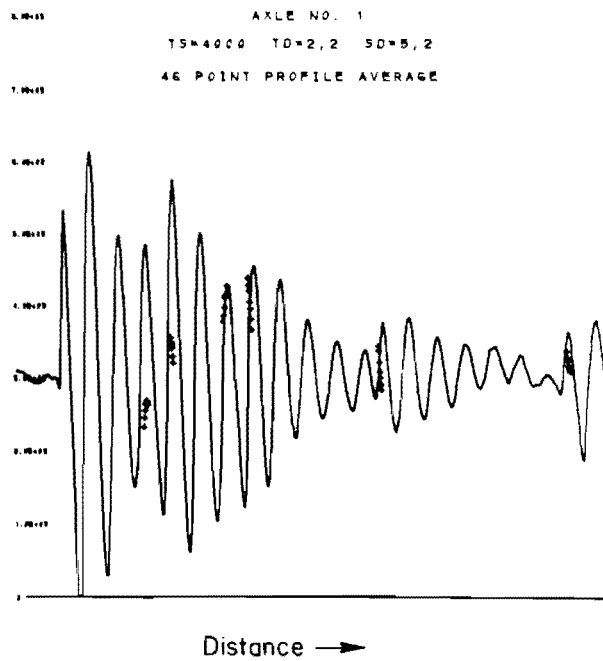


Fig 74(b). Computed tire forces resulting from an eight-inch (46 point) moving average of the input profile.

- (1) Tire stiffness is the most sensitive of the model input parameters. From the sensitivity analysis, the best values for tire stiffness were found to be 4000 and 4500 pounds per inch of deflection for speeds of 30 mph or less and speeds of approximately 60 mph, respectively.
- (2) The tire subsystem in the vehicle model should include some damping. This was determined to be approximately 2 percent of critical damping for the wheel mass.
- (3) Approximate values for spring stiffness of the vehicle suspension system may be measured experimentally.
- (4) The damping of the suspension system of a vehicle may be satisfactorily simulated by viscous damping for evaluating peak dynamic forces resulting from vehicle components oscillating in the range of 6 to 12 Hz. Representative quantities for this damping action consist of 5 percent and 2 percent of critical damping for front and rear wheels of the Class I vehicle.

This page replaces an intentionally blank page in the original.

-- CTR Library Digitization Team

CHAPTER 10. BRIDGE STUDY

One objective of the research study was to evaluate the interaction of the mathematical vehicle models described in Chapter 4 with an actual bridge profile and to provide some general information about vehicle-bridge interaction. Conventional bridge structures undergoing dynamic vehicular loading deflect slightly and usually vibrate at frequencies between 2 and 12 Hz. Under these conditions, the profile over which the vehicles travel varies with time and is somewhat different than the profile of a pavement. The specific aims of the bridge study were to evaluate the behavior of the mathematical vehicle model when subjected to a varying profile which included relatively long, small amplitude waves and to gain as much information as feasible about vehicle-bridge interaction. Field studies were limited to one bridge structure near Austin.

Even though it was highly desirable to embed wheel load transducers in the bridge deck and measure applied wheel forces directly, restricted time and resources made such an installation unfeasible in this study. Alternatively, instrumentation for measuring and recording the relative displacements between the test vehicle axles and the vehicle frame was devised as a means for evaluating the mathematical vehicle model. Since previously described phases of this study indicated the adequacy of the model for predicting dynamic wheel forces directly from known vehicle characteristics and road profile information, good agreement between measured and computed axle-frame displacements would lend further credence to the model.

Experimental Program

The field studies were conducted on a three-lane, three-span continuous, steel girder bridge with reinforced concrete deck at Brushy Creek on the south-bound lanes of IH-35 about 20 miles north of Austin. Vertical displacements of six points on the bottom flange of one girder under the median lane of the bridge were measured and recorded simultaneously with the relative vertical movements between the axles and the frame of a loaded 2-axle test truck. The

instrumental test truck was run at several speeds over the existing roadway surface and then over a series of bumps created by placing 3/4-inch plywood panels at selected positions on the bridge approach and on the deck of the first span of the bridge.

Bridge Instrumentation

The instrumentation on the bridge consisted of six strain-gaged cantilever beams furnished by the Texas Highway Department; these were supported at ground level and connected to the lower flange of a girder by music wire for measuring vertical deflections (see Fig 75). Two pneumatic road tubes were used on the deck surface for determining the longitudinal position of the test vehicle with respect to time. Electrical signals from these detectors were recorded on a multichannel light-beam oscillograph equipped with galvanometers capable of frequency response to 500 Hz.

Music wire 0.014 inch in diameter was used between the bridge girder and each cantilever beam in preference to a larger diameter wire in order to minimize errors induced by coiling or kinking of the larger wire under the varying dynamic load. Elongation of the small diameter wire even under the relatively small forces required to deflect the cantilever beam was of a significant magnitude, and it was therefore necessary to include this effect in the design and calibration of the deflection measuring system. Laboratory experiments were conducted to determine the appropriate elastic constants for the wire and for the beam, and a calibration procedure which considered these elements as two springs connected in series was devised. Computations included adjustments for the respective lengths of wire used at each deflection measuring station.

Deflection was measured at the quarter-span points on the first 50-foot span of the three-span bridge and at the third-span points on the inner span.

Vehicle Instrumentation

The vehicle used in the experimental program (a loaded Class I truck, see Table 16) was equipped with instruments which permitted the recording of differential movements between the axles and the frame. This equipment consisted of rotary potentiometers mounted on the frame of the vehicle above each wheel to be studied and connected to the axle below by a stiff arm and a small but



Fig 75. Strain-gaged cantilever beams supported by sand-filled containers at ground level beneath bridge.

TABLE 16. TEST VEHICLE CHARACTERISTICS

Vehicle Type:	2D (Class I)
Make:	Dodge
Model:	1969
License Number:	173 479
Measurements:	$W_1 = 5 \text{ feet } 7 \text{ inches}$ $W_2 = 5 \text{ feet } 10 \text{ inches}$ $X_{12} = 11 \text{ feet } 6 \text{ inches}$
Tire Pressure:	70 psi
Static Weights:	Front Axle: 6,360 pounds Rear Axle: 17,620 pounds Gross: 23,980 pounds

relatively rigid wire (see Fig 76). As a wheel moved vertically, with respect to the frame, the potentiometer through its linkage yielded a resistance change that was directly proportional to the amount of movement. Only the right side of the truck was instrumented, since roll of the vehicle was considered to be negligible in this experiment. The voltage changes produced by the displacement transducer system were recorded on a galvanometer oscillograph carried on board the truck. The analog records were subsequently analyzed and converted into a digital form that was suitable for computer processing.

Experimental Measurements. The truck that was available for the field tests was relatively light (24,000 pounds); therefore, it was desirable to configure a series of roughness patterns which would produce the maximum feasible suspension system activity and thereby result in measurable bridge deflections. The mathematical model of the Class I vehicle was used to study the effects of various bump spacings on the resulting dynamic wheel forces, and seven patterns of roughness which would best accomplish the desired results for various vehicle speeds were determined. A preliminary series of tests in which the instrumented vehicle made 22 passes over selected roughness patterns placed on a smooth pavement indicated that the computed spacings were near optimum for the chosen speed conditions.

The four roughness patterns illustrated in Fig 77 were used in the bridge study, and the test truck made a total of 31 runs over the bridge at speeds up to 60 miles per hour. Information concerning axle-frame movements and vehicle position on the bridge was recorded by the on-board instruments in the truck while bridge girder deflections at six points and vehicle position data were recorded simultaneously on another oscillograph at the roadside.

Data Reduction and Analysis. All analog data from the field experiments were converted to a digital format suitable for computer processing in the mathematical vehicle model. The road surface profile of the "unloaded" bridge as measured by the GMR profilometer was corrected to reflect the artificial roughness patterns and the deflected shape of the bridge with respect to time and position of the test truck. The deflection of the structure actually had little influence on the dynamic loads since the light test truck caused maximum girder displacements on the order of 0.1 inch. The axle-frame deflection data were digitized and compared with computed data from the model by visual inspection on a CDC 252 cathode ray tube display unit.

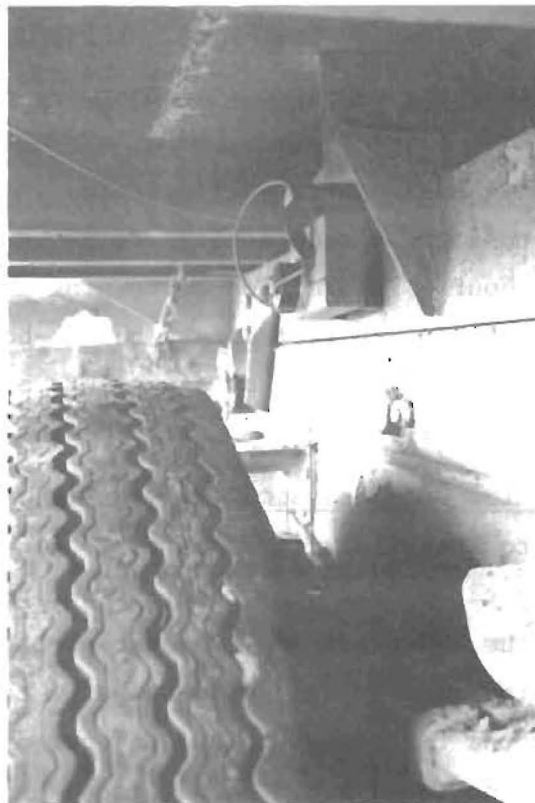
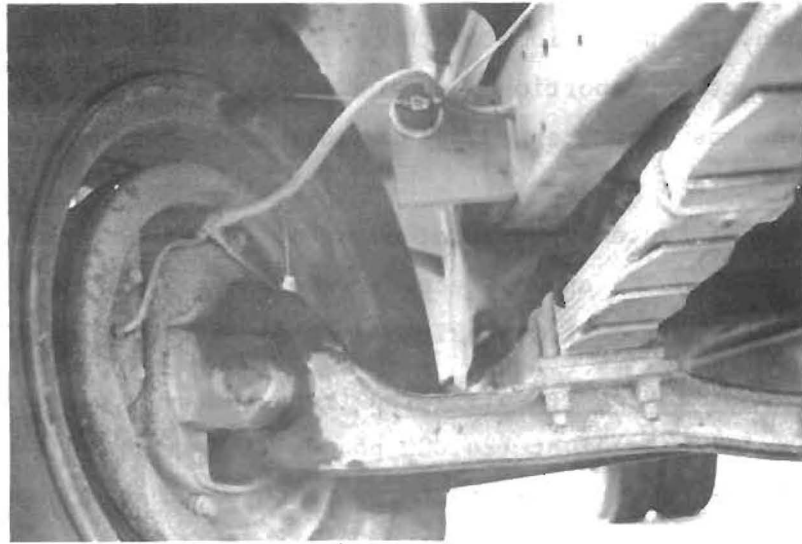


Fig 76. Potentiometers for measuring axle-body deflections.

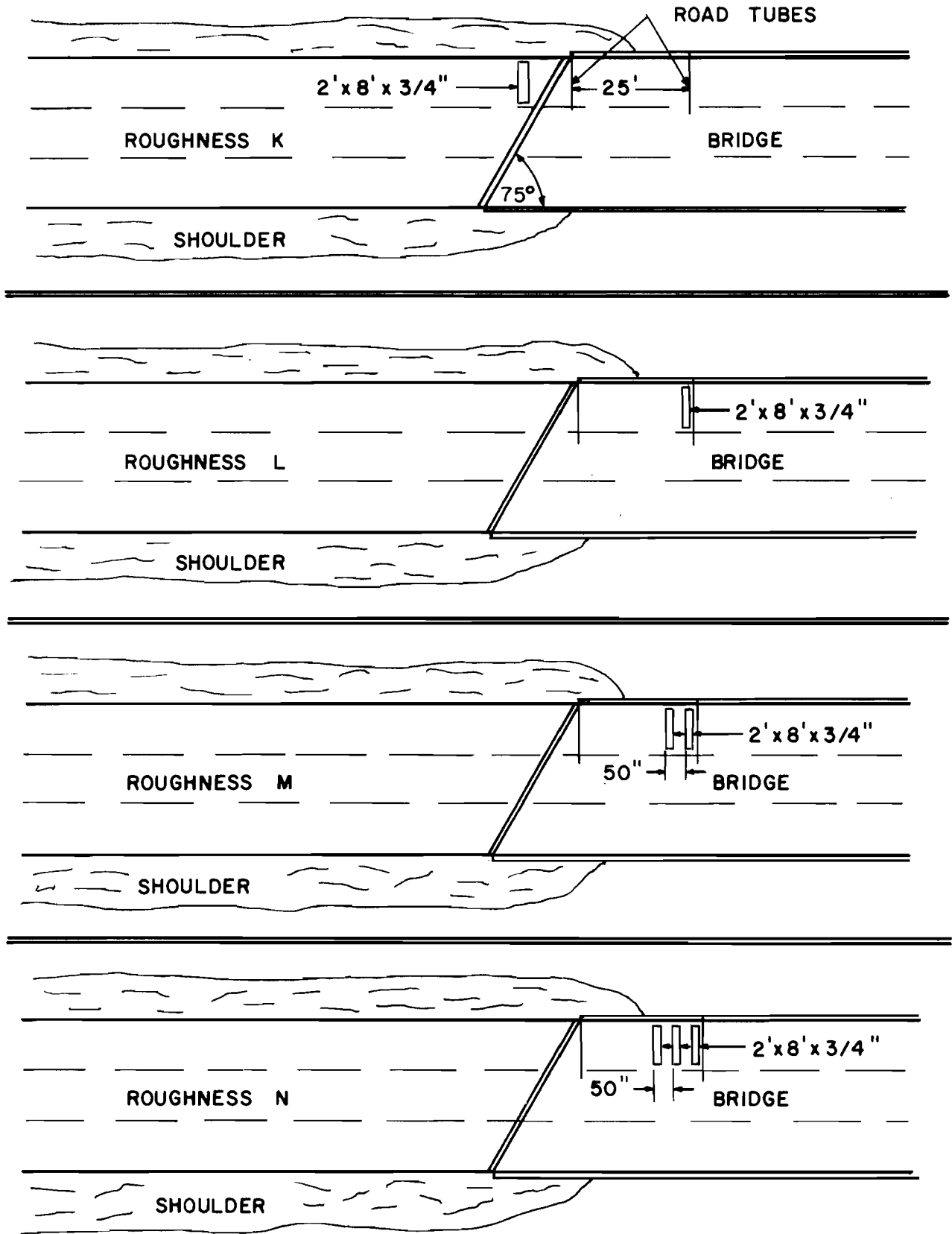
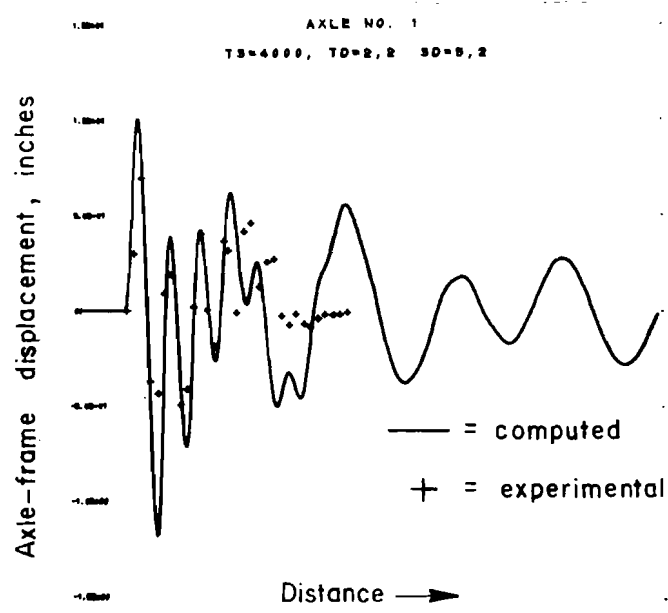


Fig 77. Roughness patterns for bridge study.

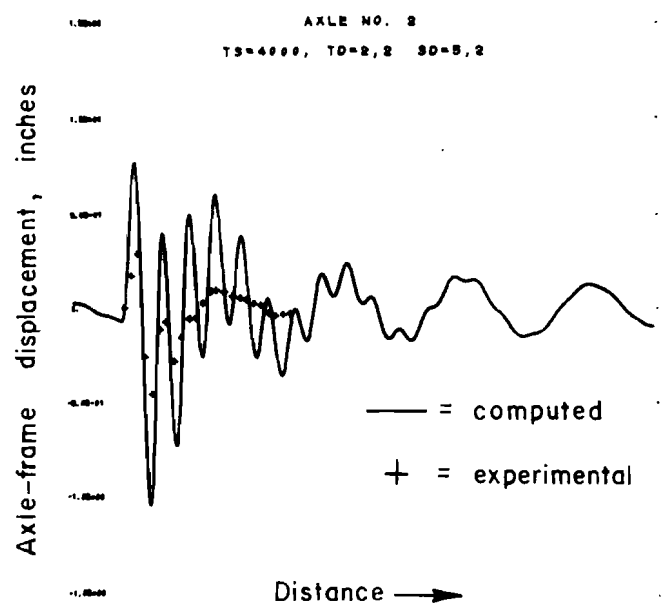
The mathematical vehicle model was "run" successively at the proper speeds over the corrected profile in the CDC 6600 computer, and calculated axle-frame displacements were displayed for each of the 31 vehicle passes. Figure 78 is an example of the display of experimental values along with the computed displacements. Agreement is quite good in the region of maximum suspension excitation, but the viscous damping used in the model does not adequately simulate vehicle behavior in the low-frequency, small amplitude realm. Friction damping of the type suggested in Ref 21 would probably improve the model performance in this area of interest. But, because computed and measured axle-frame displacements in the zone of maximum dynamic activity were found generally to agree closely throughout the range of speed and profile conditions evaluated, the mathematical vehicle model was used to study vehicle-bridge interaction under critical loading conditions. Ideally, axle-frame displacements should have been measured simultaneously with the dynamic wheel forces in the pavement experiments in order to validate the model, but no on-board instrumentation was utilized in this earlier phase of the study.

After finding the model to be adequate for predicting maximum axle-frame displacements and peak wheel forces, the effects of the four selected roughness patterns on bridge loading were compared. The computed wheel forces resulting from a 3/4-inch step bump on the bridge approach (roughness K, see Fig 77) are shown in Fig 79 for the test truck running at 60 miles per hour. Peak dynamic wheel forces are shown to be in excess of 170 percent of static wheel loads just beyond the step bump. As might be expected, the computed dynamic forces were less when the speed of the vehicle was reduced to 30 miles per hour (see Fig 80).

The wheel force diagrams generated by the model for a vehicle operating at 30 miles per hour over roughness patterns L, M, and N are shown in Figs 81, 82, and 83, respectively. Even small irregularities on the roadway surface cause large dynamic wheel loads. A single 3/4-inch step bump (roughness L, see Fig 77) generated dynamic wheel forces which were more than 180 percent of static weight. More dramatic, but perhaps less likely to occur in routine practice, are the dynamic wheel forces that reach magnitudes greater than 2-1/2 times the static wheel weight when the vehicle travels at 30 miles per hour over three 3/4-inch high bumps spaced 50 inches apart (see Fig 83). Certain types of bridge deck deterioration can, however, conceivably produce roughness patterns of this general types, and under these conditions,



(a)



(b)

Fig 78. Theoretical and experimental axle-frame displacements for truck traveling at 30 mph.

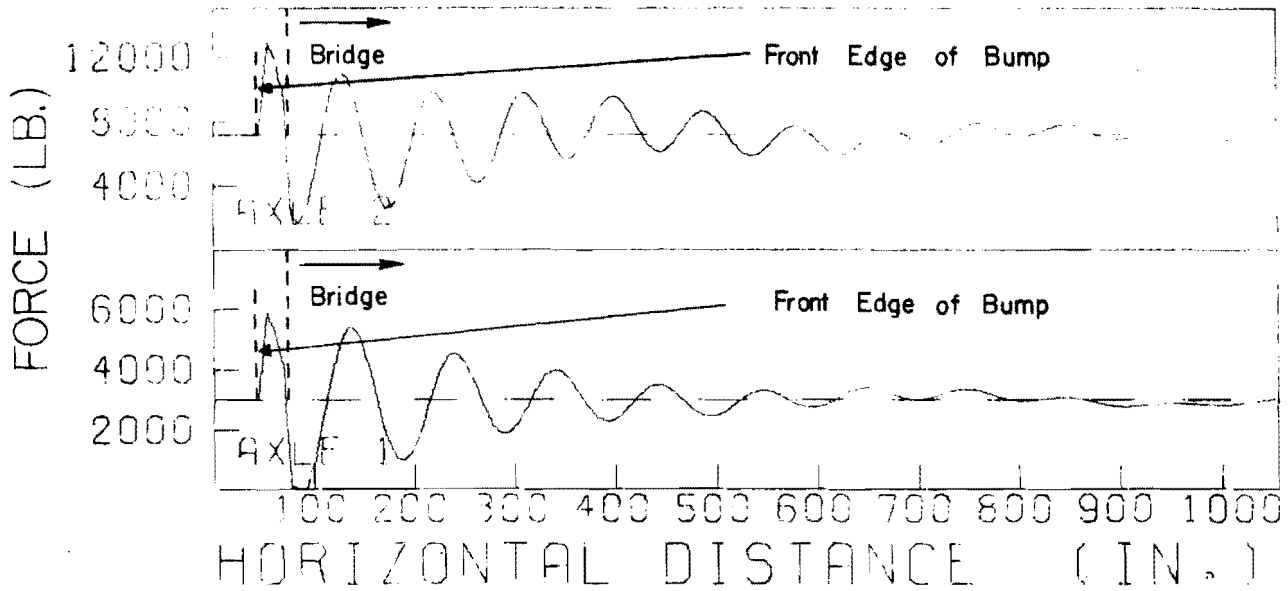


Fig 79. Predicted tire forces, vehicle speed 60 mph, roughness K.

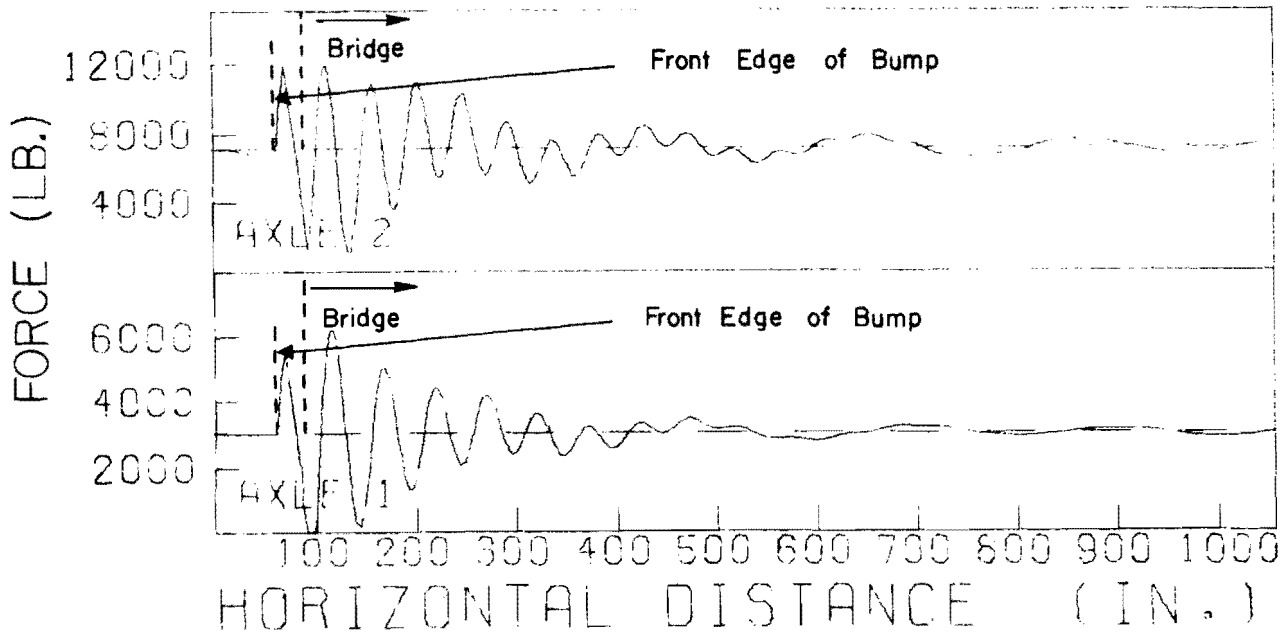


Fig 80. Predicted tire forces, vehicle speed 30 mph, roughness K.

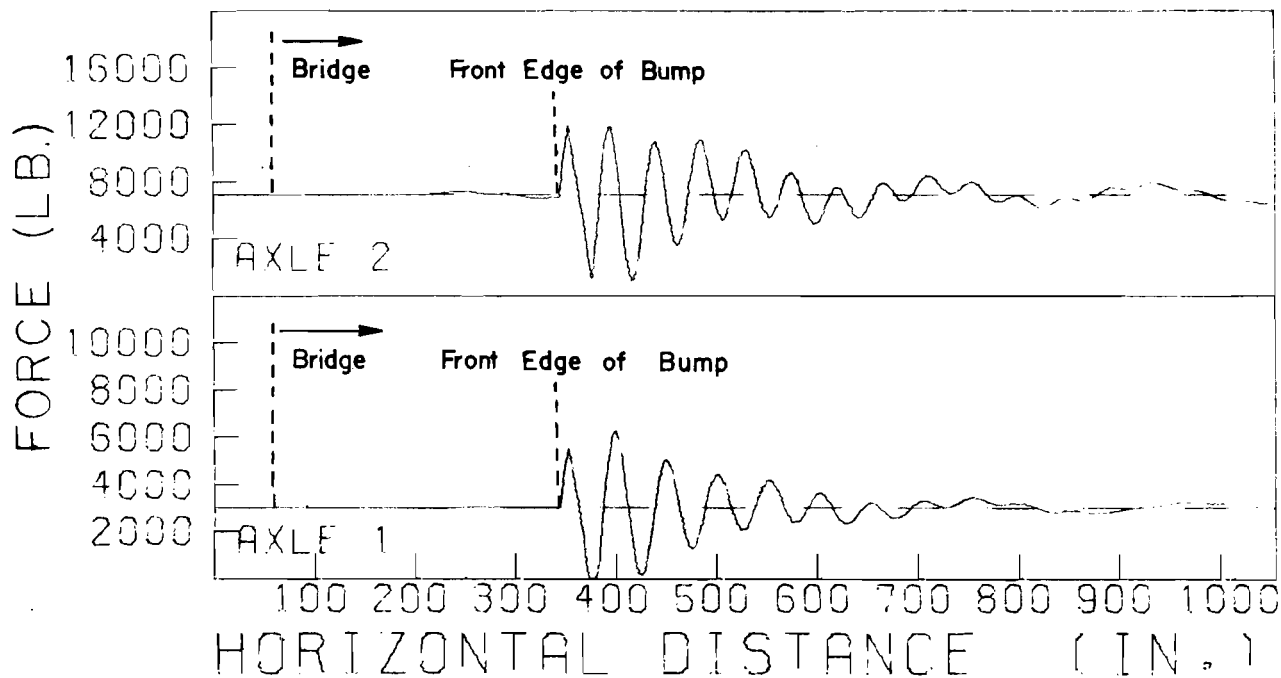


Fig 81. Predicted tire forces, vehicle speed 30 mph, roughness L.

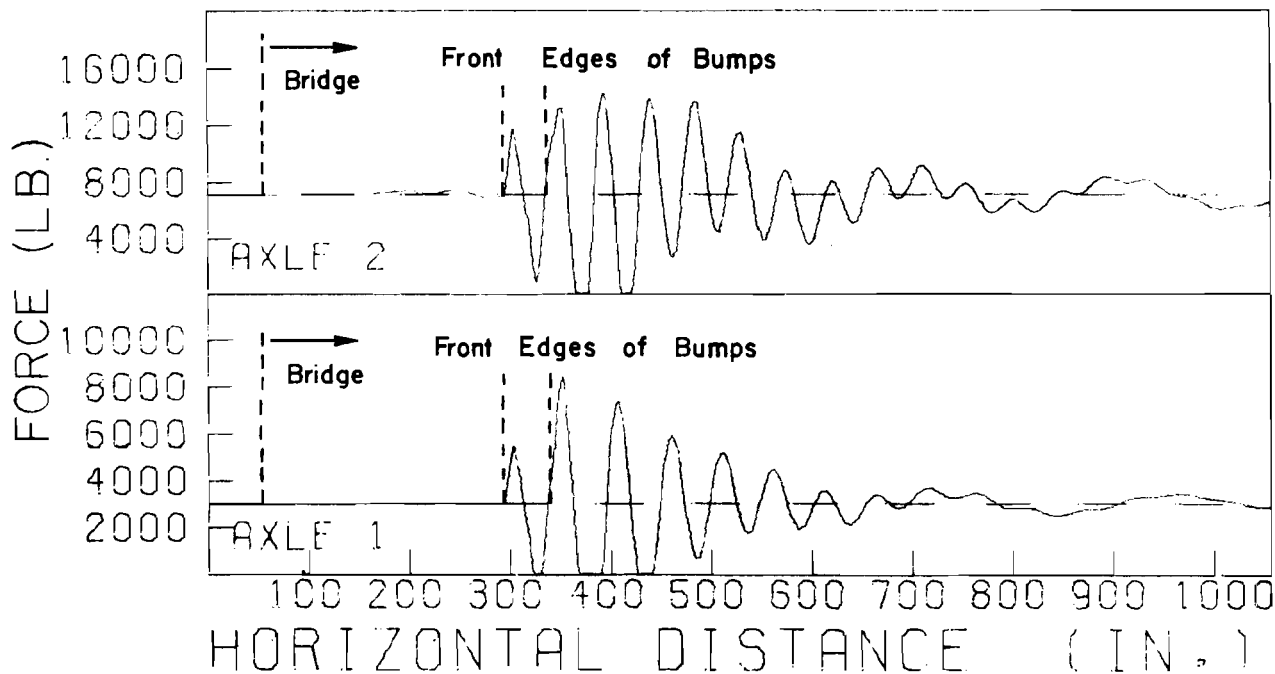


Fig 82. Predicted tire forces, vehicle speed 30 mph, roughness M.

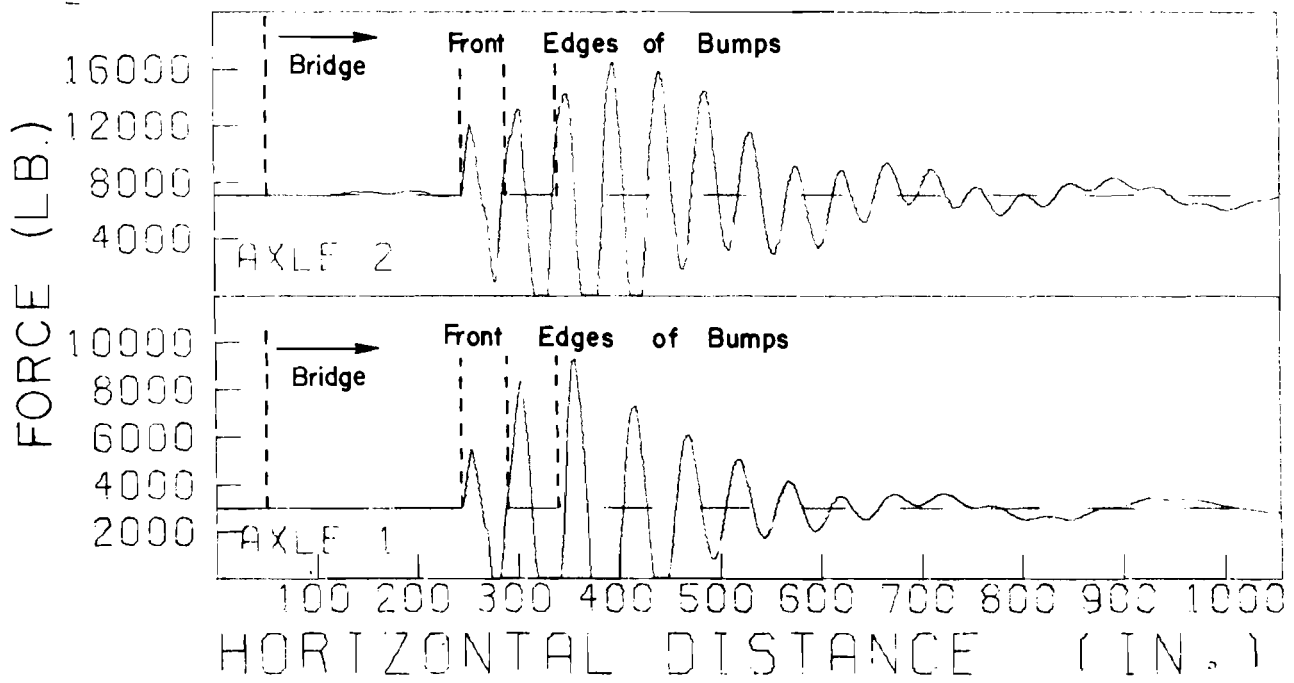


Fig 83. Predicted tire forces, vehicle speed 30 mph, roughness N.

concentrations of very high wheel loads on the deck are to be expected. The model can be used to analyze any particular situation of interest.

The energy imparted to the massive bridge structure by the varying dynamic wheel loads is not reflected directly as deflection or strain in the girders or other structural members below the deck. Inertia of the bridge prevents this, but the deck receives the full impact of the dynamic loading and should be designed to withstand large numbers of repetitions of critical dynamic wheel loads. Results of this study indicate that road surface irregularities less than an inch high can easily result in dynamic wheel loads that are 150 to 250 percent of static wheel weight. Bumps of this size are not uncommon, particularly on bridge approaches and at some structural joints. As bridge deck design procedures are refined to account directly for such factors as localized load distribution through the tires and for repetitions of dynamic wheel loads, consideration should be given to using wheel load impact factors in the range of 150 to 200 percent.

Summary of Bridge Study

From the model analysis and field study of rather limited scope, the following observations and conclusions are warranted:

- (1) The technique for measuring bridge deflections with strain-gaged cantilever beams and small-diameter music wire is convenient and accurate, but proper calibration procedures must be utilized.
- (2) Axle-frame displacements in a moving vehicle can be measured successfully with simple, inexpensive potentiometer transducers and on-board analog recording equipment. These experimental data provided a secondary check on the validity of the mathematical vehicle model described in Chapter 4.
- (3) Computed axle-frame displacements agreed well with experimental values in the critical realm of maximum suspension system activity, but for low-frequency, small-amplitude displacements, the viscous damping utilized in the model was inadequate. Friction damping of the type suggested in Ref 21 might produce better simulation.
- (4) Under the 24,000 test truck running at 30 mph, maximum girder deflection was on the order of 0.1 inch when three 3/4-inch high bumps spaced at 50 inches were placed on the first span of the bridge deck. This deflection had negligible effect on the dynamic behavior of the model but represented considerable structural displacement for such a light vehicle. The bridge oscillated at about 10 Hz; this was approximately the same frequency at which the truck under carriage oscillated after having been driven by the step bumps.

- (5) Surface irregularities less than an inch high can produce dynamic wheel forces that are 150 to 250 percent of static wheel weight. Procedures for designing bridge decks should take these dynamic loads into consideration.

CHAPTER 11. ESTIMATING STATIC VEHICULAR WEIGHTS

An idealized vehicle traveling on a perfectly smooth pavement at normal roadway speeds exerts dynamic wheel forces on the pavement that are essentially equal to the static weight of the vehicle. In practice, these ideal conditions are never realized completely, but when variations from the ideal are small, static weight estimates of acceptable precision for certain purposes can be made from one or more samples of dynamic wheel force. Some of the experimental data obtained in this study are representative of actual roadway and truck traffic conditions and are analyzed to determine the accuracy with which static wheel weights and gross vehicle weights can be estimated from dynamic wheel forces measured with transducers in the pavement. A stepwise multiple regression computer program, BMD-2R(Ref 51) has been used for the statistical analysis.

The technique of obtaining the experimental data for five classes of test trucks is described in preceding chapters and in the appendices of this report. Static wheel weights that are used as a basis for comparison are average values of between four and ten weighings of each wheel of five test vehicles that were obtained from careful use of portable wheel load weighers as detailed in Appendix A. The maximum coefficient of variation in these static wheel weight data was 4 percent, but most coefficients of variation were less than 2 percent. Dynamic wheel force data are average values of force on the wheel load transducer while the wheel was fully supported on the 18-inch effective length of the transducer.

Static Wheel Weights

For visual inspection, dynamic wheel forces measured by a wheel load transducer in the left wheel path of the test vehicles are plotted versus the corresponding static wheel weights in Figs 84, 85, and 86 for speeds of 10, 30, and 60 mph, respectively. Each test truck used in the experiment made several passes over the transducer at each speed indicated. At 10 mph, the data points are clustered rather evenly about the 45 degree line of perfect agreement, but

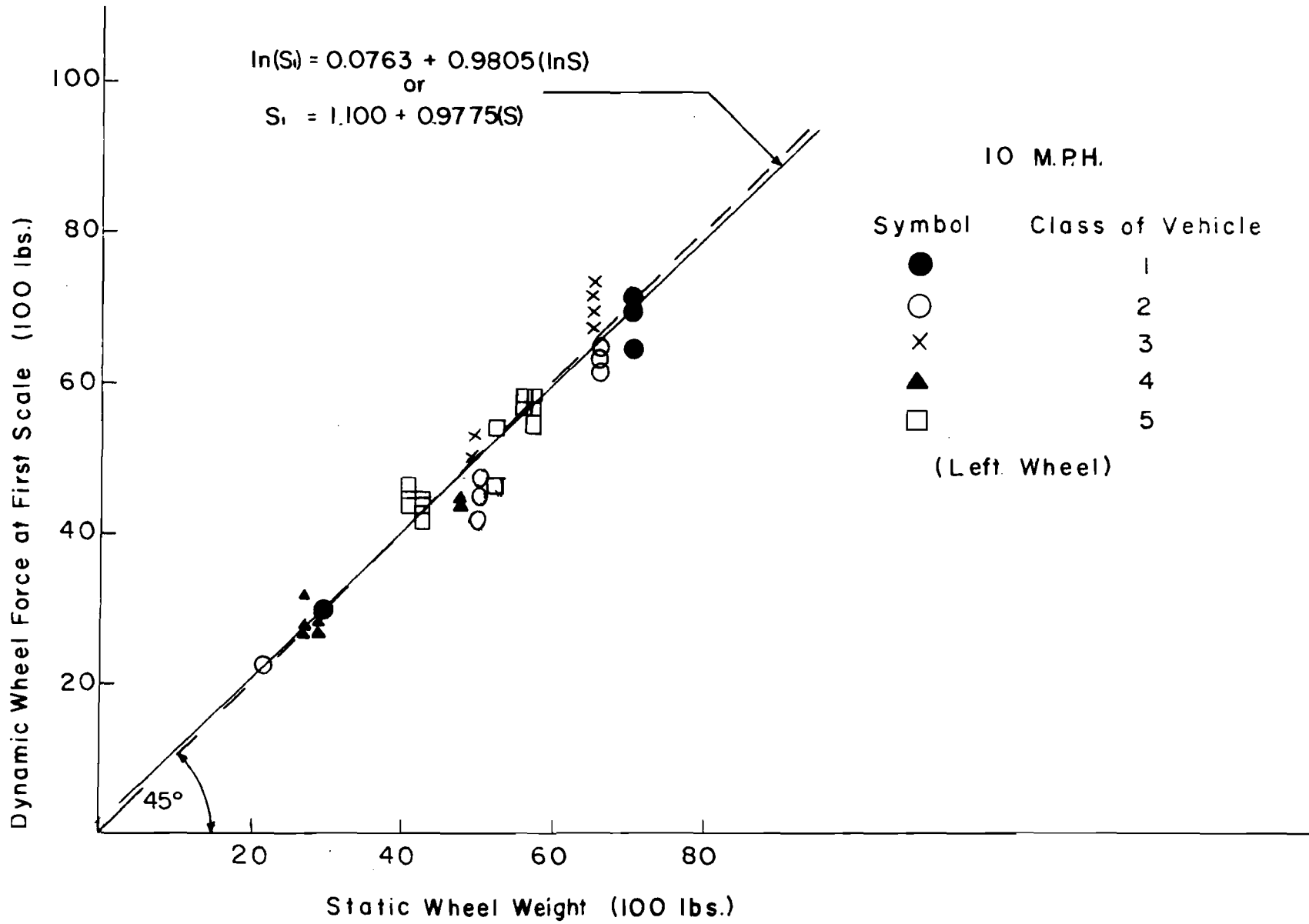


Fig 84. Predicted vs static wheel weights, vehicle speed 10 mph.

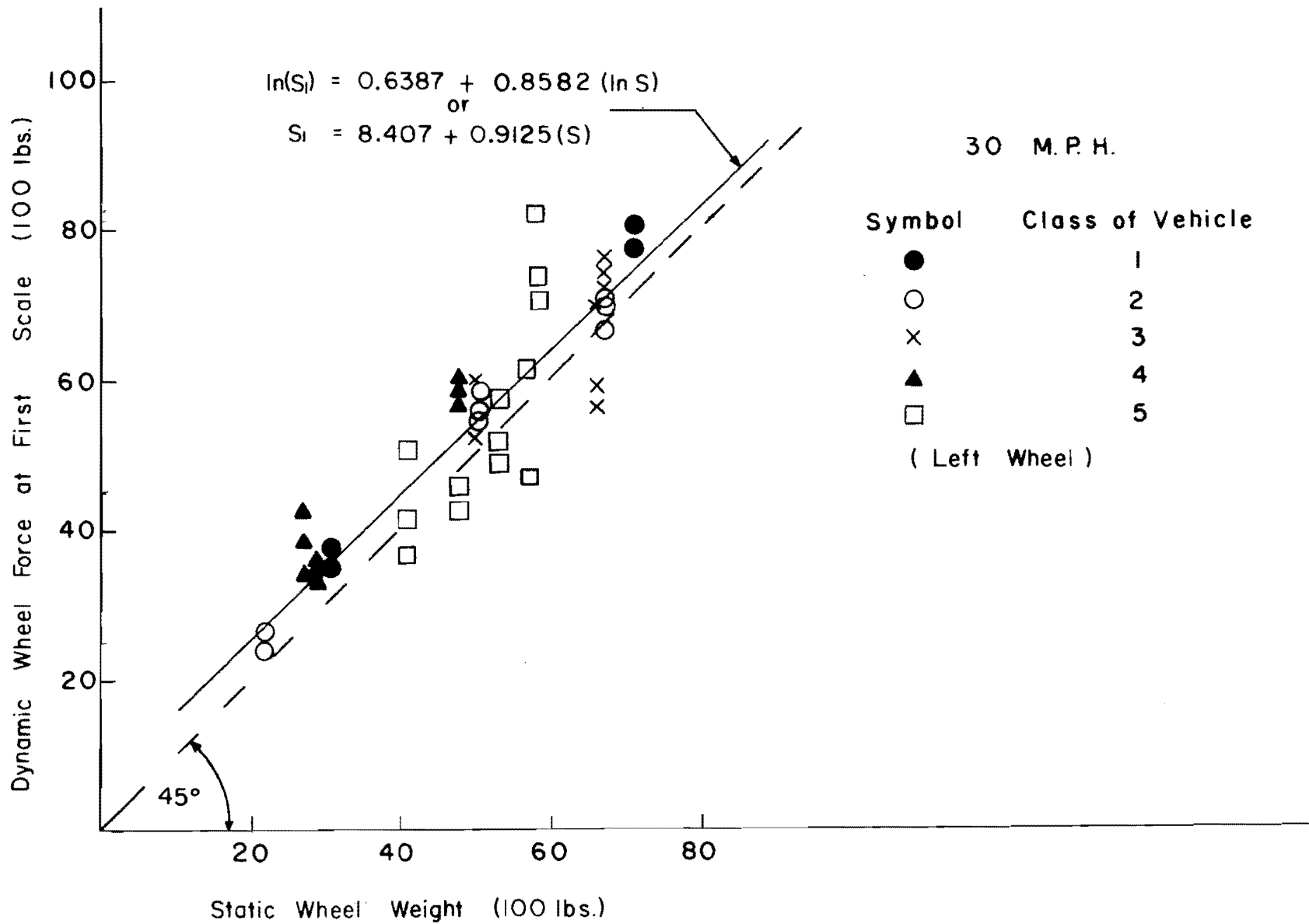


Fig 85. Predicted vs static wheel weights, vehicle speed 30 mph.

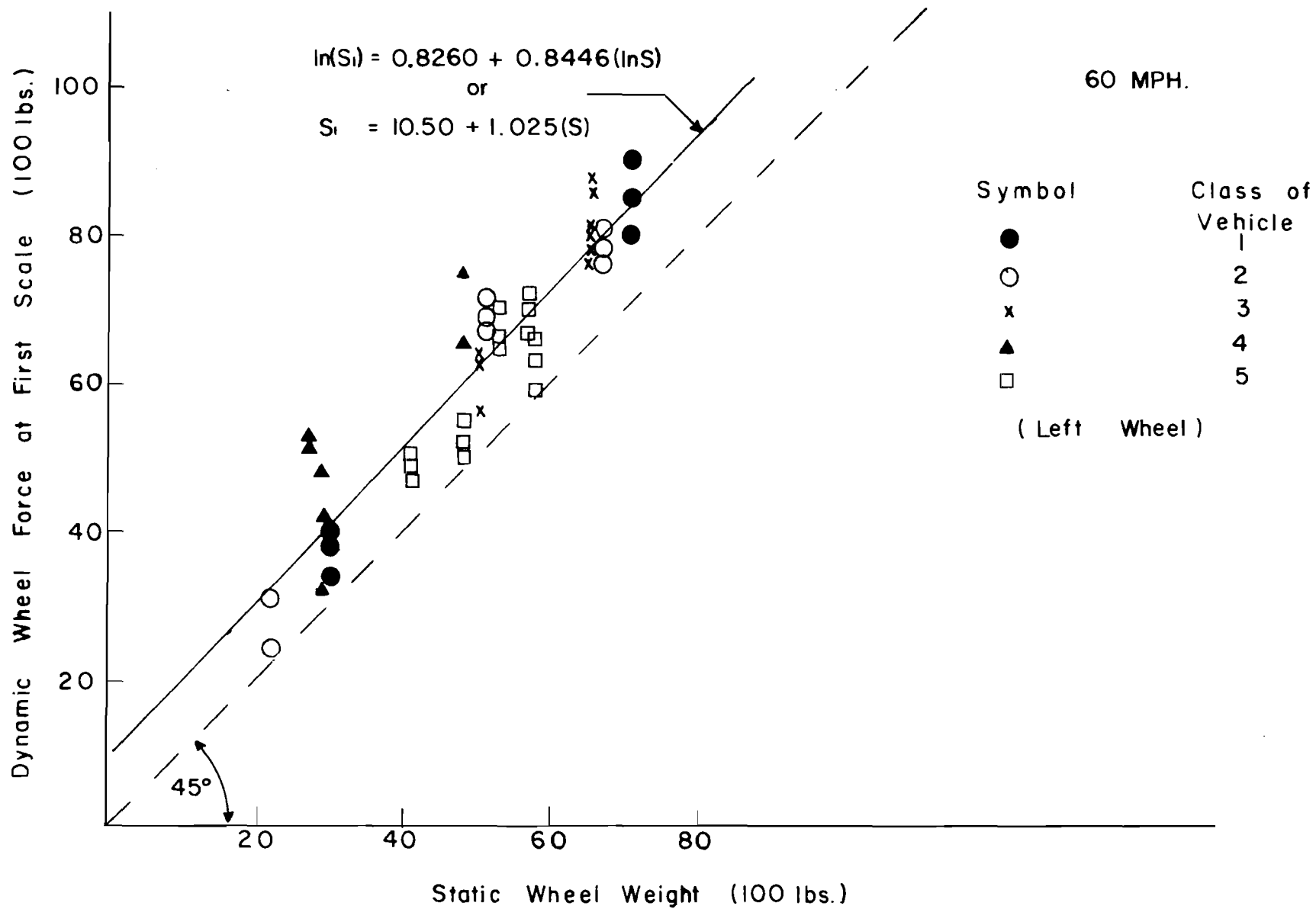


Fig 86. Predicted vs static wheel weights, vehicle speed 60 mph.

for 30 and 60 mph, the dynamic wheel forces are generally somewhat greater than the corresponding static weights. A number of factors could account for this difference, but one likely explanation is that when these tests were run the wheel load transducers were standing slightly above the surrounding pavement by perhaps 1/8 to 1/4 inch in the wheel paths. During the several months of experimental work, the flexible pavement in the test section and for a half mile or so in advance rutted in each wheel path. Profile measurements with the GMR profilometer indicated that the transducers were standing somewhat proud of the approach pavement (see Fig 55, Chapter 7). The dynamic effects of these "bumps" would tend to be greater at the higher speeds. However, profile irregularities of this magnitude may exist in practice; therefore, the data are considered to be representative of a worst condition.

In order to examine the relationship between static weight and dynamic wheel force numerically, a linear multiple regression analysis was performed. Although the obvious purpose of this analysis was to determine the precision with which static wheel weights can be predicted from samples of dynamic wheel force, the regression equations were derived by using static weights to estimate dynamic wheel forces. This was necessary since in a normal regression equation ($y = A + Bx$), the independent variable (x) is assumed to be virtually error free, while the dependent variable (y) may have errors associated with it. The static wheel weight information averaged from multiple weighings of each wheel was taken as the independent, or error-free, variable (x) in developing the regression equations. These equations may be inverted, or solved for x , so that dynamic wheel forces can be used to estimate static wheel weight. This inversion technique is called inverse estimation and is fully documented in Ref 52.

Results of the regression analysis are summarized in Table 17. A regression equation was developed for each of the three truck speed classes and for various combinations of scales used in the experiment. A log transformation of the data was utilized in the statistical analysis, and the resulting equations are presented in this form. The coefficient of variation for each regression equation is a measure of the precision with which estimates of static wheel weight can be predicted by the equation. As explained above, these coefficients were computed on the basis of static wheel weight being the independent variable; therefore, small inaccuracies can result from applying the coefficients to the inverted equations. These inaccuracies, however, cannot

TABLE 17. REGRESSION ANALYSIS FOR WHEEL WEIGHT STUDY

Speed (mph) Number of Scales	10 mph	30 mph	60 mph	Statistic
1	$\ln(s_1) = .0763$ $+ .9805(\ln S)$	$\ln(s_1) = .6387$ $+ .8582(\ln S)$	$\ln(s_1) = .8260$ $+ .8446(\ln S)$	Equation
	6.6	11.5	13.4	Coefficient of Variation (%)
	0.97	0.88	0.84	R^2
2	$\ln(s_1 + s_5) = .7564$ $+ .9838(\ln S)$	$\ln(s_1 + s_4) = 1.408$ $+ .8386(\ln S)$	$\ln(s_1 + s_3) = 1.177$ $+ .9162(\ln S)$	Equation
	5.1	7.7	11.7	Coefficient of Variation (%)
	0.98	0.94	0.89	R^2

(Continued)

TABLE 17. (Continued)

Speed (mph) Number of Scales	10 mph	30 mph	60 mph	Statistic
3	$\ln(s_1 + s_5 + s_6)$ = 1.256 + .9630(lnS)	$\ln(s_1 + s_4 + s_5)$ = 1.751 + .8557(lnS)	$\ln(s_1 + s_3 + s_4)$ = 1.753 + .8682(lnS)	Equation
	4.9	6.7	11.5	Coefficient of Variation (%)
	0.98	0.96	0.88	R ²

where S = static weight

s₁ = scale 1 estimate

s₂ = scale 2 estimate

s₃ = scale 3 estimate

s₄ = scale 4 estimate

s₅ = scale 5 estimate

s₆ = scale 6 estimate

Note: All weights and estimates must be expressed in 100 lb units.

The following confidence levels may be applied to the data in this table:

<u>Number of Standard Deviations</u> <u>(Coefficient of Variation)</u>	<u>Confidence (%)</u>
1	68
2	95

possibly be large because of the relatively small scatter in the observed data and the fact that all data points cluster near the 45 degree line in Figs 84, 85, and 86.

The following interpretation of the regression equations and associated statistics shown in Table 17 is warranted. Static wheel forces estimated by the regression equations from dynamic wheel force measurements will be within

$$\pm n \times \text{coefficient of variation}$$

of the true value, where n is the number of standard deviations from the mean that will satisfy an associated confidence level in the estimate. For example, if n is 1, then approximately 68 percent of any random group of dynamic wheel weight observations will, from the regression equations, yield static wheel weights that vary no more than $\pm 1 \times$ coefficient of variation from the true values. If n is 2, approximately 95 percent of the observations would produce estimates within $\pm 2 \times$ coefficient of variation of the true values.

Two trends in the data shown in Table 17 are important. First, at the scale installation under consideration where profile roughness was caused by pavement rutting around the wheel load transducers, speed of the vehicles influenced the accuracy of the static wheel weight estimates. At vehicle speeds of 10 mph, a single sample of the dynamic wheel force used with the appropriate regression equation yielded static wheel weight estimates within ± 6.6 percent approximately 68 percent of the time while at 60 mph comparable limits of accuracy were ± 13.4 percent. The higher speeds resulted in poorer estimates of static wheel weight at this multiple scale installation.

Second, increasing the number of scales improved the estimates of static wheel weight. The greatest improvement indicated in Table 17 was at 30 mph where the coefficient of variation decreased from ± 11.5 percent to ± 6.7 percent when three transducers were used instead of one. The advantage of multiple scales is less pronounced at the other vehicle speeds with reductions in the coefficient of variation being generally less than 2 percent when considering two or three scales. It is interesting to note that Scale 1 always contributed most to explaining the relationship between dynamic and static wheel loads as evidenced by the sequence in which the scales were added in the regression equations, and that various scales combined in an orderly way to improve the estimate. At 10 mph, the scales farthest downstream (Scale 5, then 6) were

found to further reduce the error of estimate; whereas, at 30 and 60 mph, the scales nearer to Scale 1 (Scales 3, 4, and 5) made larger contributions than those downstream. The fact that various scales were combined in the regression equations to yield the best estimate of static wheel weight and that the regression coefficients were somewhat different in each equation is further evidence that the profile roughness caused by pavement rutting interacted in a complex manner with the suspension system of the moving vehicles. Judgment should be exercised in deciding whether or not the relatively small improvements in accuracy justify the expense of more than one wheel load transducer in each wheel path.

Static Gross Vehicle Weight

Part of the wheel weight data used in the previous analysis were combined with additional output from a transducer in the right wheel path to yield gross vehicle weights, and the same regression technique was employed to evaluate the accuracy with which static gross vehicle weights can be predicted from dynamic wheel forces measured by a single pair of wheel load transducers. Results of the regression analysis are presented in Table 18, and since the prediction errors are relatively small, multiple transducer combinations were not investigated.

Using the regression equations that were developed for the subject scale site and shown on the second page of Table 18, gross vehicle weights can be predicted within ± 3.4 , ± 4.5 , or ± 8.0 percent with 68 percent confidence for vehicular speeds of 10, 30, and 60 mph, respectively. Or, without using a regression equation (see first page of Table 18), gross weights can be predicted with 68 percent confidence within ± 4.6 , ± 9.7 , or ± 15.5 percent for speeds of 10, 30, or 60 mph, respectively.

As with wheel weight predictions, the rutted pavement apparently induced dynamic effects that caused larger errors in static gross weight estimates at the higher speeds. Speed effects were found to be much less pronounced at this site before the pavement rutted and after the roadway was overlaid with approximately 1-1/2 inches of asphaltic concrete to smooth and deslick the surface. The variations in estimated static gross vehicle weight indicated in Table 18 represent a worst case scale installation condition that would be considered acceptable in practice. It is recognized that the wheel load

TABLE 18. ANALYSIS OF STATIC CROSS WEIGHTS

Speed (mph) Type of Analysis	10 mph	30 mph	60 mph	Statistic
Variation About 45° Line (X = X)	x = y	x = y	x = y	Equation
	4.6	9.7	15.5	Coefficient of Variation (%)
	--	--	--	R ²
Zero Regression Intercept (X = 0 + bX)	$\ln X = 0 + .998 \ln X$	$\ln X = 0 + 1.01 \ln X$	$\ln X = 0 + 1.01 \ln X$	Equation
	4.3	5.3	8.0	Coefficient of Variation (%)
	.99	.99	.99	R ²

(Continued)

TABLE 18. (Continued)

Speed (mph) Type of Analysis	10 mph	30 mph	60 mph	Statistic
Regression Equation of the Form (X = a + b)	$\ln X = -.925 + 1.087 \ln Y$	$\ln X = .966 + .915 \ln Y$	$\ln X = .723 + .943 \ln Y$	Equation
	3.4	4.5	8.0	Coefficient of Variation (%)
	.99	.98	.94	R ²

where Y = static gross weight

X = composit transducer estimate of gross weight

ln = natural logarithm

Confidence levels may be applied to the data in this table as follows:

<u>Number of Standard Deviations (Coefficient of Variation)</u>	<u>Confidence (%)</u>
1	68
2	95

transducers must be flush with the surface of a smooth approach pavement if dynamic effects are to be minimized.

Summary

Based on the data available from the pavement dynamics study and on the statistical analysis described above, the following statements can be made regarding the accuracy with which static vehicle weights can be predicted from measurements of dynamic wheel force with transducers in the pavement.

- (1) For best accuracy, the wheel load transducers must be maintained flush with the pavement surface in order to minimize dynamic effects. The influence of pavement rutting that was approximately 1/4 inch deep in the wheel paths around the transducers at the test site is included in the coefficient of variation shown in Tables 17 and 18 and referred to subsequently in relation to expected accuracy. This condition probably represents a worst case that would be considered tolerable in practice, and the estimates of possible accuracy discussed in this chapter should be interpreted accordingly.
- (2) Examination of the experimental data indicated that measured dynamic wheel forces were generally greater than corresponding average static wheel weights; therefore, it was desirable to utilize a linear multiple regression technique to quantify and evaluate the relationship. While the resulting regression equations are applicable only for the conditions at the experimental site, they serve to indicate the nature of the relationship that can be expected if the pavement and the transducers are not maintained as a smooth riding surface.
- (3) When appropriate regression equations for a particular site are used, static wheel weights can be estimated from the dynamic wheel force information produced by a single transducer with an expected accuracy of ± 7 percent for speeds near 10 mph or ± 13 percent for vehicles traveling at 60 mph with about 70 percent confidence. At a 95 percent confidence level, the range in the expected accuracy of the estimate is approximately twice these percentages.
- (4) Estimates of static wheel weight can be improved by using multiple wheel load transducers. The regression equations developed from multiple transducer experimental data yielded somewhat smaller coefficients of variation than those based on information from a single transducer. The regression equations were different for the two cases, but the error of estimate, as indicated by the coefficient of variation, was generally reduced by less than 2 percent when two or three transducers were used rather than one.
- (5) Static gross vehicle weight can be estimated by a regression equation using information from a single pair of wheel load transducers with an accuracy between ± 3 percent at 10 mph and ± 8 percent at 60 mph with 68 percent confidence. When no regression equation was used with the experimental data (see first page of Table 18), the

coefficient of variation ranged between ± 4.6 and ± 15.5 percent for the same confidence level. A smooth pavement surface around flush-mounted transducers will reduce this error of estimation. Static gross vehicle weight estimates were more accurate than individual wheel weight estimates on a percentage basis.

- (6) Even though individual static weight estimates from dynamic measurements do not agree perfectly with average weights obtained from wheel load weighers* the in-motion weighing technique can be used to yield adequate data for certain purposes such as traffic weight surveys. For such surveys, the technique makes it feasible to obtain very large samples of traffic (up to 100 percent for any selected period of time) and determine weight characteristics of individual classes of vehicles or of the traffic stream as a whole without hazard or delay to any vehicle. Mean weights computed from a large sample, even though individual measurements are not determined as accurately, are probably more representative of the true weight characteristics of traffic than are mean values computed from a small sample consisting of more accurately measured weights.
- (7) In order to evaluate comprehensively the accuracy with which static vehicle weights can be estimated from dynamic wheel force measurements, it will be necessary to analyze data from controlled tests at a minimum of five field sites. The analysis presented in this chapter points out again the strong interaction between the moving vehicle and the pavement surface profile and indicates the range of accuracy that can be feasibly achieved in practice.

An interactive graphics technique that utilized a cathode ray tube display was found to be a fast and efficient means of comparing the results of mathematical simulation with experimental data. An analysis of the vehicle simulation model by this technique lead to the following conclusions:

- (1) Of the model input parameters, tire stiffness was the most sensitive. Computed wheel forces agreed most closely with observed wheel forces when values of tire stiffness of 4000 and 4500 pounds per inch of deflection for speeds of 30 mph and 60 mph, respectively, were used.
- (2) A small amount of viscous damping in the tire simulation subsystem of the model produced the best results. Approximately 2 percent of critical damping for the wheel mass was found most satisfactory.
- (3) For model input parameters, the suspension stiffness of any vehicle can be adequately estimated from experimental measurements of axle-frame displacements resulting from application of known static load increments.
- (4) Viscous damping in the suspension subsystem of the model resulted in wheel forces that agreed well with observed values in the realm of

* The National Conference on Weights and Measures recommends a maintenance tolerance of 3 percent of a known test load for wheel load weighers, Ref 53.

maximum suspension system activity where dynamic forces were produced by oscillations of the unsprung mass in the range of about 6 to 12 Hz. For the Class I (2-axle) vehicle, suspension damping of 5 percent and 2 percent of computed critical damping for the front and rear tire-axle-suspension subsystem, respectively, were found to yield best results. Friction damping might possibly give better results in the range of low frequency, small amplitude oscillations.

- (5) Tire enveloping can be simulated by averaging the road surface profile over a distance approximately equal to the tire contact length. This is a better representation of the real tire-pavement interface than the moving point contact frequently used in simulation models.

CHAPTER 12. CONCLUSIONS AND RECOMMENDATIONS

According to the objectives stated in the early part of this report, this investigation was divided into two phases: (1) theoretical and (2) experimental. The theoretical phase involved the development of a mathematical technique which can be used to predict the magnitude, position, and duration of the dynamic wheel loads applied normal to the roadway surface by the wheels of moving traffic. The experimental phase involved the design of a portable electronic data collection system capable of sampling dynamic loads applied by the wheels of several classes of vehicles operating at wide ranges of speeds. The measured dynamic wheel loads were then used to validate the accuracy of the mathematical technique by comparing the predicted and the measured loads. In addition, a statistical analysis was performed to evaluate the significance of some of the factors which influence the magnitude and variation of dynamic wheel loads. The conclusions drawn from this statistical analysis, as emphasized in the preceding chapter, are applicable only within the inference space defined by the general layout of the experiment design.

Conclusions

Based on the work described in the preceding chapters, the following conclusions are warranted:

A generalized mathematical model which consists of a series of interconnected masses, springs, and dashpots has been developed to characterize five classes of highway vehicles.

The normal component of the dynamic forces applied to the roadway surface by the wheels of each of these several classes of single unit and articulated vehicles operating under various conditions can be predicted with reasonable accuracy by using this model in a simple mathematical simulation procedure.

At vehicle speeds of 10 and 30 miles per hour, the model accuracy is quite satisfactory since 92 and 82 percent, respectively, of the total observed wheel loads (2,448 observations at these speeds) were found to fall within

10 percent of the range predicted by model simulation. At high speeds many of the observed oscillations were not in phase with the predicted oscillations. This resulted in a poorer agreement whereby only 53 percent of the observed values were within 10 percent of the predicted range of wheel loads. With relatively few exceptions, however, the average difference between observed and predicted wheel loads was less than 10 percent.

The computer program which solves the sets of differential equations necessary for calculating the dynamic wheel load forces is operational, efficient, and easy to use. Although this computer program has been written for the CDC 6600 computer, it may easily be adapted for use on other machines of comparable size or capacity. Furthermore each class of vehicle is handled separately in a subroutine thus allowing flexibility for modifying the characteristics of each particular class individually.

An analysis of variance was performed on the data in accordance with the experimental design in order that inference concerning the statistical significance of the various factors considered could be made. Four main effects, six two-factor interactions, and four three-factor interactions were found to have significant influence on the magnitude of dynamic wheel loads. According to their order of decreasing significance, the main effects included:

- (1) axle,
- (2) sample location,
- (3) speed, and
- (4) roughness.

The two-factor interactions include

- (1) speed-sample location,
- (2) roughness-sample location,
- (3) axle-speed,
- (4) axle-sample location,
- (5) axle-roughness, and
- (6) speed-roughness.

The three-factor interactions include

- (1) speed-roughness-sample location,
- (2) speed-sample location-axle,
- (3) axle-sample location-roughness, and
- (4) speed-roughness-axle.

Average dynamic wheel loads increased with an increase in speed. A total of 3,672 observations of dynamic wheel force were made at six scale locations along a 64 foot instrumented section for five test vehicles operating at 10, 30, and 60 miles per hour over four patterns of surface roughness. The average dynamic wheel load components resulting from these tests were 6, 15, and 19 percent of static load for the respective speed levels.

Dynamic wheel loads also vary as vehicles move along the roadway surface. Dynamic wheel load components calculated by averaging the wheel force observations from the test conditions described above were found to vary by as much as 27 percent of the static load.

Even though the four pavement roughness patterns studied produced relatively small dynamic wheel load components when considered in terms of the average force applied along the 64 foot long test section, large dynamic loads at or near the step bumps were frequently observed. An obstruction in the roadway surface as small as 3/8-inch high caused the tire of a vehicle traveling at high speeds to lose contact with the roadway surface. Impact factors of more than 100 percent were produced as the tire mounted the step bump and again as the tire regained contact with the roadway surface.

The following conclusions and observations characterize the dynamic behavior of Class I single-unit vehicles. The left wheel path was more heavily instrumented and vehicle roll was found to be negligible; therefore, reference is made primarily to wheels on the left side of the vehicle.

- (1) The overall average dynamic load component produced by the left wheel of the front axle is 1-1/2 times the corresponding component produced by the left wheels of the rear axle (drive axle).
- (2) Higher speeds resulted in greater average dynamic wheel load components for both axles.
- (3) The maximum range of variation in the average dynamic load component along the test section was produced by the left wheel of the axle with the least static load.
- (4) A step bump 3/8-inch high on scale 1L produced an average increase in the dynamic component at this scale of about 40 percent for both left wheels as compared with no bump.

The following conclusions and observations characterize the dynamic behavior of Class II articulated vehicles:

- (1) The overall average dynamic load component produced by the left wheel of the front axle is 2 times the corresponding component produced by the left wheel of axle 2 (drive axle) and approximately

1-1/4 times the component produced by the left wheel of axle 3. The magnitude of these dynamic load components is inversely proportional to the corresponding static wheel load.

- (2) Higher speeds resulted in greater average dynamic wheel load components for the drive axle and the trailer axle. Axle 1, however, produced its maximum dynamic load component at 30 miles per hour.
- (3) The maximum range of variation in the average dynamic load component along the test section was produced by the left wheel of the axle with the least static load.
- (4) A step bump 3/8-inch high on scale 1L produced an average increase in the dynamic component of about 40 percent for all left wheels studied.

The following conclusions and observations characterize the dynamic behavior of Class III single-unit vehicles:

- (1) There appears to be no consistent relationship between the overall average dynamic wheel load components and the corresponding static wheel loads for the conditions observed.
- (2) In general, higher speeds produced greater average dynamic components.
- (3) The maximum range of variation in the average dynamic load component along the test section was produced by the left wheel of the forward tandem axle.
- (4) A step bump 3/8-inch high on scale 1L produced an average increase in the dynamic load component of about 20 percent for all left wheels studied.

The following conclusions and observations characterize the dynamic behavior of Class IV articulated vehicles:

- (1) The overall average dynamic load component produced by the front axle of this class of vehicle is much less than the corresponding components for the remaining axles where the magnitude is inversely proportional to static load. Although the left wheel of axles 1, 3, and 4 have nearly the same static load, the dynamic components produced by the latter two (tandem pairs) are much higher.
- (2) Higher speeds resulted in greater average dynamic components for all axles.
- (3) The maximum range of variation in the average dynamic load component along the test section was approximately the same for left wheel of the drive axle and for the fore-and-aft trailer tandem axle.
- (4) A step bump 3/8-inch high on scale 1L produced an average increase in the dynamic load component of about 50 percent for all left wheels studied.
- (5) In general there is no difference in the behavior of the fore-and-aft tandem axles with regard to their effect on the magnitude and pattern of variation of dynamic wheel load component.

The following conclusions and observations characterize the dynamic behavior of Class V articulated vehicles:

- (1) As in the case of Class IV vehicles, the average dynamic component produced by the left wheel of the front axle is much less than the corresponding components for the remaining axles where the magnitudes of these components have also been found to be inversely proportional to the static load.
- (2) In general higher speeds resulted in greater average dynamic components.
- (3) The maximum variation in the average dynamic component along the test section was produced by the left wheel of axle 3.
- (4) A step bump 3/8-inch high on scale 1L produced an average increase in the dynamic load component of about 40 percent for all left wheels studied.
- (5) In general there was no difference in the behavior of the fore-and-aft axles of each tandem with regard to their effect on the magnitude and pattern of variation of dynamic wheel load component. The drive tandem, however, produced greater dynamic components than the trailer tandem.

The bridge study was of limited scope, but it served to further verify the adequacy of the vehicle simulation model for predicting maximum dynamic wheel forces. The on-board instrumentation used in the test truck for measuring axle-frame displacements was simple and inexpensive, but satisfactory. Small displacements of the bridge had little effect on the performance of the mathematical model in predicting peak dynamic wheel loads, but the axle-frame displacement measurements again indicated the inadequacy of the viscously damped model for predicting low-frequency, small-amplitude oscillations. Friction damping in the suspension subsystem might be better. Certain patterns of road surface irregularities only 3/4-inch high produced dynamic wheel forces up to 250 percent of static wheel weight, and the field tests demonstrated that even small bumps on a bridge deck can result in impact factors up to 100 percent. Bridge decks should be designed to accommodate loads of this kind.

Samples of dynamic wheel forces measured by wheel load transducers that are appropriately designed and installed can be used to estimate static vehicle weights with acceptable precision for certain purposes. Where the pavement surrounding the transducers is not maintained in a smooth condition, dynamic effects resulting from different vehicle speeds affect the accuracy of the estimate. For a worst tolerable installation, static wheel weights can

probably be estimated from regression equations within about ± 7 percent for slow moving vehicles and within about ± 13 percent for high speed vehicles with 68 percent confidence. Relatively small improvements in the expected accuracy of these estimates will result from using two or three transducers in each wheel path rather than one. Static gross vehicle weights can be estimated from a single sample of dynamic wheel forces with an expected accuracy between ± 3 percent at 10 mph and ± 8 percent at 60 mph with 68 percent confidence from appropriate regression equations or within about ± 4 to ± 15 percent for these conditions without regression equations. Better estimates can be expected from smooth pavement approaches. Up to a 100 percent sample of traffic is feasible with the in-motion weighing technique, and the large sample size tends to compensate for the inaccuracies in estimated static weight based on samples of dynamic wheel force.

Recommendations

Experience gained in the conduct of this study suggests recommendations for further study or development in three general areas: mathematical model refinement, field experimentation, and analysis of dynamic bridge loading.

Model Refinement. The viscous damping utilized in the mathematical model failed to represent adequately the effect of long period, small amplitude oscillations observed in the test vehicles. Friction damping of the type outlined in Ref 24 can be readily incorporated into the model damping subsystem and future modeling of vehicle suspension systems should combine friction and viscous damping as elements in the simulation. Interactive graphics can aid in determining the best values for friction breakaway steps to use in the subsystem.

Further study should be given to modeling the tandem axle. There is some interaction between the fore and aft axles, but the best technique for simulating this phenomenon is not readily apparent. Field data described in Chapter 6 will serve to evaluate the adequacy of trail configurations.

Field Experimentation. In future field studies, instrumentation should include both on-board vehicle force or displacement recorders and in-road dynamic force transducers. These measurements are complementary, and if obtained simultaneously, provide the necessary parameters for evaluating a mathematical simulation model.

Test vehicles of known static weight and operating at a range of speeds should be utilized at a minimum of five different field installations to yield data for a comprehensive analysis of the accuracy with which static vehicle weights can be estimated from dynamic wheel force measurements. Pavements at these sites should be maintained in as smooth a condition as feasible.

Bridge Studies. The instrumentation techniques described herein give valuable information for analyzing dynamic bridge behavior under known vehicle loads; however, future studies should utilize a wider range of vehicle types, a larger variety of profiles, and strain gages on the bridge deck. Impact factors of up to 100% of an individual wheel load should be considered in deck design even though the maximum impact loads from all wheels do not necessarily occur simultaneously.

This page replaces an intentionally blank page in the original.

-- CTR Library Digitization Team

REFERENCES

1. Anderson, Virgil L., "Design and Optimum Techniques for Consulting Statisticians and Experimenters," lecture notes prepared for publication.
2. Apetaur, Milan, Jaromir Cmiral, Karel Janac, and Jiri Skrivanek, "Ride and Road Holding, Statistical Analysis of Suspension Problem on an Analog Computer," Automobile Engineer, April 1966, pp 142-148.
3. Bachmann, I. W., "Weighing Moving Vehicles," German Construction Engineering, June 1959, pp 870-871.
4. Bellini, W. R., and E. N. Thrower, "A Digital Computer Program to Simulate the Passage of a Vehicle Over a Road Surface," Road Research Laboratory Report LR 181, Ministry of Transport, Crothorne, England, 1968.
5. Bieniek, M. P., "Suspension Dynamics," Automobile Engineer, Vol 50, April 1960, pp 143-147.
6. Bundorf, R. T., D. E. Pollock, and M. C. Hardin, "Vehicle Handling Response to Aerodynamic Inputs," Society of Automotive Engineering Transactions, Vol 72, 1964, pp 7-23.
7. Cain, B. S., Vibration of Rail and Road Vehicles, Pitman Publishing Corporation, New York, 1940.
8. Clark, D. C., "A Preliminary Investigation into the Dynamic Behavior of Vehicles and Highways," Society of Automotive Engineering Transactions, Vol 70, 1962, pp 447-455.
9. Cochran, W. G., and G. M. Cox, Experimental Designs, 2nd Edition, Wiley and Sons, 1957.
10. Crandall, S. H., and W. D. Marks, Random Vibration in Mechanical Systems, Academic Press, New York and London, 1963.
11. Cudney, G. R., "The Effects of Loading on Bridge Life," Research Report No. R-638, Michigan State Highway Department, January 1968.
12. Dearinger, John A., "Dynamic Weighing of Vehicles," Public Roads, Vol 31, No. 10, October 1961, pp 200-204.
13. Den Hartog, J. P., Mechanical Vibrations, 4th Edition, McGraw-Hill, New York, 1956.

14. Ditlevsen, Ove, "Statistical Description of Traffic Loads on Structures," ACTA Polytechnica Scandinavica, Copenhagen, 1964.
15. "Dynamic Studies of Bridges on the AASHO Road Test," Special Report 71, Highway Research Board, 1962.
16. Ellis, J. R., "An Introduction to the Dynamic Properties of Vehicle Suspensions," Proceedings of Institution of Mechanical Engineers, Vol 179, 1964-65, pp 98-111.
17. Epsco Incorporated, "The Design and Installation of a Complete System for the Automatic Weighing of Vehicles in Motion and Collection of Traffic Data," Report for Project S2F-26, Michigan State Highway Department, October 1963.
18. Fabian, G. J., D. C. Clark, and C. H. Hutchinson, "Preliminary Analysis of Road Loading Mechanics," Bulletin 250, Highway Research Board, 1960, pp 1-19.
19. Fenves, S. J., A. S. Veletsos, and C. P. Siess, "Dynamic Studies of the AASHO Road Test Bridges," Special Report 73, Highway Research Board, 1962, pp 83-96.
20. Fisher, J. W., and H. C. Huckins, "Measuring Dynamic Vehicle Loads," Special Report 73, Highway Research Board, 1962, pp 138-148.
21. General Motors Corporation, "Dynamic Pavement Loads of Heavy Highway Vehicles," National Cooperative Highway Research Program Report 105, Highway Research Board, 1970.
22. Gilliam, R. P., "Dynamic Response of Nonlinear Automotive Suspension Systems," Master's Thesis, The University of Texas, Austin, 1962.
23. Hadley, William O., W. Ronald Hudson, and Thomas W. Kennedy, "An Evaluation of the Factors Affecting the Tensile Properties of Asphalt-Treated Materials," Research Report No. 98-2, Center for Highway Research, The University of Texas at Austin, March 1969.
24. Hopkins, R. C., and H. H. Boswell, "A Comparison of Methods Used for Measuring Vibrations in Loads Transferred Through Vehicle Tires to the Road Surface," Public Roads, Vol 29, No. 10, October 1957, pp 221-226.
25. Hudson, W. Ronald, "High Speed Road Profile Equipment Evaluation," Research Report No. 73-1, Center for Highway Research, The University of Texas, Austin, 1966.
26. Lee, Clyde E., and Nasser I. Al-Rashid, "A Portable Electronic Scale for Weighing Vehicles in Motion," Research Report No. 54-1F, Center for Highway Research, The University of Texas at Austin, 1968.
27. McCracken, D. D., and W. S. Dorn, Numerical Methods and Fortran Programming, Wiley and Sons, New York, 1964.

28. McDowell, Edward L., "Transverse Vibration of Beam Resting on Elastic Foundation," Ph.D. Dissertation, Illinois Institute of Technology, 1954.
29. Mitschke, Eng. M., "Influence of Road and Vehicle Dimensions on the Amplitude of Body Motions and Dynamic Wheel Loads," Society of Automotive Engineering Transactions, Vol 70, 1962, pp 434-446.
30. Newmark, N. M., "A Method of Computation for Structural Dynamics," Transactions, Vol 127, Proceedings of the American Society of Civil Engineers, 1962, pp 1406-1435.
31. Norman, D. K., and R. C. Hopkins, "Weighing Vehicles in Motion," Bulletin 50, Highway Research Board, January 1952.
32. Ostle, B., Statistics in Research, 2nd Edition, Iowa State University Press, 1963.
33. Philco-Ford Corporation, "Dynamic Vehicular Weighing System," Philco Project for Pennsylvania Department of Highways, June 15, 1967.
34. Philco-Ford Corporation, "Dynamic Vehicular Weighing System," Philco Project for Pennsylvania Department of Highways, June 3, 1966.
35. Pradko, F., "Computer Simulates Vehicle Suspension Systems," Society of Automotive Engineering Journal, Vol 71, April 1963.
36. Ragazzini, J. R., and G. F. Franklin, Sampled-Data Control Systems, McGraw Hill, New York, 1958.
37. Salvadori, M. G., and M. L. Baron, Numerical Method in Engineering, Prentice-Hall, Englewoods, New Jersey, 1961.
38. Sethna, D. R., "Dynamics of a Four-Wheeled Vehicle and the Effects of Suspended Geometry," Proceedings of Automobile Division, No. 6, Institute of Mechanical Engineers, 1962-63.
39. Stiffler, W. W., and R. C. Bensly, "Weighing Trucks in Motion and the Use of Electronic Scales for Research," Traffic Engineering, Vol 26, No. 5, February 1956, pp 195-199, 206.
40. Symonds, P. S., "Traveling Loads on Rigid Plastic Beams," Engineering Mechanics Division Journal, Proceedings of the American Society of Civil Engineers, January 1960, pp 79-89.
41. Texas Highway Department, Design Manual of Controlled Access Highways, Chapter 3, "Design of Pavement Structures," 1960.
42. "The AASHO Road Test Report 6: Special Studies," Special Report 61F, Highway Research Board, 1962.
43. Timoshenko, S., Vibration Problems in Engineering, D. Van Nostrand, New York, 1937.

44. Trott, J. J., and J. W. Grainger, "Design of a Dynamic Weighbridge for Recording Vehicle Wheel Loads," Road Research Laboratory Report LR219, Ministry of Transport, Crowthorne, Berkshire, England.
45. Trott, J. J., and A. C. Whiffin, "Measurements of the Axle Loads Moving on Truck Roads," Roads and Construction, July 1965, pp 209-214.
46. Tung, C. C., "Random Response of Highway Bridges to Vehicle Loads," Engineering Mechanics Division Journal, Proceedings of the American Society of Civil Engineers, October 1967, pp 79-94.
47. Volterra, E., and E. C. Zachmanaglou, Dynamics of Vibrations, Merrill Books, Columbus, Ohio, 1965.
48. "Weigh Axles in Motion," Taller and Cooper, Incorporated, 75 Front Street, Brooklyn, New York (commercial advertisement).
49. Wen, Robert K., "Dynamic Response of Beams Traversed by Two-Axle Loads," Engineering Mechanics Division Journal, Proceedings of the American Society of Civil Engineers, October 1960, pp 91-111.
50. Yoder, E. J., Principles of Pavement Design, John Wiley, New York, 1959.
51. Biomedical Computer Programs, "BMD-2R-Stepwise Multiple Regression," University of California at Los Angeles, 1964.
52. Halperin, Max, "Inverse Estimation in Linear Regression," Technometrics, Vol 12, No. 4, November 1970, pp 727-730.
53. National Bureau of Standards Handbook 44-3rd Edition 1965, "Specifications, Tolerances, and Other Technical Requirements for Commercial Weighing and Measuring Devices," Superintendent of Documents, U. S. Government Printing Office, Washington, D. C. 20402 (including 1968 Replacement Sheets).

APPENDIX A

STATIC WHEEL LOADS OF TEST VEHICLES

This page replaces an intentionally blank page in the original.

-- CTR Library Digitization Team

APPENDIX A. STATIC WHEEL LOADS OF TEST VEHICLES

The static load for each wheel of each test vehicle was determined immediately prior to use of the vehicle in testing by means of a pair of loadometers. The loadometers had been previously calibrated in the laboratory and periodically checked by the Texas Department of Public Safety.

The loadometers were set in pits in each wheel path on a specially constructed level ramp in the equipment yard of the Texas Highway Department warehouse located on Highway 183 southeast of Austin (Figs A.1 and A.2).

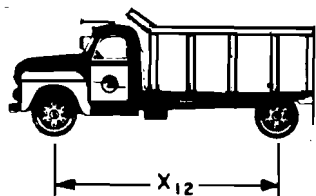
Each vehicle was weighed at least eight times (Figs A.3 and A.4) except for vehicles I-1 and I-2 which were weighed only four times. Summaries of these static weights are tabulated in the following figures.



Fig A.1. Static weighing operation
(front axle).



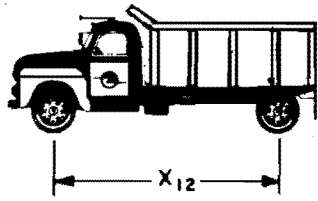
Fig A.2. Static weighing operation
(rear axle).



Vehicle No.	I-1	X_{12}	11' 2"
Model	1967 Dodge		
License No.	135456		
Tire Press.	65-70		

1	2	3	4	5	6	7	8	9	10
Loading Condition	Axle	Number of Weighings	Avg Static Weight lb	Standard Deviation lb	Variance lb ²	Coefficient of Var. %	Maximum Weight lb	Minimum Weight lb	Range lb
Fully Loaded	1 - R	4	2240	5.7	33	0.25	2245	2235	10
	1 - L	4	2335	5.7	33	0.24	2340	2330	10
	2 - R	4	7844	31.7	1004	0.40	7880	7815	65
	2 - L	4	8371	11.8	140	0.14	8380	8355	25
	1 - R								
	1 - L								
	2 - R								
	2 - L								

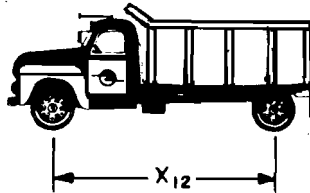
Fig A.3. Summary of static weights (vehicle No. I-1).



Vehicle No.	I-2	X_{12}	13' 2"
Model	1963 Dodge		
License No.	44002		
Tire Press.	65 - 70		

1	2	3	4	5	6	7	8	9	10
Loading Condition	Axle	Number of Weighings	Avg Static Weight lb	Standard Deviation lb	Variance lb ²	Coefficient of Var. %	Maximum Weight lb	Minimum Weight lb	Range lb
Partially Loaded	1 - R	4	2298	19.0	360	0.83	2310	2270	40
	1 - L	4	2539	8.54	73	0.34	2550	2530	20
	2 - R	4	3940	0.0	0	0.00	3940	3940	0
	2 - L	4	4177	79.0	6240	1.90	4250	4090	160
	1 - R								
	1 - L								
	2 - R								
	2 - L								

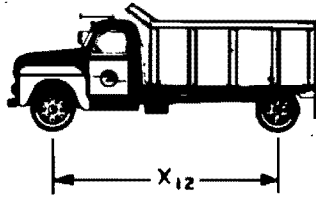
Fig A.4. Summary of static weights (vehicle No. I-2).



Vehicle No.	I-3	X_{12}	12'9"
Model	International 1969		
License No.	162 - 058		
Tire Press.	65 - 70		

1	2	3	4	5	6	7	8	9	10	11
Loading Condition	Axle	Number of Weighings	Avg Static Weight lb	Standard Deviation lb	Variance lb ²	Coefficient of Var. %	Maximum Weight lb	Minimum Weight lb	Range lb	Comm. Scale
EMPTY	1 - R	10	2265	13	161	0.57	2280	2245	35	4430
	1 - L	10	2238	14	201	0.63	2265	2220	45	
	2 - R	10	2847	5	29	0.18	2850	2835	15	5250
	2 - L	10	2587	9	73	0.35	2600	2575	25	
LOADED	1 - R	10	3139	12	143	0.38	3170	3130	40	6120
	1 - L	10	3012	44	1950	1.46	3090	2930	160	
	2 - R	10	7780	14	189	0.18	7810	7760	50	14660
	2 - L	10	7103	37	1335	0.52	7145	7030	115	

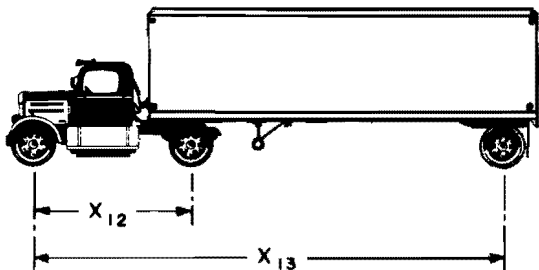
Fig A.5. Summary of static weights (vehicle No. I-3).



Vehicle No.	I-4	X_{12}	
Model	Dodge 1965		
License No.	156 - 395		
Tire Press.	65 - 70		

1	2	3	4	5	6	7	8	9	10	11
Loading Condition	Axle	Number of Weighings	Avg Static Weight lb	Standard Deviation lb	Variance lb ²	Coefficient of Var. %	Maximum Weight lb	Minimum Weight lb	Range lb	Comm. Scale
EMPTY	1 - R	10	2029	9	81	.44	2040	2010	30	4030
	1 - L	10	2068	7	51	.30	2080	2060	20	
	2 - R	10	2907	6	34	.20	2915	2900	15	5760
	2 - L	10	3107	8	62	.25	3120	3095	25	
LOADED	1 - R	10	2164	12	134	.55	2180	2140	40	4300
	1 - L	10	2164	8	60	.36	2175	2150	25	
	2 - R	10	7907	37	1401	.46	7960	7850	110	15550
	2 - L	10	7979	90	8173	1.12	8125	7865	260	

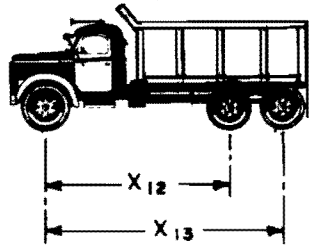
Fig A.6. Summary of static weights (vehicle No. I-4).



Vehicle No.	II-1	X ₁₂	10'8"
Model	FORD 1967	X ₁₃	31'3"
License No.	J - 734		
Tire Press.	70 - 75		

1	2	3	4	5	6	7	8	9	10	11
Loading Condition	Axle	Number of Weighings	Avg Static Weight lb	Standard Deviation lb	Variance lb ²	Coefficient of Var. %	Maximum Weight lb	Minimum Weight lb	Range lb	Comm. Scale
	1 - R	8	2161	22	498	1.01	2200	2130	70	4220
	1 - L	8	2200	44	1971	2.00	2300	2160	140	
	2 - R	8	6013	113	12679	1.87	6110	5850	260	12560
	2 - L	8	6678	91	8279	1.36	6780	6570	210	
	3 - R	8	4560	50	2457	1.09	4630	4500	130	9530
	3 - L	8	5121	69	4727	1.34	5210	5020	190	

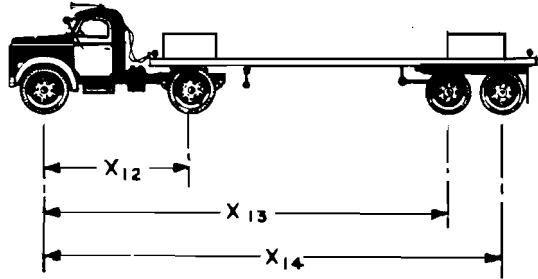
Fig A.7. Summary of static weights (vehicle No. II-1).



Vehicle No.	III-1	X ₁₂	18'10"
Model	GMC - 1962 Chevy	X ₁₃	22'10"
License No.	146 - 493		
Tire Press.	70 - 75		

1	2	3	4	5	6	7	8	9	10	11
Leading Condition	Axle	Number of Weighings	Avg Static Weight lb	Standard Deviation lb	Variance lb ²	Coefficient of Var. %	Maximum Weight lb	Minimum Weight lb	Range lb	Comm. Scale
	1 - R	8	4729	11	127	.23	4750	4720	30	9530
	1 - L	8	4986	12	141	.24	5010	4970	40	
	2 - R	8	6624	39	1541	.58	6690	6550	140	13640
	2 - L	8	6575	103	10543	1.56	6750	6410	340	
	3 - R	8	6516	19	370	.29	6540	6580	60	12880
	3 - L	8	6585	22	486	.33	6610	6540	70	

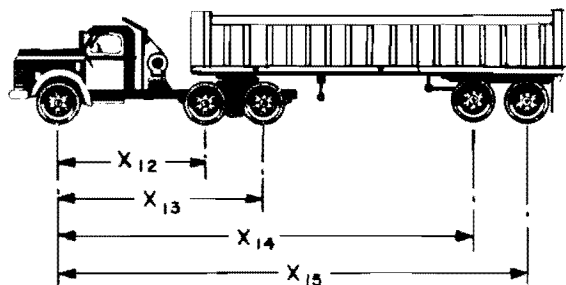
Fig A.8. Summary of static weights (vehicle No. III-1).



Vehicle No.	IV-1	X ₁₂	12'1"
Model	International '67	X ₁₃	41'11"
License No.	J23 - 302	X ₁₄	46'0"
Tire Press.	70 - 75		

1	2	3	4	5	6	7	8	9	10	11
Loading Condition	Axle	Number of Weighings	Avg Static Weight lb	Standard Deviation lb	Variance lb ²	Coefficient of Var. %	Maximum Weight lb	Minimum Weight lb	Range lb	Comm. Scale
	1 - R	10	2906	42	1738	1.44	2970	2850	120	5430
	1 - L	10	2872	65	4262	2.26	3010	2800	210	
	2 - R	10	4855	43	1850	.88	4920	4780	140	9560
	2 - L	10	4751	48	2321	.99	4800	4650	150	
	3 - R	10	2904	31	938	1.07	2940	2840	100	10690
	3 - L	10	2689	23	521	0.86	2730	2650	80	
	4 - R	10	2984	24	582	0.80	3010	2930	80	
	4 - L	10	2888	24	596	0.83	2920	2860	60	

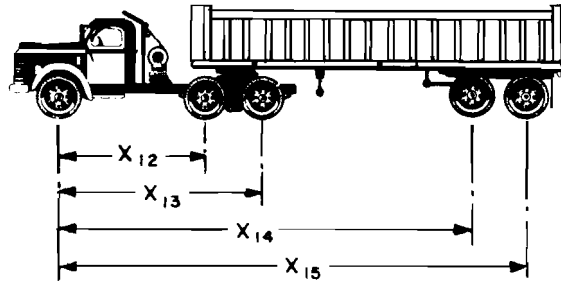
Fig A.9. Summary of static weights (vehicle No. IV-1).



Vehicle No.	V-1	X ₁₂	
Model	MACK	X ₁₃	
License No.	J - 1165	X ₁₄	
Tire Press.	70 - 75	X ₁₅	

1	2	3	4	5	6	7	8	9	10	11
Loading Condition	Axle	Number of Weighings	Avg Static Weight lb	Standard Deviation lb	Variance lb ²	Coefficient of Var. %	Maximum Weight lb	Minimum Weight lb	Range lb	Comm. Scale
	1 - R	8	4335	31	943	0.72	4380	4290	90	8930
	1 - L	8	5129	57	3270	1.11	5200	5030	170	
	2 - R	8	8233	22	479	0.27	8270	8210	60	31780
	2 - L	8	8738	33	1079	0.38	8800	8700	100	
	3 - R	8	6479	55	3041	0.85	6570	6380	190	
	3 - L	8	7320	28	800	0.38	7350	7270	80	
	4 - R	8	7886	116	13513	1.47	8110	7770	340	32960
	4 - L	8	8626	166	27684	1.92	8790	8310	480	
	5 - R	8	7691	99	9841	1.29	7820	7540	280	
	5 - L	8	8998	123	15221	1.37	9160	8820	340	

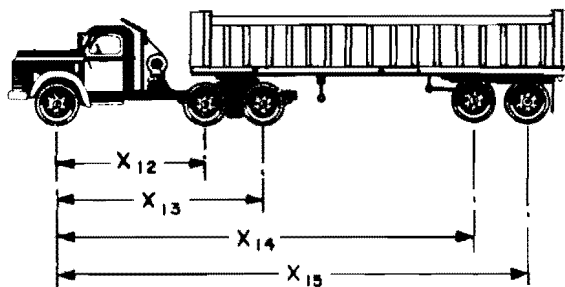
Fig A.10. Summary of static weights (vehicle No. V-1).



Vehicle No.	V-2	X_{12}	10'7"
Model	International	X_{13}	14'10"
License No.	J - 1162	X_{14}	32'7"
Tire Press.	70 - 75	X_{15}	36'10"

1	2	3	4	5	6	7	8	9	10	11
Loading Condition	Axle	Number of Weighings	Avg Static Weight lb	Standard Deviation lb	Variance lb ²	Coefficient of Var. %	Maximum Weight lb	Minimum Weight lb	Range lb	Comm. Scale
	1 - R	1	4180							8360
	1 - L	1	4180							
	2 - R	8	8233	22	479	0.26	8270	8210	60	33690
	2 - L	8	8790	76	5714	0.86	8840	8610	230	
	3 - R	8	6479	55	3041	0.85	6570	6380	190	
	3 - L	8	8691	75	5670	0.86	8820	8590	230	
	4 - R	8	7886	116	13513	1.47	8110	7770	340	34540
	4 - L	8	8626	166	27684	1.92	8790	8310	480	
	5 - R	8	7691	99	9841	1.29	7820	7540	280	
	5 - L	8	8998	123	15221	1.37	9160	8820	340	

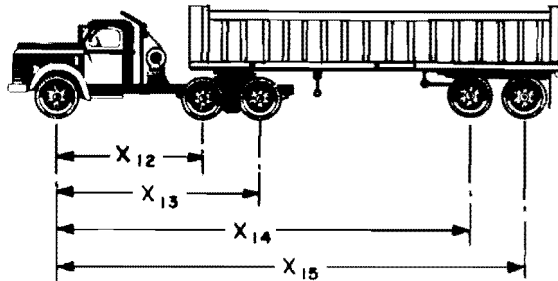
Fig A.11. Summary of static weights (vehicle No. V-2).



Vehicle No.	V-3	X_{12}	12'3"
Model	MACK 1957	X_{13}	16'4"
License No.	J - 1161	X_{14}	34'1"
Tire Press.	70 - 75	X_{15}	38'4"

1	2	3	4	5	6	7	8	9	10	11
Loading Condition	Axle	Number of Weighings	Avg Static Weight lb	Standard Deviation lb	Variance lb ²	Coefficient of Var. %	Maximum Weight lb	Minimum Weight lb	Range lb	Comm. Scale
	1 - R	10	3998	28	796	0.70	4020	3930	90	8270
	1 - L	10	4270	40	1578	0.94	4330	4190	140	
	2 - R	10	5680	47	2178	0.83	5770	5600	170	10530
	2 - L	10	5341	87	7543	1.63	5560	5250	310	
	3 - R	10	4681	38	1477	0.81	4760	4630	130	9210
	3 - L	10	4115	36	1272	0.87	4180	4050	130	
	4 - R	10	5729	77	5943	1.34	5920	5660	260	11450
	4 - L	10	5710	79	6267	1.38	5920	5650	270	
	5 - R	10	5641	69	4699	1.22	5770	5550	220	10930
	5 - L	10	5839	94	8743	1.61	5970	5660	310	

Fig A.12. Summary of static weights (vehicle No. V-3).



Vehicle No.	V-4	X_{12}	9'4"
Model	INTERNATIONAL 1960	X_{13}	13'5"
License No.	J - 1240	X_{14}	31'1"
Tire Press.	70 - 75	X_{15}	35'4"

1	2	3	4	5	6	7	8	9	10	11
Loading Condition	Axle	Number of Weighings	Avg Static Weight lb	Standard Deviation lb	Variance lb ²	Coefficient of Var. %	Maximum Weight lb	Minimum Weight lb	Range lb	Comm. Scale
	1 - R	10	4524	36	1316	0.79	4580	4480	100	8950
	1 - L	10	4378	60	3573	1.37	4490	4310	180	
	2 - R	10	3409	49	2432	1.44	3520	3350	170	21100
	2 - L	10	3446	139	19449	4.03	3540	3070	470	
	3 - R	10	6740	71	4978	1.05	6910	6680	230	
	3 - L	10	6650	95	8933	1.43	6890	6520	370	
	4 - R	10	5461	28	766	0.51	5490	5410	80	21060
	4 - L	10	5192	30	929	0.58	5240	5160	80	
	5 - R	10	5810	11	111	1.89	5830	5800	30	
	5 - L	10	5157	33	1112	0.64	5210	5120	90	

Fig A.13. Summary of static weights (vehicle No. V-4).

This page replaces an intentionally blank page in the original --- CTR Library Digitization Team

APPENDIX B

EXPERIMENT DESIGN

This page replaces an intentionally blank page in the original.

-- CTR Library Digitization Team

APPENDIX B. EXPERIMENT DESIGN

In Chapter 6 the procedure for carrying out the major experiment has been described. This procedure introduced several restrictions on randomization and caused "splits" in the design. Thus, under these conditions, the best suited experiment design is a split-split-split plot. According to this design, the general layout for the major experiment is shown in Fig B.1. In this figure X_1, \dots, X_n represent the random order of individual passes by each test vehicle. The appropriate model for the statistical analysis of the data is:

$$\begin{aligned}
 Y_{ijklm} = & \mu + T_i + a_{(i)j} + S_k + ST_{ik} + b_{(ij)k} + A_l + AT_{il} \\
 & + AS_{lk} + AST_{ikl} + C_{(ijk)l} + V_m + VT_{im} + VS_{km} + VTS_{ikm} \\
 & + VA_{lm} + VAT_{ilm} + VAS_{lkm} + VAST_{iklm} + d_{(ijkl)m}
 \end{aligned}$$

where:

μ = the common effect (mean),

T_i = the effect of the i^{th} level of ROUGHNESS where $i = 1, 2, 3, 4$,

S_k = the effect of the k^{th} level of SCALE POSITION where
 $k = 1, 2, 3, \dots, 6$,

A_l = the effect of the l^{th} axle, where $l = 1, 2, \dots, 17$, and

V_m = the effect of the m^{th} level of SPEED, where $m = 1, 2, 3$.

Error "a", "b", "c", and "d" are the errors at each split.

Accordingly, the analyses of variance table is shown in Table B.1.

		Roughness																									
		1						2						3						4							
		Replicate						Replicate						Replicate						Replicate							
		Axes	(1) Speed		(2) Speed		(3) Speed		(4) Speed		(5) Speed		(6) Speed		(7) Speed		(8) Speed		(9) Speed		(10) Speed		(11) Speed		(12) Speed		
10	30		60	10	30	60	10	30	60	10	30	60	10	30	60	10	30	60	10	30	60	10	30	60			
Classes	I	1	X_1	-	-																						
		2	X_1	-	-																						
	II	3																									
		4																									
		5																									
	III	6																									
		7																									
		8																									
	IV	9																									
		10																									
		11																									
		12																									
	V	13																							-	-	X_n
		14																							-	-	X_n
		15																							-	-	X_n
		16																							-	-	X_n
		17																							-	-	X_n

Fig B.1. Major experiment layout.

TABLE B.1 ANALYSIS OF VARIANCE TABLE

Source of Variation	Degrees of Freedom	Expected Mean Square
T	3	$\sigma^2 + 3\sigma_c^2 + 51\sigma_b^2 + 306\sigma_a^2$ 918 ϕ (T)
Error "a"	8	$\sigma^2 + 3\sigma_c^2 + 51\sigma_b^2 + 306\sigma_a^2$
<hr/>		
S	5	$\sigma^2 + 3\sigma_c^2 + 51\sigma_b^2 + 612 \phi$ (S)
S x T	15	$\sigma^2 + 3\sigma_c^2 + 51\sigma_b^2 + 153 \phi$ (ST)
Error "b"	40	$\sigma^2 + 3\sigma_c^2 + 51\sigma_b^2$
<hr/>		
A	16	$\sigma^2 + 3\sigma_c^2 + 216 \phi$ (A)
A x T	48	$\sigma^2 + 3\sigma_c^2 + 54 \phi$ (AT)
A x S	80	$\sigma^2 + 3\sigma_c^2 + 36 \phi$ (AS)
A x S x T	240	$\sigma^2 + 3\sigma_c^2 + 9 \phi$ (AST)
Error "c"	768	$\sigma^2 + 3\sigma_c^2$
<hr/>		
V	2	$\sigma^2 + 1224 \phi$ (V)
V x T	6	$\sigma^2 + 306 \phi$ (VT)
V x S	10	$\sigma^2 + 204 \phi$ (VS)
V x A	32	$\sigma^2 + 72 \phi$ (VA)
V x T x S	30	$\sigma^2 + 51 \phi$ (VTS)
V x T x A	96	$\sigma^2 + 18 \phi$ (VTA)
V x S x A	160	$\sigma^2 + 12 \phi$ (VSA)
V x S x A x T	480	$\sigma^2 + 3 \phi$ (VSAT)
Error "d"	1632	σ^2

This page replaces an intentionally blank page in the original.

-- CTR Library Digitization Team

APPENDIX C

EXPERIMENTAL RESULTS

This page replaces an intentionally blank page in the original.

-- CTR Library Digitization Team

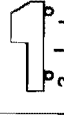
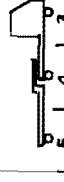
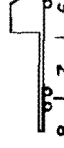
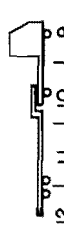
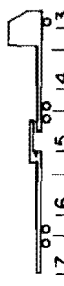
APPENDIX C. EXPERIMENTAL RESULTS

This appendix contains tabular documentation of the experimental data recorded in the field and reduced by visual inspection of the analog records. Samples of observed wheel loads in both the left* and the right** wheel paths are presented in Tables C.1 through C.36. The average of each set of samples, the static load, the difference between the average and the static load expressed in percent of static, the serial number assigned to the corresponding vehicle pass, and the date of field collection are also included in these tables.


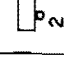


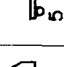

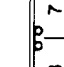
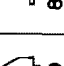
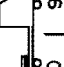

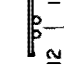

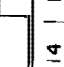
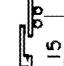
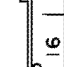
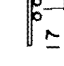
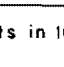
The average dynamic load components of the three observations at each sampling location in the left wheel path at the different combinations of roughness and speed and which have been used in the comparative study in Chapter 7 are summarized in Tables C.37 through C.48.

* Six samples per axle for each run.




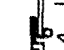
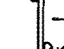
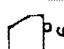
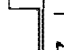
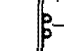
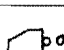
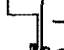

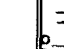
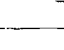
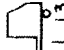
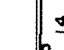
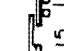
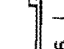
** Three samples per axle for each run.

Table No. C.1		Roughness: <u>1</u> Replicate No: <u>1</u> Speed: <u>10</u> Site: <u>I-35</u>																
Vehicle Class	Experimental Results	Left Wheel Path Scales									Right Wheel Path Scales						Ser'o'l No	Date
		1 (1L)	2 (2L)	3 (4L)	4 (5L)	5 (6L)	6 (7L)	Average	Static	Diff.	1 (1R)	2 (2R)	3 (4R)	Average	Static	Diff.		
I		30	34	35	35	32	31	33	30	9	29	35	33	32	31	4	111	5/20/69
		72	81	74	82	77	65	75	71	6	65	79	76	73	78	- 6		
II		23	21	22	23	20	20	21	22	- 2	21	22	20	21	22	- 5	425	7/1/69
		65	64	65	69	69	68	67	67	0	59	68	66	64	60	7		
		48	55	49	64	51	57	54	51	6	39	59	55	51	46	11		
III		51	50	53	55	50	48	51	50	2	47	48	49	48	47	2	324	5/29/69
		71	70	68	87	70	62	71	66	8	73	71	71	72	66	9		
IV		74	68	80	81	66	66	72	66	10	70	72	71	71	65	9	424	7/1/69
		29	32	29	33	31	28	30	29	5	29	32	28	30	29	2		
		45	48	48	50	43	50	47	48	- 1	42	55	48	48	49	- 1		
		31	23	23	16	28	31	25	27	- 6	29	28	28	28	29	- 2		
V		27	28	18	28	31	35	28	29	- 4	19	20	20	20	30	-34	423	7/1/69
		42	43	45	43	41	43	43	43	0	39	39	33	37	40	- 7		
		55	57	60	54	53	56	56	53	5	57	60	64	60	57	6		
		47	44	56	47	43	45	47	41	12	45	47	45	46	47	- 3		
		57	69	65	68	60	63	64	57	12	58	73	67	66	57	16		
		55	70	77	61	64	68	66	58	14	53	63	53	56	56	0		


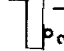


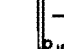
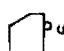

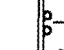
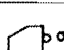

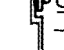
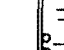


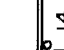
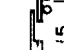
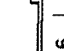
All Weights in 100 Pounds

Table No. C-2		Roughness: <u>1</u>		Replicate No: <u>1</u>		Speed: <u>30</u>		Site: <u>I-35</u>											
Experimental Results		Left Wheel Path Scales									Right Wheel Path Scales						Serial No Date		
		1 (1L)	2 (2L)	3 (4L)	4 (5L)	5 (6L)	6 (7L)	Average	Static	Diff	1 (1R)	2 (2R)	3 (4R)	Average	Static	Diff			
Vehicle Class	I		38	37	30	37	31	32	34	30	14	35	38	38	37	31	19	107	5/20/69
			77	69	86	75	77	81	77	71	9	81	78	82	80	78	3		
	II		26	35	33	31	22	26	29	22	31	21	21	30	24	22	9	417	7/1/69
			70	67	77	71	65	76	71	67	6	71	88	70	76	60	27		
			55	51	50	53	63	67	56	51	11	41	67	51	53	46	15		
	III		52	49	60	53	48	52	52	50	5	49	51	50	50	47	6	322	5/29/69
			70	73	90	74	67	70	74	66	12	72	84	71	76	66	15		
			75	68	76	71	68	68	71	66	8	62	85	57	68	65	5		
	IV		33	25	24	29	31	34	29	29	1	27	35	46	36	29	24	416	7/1/69
			60	51	61	47	63	60	57	48	19	59	64	67	63	49	29		
			34	34	32	31	43	36	35	27	30	27	39	43	36	29	25		
			34	36	36	35	39	42	37	29	28	28	31	24	28	30	- 8		
	V		44	40	49	39	46	47	44	43	3	42	62	25	43	40	7	415	7/1/69
			51	60	69	61	64	60	61	53	15	63	88	61	71	57	24		
			36	45	59	52	48	46	48	41	16	44	72	37	51	47	9		
			47	43	58	68	46	57	53	57	- 7	50	60	60	57	57	- 1		
			70	65	65	39	61	55	59	58	2	62	82	41	62	56	10		

All Weights in 100 Pounds

Table No. C.3		Roughness: <u>1</u> Replicate No: <u>1</u> Speed: <u>60</u> Site: <u>I-35</u>														Serial No	Date		
Experimental Results		Left Wheel Path Scales									Right Wheel Path Scales								
		1 (1L)	2 (2L)	3 (4L)	4 (5L)	5 (6L)	6 (7L)	Average	Static	Diff.	1 (1R)	2 (3R)	3 (4R)	Average	Static			Diff.	
Vehicle Class	I		40	39	34	42	38	32	38	30	25	26	35	41	34	31	10	105	5/20/69
			90	88	82	91	79	71	83	71	18	68	73	87	76	78	-3		
	II		24	21	21	19	29	26	23	22	6	20	27	27	25	22	12	413	7/1/69
			76	83	69	56	76	81	73	67	10	64	76	88	76	60	27		
			69	56	55	44	54	63	57	51	11	51	62	58	57	46	24		
	III		56	51	54	55	55	55	54	50	9	49	52	59	53	47	13	321	5/29/69
			76	75	69	73	76	74	74	66	12	78	75	87	80	66	21		
			75	75	70	66	81	69	73	66	10	70	75	90	78	65	21		
	IV		27	25	26	21	25	27	25	29	-13	4	8	19	10	29	-64	412	7/1/69
			28	34	31	36	38	53	37	48	-24	22	30	31	28	49	-44		
			15	17	12	17	19	29	18	27	-33	12	12	18	14	29	-52		
			12	15	12	21	20	24	17	29	-40	6	7	8	7	30	-77		
	V		50	44	39	50	49	47	46	43	8	40	49	62	50	40	26	411	7/1/69
			66	63	57	65	60	64	63	53	18	62	79	98	80	57	40		
			47	56	40	51	58	46	50	41	21	42	55	102	66	47	41		
			67	80	74	47	74	72	69	57	21	57	50	113	73	57	29		
			59	87	69	60	77	65	69	58	20	42	44	112	66	56	18		




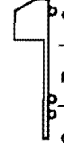


All Weights in 100 Pounds

Table No. C.4		Roughness: <u>1</u>		Replicate No: <u>2</u>		Speed: <u>10</u>		Site: <u>I-35</u>		Serial No	Date						
Experimental Results		Left Wheel Path Scales						Right Wheel Path Scales									
		1 (1L)	2 (2L)	3 (4L)	4 (5L)	5 (6L)	6 (7L)	Average	Static			Diff.	1 (1R)	2 (2R)	3 (4R)	Average	Static
Vehicle Class	I		30	32	36	35	32	33	33	30	10	29	35	35	33	31	6
			65	80	73	91	70	70	74	71	5	64	80	77	74	78	-6
	II		22	24	21	24	20	20	22	22	0	21	23	22	22	22	0
			64	66	63	64	69	70	66	67	-1	55	70	63	63	60	4
			45	55	48	56	48	56	51	51	0	39	61	50	50	46	9
	III		54	45	50	55	50	45	50	50	0	52	50	44	49	47	4
			70	66	72	79	60	70	70	66	5	72	65	77	71	66	8
			70	64	80	73	68	66	70	66	5	68	70	69	69	65	6
	IV		30	30	32	32	31	30	31	29	6	29	30	29	29	29	0
			44	47	53	47	43	52	48	48	0	39	57	47	48	49	-3
			27	19	21	16	27	33	24	27	-12	24	27	24	25	29	-14
			29	28	22	28	31	37	29	29	0	22	28	21	24	30	-21
	V		44	41	45	44	42	43	43	43	0	40	40	37	39	40	-2
			47	55	67	58	51	54	55	53	4	52	60	73	62	57	8
			42	48	47	50	42	46	46	41	12	45	49	42	45	47	-4
			59	59	66	86	47	59	63	57	10	62	65	75	67	57	18
			56	58	61	76	57	56	61	58	5	49	55	56	53	56	-5

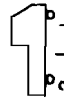
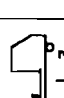

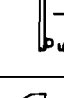


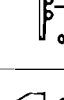
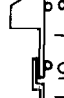
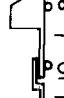
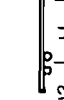
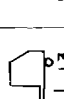
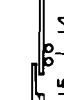
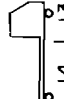
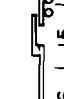
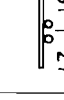
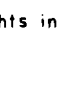

All Weights in 100 Pounds

Table No. C. 5		Roughness: <u>1</u> Replicate No.: <u>2</u> Speed: <u>30</u> Site: <u>I-35</u>															Serial No	Date	
Experimental Results	Vehicle Class	Left Wheel Path Scales									Right Wheel Path Scales								
		1 (1L)	2 (2L)	3 (4L)	4 (5L)	5 (6L)	6 (7L)	Average	Static	Diff.	1 (1R)	2 (3R)	3 (4R)	Average	Static	Diff.			
I		1	36	34	32	35	33	29	33	30	11	32	35	34	34	31	9	109	5/20/69
		2	80	71	78	67	71	79	74	71	5	81	80	87	83	78	6		
II		3	24	32	35	37	28	22	30	22	35	20	24	26	23	22	6	421	7/1/69
		4	69	67	75	64	74	70	70	67	4	70	85	68	74	60	24		
		5	58	47	45	54	60	57	53	51	5	45	72	47	55	46	19		
III		6	59	47	59	55	50	50	53	50	7	51	51	51	51	47	9	323	5/29/69
		7	76	68	90	83	60	68	74	66	12	75	79	78	77	66	17		
		8	59	62	68	70	71	65	66	66	0	61	85	65	70	65	8		
IV		9	35	26	25	30	30	35	30	29	4	29	38	53	40	29	38	420	7/1/69
		10	57	56	59	47	63	60	57	48	19	49	74	70	64	49	31		
		11	38	43	32	30	35	41	36	27	35	28	45	41	38	29	31		
		12	33	42	33	33	33	35	35	29	20	28	33	26	29	30	-3		
V		13	45	36	52	35	45	46	43	43	0	42	53	23	39	40	-2	419	7/1/69
		14	48	55	65	73	68	55	61	53	14	58	87	50	65	57	14		
		15	40	50	55	55	49	52	50	41	22	46	67	37	50	47	6		
		16	50	43	64	63	55	43	53	57	2	52	70	55	59	57	4		
		17	73	63	68	43	63	69	63	58	9	62	82	51	65	56	16		

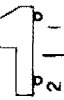
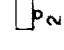
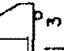

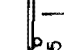
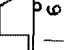
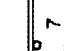
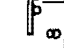
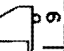
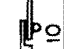
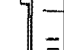
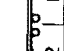
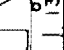
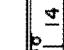
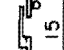
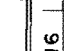
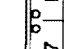
All Weights in 100 Pounds

Experimental Results		Roughness: <u>1</u> Replicate No: <u>2</u> Speed: <u>60</u> Site: <u>I-35</u>															Serial No	Date		
		Left Wheel Path Scales									Right Wheel Path Scales									
		1 (1L)	2 (2L)	3 (4L)	4 (5L)	5 (6L)	6 (7L)	Average	Static	Diff	1 (1R)	2 (3R)	3 (4R)	Average	Static	Diff				
Vehicle Class	I		34	33	35	40	37	35	36	30	19	28	35	41	35	31	12	117	5/20/69	
			80	82	75	81	81	79	80	71	12	75	78	93	82	78	5			
	II		3	31	17	14	33	26	27	25	22	12	19	30	25	25	22	12	437	7/1/69
			4	81	78	69	72	78	83	77	67	15	62	85	97	81	60	36		
			5	67	55	59	52	55	72	60	51	18	49	63	67	60	46	30		
	III		6	62	50	52	57	57	52	55	50	10	47	51	56	51	47	9	327	5/29/69
			7	88	75	70	85	82	73	79	66	19	73	66	94	78	66	18		
			8	78	80	73	67	84	72	75	66	15	63	60	95	73	65	12		
	IV		9	32	23	30	26	31	32	29	29	0	27	36	43	35	29	22	436	7/1/69
			10	65	51	59	51	58	62	58	48	20	52	75	79	69	49	40		
			11	51	46	38	36	45	43	43	27	60	33	44	51	43	29	47		
			12	42	43	37	37	46	35	40	29	38	25	35	36	32	30	7		
	V		13	52	47	37	53	45	50	47	43	10	36	51	66	51	40	27	435	7/1/69
			14	65	61	57	71	65	66	64	53	21	59	75	95	76	57	34		
			15	49	62	45	51	54	61	54	41	31	40	56	97	64	47	37		
			16	70	67	67	50	67	68	65	57	14	62	58	106	75	57	32		
			17	63	79	71	58	66	68	67	58	16	39	51	97	62	56	11		

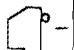
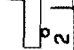
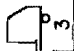
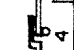

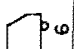

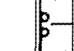
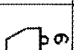
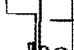
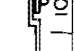
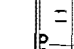

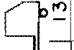
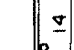
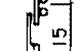
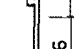
All Weights in 100 Pounds

Table No. C.7		Roughness: <u>1</u>		Replicate No: <u>3</u>		Speed: <u>10</u>		Site: <u>I-35</u>											
Experimental Results	Left Wheel Path Scales									Right Wheel Path Scales						Serial No.	Date		
	1 (1L)	2 (2L)	3 (4L)	4 (5L)	5 (6L)	6 (7L)	Average	Static	Diff.	1 (1R)	2 (3R)	3 (4R)	Average	Static	Diff.				
Vehicle Class	I		30	35	35	36	30	32	33	30	10	27	32	33	31	31	0	115	5/20/69
			70	78	76	89	71	69	75	71	6	68	79	77	75	78	- 4		
	II		22	19	22	24	22	22	22	22	0	22	24	21	22	22	0	433	7/1/69
			62	63	63	70	68	68	66	67	- 2	56	71	63	63	60	6		
			49	51	45	61	49	51	51	51	0	39	59	52	50	46	9		
	III		51	47	52	53	49	47	50	50	0	50	48	46	48	47	2	326	5/29/69
			65	72	70	82	61	64	69	66	5	66	72	71	70	66	6		
			73	66	81	75	65	66	71	66	8	70	70	72	71	65	9		
	IV		30	30	31	31	30	32	31	29	6	29	28	31	29	29	0	432	7/1/69
			45	49	59	55	42	41	48	48	0	42	64	50	52	49	6		
			28	25	28	20	28	33	27	27	0	25	29	27	27	29	- 7		
			27	35	28	24	28	35	30	29	2	22	28	21	24	30	-21		
	V		45	41	44	43	42	45	43	43	0	43	43	41	42	40	6	431	7/1/69
			47	53	65	56	53	56	55	53	4	56	61	72	63	57	11		
			44	51	44	50	46	48	47	41	15	47	50	44	47	47	0		
			59	63	77	77	55	59	65	57	16	58	68	78	68	57	19		
			57	57	61	65	63	59	60	58	4	51	55	53	53	56	- 5		

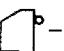

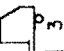
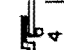
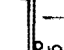
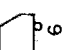
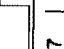
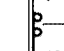
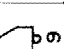
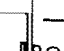
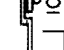
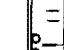


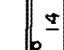
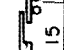
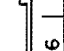
All Weights in 100 Pounds

Experimental Results		Roughness: <u>1</u> Replicate No: <u>3</u> Speed: <u>30</u> Site: <u>I-35</u>															Serial No	Date	
		Left Wheel Path Scales									Right Wheel Path Scales								
		1 (1L)	2 (2L)	3 (4L)	4 (5L)	5 (6L)	6 (7L)	Average	Static	Diff.	1 (1R)	2 (3R)	3 (4R)	Average	Static	Diff.			
Vehicle Class	I		36	36	37	40	32	34	36	30	19	33	39	37	36	31	17	119	5/20/69
			77	70	80	73	76	78	76	71	7	81	77	83	80	78	3		
	II		24	38	32	28	25	26	29	22	31	23	23	30	25	22	15	441	7/1/69
			67	79	72	65	73	67	70	67	5	64	91	77	77	60	29		
			56	42	54	46	53	60	52	51	2	55	75	59	63	46	37		
	III		52	49	59	53	48	51	52	50	4	50	51	49	50	47	6	328	5/29/69
			71	75	87	87	68	66	76	66	15	72	82	74	76	66	15		
			56	67	68	73	68	72	67	66	2	61	81	64	69	65	6		
	IV		33	28	30	28	32	31	30	29	5	29	32	40	34	29	16	440	7/1/69
			58	44	57	51	46	63	53	48	11	45	80	58	61	49	24		
			42	27	35	32	31	43	35	27	30	33	42	42	39	29	34		
			34	32	36	37	39	32	35	29	21	26	41	32	33	30	10		
	V		43	35	54	40	43	45	43	43	0	42	53	24	40	40	0	439	7/1/69
			57	51	70	70	60	58	61	53	15	62	79	60	67	57	18		
			50	46	54	57	44	44	49	41	20	46	77	50	58	47	23		
			61	44	50	56	64	62	56	57	- 1	57	53	59	56	57	- 1		
			82	58	78	50	76	69	69	58	19	73	88	46	69	56	23		

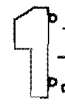

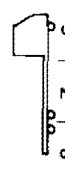
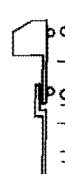

All Weights in 100 Pounds

Table No. C.9		Roughness: <u>1</u> Replicate No.: <u>3</u> Speed: <u>60</u> Site: <u>I-35</u>															Serial No	Date	
Experimental Results		Left Wheel Path Scales									Right Wheel Path Scales								
		1 (1L)	2 (2L)	3 (4L)	4 (5L)	5 (6L)	6 (7L)	Average	Static	Diff	1 (1R)	2 (2R)	3 (4R)	Average	Static	Diff			
Vehicle Class	I		38	36	31	41	38	30	36	30	19	27	34	41	34	31	10	121	5/20/69
			85	86	75	83	82	72	80	71	13	75	71	87	78	78	0		
	II		31	19	20	28	27	31	26	22	18	24	32	29	28	22	29	445	7/1/69
			78	76	69	73	80	86	77	67	15	65	81	99	82	60	36		
			71	56	61	56	59	79	64	51	25	50	64	65	60	46	30		
	III		60	45	50	54	53	51	52	50	4	49	50	58	52	47	11	329	5/29/69
			86	67	65	79	79	66	74	66	12	77	70	88	78	66	19		
			81	70	70	65	81	65	72	66	9	65	75	92	77	65	19		
	IV		32	21	30	28	30	34	29	29	0	30	35	39	35	29	20	444	7/1/69
			75	38	61	58	62	74	61	48	28	49	79	73	67	49	37		
			53	41	36	48	50	53	47	27	73	33	46	50	43	29	48		
			48	35	36	55	53	44	45	29	56	26	42	46	38	30	27		
	V		53	51	37	54	47	50	49	43	13	36	52	66	51	40	28	443	7/1/69
			70	63	56	61	68	73	65	53	23	66	82	108	85	57	50		
			50	63	44	47	55	65	54	41	32	42	61	115	73	47	55		
			72	66	72	42	53	77	64	57	12	63	67	121	84	57	47		
			66	95	63	48	76	68	69	58	20	43	50	117	70	56	25		

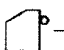
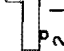
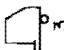
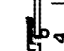
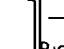
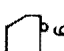
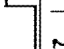
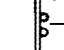
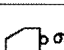
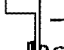

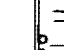

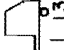
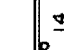
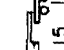
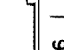
All Weights in 100 Pounds

Table No. C.10		Roughness: <u>2</u> Replicate No: <u>1</u> Speed: <u>10</u> Site: <u>I-35</u>															Serial No	Date	
Experimental Results		Left Wheel Path Scales									Right Wheel Path Scales								
		1 (1L)	2 (2L)	3 (4L)	4 (5L)	5 (6L)	6 (7L)	Average	Static	Diff	1 (1R)	2 (2R)	3 (4R)	Average	Static	Diff			
Vehicle Class	I		34	30	38	36	33	24	32	30	8	37	30	35	34	31	10	129	5/20/69
			67	77	73	90	74	86	78	71	10	67	77	79	74	78	- 5		
	II		22	23	23	24	19	21	22	22	0	24	23	22	23	22	5	461	7/1/69
			63	67	69	77	67	69	69	67	2	62	73	65	67	60	11		
			52	58	53	65	51	58	56	51	10	43	60	57	53	46	16		
	III		56	48	50	57	50	48	52	50	3	52	49	46	49	47	4	339	5/29/69
			84	63	71	83	68	64	72	66	9	86	74	75	78	66	19		
			62	69	75	74	65	65	68	66	4	60	80	70	70	65	8		
	IV		26	32	31	32	29	30	30	29	3	28	26	29	28	29	- 5	460	7/1/69
			45	52	58	53	58	56	54	48	12	39	55	60	51	49	5		
			24	31	43	37	25	32	32	27	19	25	44	45	38	29	31		
			42	47	43	41	38	34	41	29	41	30	37	31	33	30	9		
	V		42	42	45	44	41	44	43	43	0	40	40	33	38	40	- 6	459	7/1/69
			51	56	70	64	51	53	57	53	8	58	47	82	62	57	9		
			47	46	52	56	50	45	49	41	20	44	50	40	45	47	- 5		
			58	72	77	81	57	61	68	57	19	49	70	80	66	57	16		
			58	55	72	69	52	62	61	58	6	45	55	62	54	56	- 4		

All Weights in 100 Pounds

Table No. C. 11		Roughness: <u>2</u> Replicate No: <u>1</u> Speed: <u>30</u> Site: <u>I-35</u>														Serial No.	Date		
Experimental Results		Left Wheel Path Scales									Right Wheel Path Scales								
		1 (1L)	2 (2L)	3 (4L)	4 (5L)	5 (6L)	6 (7L)	Average	Static	Diff	1 (1R)	2 (2R)	3 (4R)	Average	Static			Diff	
Vehicle Class	I 	1	30	39	34	40	36	32	35	30	17	35	39	33	36	31	15	125	5/20/69
		2	76	76	79	81	77	75	77	71	9	88	76	81	82	78	5		
	II 	3	8	34	39	35	25	20	27	22	22	18	25	23	22	22	0	453	7/1/69
		4	74	63	77	63	59	67	67	67	0	74	79	67	73	60	22		
		5	56	55	57	48	61	67	57	51	12	41	65	57	54	46	18		
	III 	6	68	48	57	53	50	50	54	50	8	53	53	49	52	47	11	333	5/29/69
		7	125	102	114	98	69	58	94	66	42	107	91	90	96	66	45		
		8	47	38	79	85	57	70	63	66	- 5	40	75	93	70	65	8		
		9	40	29	25	31	30	34	32	29	9	33	30	45	36	29	24		
	IV 	10	53	49	64	51	58	57	55	48	15	48	70	69	62	49	27	452	7/1/69
		11	18	46	27	35	28	39	32	27	19	11	38	47	32	29	10		
		12	44	30	39	30	34	33	35	29	21	41	33	31	35	30	17		
		13	47	38	53	50	44	45	46	43	7	42	58	23	41	40	2		
	V 	14	76	71	75	63	57	57	67	53	25	81	112	61	85	57	49	451	7/1/69
		15	25	48	55	63	43	40	46	41	11	25	70	30	42	47	-11		
		16	83	81	60	22	82	62	65	57	14	90	90	43	74	57	30		
		17	56	55	105	82	65	52	69	58	19	59	108	59	75	56	35		


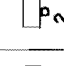


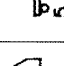
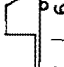
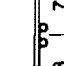
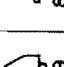
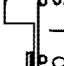

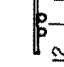
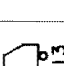
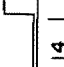
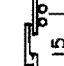
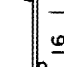
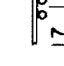
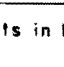
All Weights in 100 Pounds

Table No. C . 12		Roughness: <u>2</u> Replicate Na: <u>1</u> Speed: <u>60</u> Site: <u>I-35</u>															Serial No	Date	
Experimental Results		Left Wheel Path Scales									Right Wheel Path Scales								
		1 (1L)	2 (2L)	3 (4L)	4 (5L)	5 (6L)	6 (7L)	Average	Static	Diff.	1 (1R)	2 (2R)	3 (3R)	Average	Static	Diff.			
Vehicle Class	I		58	23	30	39	39	30	37	30	22	44	36	35	38	31	24	123	5/20/69
			70	96	80	84	80	71	80	71	13	54	81	99	78	78	0		
	II		51	5	20	12	32	31	25	22	14	37	47	15	33	22	50	449	7/1/69
			66	80	73	82	93	80	79	67	18	52	84	101	79	60	32		
			68	56	61	54	61	72	62	51	22	54	63	71	63	46	36		
	III		57	53	52	57	59	52	55	50	10	45	58	60	54	47	16	330	5/29/69
			127	25	24	147	40	100	77	66	17	139	138	65	114	66	73		
			133	28	24	134	44	87	75	66	14	120	141	60	107	65	65		
	IV		31	29	34	25	31	31	30	29	4	36	54	29	40	29	37	448	7/1/69
			88	51	61	52	62	79	66	48	36	68	79	77	75	49	52		
			20	72	18	29	37	45	37	27	36	17	62	50	43	29	48		
			75	58	22	36	54	38	47	29	63	40	30	10	27	30	-11		
	V		43	45	33	60	41	50	45	43	5	40	55	67	54	40	35	447	7/1/69
			113	31	38	100	84	54	70	53	32	99	103	84	95	57	67		
			97	10	10	80	54	57	51	41	25	81	72	69	74	47	57		
			115	0	0	132	57	30	56	57	- 2	107	143	19	90	57	57		
			140	0	5	130	78	54	68	58	17	120	175	0	98	56	76		


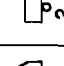

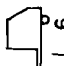
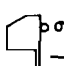

All Weights in 100 Pounds

Table No. C . 13		Roughness: <u>2</u>		Replicate No: <u>2</u>		Speed: <u>10</u>		Site: <u>I-35</u>											
Experimental Results		Left Wheel Path Scales									Right Wheel Path Scales						Serial No. Date		
		1 (1L)	2 (2L)	3 (4L)	4 (5L)	5 (6L)	6 (7L)	Average	Static	Diff.	1 (1R)	2 (3R)	3 (4R)	Average	Static	Diff.			
Vehicle Class	I		34	30	40	36	32	34	34	30	14	37	28	35	33	31	8	131	5/20/69
			60	77	76	88	74	73	75	71	5	66	80	79	75	78	- 4		
	II		20	22	22	22	19	20	21	22	- 5	22	20	21	21	22	- 5	465	7/1/69
			63	68	70	83	71	67	70	67	5	61	69	67	66	60	9		
			50	54	59	67	50	55	56	51	9	42	62	64	56	46	22		
	III		53	47	52	57	48	47	51	50	1	55	48	47	50	47	6	342	5/29/69
			88	71	70	86	65	64	74	66	12	93	70	75	79	66	20		
			70	73	78	72	66	64	71	66	7	67	79	74	73	65	13		
	IV		29	27	30	32	32	34	31	29	6	30	32	28	30	29	3	464	7/1/69
			41	52	59	48	45	44	48	48	0	33	67	49	50	49	1		
			36	28	25	19	30	33	28	27	6	33	34	26	31	29	7		
			29	29	25	23	29	34	28	29	-3	22	27	22	24	30	-21		
	V		41	42	46	46	43	44	44	43	2	40	40	39	40	40	0	463	7/1/69
			49	54	71	68	53	58	59	53	11	55	60	85	67	57	17		
			41	46	50	58	46	45	48	47	1	47	59	45	50	47	7		
			52	62	73	84	55	56	64	57	12	54	70	80	68	57	19		
			64	58	66	78	62	61	65	58	12	60	57	59	59	56	5		


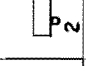
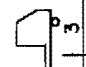

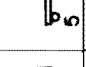

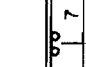
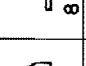
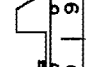

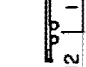
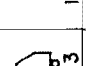
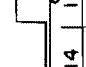
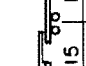
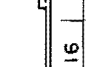
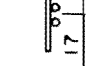
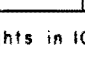
All Weights in 100 Pounds

Table No. C. 14		Roughness: <u>2</u>		Replicate No.: <u>2</u>		Speed: <u>30</u>		Site: <u>I-35</u>		Serial No	Date								
Experimental Results		Left Wheel Path Scales						Right Wheel Path Scales											
		1 (1L)	2 (2L)	3 (4L)	4 (5L)	5 (6L)	6 (7L)	Average	Static			Diff	1 (1R)	2 (2R)	3 (4R)	Average	Static	Diff	
Vehicle Class	I		26	36	29	40	36	34	34	30	12	34	36	34	35	31	12	127	5/20/69
			77	70	79	78	73	75	75	71	6	89	77	77	81	78	4		
	II		19	25	25	32	26	23	25	22	14	25	25	30	27	22	21	457	7/1/69
			82	69	78	70	64	72	73	67	8	74	83	74	77	60	28		
			60	54	58	50	64	70	59	51	16	42	65	60	56	46	21		
	III		67	47	54	53	49	49	53	50	6	53	52	50	52	47	11	336	5/29/69
			127	107	107	90	77	57	94	66	42	111	88	80	93	66	41		
			44	41	83	86	54	71	63	66	- 5	40	79	95	71	65	9		
	IV		38	27	31	28	32	33	31	29	9	33	33	39	35	29	21	456	7/1/69
			55	57	49	58	74	64	60	48	24	43	88	64	65	49	33		
			25	47	44	34	40	45	39	27	45	30	41	49	40	29	38		
			47	29	29	37	33	33	35	29	20	34	43	26	34	30	14		
	V		43	41	54	37	45	45	44	43	3	42	59	33	45	40	12	455	7/1/69
			64	66	68	55	63	59	63	53	18	68	97	107	91	57	59		
			40	76	63	52	55	52	56	41	37	50	40	50	47	47	0		
			84	50	50	79	61	64	65	57	13	91	46	88	75	57	32		
			91	97	49	46	52	52	65	58	11	85	59	50	65	56	15		


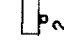

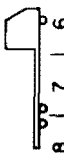
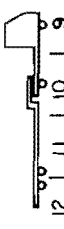

All Weights in 100 Pounds

Table No. C. 15		Roughness: <u>2</u> Replicate No: <u>2</u> Speed: <u>60</u> Site: <u>I-35</u>															Serial No.	Date	
Experimental Results		Left Wheel Path Scales									Right Wheel Path Scales								
		1 (1L)	2 (2L)	3 (4L)	4 (5L)	5 (6L)	6 (7L)	Average	Static	Diff.	1 (1R)	2 (2R)	3 (4R)	Average	Static	Diff.			
Vehicle Class	I		52	25	32	36	35	31	35	30	17	41	38	37	39	31	25	135	5/20/69
			68	98	73	79	80	71	78	71	10	58	83	102	81	78	4		
	II		56	6	18	26	27	37	28	22	29	33	41	21	32	22	44	473	7/1/69
			73	82	72	83	90	85	81	67	21	61	87	108	85	60	42		
			73	56	59	59	59	75	64	51	25	60	65	71	65	46	42		
	III		57	51	51	56	59	53	54	50	8	45	59	60	55	47	17	348	5/29/69
			127	28	31	145	48	102	80	66	21	138	139	64	57	66	-14		
			131	35	25	131	47	92	77	66	17	122	140	64	110	65	69		
	IV		35	33	33	31	34	38	34	29	17	25	46	44	38	29	32	472	7/1/69
			99	62	61	50	72	65	68	48	42	68	91	84	81	49	65		
			35	67	9	44	52	46	42	27	56	35	45	51	44	29	51		
			91	43	27	61	56	47	54	29	87	53	28	24	35	30	17		
	V		42	48	35	60	52	54	49	43	14	35	56	68	53	40	18	471	7/1/69
			102	44	50	88	95	68	75	53	42	98	98	105	100	57	75		
			62	39	12	86	62	65	54	41	32	81	75	95	84	47	79		
			132	0	0	140	40	47	60	57	5	100	122	47	90	57	59		
158			0	0	128	37	44	61	58	5	117	112	78	102	56	82			

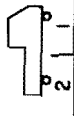


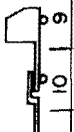
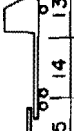
All Weights in 100 Pounds

Table No. C. 16		Roughness: <u>2</u>		Replicate No: <u>3</u>		Speed: <u>10</u>		Site: <u>I-35</u>												
Experimental Results		Left Wheel Path Scales									Right Wheel Path Scales						Serial No		Date	
		1 (1L)	2 (2L)	3 (4L)	4 (5L)	5 (6L)	6 (7L)	Average	Static	Diff	1 (1R)	2 (2R)	3 (4R)	Average	Static	Diff				
Vehicle Class	I		30	34	33	35	29	30	32	30	6	28	27	31	29	31	-8	133	5/20/69	
			65	77	77	90	72	70	75	71	6	66	82	77	75	78	-4			
	II		24	21	23	21	20	20	21	22	-2	23	22	21	22	22	0	469	7/1/69	
			67	64	68	78	72	70	70	67	4	66	68	67	67	60	12			
			57	57	53	65	53	56	57	51	11	50	63	59	57	46	25			
	III		50	46	54	52	48	44	49	50	-2	46	50	46	47	47	0	345	5/29/69	
			69	65	71	45	62	66	63	66	-5	71	74	78	74	66	13			
			67	68	78	74	68	61	69	66	5	69	75	72	72	65	11			
	IV		30	27	30	32	31	33	31	29	5	30	33	30	31	29	7	468	7/1/69	
			41	52	60	50	45	50	50	48	3	38	64	52	51	49	5			
			40	28	29	24	33	35	31	27	17	35	37	30	34	29	17			
	V		28	32	30	27	33	35	31	29	6	23	31	25	26	30	-12	467	7/1/69	
			41	42	47	41	41	45	43	43	0	40	40	41	40	40	0			
			49	55	75	65	57	60	60	53	14	58	64	87	70	57	22			
			42	47	48	57	42	49	47	41	16	46	49	51	49	47	4			
			54	63	75	84	53	59	65	57	13	60	64	78	67	57	18			
				62	62	65	71	61	61	64	58	10	59	60	61	60	56	7		

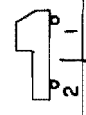
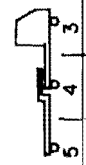
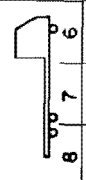
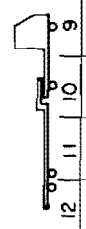
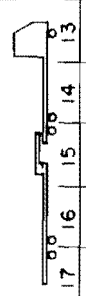
All Weights in 100 Pounds

Table No. C.17		Roughness: <u>2</u> Replicate No: <u>3</u> Speed: <u>30</u> Site: <u>I-35</u>															Serial No	Date		
Experimental Results		Left Wheel Path Scales									Right Wheel Path Scales									
		1 (1L)	2 (2L)	3 (4L)	4 (5L)	5 (6L)	6 (7L)	Average	Static	Diff	1 (1R)	2 (2R)	3 (4R)	Average	Static	Diff				
Vehicle Class	I		43	36	41	46	31	34	39	30	28	38	40	34	37	31	20	137	5/20/69	
			81	62	80	76	78	80	76	71	7	91	75	88	85	78	9			
	II		3	29	28	28	32	27	23	28	22	27	27	27	32	29	22	30	477	7/1/69
			4	76	70	78	66	70	72	72	67	7	74	86	74	78	60	30		
			5	56	47	47	54	64	58	54	51	7	51	73	51	58	46	27		
	III		6	66	49	55	54	48	49	53	50	6	50	52	50	51	47	9	351	5/29/69
			7	133	106	101	90	76	59	94	66	42	117	86	81	95	66	44		
			8	38	36	88	88	50	68	60	66	9	39	82	98	73	65	12		
	IV		9	38	28	32	33	32	35	33	29	14	33	36	47	39	29	33	476	7/1/69
			10	54	57	50	55	74	66	59	48	24	49	82	61	64	49	31		
			11	28	44	40	28	42	37	36	27	35	22	50	48	40	29	38		
			12	50	28	32	36	34	35	36	29	24	40	47	36	41	30	37		
	V		13	52	44	55	56	49	47	50	43	17	45	59	44	49	40	23	475	7/1/69
			14	62	61	72	62	53	57	61	53	15	73	90	72	78	57	37		
			15	44	76	45	73	57	46	57	41	39	49	86	70	68	47	45		
			16	65	65	82	62	68	64	68	57	19	73	95	63	77	57	35		
			17	48	65	85	69	65	70	67	58	16	44	98	45	62	56	11		

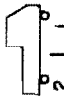

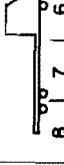

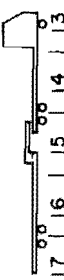
All Weights in 100 Pounds

Experimental Results		Roughness: <u>2</u> Replicate No.: <u>3</u> Speed: <u>60</u> Site: <u>I-35</u>															Serial No	Date	
		Left Wheel Path Scales									Right Wheel Path Scales								
		1 (1L)	2 (2L)	3 (4L)	4 (5L)	5 (6L)	6 (7L)	Average	Static	Diff	1 (1R)	2 (2R)	3 (4R)	Average	Static	Diff			
Vehicle Class	I		58	21	28	42	40	29	36	30	21	42	35	38	38	31	24	139	5/20/69
		83	104	80	83	80	72	84	71	18	59	76	97	77	78	-1			
	II		57	6	21	10	35	33	27	22	23	42	46	19	36	22	62	481	7/1/69
		74	85	77	83	94	89	84	67	25	59	87	107	84	60	41			
		76	62	62	62	60	76	66	51	30	57	65	69	64	46	38			
	III		58	49	50	55	58	54	54	50	8	46	60	61	56	47	18	354	5/29/69
		128	30	37	143	56	104	83	66	26	136	140	63	113	66	71			
		130	41	26	128	51	96	79	66	19	124	139	69	111	65	70			
	IV		31	31	35	27	31	38	32	29	11	45	55	36	45	29	56	480	7/1/69
		87	50	60	53	64	92	68	48	41	66	97	83	82	49	67			
		7	80	24	12	33	56	35	27	31	35	75	59	56	29	94			
		43	74	31	12	42	39	40	29	39	63	32	11	35	30	18			
	V		42	52	38	59	54	59	51	43	20	34	55	64	51	40	28	479	7/1/69
		108	35	50	87	97	81	76	53	43	97	99	97	98	57	72			
		62	45	15	90	78	73	61	41	49	84	74	104	87	47	85			
		140	0	0	135	31	46	59	57	4	115	149	40	101	57	77			
		160	0	0	128	39	47	62	58	7	130	165	66	120	56	114			


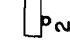
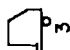

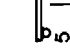

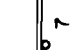
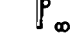
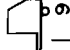
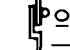
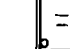
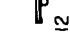
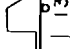
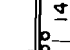
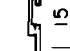
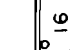
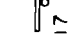
All Weights in 100 Pounds

Table No. C. 19		Roughness: <u>3</u> Replicate No.: <u>1</u> Speed: <u>10</u> Site: <u>I-35</u>															Serial No.	Date	
Experimental Results	Vehicle Class	Left Wheel Path Scales									Right Wheel Path Scales								
		1 (1L)	2 (2L)	3 (4L)	4 (5L)	5 (6L)	6 (7L)	Average	Static	Diff.	1 (1R)	2 (2R)	3 (4R)	Average	Static	Diff.			
I		1	38	28	34	28	30	31	31	30	5	35	33	36	35	31	12	147	5/20/69
		2	87	70	78	86	73	68	77	71	8	90	77	78	81	78	5		
II		3	25	21	24	22	22	21	22	22	0	24	25	24	24	22	11	497	7/1/69
		4	54	71	66	70	68	68	66	67	-1	55	71	66	64	60	7		
		5	62	63	52	67	52	57	59	51	15	59	63	57	60	46	30		
III		6	54	40	54	49	49	45	48	50	-3	46	49	49	48	47	2	366	5/29/69
		7	64	81	62	88	61	64	70	66	6	57	73	67	66	66	0		
		8	89	65	86	71	62	65	73	66	11	71	64	78	71	65	9		
IV		9	34	22	32	29	32	28	30	29	2	31	31	31	31	29	7	496	7/1/69
		10	38	54	57	58	54	52	52	48	9	38	60	56	51	49	5		
		11	47	29	36	36	26	30	34	27	26	53	40	46	46	29	60		
		12	38	35	43	43	30	28	36	29	25	36	31	39	35	30	18		
V		13	46	41	43	44	42	45	43	43	0	45	43	39	42	40	6	495	7/1/69
		14	63	55	68	53	53	58	58	53	10	70	61	79	70	57	23		
		15	52	55	37	58	42	49	49	41	19	53	64	48	55	47	17		
		16	74	66	71	83	55	57	68	57	19	82	67	73	74	57	30		
		17	68	62	64	78	64	59	66	58	14	54	61	61	59	56	5		

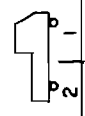
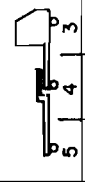


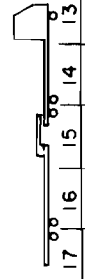
All Weights in 100 Pounds

Table No. C. 20		Roughness: <u>3</u>		Replicate No: <u>1</u>		Speed: <u>30</u>		Site: <u>I-35</u>												
Experimental Results		Left Wheel Path Scales									Right Wheel Path Scales						Serial No		Date	
		1 (1L)	2 (2L)	3 (4L)	4 (5L)	5 (6L)	6 (7L)	Average	Static	Diff.	1 (1R)	2 (2R)	3 (4R)	Average	Static	Diff.				
Vehicle Class	I 	1	15	28	44	40	33	34	32	30	8	33	41	36	37	31	18	143	5/20/69	
		2	69	66	85	72	79	79	75	71	6	77	87	80	81	78	4			
	II 	3	41	35	28	27	26	23	30	22	36	40	27	29	32	22	45	489	7/1/69	
		4	83	89	71	62	79	72	76	67	13	76	100	73	83	60	38			
		5	64	48	54	51	59	55	55	51	8	62	69	56	62	46	36			
	III 	6	50	48	58	55	48	50	51	50	3	46	60	52	53	47	12	360	5/29/69	
		7	41	85	97	97	59	75	76	66	15	29	115	90	78	66	18			
		8	82	73	40	57	75	60	64	66	-2	92	77	42	70	65	8			
	IV 	9	18	33	29	24	30	35	28	29	-3	39	45	50	45	29	54	488	7/1/69	
		10	69	76	48	56	66	51	61	48	27	69	73	63	68	49	39			
		11	31	47	40	32	35	39	37	27	38	23	22	58	34	29	18			
		12	80	32	31	28	37	29	39	29	36	54	50	39	48	30	59			
	V 	13	46	47	47	35	46	45	44	43	3	45	60	25	43	40	8	487	7/1/69	
		14	69	94	75	66	67	61	72	53	36	68	97	71	79	57	38			
		15	39	44	75	57	53	48	53	41	28	41	83	49	58	47	23			
		16	84	115	70	39	38	72	70	57	22	100	123	59	94	57	65			
		17	48	62	133	68	61	70	74	58	27	37	115	99	84	56	49			

All Weights in 100 Pounds

Table No. C. 21		Roughness: <u>3</u> Replicate No: <u>1</u> Speed: <u>60</u> Site: <u>I-35</u>															Serial No	Date	
Experimental Results		Left Wheel Path Scales									Right Wheel Path Scales								
		1 (1L)	2 (2L)	3 (4L)	4 (5L)	5 (6L)	6 (7L)	Average	Static	Diff.	1 (1R)	2 (2R)	3 (4R)	Average	Static	Diff.			
Vehicle Class	I		62	5	10	58	46	33	36	30	19	63	48	31	47	31	53	141	5/20/69
			118	66	84	83	77	76	84	71	18	98	63	100	87	78	12		
	II		52	79	68	36	25	36	49	22	124	39	54	14	36	22	62	485	7/1/69
			66	54	59	72	70	81	67	67	0	55	72	99	75	60	26		
			48	0	0	46	53	70	36	51	-29	42	72	75	63	46	37		
	III		73	42	52	64	49	49	55	50	10	58	51	58	56	47	18	357	5/29/69
			152	10	46	93	94	34	71	66	8	155	95	58	103	66	56		
			148	11	78	102	98	33	78	66	19	133	89	99	107	65	65		
	IV		38	18	40	22	30	36	31	29	6	50	61	22	44	29	53	484	7/1/69
			103	7	31	93	67	63	61	48	26	80	112	71	88	49	79		
			83	70	71	45	65	45	63	27	134	30	53	52	45	29	55		
			0	0	52	47	44	55	33	29	14	16	62	76	51	30	71		
	V		22	50	39	54	59	51	46	43	7	12	67	70	50	40	24	483	7/1/69
			83	50	18	95	67	72	64	53	21	68	102	51	74	57	30		
			126	51	78	133	61	50	83	41	102	81	91	111	94	47	100		
			29	0	140	37	33	79	53	57	-7	30	69	52	50	57	-12		
			15	0	0	27	75	55	29	58	-50	7	52	133	64	56	14		

All Weights in 100 Pounds

Table No. C. 22		Roughness: <u>3</u> Replicate No: <u>2</u> Speed: <u>10</u> Site: <u>I-35</u>															Serial No	Date	
Experimental Results		Left Wheel Path Scales									Right Wheel Path Scales								
		1 (1L)	2 (2L)	3 (4L)	4 (5L)	5 (6L)	6 (7L)	Average	Static	Diff.	1 (1R)	2 (3R)	3 (4R)	Average	Static	Diff.			
Vehicle Class	I		30	29	36	31	32	32	32	30	6	35	33	37	35	31	13	149	5/20/69
			87	63	79	87	72	70	76	71	8	94	80	78	84	78	8		
	II		27	21	25	21	21	19	22	22	0	27	24	26	26	22	17	501	7/1/69
			60	63	62	63	66	66	63	67	-5	57	69	66	64	60	7		
			65	57	56	64	48	54	57	51	12	61	61	60	61	46	32		
	III		55	47	50	50	48	47	49	50	-2	47	49	45	47	47	0	369	5/29/69
			64	78	63	87	60	65	70	66	5	59	69	68	65	66	-1		
			85	65	86	72	69	65	74	66	12	68	65	80	71	65	6		
	IV		27	30	27	33	30	30	29	29	0	27	40	29	32	29	10	500	7/1/69
			57	48	45	48	50	48	49	48	3	60	58	47	55	49	12		
			10	17	20	16	25	30	20	27	-27	22	38	32	31	29	6		
			27	31	20	28	29	32	28	29	-4	28	25	26	26	30	-12		
	V		48	40	43	44	42	45	44	43	2	45	46	39	43	40	8	499	7/1/69
			63	55	68	52	55	58	58	53	10	72	65	77	71	57	25		
			52	55	39	56	47	49	50	41	21	53	59	41	51	47	9		
			77	73	70	82	53	56	69	57	20	87	68	71	75	57	32		
			71	68	67	78	64	63	68	58	18	60	60	62	61	56	8		

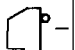
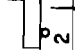
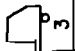
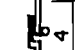
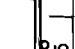
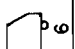
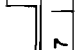
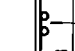
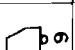
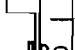
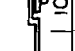
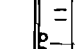
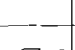
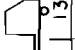
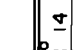
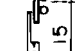
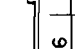
All Weights in 100 Pounds

Table No. C . 23		Roughness: 3		Replicate No.: 2		Speed: 30		Site: I-35											
Vehicle Class	Experimental Results	Left Wheel Path Scales									Right Wheel Path Scales						Serial No	Date	
		1 (1L)	2 (2L)	3 (4L)	4 (5L)	5 (6L)	6 (7L)	Average	Static	Diff	1 (1R)	2 (2R)	3 (4R)	Average	Static	Diff			
I		24	33	41	40	34	33	34	30	14	37	47	40	41	31	33	145	5/20/69	
		75	64	75	73	77	80	74	71	4	73	86	85	81	78	4			
	II		44	38	30	30	27	25	32	22	47	40	31	32	34	22	56	493	7/1/69
			82	79	69	67	78	78	75	67	13	73	103	68	81	60	36		
			64	52	51	56	64	69	59	51	16	62	75	56	64	46	40		
	III		48	48	57	56	50	50	51	50	3	38	57	51	49	47	4	363	5/29/69
			37	93	107	98	61	70	78	66	18	22	130	100	84	66	27		
			75	63	28	69	77	67	63	66	-4	78	62	43	61	65	-6		
	IV		19	33	30	23	31	34	28	29	-2	41	41	46	43	29	47	492	7/1/69
			57	77	48	53	65	54	59	48	23	57	73	67	66	49	34		
			28	47	33	34	40	37	36	27	35	22	22	56	33	29	15		
			85	29	38	26	32	34	41	29	40	57	43	41	47	30	57		
	V		37	42	54	49	49	48	46	43	8	41	62	31	45	40	12	491	7/1/69
			84	72	81	90	64	60	75	53	42	90	105	76	90	57	58		
			41	42	43	58	45	51	47	41	14	36	64	49	50	47	6		
			31	57	96	78	55	56	62	57	9	36	87	84	69	57	21		
			114	65	60	44	66	69	70	58	20	94	86	40	73	56	31		

All Weights in 100 Pounds

Table No. C. 24		Roughness: <u>3</u>		Replicate No: <u>2</u>		Speed: <u>60</u>		Site: <u>I-35</u>										
Vehicle Class	Experimental Results	Left Wheel Path Scales									Right Wheel Path Scales						Serial No	Date
		1 (1L)	2 (2L)	3 (4L)	4 (5L)	5 (6L)	6 (7L)	Average	Static	Diff.	1 (1R)	2 (3R)	3 (4R)	Average	Static	Diff.		
		I		II		III		IV		V		I		II		III		
I		68	10	19	48	41	32	36	30	21	61	43	34	46	31	48	157	5/20/69
		122	80	79	83	78	72	86	71	21	103	60	94	86	78	10		
		55	0	11	4	49	20	23	22	5	41	52	9	34	22	55	509	7/1/69
		91	57	60	90	78	90	78	67	16	61	85	85	77	60	28		
		57	57	67	68	58	76	64	51	25	39	65	72	59	46	28		
		68	45	53	62	51	46	54	50	8	46	51	58	52	47	10	375	5/29/69
		140	0	12	160	14	79	67	66	2	122	135	15	91	66	37		
		149	0	21	176	25	75	74	66	13	111	125	41	92	65	42		
		42	24	96	22	33	36	42	29	45	43	60	17	40	29	38	508	7/1/69
		96	3	33	92	73	61	60	48	24	67	100	76	81	49	65		
		70	0	87	75	59	51	57	27	111	30	55	63	49	29	70		
		0	73	75	43	37	58	48	29	64	24	74	73	57	30	90		
		22	72	42	61	55	58	52	43	20	13	28	97	46	40	15	507	7/1/69
		124	0	40	82	82	74	67	53	26	82	105	93	93	57	63		
		113	0	86	58	60	76	65	41	59	113	111	107	110	47	134		
		86	0	0	52	41	91	45	57	-21	82	145	16	81	57	42		
		128	0	0	48	31	66	46	58	-21	75	126	74	92	56	64		

All Weights in 100 Pounds

Table No. C-25		Roughness: <u>3</u> Replicate No: <u>3</u> Speed: <u>10</u> Site: <u>I-35</u>															Serial No	Date	
Experimental Results		Left Wheel Path Scales									Right Wheel Path Scales								
		1 (1L)	2 (2L)	3 (4L)	4 (5L)	5 (6L)	6 (7L)	Average	Static	Diff	1 (1R)	2 (2R)	3 (4R)	Average	Static	Diff			
Vehicle Class	I		37	30	34	30	32	33	33	30	9	36	33	35	35	31	12	151	5/20/69
			89	73	77	90	72	69	78	71	10	89	76	77	81	78	3		
	II		25	19	23	20	21	20	21	22	-3	26	26	24	25	22	15	505	7/1/69
			63	67	69	70	64	67	67	67	0	57	71	65	64	60	7		
			62	58	54	65	50	56	57	51	13	55	60	57	57	46	25		
	III		55	42	53	48	47	44	48	50	-4	45	48	49	47	47	0	372	5/29/69
			64	78	63	83	58	67	69	66	4	57	72	66	65	66	-2		
			84	67	85	75	70	60	74	66	11	69	65	80	71	65	10		
	IV		27	32	27	33	30	30	30	29	3	27	40	30	32	29	11	504	7/1/69
			55	50	40	42	57	45	48	48	0	58	57	44	53	49	8		
			18	23	24	16	24	30	22	27	-17	18	38	32	29	29	0		
			33	30	20	26	27	32	28	29	-3	32	23	25	27	30	-11		
	V		47	40	40	43	40	44	42	43	-2	44	44	39	42	40	6	503	7/1/69
			62	54	63	49	50	55	55	53	5	70	58	73	67	57	18		
			55	56	48	58	46	46	52	41	26	56	59	50	55	47	17		
			88	75	58	80	53	60	69	57	21	92	69	74	78	57	37		
			76	74	65	71	57	65	68	58	17	69	65	58	64	56	14		

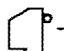



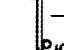
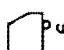
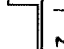
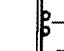
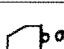


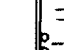

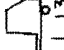
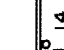
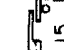
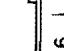
All Weights in 100 Pounds

Table No. C. 26		Roughness: <u>3</u>		Replicate No.: <u>3</u>		Speed: <u>30</u>		Site: <u>I-35</u>										
Experimental Results	Left Wheel Path Scales									Right Wheel Path Scales						Serial No	Date	
	1 (1L)	2 (2L)	3 (4L)	4 (5L)	5 (6L)	6 (7L)	Average	Static	Diff.	1 (1R)	2 (2R)	3 (4R)	Average	Static	Diff.			
	Vehicle Class																	
I		28	33	43	39	34	34	35	30	17	37	44	37	39	31	27	155	5/20/69
		77	61	79	67	75	79	73	71	3	74	84	82	80	78	3		
II		41	32	23	26	26	24	29	22	30	38	28	31	32	22	47	513	7/1/69
		88	83	73	70	83	76	79	67	18	80	105	75	87	60	44		
		66	50	52	53	63	65	58	51	14	64	75	56	65	46	41		
III		47	49	59	56	49	49	51	50	3	39	56	50	48	47	3	378	5/29/69
		39	101	113	100	70	64	81	66	28	24	136	103	88	66	33		
		80	62	30	74	69	74	65	66	-2	71	56	50	59	65	-9		
IV		20	32	29	25	32	35	29	29	0	41	44	38	41	29	41	512	7/1/69
		76	70	51	59	69	65	65	48	35	67	72	61	67	49	36		
		36	65	47	28	35	42	42	27	56	30	21	59	37	29	26		
		65	29	22	32	37	28	35	29	22	48	59	32	46	30	54		
V		38	43	52	40	47	46	44	43	3	47	61	20	43	40	7	511	7/1/69
		73	94	79	82	66	62	76	53	43	81	103	87	90	57	58		
		30	35	62	56	46	49	46	41	13	42	64	45	50	47	7		
		53	73	101	70	83	72	75	57	32	68	115	78	87	57	53		
		73	36	90	64	63	73	66	58	15	63	74	78	72	56	28		

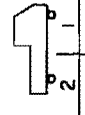
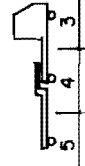
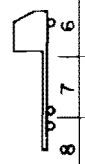
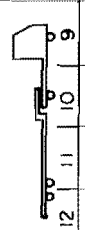
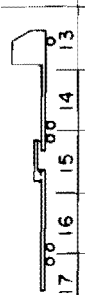
All Weights in 100 Pounds

Table No. C. 27		Roughness: <u>3</u>		Replicate No: <u>3</u>		Speed: <u>60</u>		Site: <u>I-35</u>											
Experimental Results		Left Wheel Path Scales									Right Wheel Path Scales						Serial No. Date		
		1 (1L)	2 (2L)	3 (4L)	4 (5L)	5 (6L)	6 (7L)	Average	Static	Diff.	1 (1R)	2 (3R)	3 (4R)	Average	Static	Diff.			
Vehicle Class	I		74	8	16	54	44	33	38	30	27	61	41	35	46	31	47	153	5/20/69
			120	75	83	89	77	79	87	71	23	94	53	100	82	78	6		
	II		33	0	10	17	44	24	21	22	- 3	39	48	14	34	22	53	517	7/1/69
			74	67	69	80	71	76	73	67	9	65	79	97	80	60	34		
			53	52	65	59	53	59	57	51	12	42	65	76	61	46	33		
	III		76	47	46	54	50	51	54	50	8	61	52	56	56	47	20	381	5/29/69
			115	76	44	106	76	50	78	66	18	108	79	82	90	66	36		
			135	46	64	102	86	47	80	66	21	91	79	82	84	65	29		
	IV		41	20	39	21	32	29	30	29	5	42	58	20	40	29	38	516	7/1/69
			88	9	37	98	68	52	59	48	23	66	103	63	77	49	57		
			60	0	88	58	64	41	52	27	93	31	48	63	47	29	62		
			0	71	60	43	35	44	42	29	45	17	68	72	52	30	74		
	V		24	70	39	62	52	57	51	43	18	9	34	65	36	40	- 10	515	7/1/69
			39	0	40	88	78	74	53	53	0	101	120	75	99	57	73		
			119	0	69	74	51	75	65	41	59	130	135	82	116	47	147		
			74	0	0	120	55	62	52	47	10	66	130	17	71	57	25		
			81	0	0	135	68	81		58		61	156	44	87	56	55		

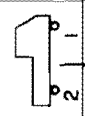
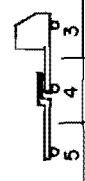
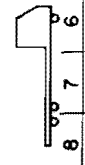
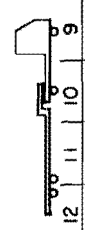
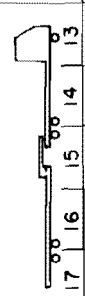
All Weights in 100 Pounds

Table No. C .28		Roughness: <u>4</u>		Replicate No: <u>1</u>		Speed: <u>10</u>		Site: <u>I-35</u>		Serial No.	Date								
Experimental Results		Left Wheel Path Scales										Right Wheel Path Scales							
		1 (1L)	2 (2L)	3 (4L)	4 (5L)	5 (6L)	6 (7L)	Average	Static			Diff	1 (1R)	2 (3R)	3 (4R)	Average	Static	Diff	
Vehicle Class	I		42	31	36	32	32	32	34	30	14	37	30	34	34	31	9	165	5/20/69
			88	73	80	87	71	71	78	71	10	87	74	81	81	78	3		
	II		26	20	24	22	20	20	22	22	0	30	24	22	25	22	15	533	7/1/69
			73	64	71	73	68	65	69	67	3	79	70	67	72	60	20		
			66	68	54	60	49	54	58	51	15	69	64	61	65	46	41		
	III		54	42	50	54	48	48	49	50	- 1	53	51	47	50	47	7	393	5/29/69
			72	83	65	85	60	63	71	66	8	83	73	68	75	66	13		
			83	64	83	77	61	62	72	66	9	86	61	75	74	65	14		
	IV		34	32	32	35	31	29	32	29	11	36	30	29	32	29	9	532	7/1/69
			63	59	48	48	42	43	51	48	5	66	66	47	60	49	22		
			38	12	20	35	27	29	27	27	0	47	25	30	34	29	17		
			32	14	17	25	26	32	24	29	-16	32	23	22	26	30	- 14		
	V		45	43	46	42	42	43	43	43	0	47	42	41	43	40	8	531	7/1/69
			60	73	65	56	53	54	60	53	14	78	60	72	70	57	23		
			43	54	55	54	44	47	49	41	21	48	47	46	47	47	0		
			67	73	75	78	53	57	67	47	43	69	70	81	73	57	29		
			60	63	68	71	60	59	63	58	9	63	62	56	60	56	8		

All Weights in 100 Pounds

Table No. C. 29		Roughness: <u>4</u>		Replicate No: <u>1</u>		Speed: <u>30</u>		Site: <u>I-35</u>											
Vehicle Class	Experimental Results	Left Wheel Path Scales									Right Wheel Path Scales						Serial No	Date	
		1 (1L)	2 (2L)	3 (4L)	4 (5L)	5 (6L)	6 (7L)	Average	Static	Diff	1 (1R)	2 (3R)	3 (4R)	Average	Static	Diff			
I		1	57	41	30	41	31	31	38	30	28	45	37	40	41	31	31	161	5/20/69
		2	111	58	85	78	76	77	81	71	14	105	79	83	89	78	12		
II		3	39	48	19	16	27	24	29	22	31	33	30	34	32	22	47	525	7/1/69
		4	112	96	78	80	71	74	85	67	27	101	88	81	90	60	50		
		5	93	43	54	52	59	64	61	51	19	75	77	58	70	46	52		
III		6	59	45	58	55	54	49	53	50	7	58	47	51	52	47	11	387	5/29/69
		7	82	75	105	74	59	72	78	66	18	94	80	77	84	66	27		
		8	62	50	71	70	79	67	66	66	0	62	84	62	69	65	7		
IV		9	48	31	31	32	30	30	34	29	16	44	43	47	45	29	54	524	7/1/69
		10	112	75	89	54	49	71	75	48	56	100	73	90	88	49	79		
		11	71	48	32	31	40	37	43	27	60	65	54	47	55	29	91		
		12	52	40	37	34	27	35	37	29	29	36	49	39	41	30	38		
V		13	61	35	55	46	47	50	49	43	14	55	58	33	49	40	22	523	7/1/69
		14	90	54	87	78	76	59	74	53	40	90	109	86	95	57	67		
		15	54	60	41	53	45	50	50	41	23	52	77	46	58	47	24		
		16	93	49	68	88	70	50	70	47	48	90	37	73	67	57	17		
		17	133	104	81	41	107	94	93	58	61	125	129	61	105	56	87		

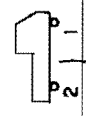
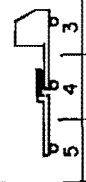
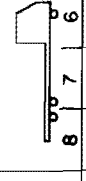
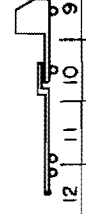
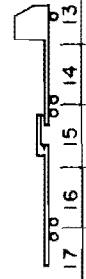
All Weights in 100 Pounds

Table No. C.30		Roughness: <u>4</u> Replicate No: <u>1</u> Speed: <u>60</u> Site: <u>I-35</u>															Serial No	Date	
Experimental Results	Vehicle Class	Left Wheel Path Scales									Right Wheel Path Scales								
		1 (1L)	2 (2L)	3 (4L)	4 (5L)	5 (6L)	6 (7L)	Average	Static	Diff.	1 (1R)	2 (2R)	3 (4R)	Average	Static	Diff.			
I		1	53	34	29	37	33	31	36	30	21	46	27	46	40	31	28	159	5/20/69
		2	110	86	61	77	73	72	80	71	12	112	80	85	92	78	18		
II		3	43	16	10	40	23	30	27	22	23	38	37	19	31	22	42	521	7/1/69
		4	107	84	65	64	80	78	80	67	- 4	99	87	102	96	60	60		
		5	96	54	57	56	54	67	64	51	25	80	61	69	70	46	52		
III		6	81	45	53	60	52	43	56	50	11	60	50	57	56	47	18	384	5/29/69
		7	123	68	30	127	41	65	76	66	15	98	87	100	95	66	44		
		8	119	42	32	120	40	52	67	66	2	96	86	57	80	65	23		
IV		9	40	19	33	24	31	33	30	29	3	47	46	33	42	29	45	520	7/1/69
		10	92	40	51	63	72	68	64	48	33	104	91	73	89	49	82		
		11	75	20	7	55	48	50	42	27	56	80	41	39	53	29	84		
		12	66	0	16	73	57	45	43	29	48	46	50	57	51	30	70		
V		13	65	66	39	57	46	52	54	43	26	59	31	71	54	40	34	519	7/1/69
		14	100	38	21	112	62	66	66	53	25	107	98	66	90	57	58		
		15	86	0	7	107	64	61	54	41	32	81	78	83	81	47	72		
		16	100	100	52	58	91	88	82	47	74	98	70	104	91	57	60		
		17	95	90	82	44	78	70	76	58	31	89	53	104	82	56	46		

All Weights in 100 Pounds

Table No. C. 31		Roughness: <u>4</u>		Replicate No: <u>2</u>		Speed: <u>10</u>		Site: <u>I-35</u>											
Vehicle Class	Experimental Results	Left Wheel Path Scales									Right Wheel Path Scales						Serial No	Date	
		1 (1L)	2 (2L)	3 (4L)	4 (5L)	5 (6L)	6 (7L)	Average	Static	Diff	1 (1R)	2 (3R)	3 (4R)	Average	Static	Diff			
		I		II		III		IV		V									
I		37	29	36	32	31	33	33	30	10	35	30	34	33	31	6	167	5/20/69	
		89	80	78	89	70	72	80	71	12	86	71	78	78	78	0			
	II		24	20	23	21	20	20	21	22	- 3	27	24	22	24	22	11	537	7/1/69
			73	65	72	69	70	67	69	67	3	74	70	68	71	60	18		
			69	71	52	62	48	56	60	51	17	64	67	60	64	46	38		
	III		54	43	50	54	47	47	49	50	- 2	57	48	44	50	47	6	397	5/29/69
			75	84	68	45	60	68	67	66	1	85	73	74	77	66	17		
			73	64	80	71	71	57	69	66	5	75	65	70	70	65	8		
	IV		33	30	29	33	30	29	31	29	6	33	29	31	31	29	7	536	7/1/69
			62	65	48	51	33	52	52	48	8	66	64	49	60	49	22		
			37	13	18	15	25	29	23	27	-15	48	35	27	37	29	26		
			40	16	19	25	28	32	27	29	- 8	37	23	24	28	30	- 7		
	V		45	43	45	49	41	43	44	43	3	47	43	38	43	40	7	535	7/1/69
			58	74	67	60	55	53	61	53	15	75	58	72	68	57	20		
			39	52	57	56	43	47	49	41	20	47	50	45	47	47	0		
			66	75	74	79	56	67	69	47	48	70	70	78	73	57	27		
			61	60	76	70	59	66	65	58	13	67	61	56	61	56	10		


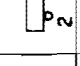


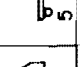

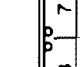
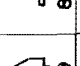
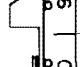

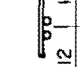
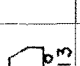
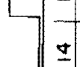
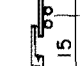
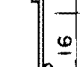
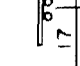
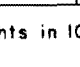
All Weights in 100 Pounds

Table No. C. 32		Roughness: <u>4</u> Replicate No: <u>2</u> Speed: <u>30</u> Site: <u>I-35</u>															Serial No	Date	
Experimental Results	Vehicle Class	Left Wheel Path Scales									Right Wheel Path Scales								
		1 (1L)	2 (2L)	3 (4L)	4 (5L)	5 (6L)	6 (7L)	Average	Static	Diff.	1 (1R)	2 (3R)	3 (4R)	Average	Static	Diff.			
I		1	50	35	37	45	31	33	38	30	28	41	41	38	40	31	29	163	5/20/69
		2	103	57	84	73	76	81	79	71	11	105	79	92	92	78	18		
II		3	36	49	23	16	27	27	30	22	35	35	31	34	33	22	52	529	7/1/69
		4	92	93	78	78	77	76	82	67	23	93	85	86	88	60	47		
		5	79	38	50	46	57	61	55	51	8	75	80	58	71	46	54		
III		6	59	50	58	53	48	52	53	50	7	59	51	53	54	47	16	390	5/29/69
		7	89	80	100	73	57	70	78	66	18	99	87	82	89	66	35		
		8	53	58	59	61	75	59	61	66	- 8	59	85	62	69	65	6		
IV		9	40	31	35	34	33	30	34	29	17	44	40	42	42	29	45	528	7/1/69
		10	83	71	66	50	46	64	63	48	32	85	82	79	82	49	67		
		11	55	31	35	32	32	37	37	27	37	58	62	37	52	29	80		
		12	47	40	40	35	30	37	38	29	32	36	49	39	41	30	38		
V		13	65	33	56	49	45	47	49	43	14	54	57	31	47	40	18	527	7/1/69
		14	104	89	86	81	75	61	83	53	56	101	94	91	95	57	67		
		15	62	55	41	50	43	49	50	41	22	57	73	47	59	47	26		
		16	105	47	73	92	49	49	69	47	47	97	47	84	76	57	33		
		17	86	103	71	32	84	78	76	58	30	98	118	38	85	56	51		


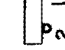

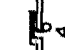
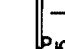
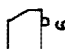
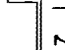
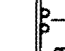
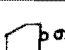


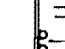
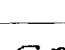
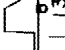
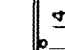
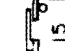

All Weights in 100 Pounds

Table No. C.33		Roughness: <u>4</u> Replicate No: <u>2</u> Speed: <u>60</u> Site: <u>I-35</u>															Experimental Results	
Vehicle Class	Diagram	Left Wheel Path Scales									Right Wheel Path Scales						Serial No	Date
		1 (1L)	2 (2L)	3 (4L)	4 (5L)	5 (6L)	6 (7L)	Average	Static	Diff	1 (1R)	2 (2R)	3 (4R)	Average	Static	Diff		
		I		52	36	33	56	37	32	41	30	37	43	26	43	37		
II		103	98	64	86	77	71	83	71	12	99	62	84	82	78	5	545	7/1/69
III		41	10	12	38	20	33	26	22	17	28	37	16	27	22	23	384	5/29/69
IV		111	77	62	74	85	78	81	67	21	98	78	93	90	60	49	544	7/1/69
V		96	55	59	60	57	70	66	51	30	79	58	69	69	46	49	543	7/1/69
		81	45	53	60	52	43	56	50	11	60	50	57	56	47	18		
		123	68	30	127	41	65	76	66	15	98	87	100	95	66	44		
		119	42	32	120	40	33	67	66	2	96	86	57	80	65	23		
		40	22	31	26	32	30	30	29	4	47	43	28	39	29	36		
		101	38	52	67	73	61	65	48	36	88	72	69	76	49	56		
		77	29	9	61	49	45	45	27	67	69	39	29	46	29	57		
		68	0	21	78	59	47	45	29	57	41	50	51	47	30	58		
		65	57	39	56	46	51	52	43	22	53	29	71	51	40	27		
		101	46	18	104	65	62	66	53	25	100	103	41	81	57	43		
		88	0	0	100	57	62	51	41	24	80	93	65	79	47	69		
		97	98	46	55	96	102	82	47	74	90	69	94	84	57	43		
		98	69	80	51	92	94	81	58	39	76	60	101	79	56	41		


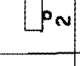


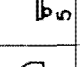
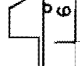
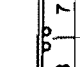
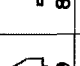
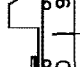

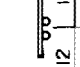
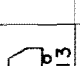
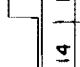
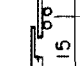
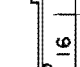
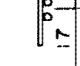
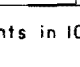
All Weights in 100 Pounds

Table No. C. 34		Roughness: <u>4</u>		Replicate No: <u>3</u>		Speed: <u>10</u>		Site: <u>I-35</u>												
Experimental Results		Left Wheel Path Scales									Right Wheel Path Scales						Serial No		Date	
		1 (1L)	2 (2L)	3 (4L)	4 (5L)	5 (6L)	6 (7L)	Average	Static	Diff.	1 (1R)	2 (3R)	3 (4R)	Average	Static	Diff.				
Vehicle Class	I		38	33	34	33	31	34	34	30	13	34	32	29	32	31	2	169	5/20/69	
			88	85	77	91	70	70	80	71	13	85	71	68	75	78	- 4			
	II		25	18	26	17	20	20	21	22	-5	27	25	21	24	22	11	541	7/1/69	
			77	62	64	73	65	72	69	67	3	79	74	64	72	60	21			
			65	64	48	63	54	54	58	51	14	64	64	57	62	46	34			
	III		54	43	50	54	47	47	49	50	- 2	57	48	44	50	47	6	397	5/29/69	
			75	84	68	45	60	68	67	66	1	85	73	74	77	66	17			
			73	64	80	71	71	57	69	66	5	75	65	70	70	65	8			
	IV		33	28	33	31	30	31	31	29	7	34	27	30	30	29	5	540	7/1/69	
			65	69	52	54	32	46	53	48	10	63	61	50	58	49	18			
			39	18	25	16	24	29	25	27	- 7	42	47	36	42	29	44			
			42	32	20	18	25	30	28	29	- 4	39	30	23	31	30	2			
	V		48	40	43	45	42	43	43	43	0	46	41	40	42	40	6	539	7/1/69	
			62	63	62	60	51	53	58	53	10	69	62	70	67	57	18			
			51	53	50	52	42	45	49	41	19	53	55	49	52	47	11			
			68	70	67	76	53	62	66	47	40	77	68	73	73	57	27			
			64	58	67	70	57	63	63	58	9	67	62	59	63	56	12			

All Weights in 100 Pounds

Table No. C. 35		Roughness: <u>4</u>		Replicate No.: <u>3</u>		Speed: <u>30</u>		Site: <u>I-35</u>											
Experimental Results		Left Wheel Path Scales									Right Wheel Path Scales						Serial No	Date	
		1 (1L)	2 (2L)	3 (4L)	4 (5L)	5 (6L)	6 (7L)	Average	Static	Diff	1 (1R)	2 (3R)	3 (4R)	Average	Static	Diff			
Vehicle Class	I		55	43	27	40	31	34	38	30	28	42	39	40	40	31	30	173	5/20/69
			116	59	85	77	75	78	82	71	15	106	78	82	89	78	14		
	II		33	42	14	15	27	25	26	22	18	29	26	29	28	22	27	549	7/1/69
			90	90	74	78	67	67	78	67	16	89	90	79	86	60	43		
			76	38	54	43	54	60	54	51	6	75	74	63	71	46	54		
	III		59	50	58	53	48	52	53	50	7	59	51	53	54	47	16	390	5/29/69
			89	80	100	73	57	70	78	66	18	99	87	82	89	66	35		
			53	58	59	61	75	59	61	66	8	59	85	62	69	65	6		
	IV		37	28	29	29	29	28	30	29	3	41	26	43	37	29	26	548	7/1/69
			60	65	74	48	50	62	60	48	25	83	75	77	78	49	60		
			61	27	25	30	35	34	35	27	31	55	54	40	50	29	71		
			51	40	27	35	27	25	34	29	18	32	46	34	37	30	24		
	V		55	37	53	50	44	45	47	43	10	50	45	36	44	40	9	547	7/1/69
			83	84	73	74	55	53	70	53	33	91	98	90	93	57	63		
			51	66	40	59	55	44	52	41	28	41	61	68	57	47	21		
			74	60	49	39	84	56	60	47	28	96	43	42	60	57	6		
			93	74	106	85	50	71	80	58	38	94	131	70	98	56	76		

All Weights in 100 Pounds

Table No. C. 36		Roughness: <u>4</u>		Replicate No: <u>3</u>		Speed: <u>60</u>		Site: <u>I-35</u>												
Experimental Results		Left Wheel Path Scales									Right Wheel Path Scales						Serial No		Date	
		1 (1L)	2 (2L)	3 (4L)	4 (5L)	5 (6L)	6 (7L)	Average	Static	Diff	1 (1R)	2 (3R)	3 (4R)	Average	Static	Diff				
Vehicle Class	I		50	37	30	39	37	30	37	30	24	45	31	41	39	31	26	175	5/20/69	
			119	94	68	88	78	76	87	71	23	107	67	84	86	78	10			
	II		35	15	11	39	26	30	26	22	18	37	38	21	32	22	45	553	7/1/69	
			98	76	67	82	80	87	82	67	22	102	87	105	98	60	63			
			84	50	58	60	53	76	64	51	25	84	62	73	73	46	59			
	III		81	45	53	60	52	43	56	50	12	60	50	57	56	47	18	384	5/29/69	
			123	68	30	127	41	65	76	66	15	98	87	100	95	66	44			
			119	42	32	120	40	52	67	66	2	96	86	57	80	65	23			
	IV		48	20	32	25	29	29	30	29	5	45	39	30	38	29	31	552	7/1/69	
			107	38	49	55	68	61	63	48	31	90	73	77	80	49	63			
			84	24	10	65	49	47	47	27	74	65	38	33	45	29	55			
			73	0	20	75	50	43	43	29	50	43	47	54	48	30	60			
	V		67	59	35	58	43	48	52	43	21	54	30	72	52	40	30	551	7/1/69	
			100	41	18	107	63	61	65	53	23	100	99	48	82	57	44			
			91	0	5	92	56	58	50	41	23	77	98	107	94	47	100			
			95	99	54	52	88	76	77	47	65	92	60	45	66	57	15			
			95	75	84	35	67	64	70	58	21	78	105	105	96	56	71			

All Weights in 100 Pounds

TABLE C.37. DYNAMIC COMPONENT (PERCENT OF STATIC)

Roughness 1 - Speed 10 mph							
Scale Number							
	1L	2L	4L	5L	6L	7L	
1	0	12	18	18	4	7	
2	-3	12	5	23	2	-4	
3	2	-3	-2	8	-6	-6	
4	-5	-4	-5	1	3	3	
5	-7	5	-7	18	-3	7	
6	4	-5	3	9	-1	-7	
7	4	5	6	25	-4	-1	
8	10	0	22	16	1	0	
9	2	6	6	10	6	3	
10	-7	0	11	6	-11	-1	
11	6	-17	-11	-36	3	20	
12	-5	5	-22	-8	3	23	
13	2	-3	4	1	-3	2	
14	-6	4	21	6	-1	4	
15	8	16	20	20	7	13	
16	2	12	22	35	-5	6	
17	-3	6	14	16	6	5	

Note: Each value is the mean of three observations at the same roughness-speed-axle combination.

TABLE C.38. DYNAMIC COMPONENT (PERCENT OF STATIC)

Roughness 1 - Speed 30 mph							
Scale Number							
	1L	2L	4L	5L	6L	7L	
1	22	19	10	24	7	6	
2	10	-1	15	1	5	12	
3	12	59	52	45	14	12	
4	3	6	11	-1	6	6	
5	11	-9	-3	0	15	20	
6	9	-3	19	7	-3	2	
7	10	9	35	23	-2	3	
8	-4	-1	7	8	5	4	
9	16	-9	-9	0	7	15	
10	22	5	23	1	19	27	
11	41	28	22	15	35	48	
12	16	26	21	21	28	25	
13	2	-14	20	-12	4	7	
14	-2	4	28	28	21	9	
15	2	15	37	33	15	15	
16	-8	-24	1	9	-4	-5	
17	29	12	21	-21	26	17	

Note: Each value is the mean of three observations at the same roughness-speed-axle combination.

TABLE C.39. DYNAMIC COMPONENT (PERCENT OF STATIC)

Roughness 1 - Speed 60 mph						
Scale Number						
	1L	2L	4L	5L	6L	7L
1	24	20	11	37	26	8
2	20	20	9	20	14	4
3	30	-14	-17	21	24	27
4	17	18	3	0	16	24
5	35	9	14	-1	10	40
6	19	-3	4	11	10	5
7	26	10	3	20	20	8
8	18	14	8	0	24	4
9	10	-21	7	-14	-1	7
10	42	-15	25	1	10	31
11	91	61	37	56	75	78
12	52	35	26	59	71	37
13	20	10	-12	22	9	14
14	26	18	7	24	21	28
15	19	47	5	21	36	40
16	22	25	25	-19	14	27
17	8	50	17	-5	26	16

Note: Each value is the mean of three observations at the same roughness-speed-axle combination.

TABLE C.40. DYNAMIC COMPONENT (PERCENT OF STATIC)

Roughness 2 - Speed 10 mph							
Scale Number							
	1L	2L	4L	5L	6L	7L	
1	9	4	23	19	4	-2	
2	-10	9	6	26	3	8	
3	0	0	3	2	-12	-8	
4	-4	-1	3	18	5	3	
5	4	11	8	29	1	11	
6	6	-6	4	11	-3	-7	
7	22	1	7	8	-2	-2	
8	1	6	17	11	1	-4	
9	-2	-1	5	10	6	12	
10	-12	8	23	5	3	4	
11	24	7	20	-1	9	24	
12	14	28	13	5	15	18	
13	-4	-2	7	2	-3	3	
14	-6	4	36	24	1	8	
15	6	13	22	39	12	13	
16	-4	15	32	46	-4	3	
17	6	1	17	25	1	6	

Note: Each value is the mean of three observations at the same roughness-speed-axle combination.

TABLE C.41. DYNAMIC COMPONENT (PERCENT OF STATIC)

Roughness 2 - Speed 30 mph						
Scale Number						
	1L	2L	4L	5L	6L	7L
1	10	23	16	40	14	11
2	10	-2	12	10	7	8
3	-15	32	39	50	18	0
4	15	1	16	-1	-4	5
5	12	2	6	-1	24	28
6	34	-4	11	7	-2	-1
7	94	59	63	40	12	-12
8	-35	-42	26	31	-19	6
9	33	-3	1	6	8	17
10	13	13	13	14	43	30
11	-12	69	37	20	36	49
12	62	0	15	18	16	16
13	10	-5	26	11	7	6
14	27	25	35	13	9	9
15	-11	63	33	53	26	12
16	36	15	12	-5	23	11
17	12	25	37	13	5	0

Note: Each value is the mean of three observations at the same roughness-speed-axle combination.

TABLE C.42. DYNAMIC COMPONENT (PERCENT OF STATIC)

Roughness 2 - Speed 60 mph							
Scale Number							
	1L	2L	4L	5L	6L	7L	
1	87	-23	0	30	27	0	
2	4	40	9	16	13	1	
3	149	-74	-11	-27	42	53	
4	6	23	10	23	38	26	
5	42	14	19	14	18	46	
6	15	2	2	12	17	6	
7	93	-58	-54	120	-27	55	
8	99	-48	-62	99	-28	39	
9	12	7	17	-5	10	23	
10	90	13	26	8	38	64	
11	-24	170	-37	5	51	82	
12	140	101	-8	25	75	43	
13	-2	12	-18	39	14	26	
14	103	-31	-13	73	74	28	
15	80	-24	-70	108	58	59	
16	126	-100	-100	138	-25	-28	
17	163	-100	-97	122	-12	-17	

Note: Each value is the mean of three observations at the same roughness-speed-axle combination.

TABLE C.43. DYNAMIC COMPONENT (PERCENT OF STATIC)

Roughness 3 - Speed 10 mph						
Scale Number						
	1L	2L	4L	5L	6L	7L
1	17	-3	16	-1	4	7
2	24	-3	10	24	2	-3
3	17	-8	9	-5	-3	-9
4	-12	0	-2	1	-2	0
5	24	16	6	28	-2	9
6	9	-14	5	-2	-4	-9
7	-3	20	-5	30	-10	-1
8	30	-1	30	10	2	-4
9	1	-3	-1	9	6	1
10	4	6	-1	3	12	1
11	-7	-15	-1	-16	-7	11
12	13	10	-5	12	-1	6
13	9	-6	-2	2	-4	4
14	18	3	25	-3	-1	8
15	29	35	1	40	10	17
16	40	25	16	43	-6	1
17	24	17	13	31	6	8

Note: Each value is the mean of three observations at the same roughness-speed-axle combination.

TABLE C.44. DYNAMIC COMPONENT (PERCENT OF STATIC)

Roughness 3 - Speed 30 mph						
	Scale Number					
	1L	2L	4L	5L	6L	7L
1	-26	4	42	32	12	12
2	4	-10	12	-1	9	12
3	91	59	23	26	20	9
4	26	25	6	-1	19	12
5	27	-2	3	5	22	24
6	-3	-3	16	11	-2	-1
7	-41	41	60	49	-4	6
8	20	0	-51	1	12	2
9	-35	13	1	-17	7	20
10	40	55	2	17	39	18
11	17	96	48	16	36	46
12	164	3	5	-1	22	5
13	-6	2	19	-4	10	8
14	42	64	48	50	24	15
15	-11	-2	46	39	17	20
16	-2	43	56	9	3	17
17	35	-6	63	1	9	22

Note: Each value is the mean of three observations at the same roughness-speed-axle combination.

TABLE C.45. DYNAMIC COMPONENT (PERCENT OF STATIC)

Roughness 3 - Speed 60 mph						
Scale Number						
	1L	2L	4L	5L	6L	7L
1	127	-74	-50	78	46	9
2	69	4	16	20	9	7
3	112	20	35	-14	79	21
4	15	-11	-7	20	9	23
5	3	-29	-14	13	7	34
6	45	-11	1	20	0	-3
7	106	-57	-49	81	-7	-18
8	118	-71	-18	92	6	-22
9	39	-29	101	-25	9	16
10	99	-87	-30	97	44	22
11	163	-14	204	120	132	69
12	-100	66	115	53	33	81
13	-47	49	-7	37	29	29
14	55	-69	-38	67	43	38
15	191	-59	89	115	40	63
16	11	-100	-18	22	-25	36
17	29	-100	-100	21	0	16

Note: Each value is the mean of three observations at the same roughness-speed-axle combination.

TABLE C.46. DYNAMIC COMPONENT (PERCENT OF STATIC)

Roughness 4 - Speed 10 mph							
Scale Number							
	1L	2L	4L	5L	6L	7L	
1	30	3	18	8	4	10	
2	24	12	10	25	-1	0	
3	14	-12	11	-9	-9	-9	
4	11	-5	3	7	1	2	
5	31	33	1	21	-1	7	
6	8	-15	0	8	-5	-5	
7	11	26	0	9	-9	-2	
8	21	-3	24	14	-3	-9	
9	15	3	8	14	5	2	
10	32	34	3	6	-26	-2	
11	41	-47	-22	-19	-6	7	
12	31	-29	-36	-22	-9	8	
13	7	-2	4	5	-3	0	
14	13	32	22	11	0	1	
15	8	29	32	32	5	13	
16	18	28	26	36	-5	9	
17	6	4	21	21	1	8	

Note: Each value is the mean of three observations at the same roughness-speed-axle combination.

TABLE C.47. DYNAMIC COMPONENT (PERCENT OF STATIC)

Roughness 4 - Speed 30 mph							
Scale Number							
	1L	2L	4L	5L	6L	7L	
1	80	32	4	40	3	9	
2	55	-18	19	7	7	11	
3	64	111	-15	-29	23	15	
4	46	39	14	17	7	8	
5	62	-22	3	-8	11	21	
6	18	-3	16	7	0	2	
7	31	19	54	11	-13	7	
8	-15	-16	-5	-3	16	-7	
9	44	3	9	9	6	1	
10	77	47	59	6	1	37	
11	131	31	14	15	32	33	
12	72	38	20	20	-3	12	
13	40	-19	27	12	5	10	
14	74	43	55	47	30	9	
15	36	47	-1	32	16	16	
16	59	-9	11	28	19	-9	
17	79	62	48	-9	39	40	

Note: Each value is the mean of three observations at the same roughness-speed-axle combination.

TABLE C.48. DYNAMIC COMPONENT (PERCENT OF STATIC)

Roughness 4 - Speed 60 mph						
Scale Number						
	1L	2L	4L	5L	6L	7L
1	72	19	2	47	19	3
2	56	31	-10	18	7	3
3	80	-38	-50	77	5	41
4	57	18	-4	10	22	21
5	80	4	14	15	7	39
6	62	-10	6	20	4	-14
7	86	3	-55	92	-38	-2
8	80	-36	-52	82	-39	-21
9	47	-30	10	-14	6	6
10	108	-19	6	29	48	32
11	191	-10	-68	124	80	75
12	138	-100	-35	160	91	55
13	53	38	-12	33	5	17
14	89	-21	-64	103	20	19
15	115	-100	-90	143	44	56
16	71	74	-11	-4	61	56
17	66	35	41	-25	36	31

Note: Each value is the mean of three observations at the same roughness-speed-axle combination.